

ASYMMETRIC SYNTHESSES, RING OPENING AND
STEREOSELECTIVE REACTIONS, ABSOLUTE CONFORMATION
AND ACTIVATION BARRIER DETERMINATIONS ON AXIALLY
CHIRAL OXAZOLIDINE DERIVATIVES

by

Öznur Demir Ordu

B.S., Chemistry, Abant İzzet Baysal University, 1998

M.S., Chemistry., Boğaziçi University, 2001

Submitted to the Institute for Graduate Studies in
Science and Engineering in partial fulfillment of
the requirements for the degree of
Doctor of Philosophy

Graduate Program in Chemistry

Boğaziçi University

2008

To my daughter Elif Berin Ordu and my husband Bülent Ordu

ACKNOWLEDGMENT

I would like to express my sincere gratitude to my thesis supervisor Prof. İlknur Doğan for her help, advice, encouragement and scientific guidance in every stage of this work. It was a great pleasure for me to work with her.

I wish to thank the members of my examination committee: Assoc. Prof. Dr. Ersin Acar, Prof. Hadi Özbal, Assit. Prof. Dr. Amitav Sanyal and Prof. Dr. Süheyla Uzman for their advices and comments on the final manuscript of my thesis.

I would like to express my heartfelt thanks to my laboratory partners Şule Erol and Esra Müjde Yılmaz for her invaluable help, understanding and motivation.

I would like to thank Dr. Sinan Şen, Dr. Funda Oğuz, Dr. Gökhan Çaylı, Hikmet Karayel, Pınar Çakır for her friendship.

I would like to thank Burcu Selen Çağlayan for recording the NMR spectra.

I would like to extend my thanks to all the members of the chemistry department who were always most helpful during my study. I wish to thank especially to Assit. Prof. Dr. Neren Ökte, Assit. Prof. Dr. Rana Sanyal, Eliza Kalvo, Hülya Metiner and Zahit Mehlep for their help, advice and understanding in every aspects.

My greatest thanks are to my mother Hacer Demir, my father Rıza Demir, my sister Hale Demir and my brother Rıdvan Demir who were always behind me, with their endless love, encouragement and support during my whole life.

Finally, my deepest thanks are extended to my daughter elif Berin Ordu and my husband Bülent Ordu for their endless love, understanding and help.

This project has been supported by Boğaziçi University Scientific Research Fund with project numbers 08B507 and 03B503.

ABSTRACT

ASYMMETRIC SYNTHESSES, RING OPENING AND STEREOSELECTIVE REACTIONS, ABSOLUTE CONFORMATION AND ACTIVATION BARRIER DETERMINATIONS ON AXIALLY CHIRAL OXAZOLIDINE DERIVATIVES

In this study, sterically hindered 5-methyl-3-(*o*-aryl)-2,4-oxazolidinediones, 5-methyl-3-(*o*-iodophenyl)-2-thioxo-4-oxazolidinedione and 5,5-dimethyl-3-(*o*-aryl)-2,4-oxazolidinediones have been synthesized. Diastereomeric isomers of the 5-methyl-3-(*o*-aryl)-2,4-oxazolidinediones and 5-methyl-3-(*o*-iodophenyl)-2-thioxo-4-oxazolidinedione and enantiomeric isomers of the 5,5-dimethyl-3-(*o*-aryl)-2,4-oxazolidinediones have been identified by ^1H NMR and ^{13}C NMR.

Activation barriers to hindered rotation around C-N single bond have been determined by using temperature dependent NMR or by thermal racemization on chiral sorbents by HPLC.

The conformational preferences of the diastereomers have been investigated by one and two dimensional NMR spectroscopy and by HPLC on an optically active sorbent. It was found that when the bulky group on C-5 and the *ortho* substituent on the aromatic ring are on opposite sites the conformation becomes more stable.

Absolute conformations of 5,5-dimethyl-3-(*o*-aryl)-2,4-oxazolidinediones have been determined by one and two dimensional ^1H NMR in the presence of a chiral auxiliary (S)-(+)-1-(9-anthryl)-2,2,2-trifluoro ethanol ((S)-TFAE). A solvation model has been proposed for the determination absolute stereochemistry on the basis of interactions between the enantiomers and (S)-TFAE.

Asymmetric alkylation and aldol reactions have been carried out on 5-methyl-3-(*o*-tolyl)-2,4-oxazolidinedione, 5-methyl-3-(*o*-iodophenyl)-2,4-oxazolidinedione and 5-methyl-3-(*o*-iodophenyl)-2-thioxo-4-oxazolidinedione over the lithium enolate forms. The enolate formation could be achieved by lithium diisopropylamide at -78 °C under nitrogen. It was found that the *o*-aryl substituents had a stereodirecting effect on the reactions taking place at C-5 of the ring. The stereoselectivity of the reactions was determined by using chiral HPLC.

Basic and reductive ring opening reactions of diastereomeric 5*S*-methyl-N-(*o*-aryl)-2,4-oxazolidinediones and enantiomeric 5,5-dimethyl-N-(*o*-aryl)-2,4-oxazolidinediones have been done to examine the stability of the ring and to synthesize various organic compounds such as chiral α -hydroxyamides, carbamoyloxyacids and carbamate derivatives via ring opening. It was observed that 5-methyl-2,4-oxazolidinedione ring cleaved more easily than 5,5-dimethyl-2,4-oxazolidinedione ring. 5-Methyl-2,4-oxazolidinedione ring was reduced to a primary alcohol after ring opening, whereas the reduction of 5,5-dimethyl-2,4-oxazolidinedione ring yielded a secondary alcohol asymmetrically without ring cleavage.

ÖZET

AKSİYEL KİRAL OKSAZOLİDİN TÜREVLERİNDE ASİMETRİK SENTEZ, HALKA AÇILMA VE STERİYOSEÇİCİ REAKSİYONLAR, KONFORMASYON VE AKTİVASYON BARIYERİ TAYİNİ

Bu çalışmada sterik engelli 5-metil-3-(*o*-aril)-2,4-oksazolidindion, 5-metil-3-(*o*-iyodofenil)-2-tiyokso-4-oksazolidinon ve 5,5-dimetil-3-(*o*-aril)-2,4-oksazolidindion bileşikleri sentezlenmiştir. Diastereomerik 5-metil-3-(*o*-aril)-2,4-oksazolidindion, 5-metil-3-(*o*-iyodofenil)-2-tiyokso-4-oksazolidindion ve enantiyomerik 5,5-dimetil-3-(*o*-aril)-2,4-oksazolidindion izomerleri ^1H NMR ve ^{13}C NMR spektroskopisi ile tanımlanmıştır.

C-N tekli bağ etrafındaki engelli dönme aktivasyon bariyeri dinamik NMR ya da termal rasemizasyon yöntemleri ile bulunmuştur.

Diastereiyomerlerin konformasyonel seçicilikleri tek ve iki boyutlu NMR spektroskopisi ve kiral HPLC ile araştırılmıştır. Bu çalışmaların sonucunda C-5 ve aril halkanın *ortho* pozisyonundaki grupların farklı yönlerde olmasının konformasyonu daha karalı hale getirdiği görülmüştür.

5,5-dimetil-3-(*o*-aril)-2,4-oksazolidindion bileşiklerinin absolut konformasyonlarının belirlenmesi için tek ve iki boyutlu NMR spektrumları (S)-(+)-1-(9-antril)-2,2,2-trifloro etanol ((S)-TFAE) varlığında alınmıştır. Enantiyomerlerin (S)-TFAE ile yapmış olduğu etkileşimler göz önüne alınarak absolute stereokimya için bir solvasyon modeli önerilmiştir.

Asimetrik alkilasyon ve aldol reaksiyonları 5-metil-3-(*o*-tolil)-2,4-oksazolidindion, 5-metil-3-(*o*-iyodofenil)-2-tiyokso-4-oksazolidinon ve 5-metil-3-(*o*-iyodofenil)-2,4-oksazolidindion bileşiklerinin enolat formları üzerinden gerçekleştirilmiştir. Enolat oluşumu için lityum diizopropilamid kullanılmış ve reaksiyon $-78\text{ }^{\circ}\text{C}$ 'de azot atmosferi

altında yapılmıştır. Bu çalışmada *o*-aril sübstitüentin C-5 de gerçekleşen reaksiyonlarda yönlendirici etkisi olduğu bulunmuştur. Stereoseçicilik, kiral HPLC kullanılarak bulunmuştur.

Diastereomeric 5-metil-3-(*o*-aril)-2,4-oksazolidindion ve enantiyomerik 5,5-dimetil-3-(*o*-aril)-2,4-oksazolidindion bileşiklerinin halka kararlılığını bulmak ve yeni organik bileşikler (kiral α -hidroksi amidler, karbamoyloksi asidler ve karbamat türevleri) sentezlemek için bazik ve indirgeyici halka açılma reaksiyonları yapılmıştır. Bu çalışmada 5-metil-3-(*o*-aril)-2,4-oksazolidindion bileşiklerinin 5,5-dimetil-3-(*o*-aril)-2,4-oksazolidindion bileşiklerinden daha kolay açıldığı gözlemlenmiştir. 5-metil-3-(*o*-aril)-2,4-oksazolidindion bileşikleri sodyum borohidür ile primer alkole indirgenirken, 5,5-dimetil-3-(*o*-aril)-2,4-oksazolidindion bileşikleri halka açılması olmadan sekonder alkole indirgenmiştir.

TABLE OF CONTENTS

ACKNOWLEDGMENTS.....	iv
ABSTRACT.....	v
ÖZET.....	vii
LIST OF FIGURES.....	xiv
LIST OF TABLES.....	xxv
LIST OF SYMBOLS/ ABBREVIATIONS.....	xxvii
1. INTRODUCTION.....	1
2. THEORY.....	5
2.1. Rotational Isomers and Stereochemistry of the N-(<i>o</i> -aryl) Substituted 2, 4- Oxazolidinedione Ring	5
2.2. Nomenclature.....	6
2.3. Determination of Absolute Conformation Using Chiral 2,2,2-Trifluoro-1-(9-anthryl)ethanol by Nuclear Magnetic Resonance.....	7
2.4. Asymmetric Synthesis.....	10
2.4.1. Methods of Asymmetric Synthesis.....	11
2.4.1.1. Substrate-Controlled Methods, First Generation Method.....	11
2.4.1.2. Auxiliary-Controlled Methods, Second Generation Method.....	12
2.4.1.3. Reagent-Controlled Methods, Third generation method.....	12
2.4.1.4. Catalyst-Controlled Methods, Fourth generation method.....	12
2.4.2. Asymmetric Alkylation and Aldol Condensation of Carbonyl Compounds.....	13
2.4.2.1. Asymmetric α -Alkylation Reactions.....	14
2.4.2.2. Asymmetric Aldol Reactions.....	17
2.5. The Gem-Dialkyl Effect in Organic Transformations.....	22
2.6. Cram and Felkin-Anh Diastereoselectivity in Nucleophilic Addition to the Carbonyl Group.....	25
3. ORGANIC SYNTHESIS.....	27
3.1. The Synthesis of (5 <i>S</i>)-methyl-3-(<i>o</i> -aryl)-2,4-oxazolidinediones.....	27

3.1.1. The General Procedure.....	27
3.1.1.1. (5S)-methyl-3-(α -naphthyl)-2,4-oxazolidinedione (2).....	27
3.1.1.2. (5S)-methyl-3-(<i>o</i> -iodophenyl)-2,4-oxazolidinedione (3).....	28
3.2. The Synthesis of 5,5-Dimethyl-3-(<i>o</i> -aryl)-2,4-oxazolidinediones.....	29
3.2.1. The General Procedure.....	29
3.2.1.1. 5,5-Dimethyl-3-(α -naphthyl)-2,4-oxazolidinedione (\pm 15)..	29
3.2.1.2. 5,5-Dimethyl-3-(<i>o</i> -iodophenyl)-2,4-oxazolidinedione (\pm 11).....	30
3.3. The Synthesis of (5S)-methyl-3-(<i>o</i> -aryl)-2-thioxo-4-oxazolidinones.....	31
3.3.1. The General Procedure.....	31
3.3.1.1. (5S)-methyl-3-(<i>o</i> -iodophenyl)-2-thioxo-4-oxazolidinone (58).....	32
3.4. The Ring Opening Reactions with Potassium Hydroxide.....	32
3.4.1. General Procedure for the Formation of Amides.....	32
3.4.1.1. N- <i>o</i> -tolyl Lactamide (20).....	32
3.4.1.2. N- α -naphthyl Lactamide (21).....	33
3.4.1.3. N- <i>o</i> -fluorophenyl Lactamide (22).....	34
3.4.1.4. N- <i>o</i> -chlorophenyl Lactamide (23).....	34
3.4.1.5. N- <i>o</i> -bromophenyl Lactamide (24).....	35
3.4.1.6. N- <i>o</i> -iodophenyl Lactamide (25).....	35
3.4.1.7. N- <i>o</i> -tolyl- \square -hydroxyisobutyramide (26).....	36
3.4.1.8. N- \square -naphthyl- \square -hydroxyisobutyramide (27).....	36
3.4.1.9. N- <i>o</i> -fluorophenyl- \square -hydroxyisobutyramide (28).....	37
3.4.1.10. N- <i>o</i> -chlorophenyl- \square -hydroxyisobutyramide (29).....	38
3.4.1.11. N- <i>o</i> -bromophenyl- \square -hydroxyisobutyramide (30).....	38
3.4.1.12. N- <i>o</i> -iodophenyl- \square -hydroxyisobutyramide (31).....	39
3.4.2. General Procedure for the Formation of Carboxylic Acids.....	40
3.4.2.1. N-(<i>o</i> -tolyl)-carbamoxyloxy-lactic Acid (32).....	40
3.4.2.2. N-(\square -naphthyl)-carbamoxyloxy-lactic Acid (33).....	40
3.4.2.3. N-(<i>o</i> -fluorophenyl)-carbamoxyloxy-lactic Acid (34).....	41
3.4.2.4. N-(<i>o</i> -chlorophenyl)-carbamoxyloxy-lactic Acid (35).....	42
3.4.2.5. N-(<i>o</i> -bromophenyl)-carbamoxyloxy-lactic Acid (36).....	42
3.4.2.6. N-(<i>o</i> -tolyl)-carbamoxyloxy-isobutyric Acid (38).....	43

3.4.2.7. N-(\square -naphthyl)-carbamoyloxy-isobutyric Acid (39).....	44
3.4.2.8. N-(<i>o</i> -fluorophenyl)-carbamoyloxy-isobutyric Acid (40).....	44
3.4.2.9. N-(<i>o</i> -chlorophenyl)-carbamoyloxy-isobutyric Acid (41).....	45
3.4.2.10. N-(<i>o</i> -bromophenyl)-carbamoyloxy-isobutyric Acid (42).....	46
3.4.2.11. N-(<i>o</i> -iodophenyl)-carbamoyloxy-isobutyric Acid (43).....	46
3.5. The Reduction Reactions with Sodium Borohydride.....	47
3.5.1. General Procedure.....	47
3.5.1.1. 1-Hydroxypropan-2-yl- <i>o</i> -tolylcarbamate ((\pm) 44).....	47
3.5.1.2. 1-Hydroxypropan-2-yl- \square -naphthylcarbamate ((\pm) 45).....	48
3.5.1.3. 1-Hydroxypropan-2-yl- <i>o</i> -fluorophenylcarbamate ((\pm) 46).....	49
3.5.1.4. 1-Hydroxypropan-2-yl- <i>o</i> -chlorophenylcarbamate ((\pm) 47).....	50
3.5.1.5. 1-Hydroxypropan-2-yl- <i>o</i> -bromophenylcarbamate ((\pm) 48).....	50
3.5.1.6. 1-Hydroxypropan-2-yl- <i>o</i> -iodophenylcarbamate ((\pm) 49).....	51
3.5.1.7. 4-Hydroxy-5,5-dimethyl-3-(<i>o</i> -tolyl)-2-oxazolidinone (50).....	52
3.5.1.8. 4-Hydroxy-5,5-dimethyl-3-(\square -naphthyl)-2-oxazolidinone (51).....	52
3.5.1.9. 4-Hydroxy-5,5-dimethyl-3-(<i>o</i> -fluorophenyl)-2-oxazolidinone (52).....	53
3.5.1.10. 4-Hydroxy-5,5-dimethyl-3-(<i>o</i> -chlorophenyl)-2-oxazolidinone (53).....	54
3.5.1.11. 4-Hydroxy-5,5-dimethyl-3-(<i>o</i> -bromophenyl)-2-oxazolidinone (54).....	54
3.5.1.12. 4-Hydroxy-5,5-dimethyl-3-(<i>o</i> -iodophenyl)-2-oxazolidinone (55).....	55
3.6. Asymmetric Alkylation and Aldol Reactions.....	56
3.6.1. General Procedure.....	56
3.6.1.1. 5-Benzyl-5-methyl-3-(<i>o</i> -tolyl)-2,4-oxazolidinedione (56).....	56
3.6.1.2. 5-Benzyl-5-methyl-3-(<i>o</i> -iodophenyl)-2,4-oxazolidinedione (57).....	57
3.6.1.3. 5-Benzyl-5-methyl-3-(<i>o</i> -iodophenyl)-2-thioxo-4-oxazolidinone (59).....	57

3.6.1.4. 5-Allyl-5-methyl-3-(<i>o</i> -iodophenyl)-2-thioxo- 4-oxazolidinone (60).....	58
3.6.1.5. 5-(1-Hydroxybenzyl)-5-methyl-3-(<i>o</i> -iodophenyl)- 2,4-oxazolidinedione (61).....	59
3.6.1.6. 5-(1-Hydroxybenzyl)-5-methyl-3-(<i>o</i> -iodophenyl)-2-thioxo- 4-oxazolidinone (62).....	59
4. RESULTS AND DISCUSSION.....	61
4.1. Conformational Preferences in Diastereomeric (5 <i>S</i>)-Methyl-3-(<i>o</i> -aryl)-2, 4 oxazolidinediones.....	61
4.1.1. ¹ H NMR.....	61
4.1.2. The Thermal Interconversion Process of the Diastereomers of 3, 4 and 6 by NMR.....	69
4.1.3. Determination of Activation Barriers by Temperature Dependent NMR.....	70
4.1.4. The Thermal Interconversion of the Diastereomers of 4 by HPLC.....	72
4.1.5. Kinetic and Thermodynamic Constants of 4.....	74
4.2. Determination of Energy Barriers to Rotation and Absolute Conformations of Thermally Interconvertible 5,5-Dimethyl-3-(<i>o</i> -aryl)-2,4- oxazolidinedione Enantiomers.....	76
4.2.1. ¹ H and ¹³ C NMR.....	76
4.2.2. Barriers to Rotation.....	78
4.2.2.1. Temperature Dependent NMR.....	78
4.2.2.2. HPLC.....	79
4.2.2.3. ¹ H NMR in the Presence of Chiral Auxiliary.....	82
4.3. Determination of the Absolute Stereochemistry and the Activation Barriers of Thermally Interconvertible Oxazolidinone Heterocycles Bearing Naphthyl Substituent.....	89
4.3.1. ¹ H a4.3.1. ¹ H NMR and ¹³ C NMR.....	90
4.3.2. ¹ H NMR in the Presence of a Chiral Auxiliary.....	92
4.3.3. Determination of Absolute Stereochemistry.....	95
4.3.4. Activation Barriers to Hindered Rotation.....	104
4.4. Ring Opening and Asymmetric Reduction Reactions of 2,4-Oxazolidinedione Derivatives.....	108

4.4.1. Reaction with Ethanol.....	111
4.4.2. Reaction with KOH.....	111
4.4.3. Reaction with NaBH ₄	114
4.4.3.1. Stereoselective Reduction of the Compounds.....	118
4.4.4. Determination of Activation Barriers.....	125
4.5. Asymmetric Alkylation and Aldol Reactions.....	128
5. CONCLUSIONS.....	146
6. APPENDIX A: SPECTROSCOPY DATA.....	149
REFERENCES.....	211

LIST OF FIGURES

Figure 1.1. The structures of the stereoisomers of thalidomide.....	1
Figure 1.2. The structure of N-acyl oxazolidinone	2
Figure 1.3. Sterically hindered heterocyclic compounds studied	3
Figure 2.1. Stereoisomers of hindered biphenyl derivatives.....	5
Figure 2.2. Rotational isomers resulting from 180° rotation around the C-N single bond	6
Figure 2.3. Descriptors for the axially chiral 5-methyl-3-(<i>o</i> -aryl)-2,4-oxazolidinediones.....	7
Figure 2.4. The structure of (S)-2,2,2-trifluoro-1-(9-anthryl)ethanol ((S)-TFAE).....	8
Figure 2.5. Chelate-like conformations	9
Figure 2.6. The (R,R) and (R,S) two-point lactone interaction	10
Figure 2.7. Reaction of carbonyl compounds	13
Figure 2.8. The metal amide bases.....	14
Figure 2.9. Intra-annular chirality transfer	15
Figure 2.10. Extra-annular chirality transfer	16
Figure 2.11. Chelate-enforced intra-annular chirality transfer	17

Figure 2.12. Aldol reaction of preformed enolates. (a) irreversible enolate formation, (b) addition of the preformed enolate to aldehydes or ketones (c) protonation.....	18
Figure 2.13. Correlation between enolate geometry and aldol configuration	20
Figure 2.14. Zimmerman-Traxler transition state models in the aldol additions of (Z) and (E) enolates.....	21
Figure 2.15. The Gem-Dialkyl Effect.....	22
Figure 2.16. The Thorpe Ingold effect.....	23
Figure 2.17. The reactive rotamer theory.....	24
Figure 2.18. Facilitated Transition.....	25
Figure 2.19. Felkin-Anh model.....	26
Figure 3.1. The synthesis of (5S)-methyl-3-(<i>o</i> -aryl)-2,4-oxazolidinediones.....	27
Figure 3.2. The synthesis of 5,5-dimethyl-3-(<i>o</i> -aryl)-2,4-oxazolidinediones.....	30
Figure 3.3. The synthesis of (5S)-methyl-3-(<i>o</i> -aryl)-2-thioxo-4-oxazolidinones.....	31
Figure 4.1. Diastereomeric (5S)-methyl-3-(<i>o</i> -aryl)-2,4-oxazolidinediones.....	61
Figure 4.2. 400 MHz ¹ H NMR signals of C-5 hydrogen and methyl protons of diastereomers of compounds a) 3 , b) 4 , c) 5 , in CDCl ₃ at 30 °C, at equilibrium.....	62
Figure 4.3. The 2D NOESY spectrum of compound 1	65

- Figure 4.4. The 2D NOESY spectrum of compound **2**. The inset shows the partly enlarged spectrum where the correlation of C-8 proton at 7.53 ppm with the lower intensity C-5 methyl at 1.78 ppm is seen..... 66
- Figure 4.5. The HMQC spectrum of compound **2**..... 67
- Figure 4.6. The 2D NOESY spectrum of compound **3**. The inset shows the partly enlarged spectrum where the correlation of ortho proton at 6.33 ppm with the higher intensity C-5 methyl at 0.5 ppm is seen..... 68
- Figure 4.7. The partial ^1H NMR spectrum of the aromatic region of compound **3**
a) before equilibrium, b) at equilibrium, S= solvent= pyridine- d_5 69
- Figure 4.8. The temperature dependent NMR spectra of **6** in acetone- d_6 71
- Figure 4.9. HPLC chromatograms of compound **4** on chiralcel OD-H column..... 73
- Figure 4.10. The ring closure leading to the **S-M** conformation..... 74
- Figure 4.11. Enantiomeric 5,5-dimethyl-3-(*o*-aryl)-2,4-oxazolidinediones..... 76
- Figure 4.12. The plot of activation barriers vs. Van der Waals radii of the *o*-substituted halogens..... 79
- Figure 4.13. The flow-rate dependent plateaus observed for (\pm) **11** on OD-H column, (a), flow-rate= 0,3 ml/min, (b), flow-rate= 0,2 ml/min, (c), flow-rate= 0,1 ml/min. Eluent composition: 80:20, v/v, hexane ethanol..... 82

- Figure 4.14. The change in enantiomer composition versus time for compound (\pm) **11** after micropreparative enrichment of the first eluted enantiomer followed by HPLC at 293 K, Eluent: ethanol: hexane (9:1, v/v), flow rate: 0,3 ml/min, t_1 : 12,85 min, t_2 : 13,89, k_1 : 0.33 , k_2 : 0.44 , α : 1.33 , detection: UV at 240 nm. Inset: The plot of $\ln(([\text{M}]-[\text{M}]_{\text{eq}})/([\text{M}]_0-[\text{M}]_{\text{eq}}))$ versus time..... 82
- Figure 4.15. The proposed solvation model for (**M,S**) compounds (\pm)-**7-11** (R= CH₃, F, Cl, Br, I) and (S)-TFAE..... 84
- Figure 4.16. The NOESY spectrum of compound (\pm)-**11** taken in the presence of (S)-TFAE. The cross-peak between the phenyl and the anthryl rings is shown in circle..... 85
- Figure 4.17. The ¹H NMR signals in the presence of eight equivalents of (S)-TFAE in C₆D₆ for the 5,5-dimethyl protons of the enantiomers (\pm) **11**, (A) At 30 °C, (B) At 22 °C, enriched in **M** conformer..... 88
- Figure 4.18. The naphthyl substituted oxazolidinone derivatives..... 91
- Figure 4.19. The naphthyl substituted rhodanine and thiazolidine derivatives..... 92
- Figure 4.20. The ¹H NMR spectra of the compounds (\pm)-**15-17** taken in the presence of six equivalents of (S)-TFAE in toluene-d₈, A= (\pm)-**15**, B= (\pm)-**16**, C= (\pm)-**17**..... 93
- Figure 4.21. The ¹H NMR spectra of the compounds (\pm)-**18** and **19** taken in the presence of six equivalents of (S)-TFAE in toluene-d₈, A= (\pm)-**18**, B= (\pm)-**19**..... 94

- Figure 4.22. The temperature dependence of the ^1H NMR signals of the methyl groups on C-5 of the compound (\pm)-**15** upon cooling from 30 °C to -70 °C, S: Solvent..... 96
- Figure 4.23. The temperature dependence of the ^1H NMR signals of the methyl protons on C-5 of the compound (\pm)-**16** upon cooling from 30 °C to -70 °C, S: Solvent..... 97
- Figure 4.24. The temperature dependence of the ^1H NMR signals of the methylene protons on C-5 of the compound (\pm)-**17** upon cooling from 30 °C to -70 °C, S: Solvent..... 97
- Figure 4.25. The NOESY spectrum of compound (\pm)-**15** taken in the presence of (S)-TFAE. The cross-peaks between the naphthyl and the anthryl rings are shown in circle..... 99
- Figure 4.26. The proposed solvation models for the **M** and the **P** enantiomers of (\pm)-**1**..... 101
- Figure 4.27. The change in enantiomer composition versus time for compound (\pm) **16** after micropreparative enrichment of the first eluted enantiomer followed by HPLC at 293 K, detection: UV at 240 nm. .Inset: The plot of $\ln\left(\frac{[A]-[A]_{\text{eq}}}{[A]_0-[A]_{\text{eq}}}\right)$ versus time..... 106
- Figure 4.28. The change in enantiomer composition versus time for compound (\pm) **17** after micropreparative enrichment of the first eluted enantiomer followed by HPLC at 293 K, detection: UV at 240 nm. .Inset: The plot of $\ln\left(\frac{[A]-[A]_{\text{eq}}}{[A]_0-[A]_{\text{eq}}}\right)$ versus time..... 107
- Figure 4.29. The compounds studied..... 109
- Figure 4.30. Ring opening reactions..... 110

Figure 4.31. The reaction of the compounds studied with KOH and controlled acidification of aq. phase.....	113
Figure 4.32. Regeneration of the heterocyclic ring at pH 2 for compounds ((±)7-11, 15).....	114
Figure 4.33. Reductive ring opening reactions of compounds 1-6.....	115
Figure 4.34. The 400 MHz ¹ H NMR spectrum of compound (±)48 in CDCl ₃	116
Figure 4.35. The reaction of compounds (±)7-11, 15 with NaBH ₄ , (i) NaBH ₄ , THF-H ₂ O, room temperature.....	117
Figure 4.36. Selective approach of hydride to the compound (±)52 from the less hindered sites	119
Figure 4.37. Molecular models of compound (±)55 showing the spatial proximity of the selected groups in Å (Lp: lone pairs).....	120
Figure 4.38. The chromatograms taken to follow the thermal equilibration of the rotational isomers of (±)55.....	121
Figure 4.39. The stereoisomers of compound (±)7, A: upon cooling, B, solution was kept for several days at RT.....	122
Figure 4.40. The NOESY spectrum of compound (±)50 in CDCl ₃	123
Figure 4.41. The NOESY spectrum of compound (±)55 in CDCl ₃	124
Figure 4.42. Molecular models of compound (±)11 showing the spatial proximity of the selected groups in Å (Lp: lone pairs).....	125
Figure 4.43. Low temperature dynamic NMR study of compound 52.....	127

Figure 4.44. The models representing the S-M and S-P conformations of compound 52	128
Figure 4.45. Asymmetric alkylation reaction of compound 1 with benzyl bromide (BnBr). Figure represents that if reaction done by only S-M or S-P the major products would be R*-M and S*-P	130
Figure 4.46. Asymmetric alkylation reaction of compound 3 with benzyl bromide (BnBr).....	132
Figure 4.47. Isomer composition of compound 57 (a), during reaction, (b) after work-up.....	132
Figure 4.48. 400 MHz ¹ H NMR spectrum of compound 57	133
Figure 4.49. 400 MHz ¹ H NMR spectrum of compound 57 in the presence of chiral auxiliary (S)-TFAE.....	133
Figure 4.50. HPLC chromatogram of compound 58 showing the presence of four isomers. Column:OD-H, eluent: 70:30 (Hexane:ethanol), λ: 254 nm, Flow: 0.4 ml/min.....	134
Figure 4.51. Alkylation reaction of compound 58 with BnBr.....	135
Figure 4.52. Alkylation reaction of compound 58 with BnBr. The composition of compound 59 was obtained during reaction after one and a half hour at -78 °C.....	136
Figure 4.53. Reaction of compound 58 with allyl bromide (Product 60) (a) after half an hour, (b) after purification.....	137
Figure 4.54. Reaction of 58 with allyl bromide and formation of stereoisomers	

of compound 60	138
Figure 4.55. 400 MHz ^1H NMR spectrum of compound 60 in CDCl_3	139
Figure 4.56. Aldol reaction of compound 3 after completion of reaction.....	140
Figure 4.57. The formation of R*-M of compound 61 through M enolate.....	140
Figure 4.58. 400 MHz ^1H NMR spectrum of compound 61 in CDCl_3	141
Figure 4.59. Aldol reaction of 58 with benzaldehyde.....	142
Figure 4.60. Aldol reaction of compound 58 (a),after completion of reaction, (b), after purification.....	143
Figure 4.61. Asymmetric aldol reaction.....	144
Figure 4.62. Asymmetric aldol reaction of 58 collected semipreparatively.....	145
Figure A.1. 400 MHz ^1H NMR spectrum of compound 2 in CDCl_3	150
Figure A.2. 400 MHz ^1H NMR spectrum of compound 3 in CDCl_3	151
Figure A.3. 400 MHz ^1H NMR spectrum of compound 11 in C_6D_6	152
Figure A.4. 400 MHz ^1H NMR spectrum of compound 15 in C_6D_6	153
Figure A.5 400 MHz ^1H NMR spectrum of compound 16 in toluene- d_8	154
Figure A.6. 400 MHz ^1H NMR spectrum of compound 17 in CDCl_3	155
Figure A.7. 400 MHz ^1H NMR spectrum of compound 20 in CDCl_3	156

Figure A.8. 400 MHz ^1H NMR spectrum of compound 21 in DMSO.....	157
Figure A.9. 400 MHz ^1H NMR spectrum of compound 22 in CDCl_3	158
Figure A.10. 400 MHz ^1H NMR spectrum of compound 23 in CDCl_3	159
Figure A.11. 400 MHz ^1H NMR spectrum of compound 24 in DMSO.....	160
Figure A.12. 400 MHz ^1H NMR spectrum of compound 26 in toluene- d_8	161
Figure A.13. 400 MHz ^1H NMR spectrum of compound 27 in CDCl_3	162
Figure A.14. 400 MHz ^1H NMR spectrum of compound 28 in toluene- d_8	163
Figure A.15. 400 MHz ^1H NMR spectrum of compound 29 in CDCl_3	164
Figure A.16. 400 MHz ^1H NMR spectrum of compound 30 in toluene- d_8	165
Figure A.17. 400 MHz ^1H NMR spectrum of compound 31 in CDCl_3	166
Figure A.18. 400 MHz ^1H NMR spectrum of compound 32 in CDCl_3	167
Figure A.19. 400 MHz ^1H NMR spectrum of compound 33 in DMSO.....	168
Figure A.20. 400 MHz ^1H NMR spectrum of compound 34 in DMSO.....	169
Figure A.21. 400 MHz ^1H NMR spectrum of compound 35 in DMSO.....	170
Figure A.22. 400 MHz ^1H NMR spectrum of compound 36 in CDCl_3	171
Figure A.23. 400 MHz ^1H NMR spectrum of compound 38 in DMSO.....	172
Figure A.24. 400 MHz ^1H NMR spectrum of compound 39 in CDCl_3	173

Figure A.25. 400 MHz ^1H NMR spectrum of compound 40 in DMSO.....	174
Figure A.26. 400 MHz ^1H NMR spectrum of compound 41 in CDCl_3	175
Figure A.27. 400 MHz ^1H NMR spectrum of compound 42 in DMSO.....	176
Figure A.28. 400 MHz ^1H NMR spectrum of compound 44 in CDCl_3	177
Figure A.29. 400 MHz ^1H NMR spectrum of compound 45 in DMSO.....	178
Figure A.30. 400 MHz ^1H NMR spectrum of compound 46 in CDCl_3	179
Figure A.31. 400 MHz ^1H NMR spectrum of compound 47 in CDCl_3	180
Figure A.32. 400 MHz ^1H NMR spectrum of compound 48 in CDCl_3	181
Figure A.33. 400 MHz ^1H NMR spectrum of compound 49 in CDCl_3	182
Figure A.34. 400 MHz ^1H NMR spectrum of compound 50 in CDCl_3	183
Figure A.35. 400 MHz ^1H NMR spectrum of compound 51 in CDCl_3	184
Figure A.36. 400 MHz ^1H NMR spectrum of compound 52 in toluene- d_8	185
Figure A.37. 400 MHz ^1H NMR spectrum of compound 53 in CDCl_3	186
Figure A.38. 400 MHz ^1H NMR spectrum of compound 54 in CDCl_3	187
Figure A.39. 400 MHz ^1H NMR spectrum of compound 55 in CDCl_3	188
Figure A.40. 400 MHz ^1H NMR spectrum of compound 56 in CDCl_3	189
Figure A.41. 400 MHz ^1H NMR spectrum of compound 57 in CDCl_3	190

Figure A.42. 400 MHz ^1H NMR spectrum of compound 58 in CDCl_3	191
Figure A.43. 400 MHz ^1H NMR spectrum of compound 59 in CDCl_3	192
Figure A.44. 400 MHz ^1H NMR spectrum of compound 60 in CDCl_3	193
Figure A.45. 400 MHz ^1H NMR spectrum of compound 61 in CDCl_3	194
Figure A.46. 400 MHz ^1H NMR spectrum of compound 62 in CDCl_3	195
Figure A.47. 100 MHz ^{13}C NMR spectrum of compound 3 in CDCl_3	196
Figure A.48. 100 MHz ^{13}C NMR spectrum of compound 20 in CDCl_3 . S: Solvent....	197
Figure A.49. 100 MHz ^{13}C NMR spectrum of compound 26 in CDCl_3 . S: Solvent....	198
Figure A.50. 100 MHz ^{13}C NMR spectrum of compound 30 in CDCl_3 . S: Solvent....	199
Figure A.51. 100 MHz ^{13}C NMR spectrum of compound 33 in CDCl_3 . S: Solvent....	200
Figure A.52. 100 MHz ^{13}C NMR spectrum of compound 35 in CDCl_3 . S: Solvent....	201
Figure A.53. 100 MHz ^{13}C NMR spectrum of compound 42 in CDCl_3 . S: Solvent....	202
Figure A.54. 100 MHz ^{13}C NMR spectrum of compound (\pm) 46 in CDCl_3	203
Figure A.55. 100 MHz ^{13}C NMR spectrum of compound 50 in CDCl_3	204
Figure A.56. 100 MHz ^{13}C NMR spectrum of compound 55 in CDCl_3	205
Figure A.57. 100 MHz ^{13}C NMR spectrum of compound 56 in CDCl_3	206
Figure A.58. 100 MHz ^{13}C NMR spectrum of compound 57 in CDCl_3	207

Figure A.59. 100 MHz ^{13}C NMR spectrum of compound 59 in CDCl_3	208
Figure A.60. 100 MHz ^{13}C NMR spectrum of compound 60 in CDCl_3	209
Figure A.61. 100 MHz ^{13}C NMR spectrum of compound 61 in CDCl_3	210

LIST OF TABLES

Table 3.1. ¹ H NMR (400 MHz) data in CDCl ₃ (Figure A.1).....	28
Table 3.2. Elemental analysis data for compound 2.....	28
Table 3.3. NMR data of compound 3.....	28
Table 3.4. Elemental analysis data for compound 3	29
Table 3.5. NMR data of compound ±15.....	30
Table 3.6. Elemental analysis data for compound ±15.....	30
Table 3.7. NMR data of compound (±11).....	31
Table 3.8. Elemental analysis data for compound ±11.....	31
Table 3.9. ¹ H NMR (400 MHz) data of compound 58 in CDCl ₃ (Figure A.42).....	32
Table 3.10. NMR data of compound 20.....	33
Table 3.11. NMR data of compound 21.....	33
Table 3.12. NMR data of compound 22.....	34
Table 3.13. NMR data of compound 23.....	35
Table 3.14. NMR data of compound 24.....	35
Table 3.15. NMR data of compound 25.....	35

Table 3.16. NMR data of compound 26.....	36
Table 3.17. NMR data of compound 27.....	37
Table 3.18. NMR data of compound 28.....	37
Table 3.19. NMR data of compound 29.....	38
Table 3.20. NMR data of compound 30.....	39
Table 3.21. NMR data of compound 31.....	39
Table 3.22. NMR data of compound 32.....	40
Table 3.23. NMR data of compound 33.....	41
Table 3.24. NMR data of compound 34.....	41
Table 3.25. NMR data of compound 35.....	42
Table 3.26. NMR data of compound 36.....	43
Table 3.27. NMR data of compound 38.....	43
Table 3.28. NMR data of compound 39.....	44
Table 3.29. NMR data of compound 40.....	45
Table 3.30. NMR data of compound 41.....	45
Table 3.31. NMR data of compound 42.....	46
Table 3.32. Elemental analysis data for compound 42.....	46

Table 3.33. NMR data of compound 43.....	47
Table 3.34. NMR data of compound (\pm) 44.....	48
Table 3.35. NMR data of compound (\pm) 45.....	49
Table 3.36. NMR data of compound (\pm) 46.....	49
Table 3.37. NMR data of compound (\pm) 47.....	50
Table 3.38. NMR data of compound (\pm) 48.....	51
Table 3.39. NMR data of compound (\pm) 49.....	51
Table 3.40. NMR data of compound 50.....	52
Table 3.41. NMR data of compound 51.....	53
Table 3.42. NMR data of compound 52.....	53
Table 3.43. NMR data of compound 53.....	54
Table 3.44. NMR data of compound 54.....	55
Table 3.45. NMR data of compound 55.....	55
Table 3.46. NMR data of compound 56.....	56
Table 3.47. NMR data of compound 57.....	57
Table 3.48. NMR data of compound 59.....	58
Table 3.49. NMR data of compound 60.....	58

Table 3.50. NMR data of compound 61.....	59
Table 3.51. NMR data of compound 62.....	60
Table 4.1. The 400 MHz ¹ H NMR chemical shift values of the compounds in different solvents at 30 °C.....	63
Table 4.2. The kinetic data of the interconversion process (S-M \rightleftharpoons S-P) of compounds 3, 4 ,6.....	70
Table 4.3. The data for the determination of activation barriers.....	71
Table 4.4. Kinetic and thermodynamic constants of the internal rotation in compound 4.....	75
Table 4.5. ¹ H and ¹³ C NMR spectral data for the synthesized compounds in the presence and absence of the optically active auxiliary, (S)-TFAE at 30 °C...	77
Table 4.6 The kinetic and thermodynamic data for the interconversion process shown in Figure 4.11.....	81
Table 4.7. ¹ H NMR chemical shifts of N- <i>o</i> -tolyl substituted O, S, N containing five membered heterocyclic systems in the presence of (S)-TFAE. Ar= <i>o</i> -tolyl.....	87
Table 4.8. ¹ H and ¹³ C NMR spectral data for compounds (±)15-17 in the presence and absence of the optically active auxiliary, (S)-TFAE at 30 °C.....	91
Table 4.9. ¹ H and ¹³ C NMR spectral data for compounds (±)18-19 in the presence and absence of the optically active auxiliary, (S)-TFAE at 30 °C.....	92

Table 4.10. The kinetic and thermodynamic data for the interconversion process shown in Figure 4.18.....	105
Table 4.11. Chromatographic parameters for the separation of enantiomers by HPLC on Chiralpak AD-H at 7 ± 2 °C.....	105
Table 4.12. Chromatographic parameters for the separation of enantiomers by HPLC at 7 ± 2 °C.....	119

LIST OF SYMBOLS/ABBREVIATIONS

ΔG^\ddagger	Free energy of activation
ΔG°	Standard free energy change
h	Planck's constant
ΔH°	Standard enthalpy change
J	Coupling constant
K	Equilibrium constant
k'	Capacity factor
k_b	Boltzmann constant
k_c	Rate constant at coalescence temperature
k_f	Rate constant for the forward reaction
k_r	Rate constant for the reverse reaction
ΔS°	Standard entropy change
t	Retention time
α	Separation factor
δ	Chemical shift
$\Delta\nu$	The difference in hertz
APT	Attached proton technique
CA	Chiral auxiliary
HPLC	High pressure liquid chromatography
(S)-TFAE	(S)-(+)-1-(9-anthryl)-2,2,2-trifluoroethanol

1. INTRODUCTION

Heterocyclic compounds are very widely distributed in nature and are essential to life. They are key components of pharmaceuticals, agrochemicals, flavourings etc. They also have a wide variety of applications in synthetic organic chemistry, especially in asymmetric synthesis.

Nature's well-known ability to produce and convert chiral compounds with a remarkable stereospecificity has always been fascinating. The insight into enzyme structure and stereochemistry has brought about a recognition of the importance of the spatial arrangement in multipoint active site-substrate interaction. Similarly, the interaction between biologically active compounds and receptor proteins often shows a high or complete stereochemical specificity. Old examples of the different physiological behaviour are found in the taste and smell of optical stereoisomers.

Numerous drugs are synthetic racemic compounds and used as such. Although this has often been quite adequate, there may exist the possibility that one of the two enantiomers is undesirable. A tragic example is the drug of thalidomide (Figure 1.1) for which both enantiomers have the desired sedative effect but only the (-) enantiomer causes foetal deformities. Unfortunately the drug was used clinically as an equal mixture of the two enantiomers but even if the pure (+) enantiomer had been used problems would have arisen since the two interconvert under physiological conditions.

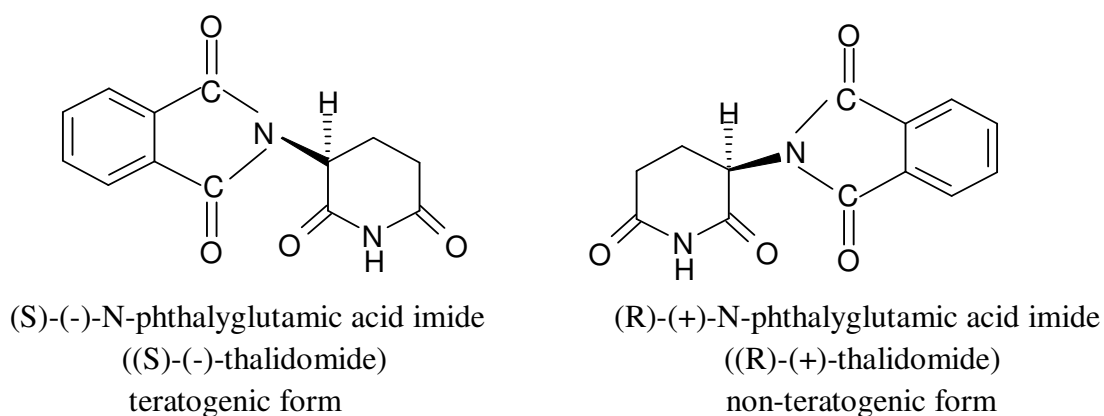


Figure 1.1. The structures of the stereoisomers of thalidomide

The resolution of racemates by chromatography has been an important technique for obtaining enantiomerically pure compounds. Asymmetric organic reactions in which an achiral unit in an ensemble of substrate molecules is converted to a chiral unit such that the possible stereoisomers are formed in unequal amounts are also very popular to synthesize new chiral compounds.

In the early 1980s, Evans *et al.* [1] and Masamune *et al.* used a series of chiral auxiliaries bearing oxazolidine ring in asymmetric reactions that led to high stereoselectivity. The chiral boron enolates generated from N-acyl oxazolidinones (Figure 1.2) (which were named Evans' auxiliaries) have proved to be among the most popular boron enolates due to the ease of their preparation, removal and recycling and to their excellent stereoselectivity.

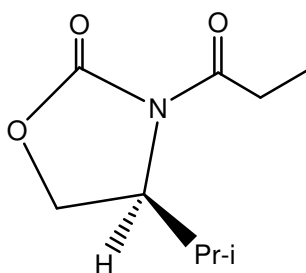


Figure 1.2. The structure of N-acyl oxazolidinone

Compounds bearing oxazolidine ring are of considerable interest due to their presence in a number of biologically active synthetic products, and their utility as directing group in asymmetric synthesis. 5,5-Dimethyl-2,4-oxazolidinedione ring is present in some antidiabetic drugs, and anticonvulsants.

In 1959, Shapiro *et al.* [2] synthesized a series of 2,4-oxazolidinone derivatives for the first time. They also examined the effect of the structural variation on anticonvulsant activity.

In 1963, Levy *et al.* tested some derivatives of 2,4-oxazolidinones for growth regulation. In 1990, Hirai *et al.* investigated herbicidal activities of some 2,4-oxazolidinones. All these researches received patents for their work.

In 1979, 60 MHz ^1H and ^{13}C NMR studies of some 3-aryl-2,4-oxazolidinediones were done by İçli, where the magnetic non-equivalence of diastereotopically and diastereomerically related protons and ^{13}C nuclei were investigated [3].

Introducing an *o*-substituted phenyl ring to the oxazolidine ring on nitrogen atom brings dissymmetry and makes these compounds axially chiral due to restricted rotation around $\text{C}_{\text{aryl}}\text{-N}_{\text{sp}^2}$ single bond (Figure 1.3). These heterocyclic analogues of biphenyls [4] are of interest in the study of conformational analysis, separation of atropisomers and activation barriers to hindered rotation.

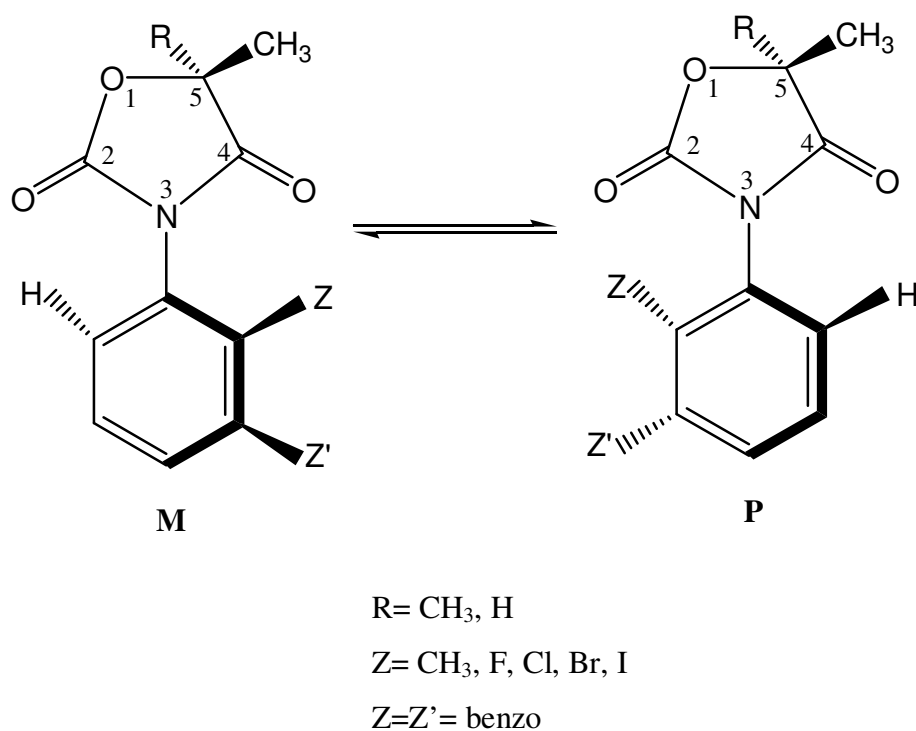


Figure 1.3. Sterically hindered heterocyclic compounds studied

The aims of the thesis are the followings:

- To investigate the conformational preferences of diastereomeric 5S-methyl-3-*o*-aryl-2,4-oxazolidinediones,
- To determine the activation barriers to hindered rotation for 5,5-dimethyl-3-*o*-aryl-2,4-oxazolidinediones,
- To determine absolute conformations of 5,5-dimethyl-3-*o*-aryl-2,4-oxazolidinediones,

- To study ring opening reactions of 2,4-oxazolidinediones,
- To carry out asymmetric alkylation reactions using lithium enolates of (5S)-methyl-3-(*o*-aryl)-2,4-oxazolidinediones and (5S)-methyl-3-(*o*-iodophenyl)-2-thioxo-4-oxazolidinone,
- To carry out asymmetric aldol reactions using lithium enolates of (5S)-methyl-3-(*o*-aryl)-2,4-oxazolidinediones and (5S)-methyl-3-(*o*-iodophenyl)-2-thioxo-4-oxazolidinone.

2. THEORY

2.1. Rotational Isomers and Stereochemistry of the N-(*o*-aryl) Substituted 2,4-Oxazolidinedione Ring

Isomers that may be interconverted by torsion around a single bond are referred to as rotational isomers or atropisomers. The atropisomerism arises due to hindered rotation about a C-C single bond. Atropisomerism is commonly encountered among the biphenyls (Figure 2.1). In these types of compounds, interconversion of stereoisomers is rendered difficult by the necessity of forcing bulky *ortho* substituents (in the example cited, X, X', Y, Y') passing one another in the transition state.

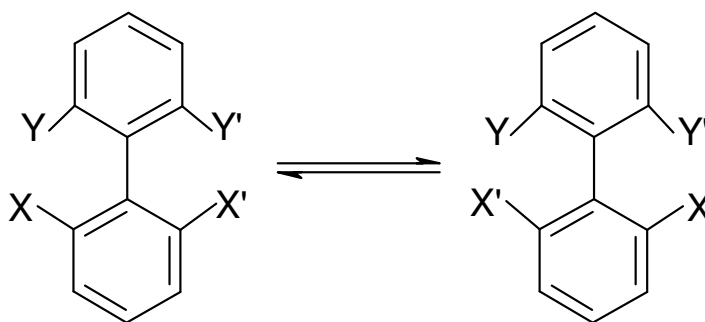


Figure 2.1. Stereoisomers of hindered biphenyl derivatives

The stereoisomerism in N-(*o*-aryl) substituted 2,4-oxazolidinedione derivatives that are analogous of biphenyls is caused by the restricted rotation around C-N single bond. The restricted rotation is due to the steric interference between the *ortho* substituents on the 3-aryl group and the carbonyl oxygen on the heterocyclic moiety (Figure 2.2). In these molecules, the substituents are too large to pass each other, resulting in configurational stability. Therefore the aryl group in the ground states of the molecules is expected to be orthogonal (or nearly orthogonal) to the heterocyclic ring. The transition state structures during the conversion of one rotamer to the other one are expected to be planar like either in T₁ or T₂ as shown in Figure 2.2.

The *ortho* aryl substitution (*Z*) brings dissymmetry to the molecule as well as causing the hindered rotation. Since the configurational difference is provided by restricted rotation around a single bond, they are called axially chiral compounds, the C-N single bond being the chiral axis. If $R=CH_3$, (A) and (B) are enantiomers of each other. If another asymmetric center exists in the molecule i.e. $R \neq CH_3$, then (A) and (B) are diastereomers of each other.

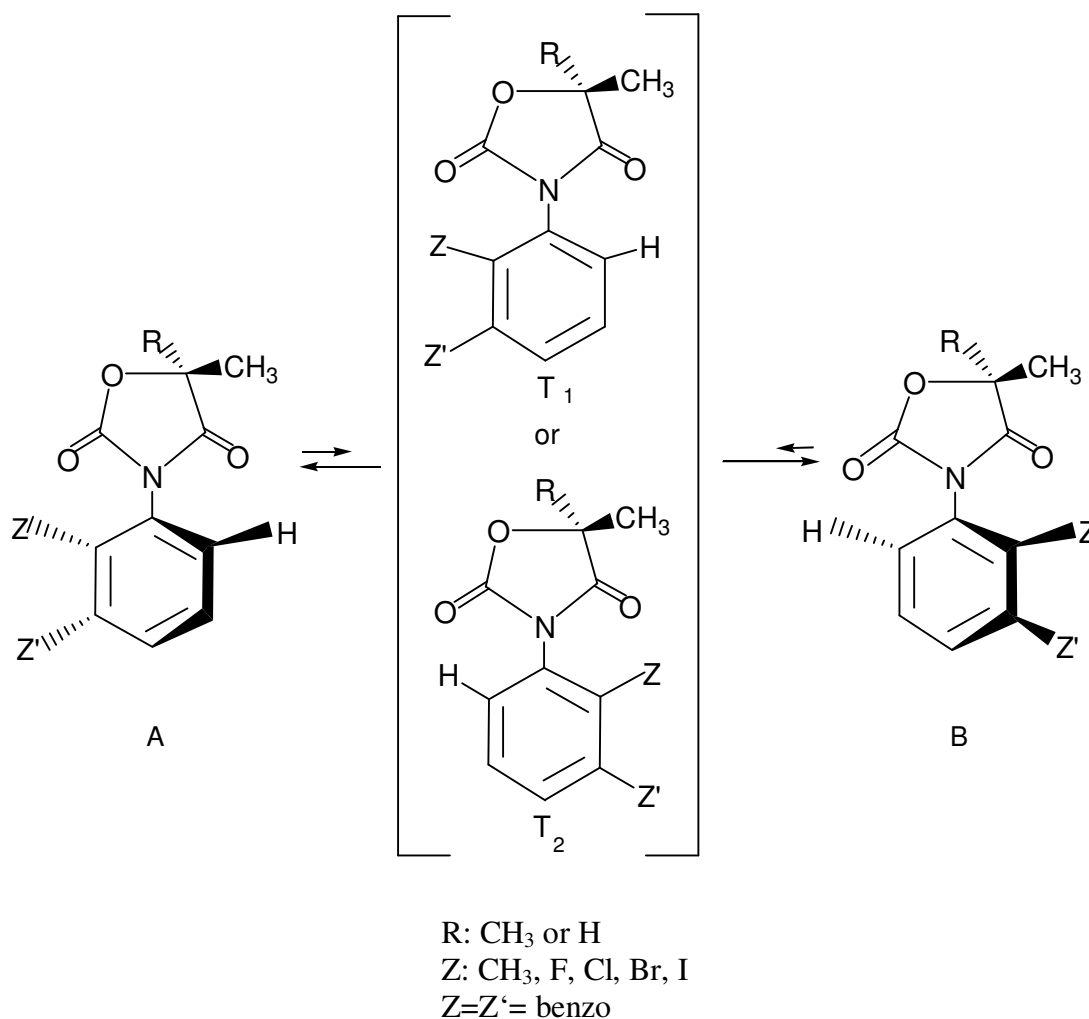


Figure 2.2. Rotational isomers resulting from 180° rotation around the C-N single bond

2.2. Nomenclature

The chirality of the axially chiral molecules is defined in terms of their helicities **M** and **P** in the Chan, Ingold, Prelog system [5]. In this system, first an axis is drawn through the single bond around which conformation is defined and the smallest torsion angle formed between the carbon atoms bearing the groups of the highest priority is used to

define the helix. Viewed along the axis, the nearer pair of groups receives the first two positions in the order of preference, and the farther groups take the third and fourth position. The nomination follows a set of rules similar to those applied in the central chiral system. A resulting clockwise rotation is denoted as “**P**” (plus) and the counter clockwise rotation is denoted as “**M**” (minus) (Figure 2.3).

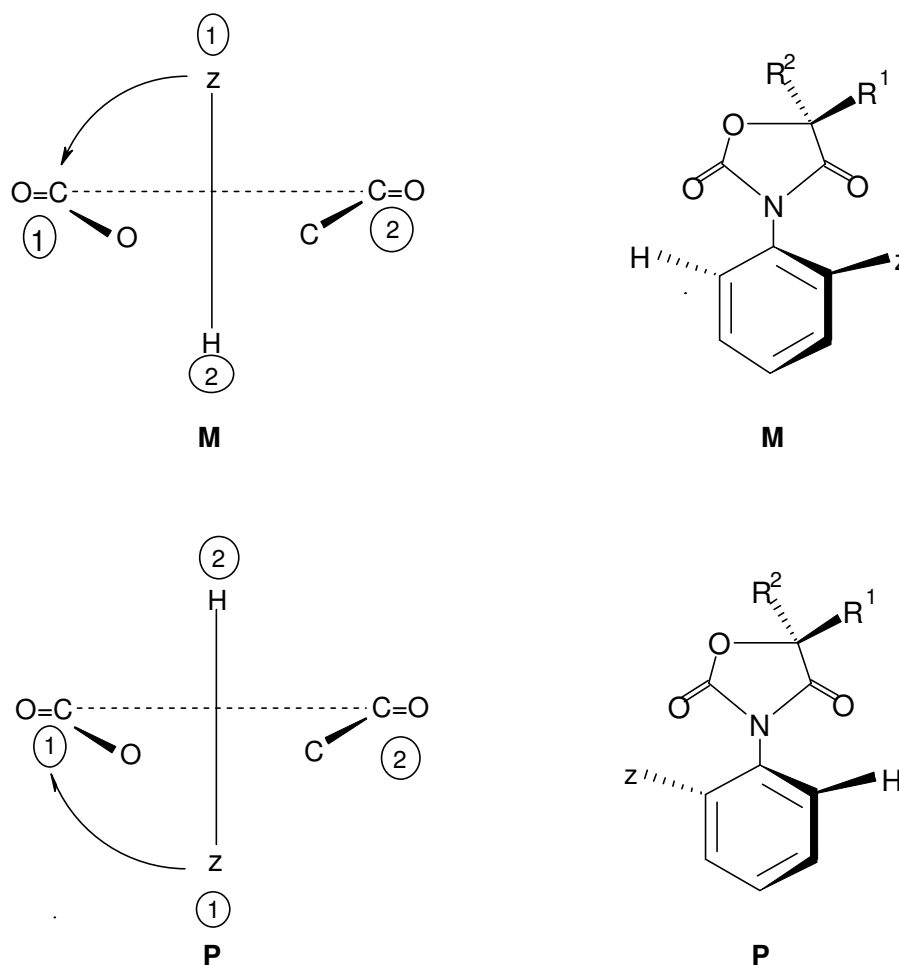


Figure 2.3. Descriptors for the axially chiral 5-methyl-3-(*o*-aryl)-2,4-oxazolidinediones

2.3. Determination of Absolute Conformation Using Chiral 2,2,2-Trifluoro-1-(9-anthryl)ethanol by Nuclear Magnetic Resonance

The absolute configuration /conformation of non-derivatizable centers are difficult to determine. Circular dichroism, chiral chromatographic methods and X-ray structural analysis have been employed for such a task, but a more readily usable technique such as

NMR analysis is preferable because the equipment is accessible and the experiments are rapid, inexpensive and can be performed with small quantities of material.

When a chiral solute dissolves in a chiral solvent then a stereochemical interaction must be involved. The expense of using a chiral material as a bulk solvent for NMR determination of enantiomeric purity is rarely justified. A chiral solvating agent is added in between 1 to 10 mole equivalents to a solution of the solute enantiomers in an achiral bulk solvent. Chiral solvating agents form diastereomeric solvation complexes with the substrate enantiomers *via* rapidly reversible equilibria in competition with the bulk solvent.

Chiral auxiliary or chiral solvating agent (CSA) (S)-2,2,2-trifluoro-1-(9-anthryl)ethanol (S)-(TFAE) (Figure 2.4) is known to render the NMR spectra of enantiomers nonequivalent for a number of solute types [6]. The observation of separate signals for each enantiomer allows the determination of enantiomeric purity without reference to an external standard of enantiomeric purity. This is done by measurement of the relative intensities of the two sets of signals.

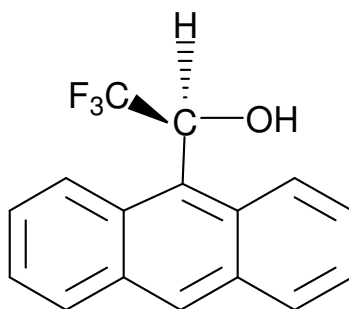


Figure 2.4. The structure of (S)-2,2,2-trifluoro-1-(9-anthryl)ethanol ((S)-TFAE)

The induced spectral nonequivalence arises from the formation of short-lived diastereomeric solvates that have non-identical spectra as a consequence of the population of rather specific conformations. Knowledge of the structures of these conformations and the absolute configuration of TFAE allows the assignment of absolute configuration to each of the solute enantiomers on the basis of the sense of nonequivalence induced by the chiral TFAE.

It is generally accepted that for induction of chemical shift non-equivalence each solvation complex must feature a minimum of three interactions. Two interactions are necessary to form a “chelate like” structure, the third interaction must be stereochemically dependent and is responsible for causing anisochronicity in solute substituents. Thus, the CSA and the solute must have complementary functionality if the necessary interactions are to occur. These can be hydrogen bonding, charge transfer (π -acid- π -base), dipole-dipole, and proton transfer.

In the short-lived diastereomeric solvates, the acidic carbinol function of TFAE interacts strongly with a hydrogen bond receptor in the enantiomeric solutes. The carbinyl hydrogen, also somewhat acidic because of the electronegative character of the perfluoroalkyl substituent, seeks interaction with a secondary basic site in the solutes (Carbinyl hydrogen bonding). The secondary site may be the π electrons of aromatic rings or multiple bonds, or the unshared electron pairs of heteroatoms.

In very general terms, solute enantiomers having appropriately situated basic sites B_1 and B_2 , will, by simultaneous interaction with the hydroxyl and carbinyl hydrogens of the chiral TFAE, assume chelate-like conformations depicted by **I** and **II** (Figure 2.5). Owing to the shielding effect of the anthryl substituent of chiral TFAE, the time-averaged chemical shifts of nuclei in R_1 will occur at higher field when R_1 is cis to the anthryl ring (as in **I**) than when it is trans (as in **II**). Thus, a sample enriched in the solute enantiomer of solvate **I** will show an upfield sense of nonequivalence for the R_1 resonance while resonance of R_2 in this sample will show an opposite (downfield) sense of nonequivalence.

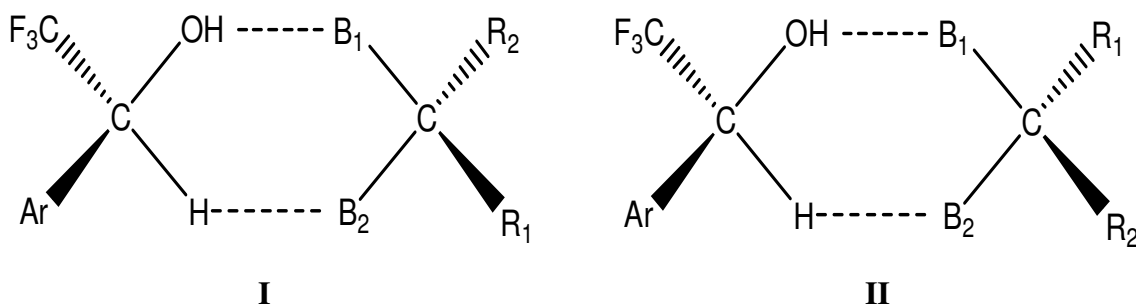


Figure 2.5 Chelate-like conformations

Many types of solute meet the requirement of this model. As an example, a two-point lactone model was proposed for lactones by Pirkle et al., 1977 [7] and is shown in Figure 2.6. In this model, the primary basic site (B_1) is the carbonyl oxygen and the secondary interaction is established between the ring oxygen (B_2) and the carbinyl hydrogen of (R)-TFAE.

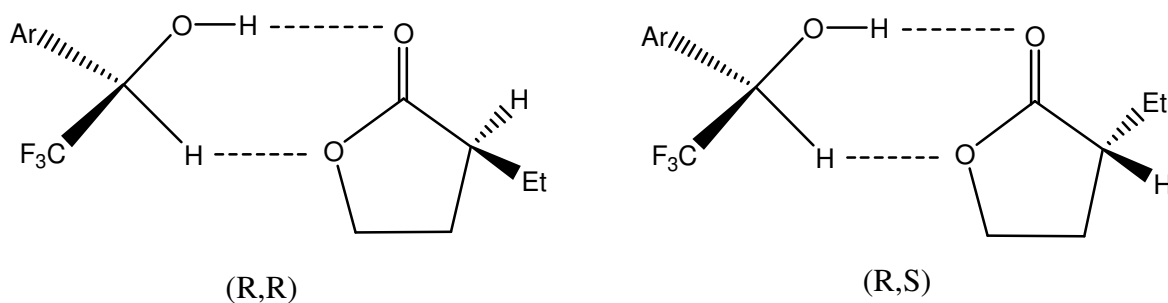


Figure 2.6. The (R,R) and (R,S) two-point lactone interaction

2.4. Asymmetric Synthesis

Asymmetric organic reactions have proved to be very valuable in the study of reaction mechanisms, in the determination of relative and absolute configuration and in the practical synthesis of optically active compounds. The pharmaceutical and the food industries have shown markedly increased interest in asymmetric organic reactions.

An asymmetric synthesis may be defined as a synthesis in which an achiral unit in an ensemble of substrate molecules is converted by a reactant to a chiral such that the possible stereoisomers are formed in unequal amounts. In an asymmetric reaction, substrate and reagent combine to form diastereomeric transition states. One of the species in the reaction medium (substrate, reagent or a catalyst) must have a chiral element to induce asymmetry at the reaction site. Most often, asymmetry is created upon conversion of trigonal carbons to tetrahedral ones at the site of the functionality.

In the simplest case an achiral substrate is converted to an unequal mixture of the two enantiomers of a chiral product containing only one stereogenic unit. The aim is obviously to achieve the highest possible proportion of the desired enantiomer: to maximise the enantioselectivity. The most commonly used measure of the degree of enantioselectivity

achieved is the enantiomeric excess (ee) (Equation 2.1). This is defined as the excess of one enantiomer over the other and is commonly expressed as a percentage:

$$ee = \left| \frac{[S] - [R]}{[S] + [R]} \right| \times 100 \quad (2.1)$$

where [R] and [S] are the composition of R and S enantiomers, respectively. If an asymmetric reaction leads to a pair of diastereomers the degree of diastereoselectivity is measured in diastereomeric excess (de) (Equation 2.2), which refers to the excess of one diastereomer over the other and is commonly expressed as a percentage:

$$de = \left| \frac{[S^*S] - [S^*R]}{[S^*S] + [S^*R]} \right| \times 100 \quad (2.2)$$

where [S*S] and [S*R] are the composition of the diastereomers, respectively.

2.4.1. Methods of Asymmetric Synthesis [8]

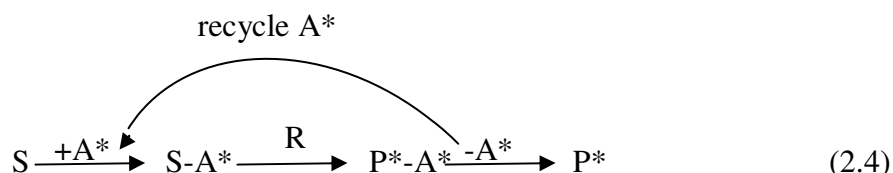
Methods of asymmetric synthesis can be divided into four major classes, depending on how this influence is exerted.

2.4.1.1. Substrate-Controlled Methods (First Generation Method). In this method, reaction is directed intramolecularly by a stereogenic unit (G*) already present in the chiral substrate (Equation 2.3). The formation of the newly formed stereogenic unit (P*) most often occurs by reaction with an achiral reagent at a diastereotopic site controlled by a nearby stereogenic unit. If we represent the part of the substrate which reacts as S, the chiral directing group as G, the reagent as R, the product as P-G and the chirality by *, the overall process becomes:



The main drawback of this procedure is the need for an enantiomerically pure starting material.

2.4.1.2. Auxiliary-Controlled Methods (Second Generation Method). This approach is similar to the first generation method in that asymmetric control is again achieved intramolecularly by a chiral group in the substrate (Equation 2.4). The difference is that the directing group, the chiral auxiliary is deliberately attached to an achiral substrate in order to direct the reaction and can be removed once it has served its purpose.



Although second generation methods have proved useful, the requirement for two extra steps, namely, the attachment and the removal of the chiral auxiliary, is a cumbersome feature.

2.4.1.3. Reagent-Controlled Methods (Third generation method). In this method, an achiral substrate is directly converted to the chiral product by the use of a chiral reagent (Equation 2.5):



In contrast to the first and second generation methods, the control is intermolecular. This is an attractive procedure but the range of reactions for which effective chiral reagents exist is somewhat limited at present.

2.4.1.4. Catalyst-Controlled Methods (Fourth generation method). In this method, conversion of an achiral substrate directly to a chiral product with an achiral reagent is achieved by the use of a chiral catalyst (Equation 2.6).



2.4.2. Asymmetric Alkylation and Aldol Condensation of Carbonyl Compounds

The carbonyl group in a ketone or an aldehyde is an extremely versatile vehicle for the introduction of functionality. Reaction can occur at the carbonyl carbon atom using the carbonyl group as an electrophile (Figure 2.7, (A)) or through enolate formation upon removal of an acidic proton at the adjacent carbon atom (Figure 2.7, (B) and (C)).

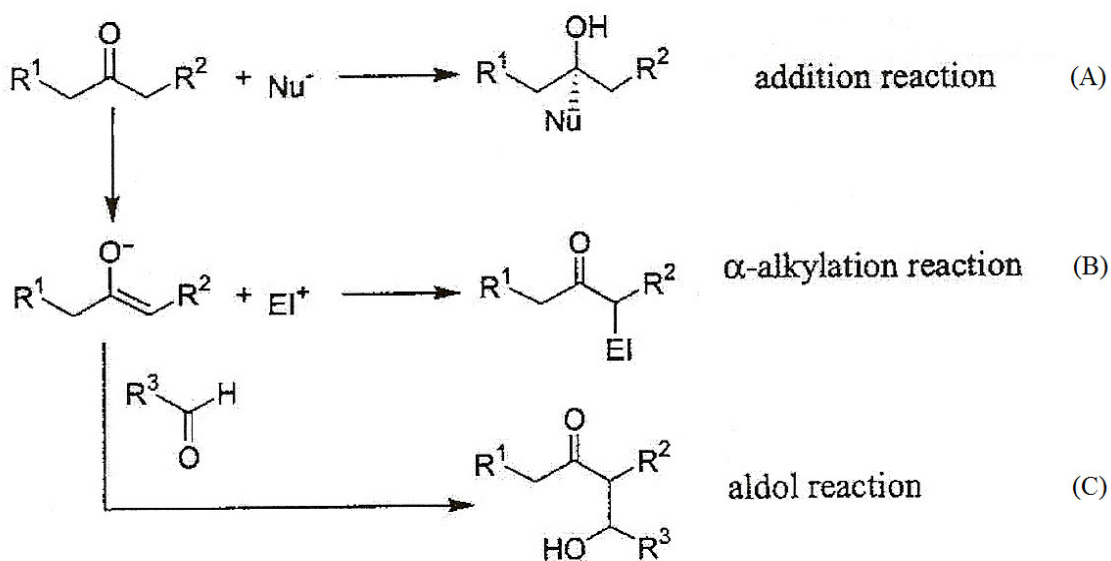


Figure 2.7. Reaction of carbonyl compounds

To generate an enolate from a carbonyl substrate, a suitable base should be chosen to meet two criteria:

1. Adequate basicity to ensure the selective deprotonation process for enolate generation
2. A sterically hindered structure so that nucleophilic attack of this base on the carbonyl centers can be prevented.

The metal amide bases had gained much popularity since the introduction of more hindered bases. The metal amide bases in Figure 2.8 (i-iii) has been a particularly important innovation in this field [8], and these reagents have now been accepted as the most suitable and commonly used bases for α -hydrogen deprotonation of carbonyl compounds. The metaldialkylamides are all quite soluble in ethereal solvent systems. Lithium

diisopropylamide (LDA,i) has been recognized as the most important strong base in organic chemistry. Both LDA (i) and lithium isopropylcyclohexyl amide (LICA,ii) exhibit similar high kinetic deprotonation selectivity. Lithium tetramethylpiperidine (LTMP, iii) is probably the most sterically hindered amide base at this time [8].

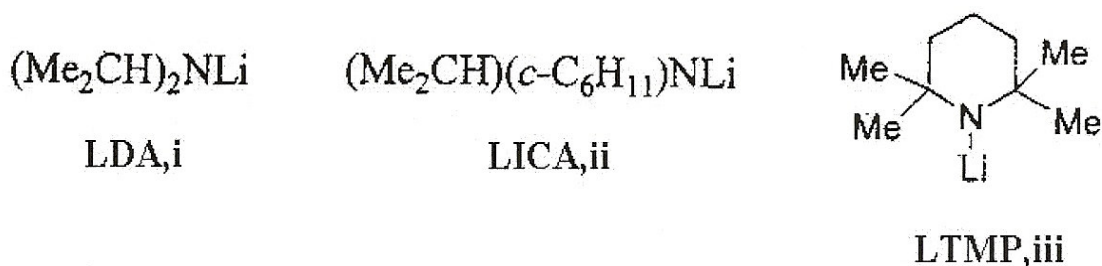


Figure 2.8. The metal amide bases

2.4.2.1. Asymmetric α -Alkylation Reactions. The asymmetric α -alkylation reactions of a carbonyl compound is one of the most commonly used chirality transfer reactions. The α -position of the carbonyl group can be transferred to the newly formed asymmetric carbon atom through this process.

α -Alkylation of a carbonyl compound can be achieved by formation of an enolate followed by condensation with an alkyl halide. In surveying chiral enolate systems as a class of nucleophile, three general subdivisions can be made in such asymmetric nucleophilic addition reactions: intra-annular, extra annular and chelation enforced intra-annular.

1. Intra-annular chirality transfer: In these cases the resident asymmetric center is interconnected via a cyclic array of covalent bonds containing the asymmetric center to the enolate framework. In such cases, the issue of enolate geometry is generally either fixed (Figure 2.9, (A)) or irrelevant to the sense of asymmetric induction (Figure 2.9, (B)). This statement should be qualified, however, for those cases in which the size of the cycle might be such that two possible enolates could be formed, as in the case illustrated by (Figure 2.9, (B) and (C)).

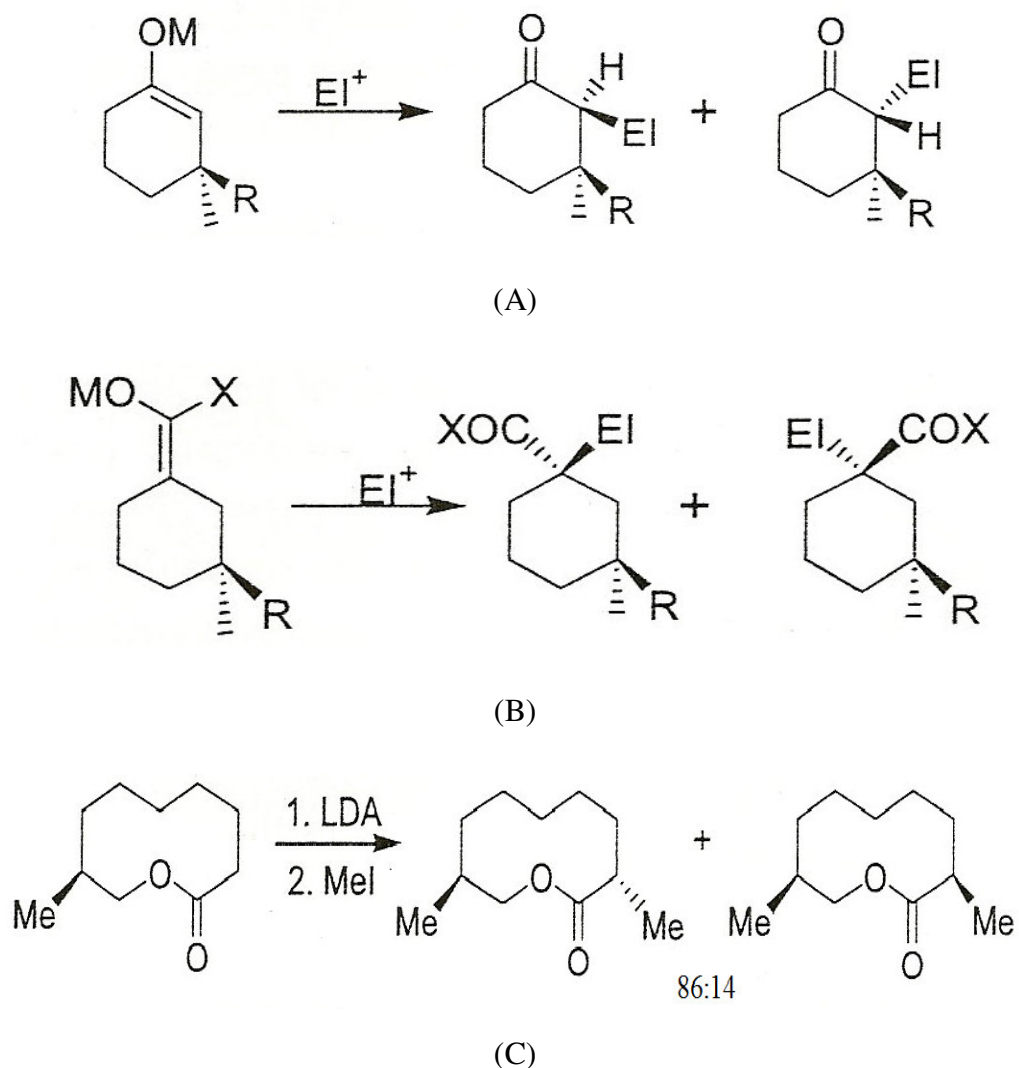


Figure 2.9. Intra-annular chirality transfer

2. Extra-annular chirality transfer: In the following examples (Figure 2.10, (A) and (B)), the resident chiral moiety (X_c) is not conformationally locked at two or more contact points via covalent bonds to the trigonal center undergoing substitution. As a consequence of such conformational ambiguity, it is frequently difficult to make predictions as to the diastereofacial bias imparted to the enolate system. Nonetheless, with an increased understanding of acyclic conformational analysis, a great level of predictability associated with acyclic diastereoselection is now possible.

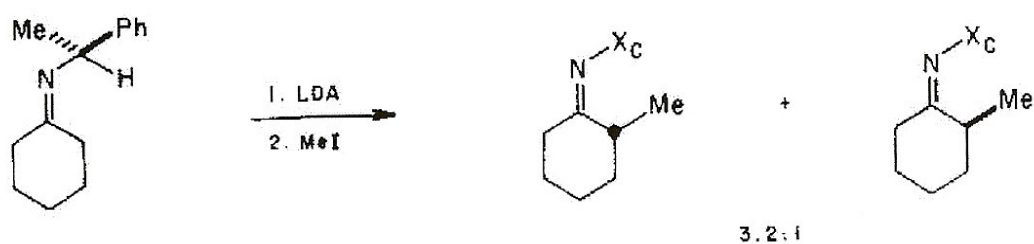
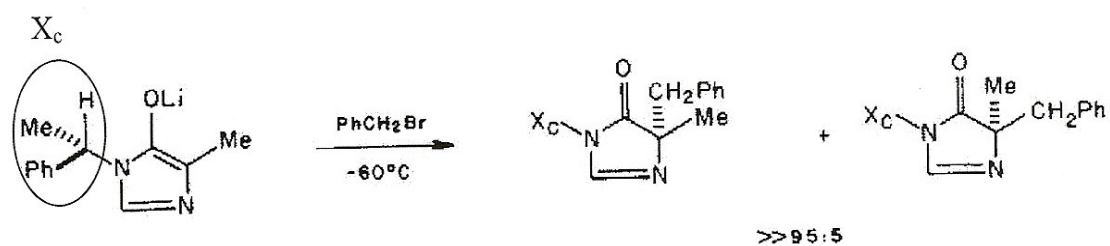


Figure 2.10. Extra-annular chirality transfer

3. Chelate-enforced intra-annular chirality transfer: One productive approach to the design of chiral enolate systems in which a structurally organized diastereofacial bias is established is illustrated in Figure 2.11, (A) and (B). In each case the presumed five- and six- membered lithium chelates provide an organizational role in fixing the orientation between the resident asymmetric center and the enolate system. Based on the preceding definitions, the postulated chelated enolates and their respective alkylation reactions constitute cases in which intra-annular chirality transfer is possible.

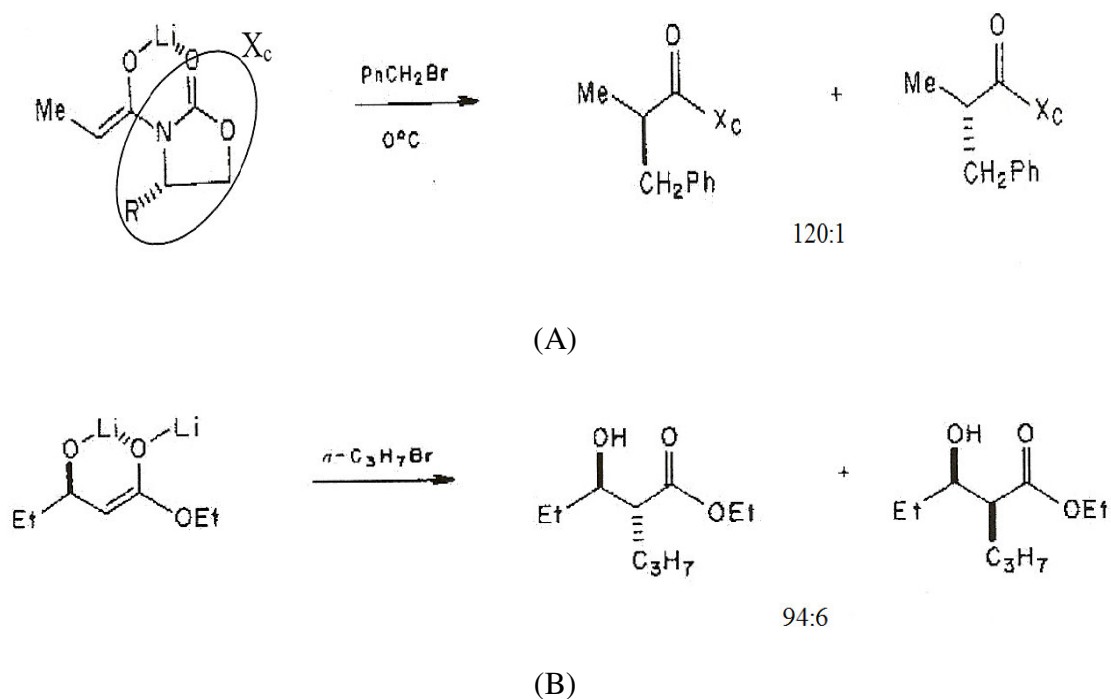


Figure 2.11. Chelate-enforced intra-annular chirality transfer

2.4.2.2. Asymmetric Aldol Reactions. In an aldol reaction, an enolizable carbonyl compound reacts with another carbonyl compound that is either an aldehyde or a ketone. The enolizable carbonyl compound, which must have at least one acidic proton in its α -position, act as a nucleophile, whereas the carbonyl active component has electrophilic reactivity. In its classical meaning the aldol reaction is restricted to aldehydes and ketones and can occur between identical or non-identical carbonyl compounds. The term “aldol reaction”, in a more advanced sense, is applied to any enolizable carbonyl compound, for example carboxylic esters, amides, carboxylates, that add to aldehydes or ketones. The traditional aldol reaction proceeds under thermodynamic control, as a reversible reaction, mediated either by acids or bases.

In contrast, modern aldol methods rely on the irreversible formation of “preformed enolates” which are added to aldehydes or ketones. In any case, the aldol reaction has proven itself by a plethora of applications to be one of the most reliable methods for carbon-carbon bond formation yielding either carbon chains, with oxygen functionality in 1,3 positions, or alkenes, by a carbonyl olefination process.

The chemistry of preformed enolates emerged in temporal and casual coherence with the “LDA area”. Although lithium and magnesium salts of diisopropylamine were first developed in the nineteen-fifties, lithium diisopropylamide (LDA) has been a widely used reagent since 1970 [8, 9], because of its behavior as a soluble, strong, and non-nucleophilic base.

Preformed enolates can be obtained not only from aldehydes and ketones, but also from carboxylic esters, amides and the acids themselves. The corresponding carbonyl compound always acts irreversibly as the CH-acidic component. Thus the term aldol reaction is no longer restricted to aldehydes and ketones but extended to all additions of preformed enolates to an aldehyde or a ketone. In contrast with the “traditional” aldol reaction, this novel approach is based on a three-step procedure (usually, however, performed as a one-pot reaction). First, the metal enolate (Figure 2.12, a) is generated irreversibly, with proton sources excluded, and, second, the compound serving as the carbonyl active, electrophilic component is added. The metal aldolate (Figure 2.12, b) thus formed is finally protonated, usually by addition of water or dilute acidic solutions, to give the aldol (Figure 2.12, c).

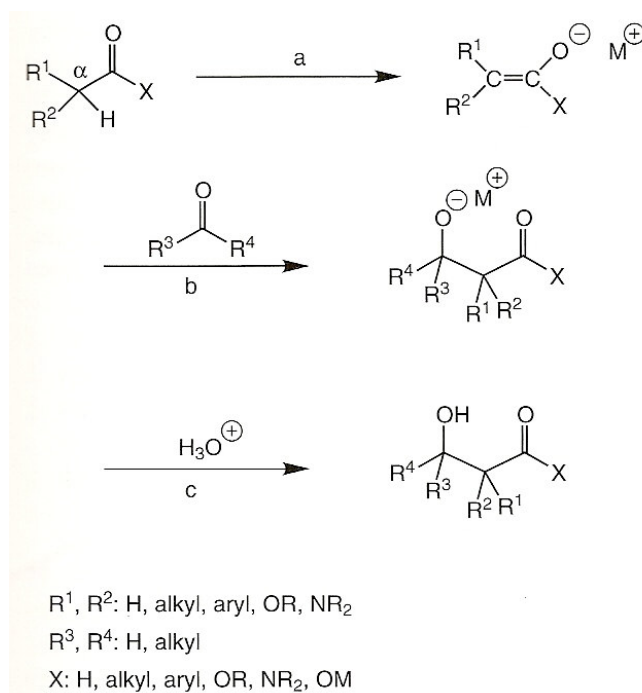


Figure 2.12. Aldol reaction of preformed enolates. (a) irreversible enolate formation; (b) addition of the preformed enolate to aldehydes or ketones; (c) protonation.

The principal aim in the development of the modern aldol was stereochemical control. In stereochemical terminology, the topic is discussed in the terms of “simple diastereoselectivity” and induced stereoselectivity”. Except for relatively rare examples when R^1 is identical with R^2 and R^3 is identical with R^4 , all aldol additions are stereogenic. If the carbonyl active compound is either an aldehyde (except formaldehyde- $R^4=H$) or a prochiral ketone ($R^3 \neq R^4$), addition of the enolate leads to formation of either one or two stereogenic centers. This depends on whether an enolate with identical α -substituents (mostly $R^1 = R^2$) or an enolate with different α -substituents is used. Under the latter conditions one of the substituents R^1 and R^2 is usually a hydrogen atom (Figure 2.12). In detail, induced stereoselectivity is postulated for the following combinations of reactants:

1. Reaction of chiral enolates with achiral or chiral aldehydes,
2. Reaction of achiral enolates with chiral aldehydes, and
3. Reaction of achiral enolates with achiral aldehydes, if they are mediated by use of a chiral catalyst, chiral ligands or all kinds of chiral solvents.

Most aldol additions of preformed enolates are run under kinetic control. In some such kinetically controlled aldol reactions simple diastereoselectivity is related to the configuration of the enolate. It was revealed that (*Z*)-configured enolates furnish mainly *syn*-aldols whereas *anti*-hydrocarbonyl compounds arise predominantly from (*E*)-enolates. Here, the descriptors E and Z refer to the relative position of the α -substituent R^2 and the oxygen metal bond (Figure 2.13).

The stereochemical outcome of the different aldol additions of preformed enolates calls for plausible transition state models. The most widely accepted transition state hypothesis for aldol additions is the Zimmerman-Traxler model [9]. This model offers a plausible explanation of the (*Z*)-*syn*, (*E*)-*anti* correlation, as shown in Figure 2.14. The diastereomeric transition states (A) and (B) in Figure 2.14, which emerge from addition of a (*Z*) enolate to an aldehyde, differ in the position of the substituent R^1 , which is equatorial in (A) and axial in (B). By analogy with conformational analysis of the cyclohexane system, the transition state (A) is expected to have a lower energy than the diastereomeric alternative (B). As a consequence the predominant formation of *syn* aldolates results from this kinetically controlled reaction.

When the (*E*) enolate is chosen as the starting material, the analogous argument indicates the transition state (C) with R^1 in an equatorial position to be favored compared with the alternative (D), in which the substituent R^1 occupies an axial position. Accordingly, the *anti* aldolate is expected to be the predominant product.

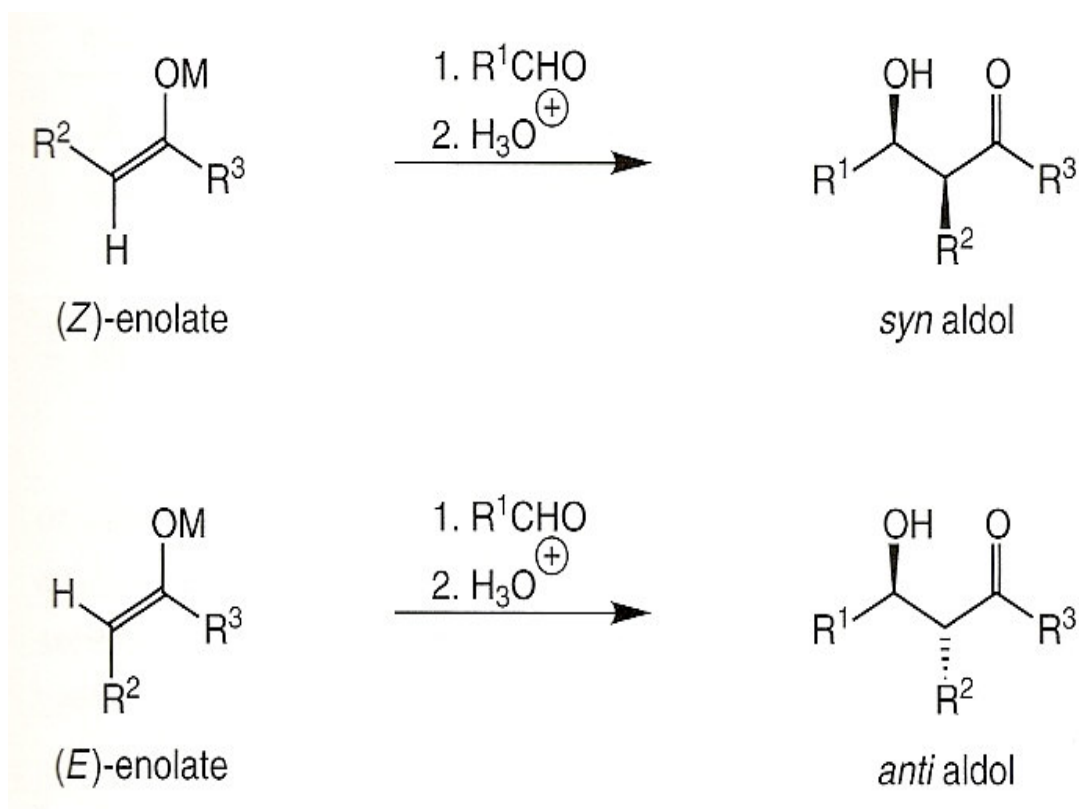


Figure 2.13. Correlation between enolate geometry and aldol configuration

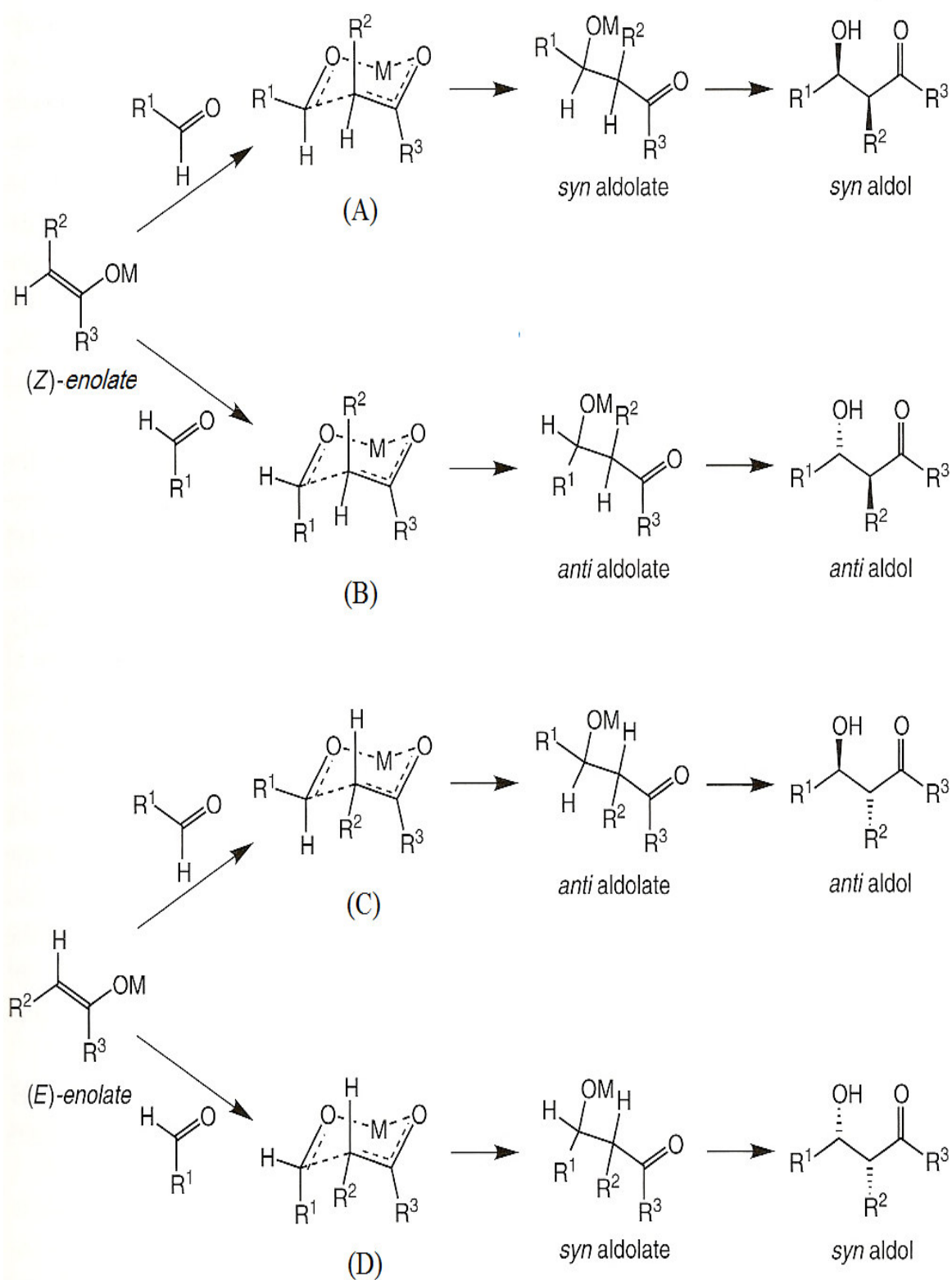


Figure 2.14. Zimmerman-Traxler transition state models in the aldol additions of (Z) and (E) enolates.

2.5. The Gem-Dialkyl Effect in Organic Transformations

Cyclization reactions are frequently critical components of natural product synthesis. Often, the nature of the target molecule requires the formation of thermodynamically disfavored seven, eight and nine-member rings as well as the formation of ring systems with a challenging steric environment about a macrocycle. To overcome these problems, chemists have taken advantage of an accelerated rate of cyclization resulting from a gem-dialkyl moiety located on the framework of the acyclic carbon backbone (Figure 2.15).

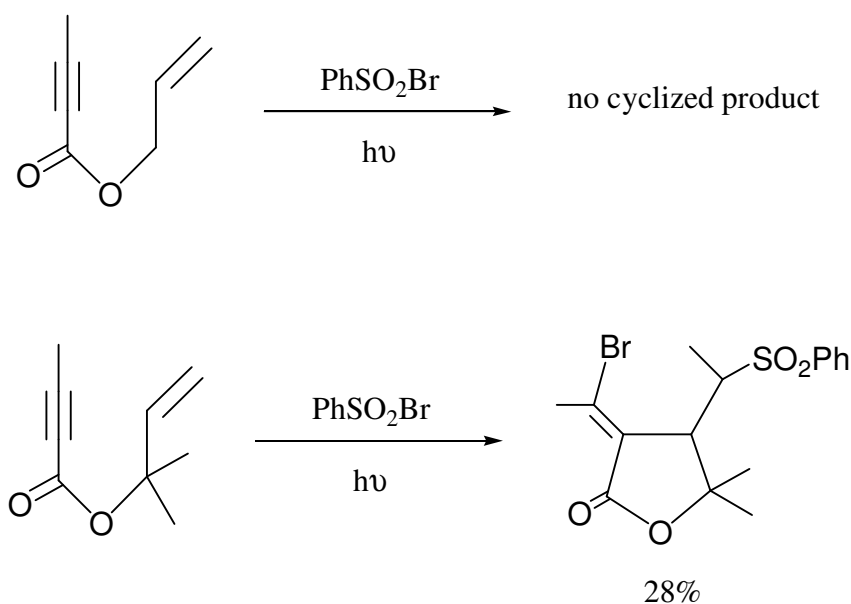


Figure 2.15. The Gem-Dialkyl Effect

This gem-dialkyl effect, first realized in 1916, has been used effectively to increase rates of reactions and allow cyclizations not possible when a dialkyl substituent is absent in the parent molecule. As well as facilitating slow reactions, the gem-dialkyl effect also generates products which possess quaternary carbon centers, as many classes of important natural products contain.

The gem-dialkyl effect was first observed and by Beesley, Ingold and Thorpe in the early 1900's when studying the cyclization of three, four, and five-membered substituted ring systems. Their postulation for an observed rate increase of cyclization when adding a gem-dialkyl functionality was attributed to the decrease in angle between the two reacting

termini (Figure 2.16). Their rationale, termed the Thorpe-Ingold effect, or angle compression explained that this compression resulted in a rate increase which was a direct result from positioning two reacting termini closer to one and other.

The broader term *gem*-dimethyl or *gem*-dialkyl effect was coined and the effect explained in terms of increased strain and a reduced entropy of rotation in the open-chain compound. Quantitatively the effect on the formation of normal rings varies considerably, and depends on the type of reaction as well as on the position of the substituent(s) in the chain. These variations can often be understood in terms of tightness or looseness of the transition state and of specific interactions in the transition state involving the substituent.

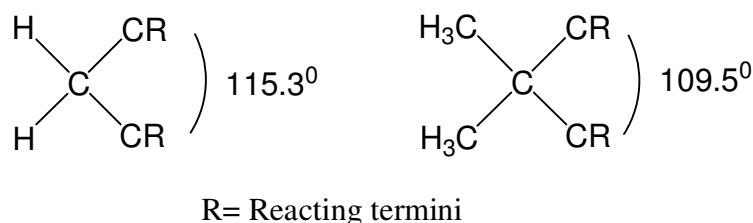


Figure 2.16. The Thorpe Ingold effect.

An alternative explanation for the *gem*-dialkyl effect was brought forth by Bruce and Pandit in 1960 and was recently advanced by Jung and co-workers. This hypothesis called the reactive rotamer effect, subscribes that there is a higher population of reactive *syn* rotamers due to alkyl substituents on the chain connecting the reaction centers, thus enabling the transformation. This can be demonstrated graphically via Newman projections of the cyclic precursors (Figure 2.17). In the case of the compound with no *gem*-dialkyl group (Figure 2.17, (a)), there is a steric bias for the two alkyl chains to be in the *anti* conformation with respect to one another by a factor of approximately 3 kcal/mol. This rotational barrier either slows or prevents cyclization as the favored conformation has the reacting centers spatially separated from one and other. However when R and R are two alkyl groups (Figure 2.17, (a)), the picture changes somewhat. Depending on the steric bulk of the R groups, the energetic difference between *anti* and *gauche* conformations can be equal or in some cases favors the *gauche* conformer, positioning the reacting substituents in proximity and thus enabling the cyclization reaction.

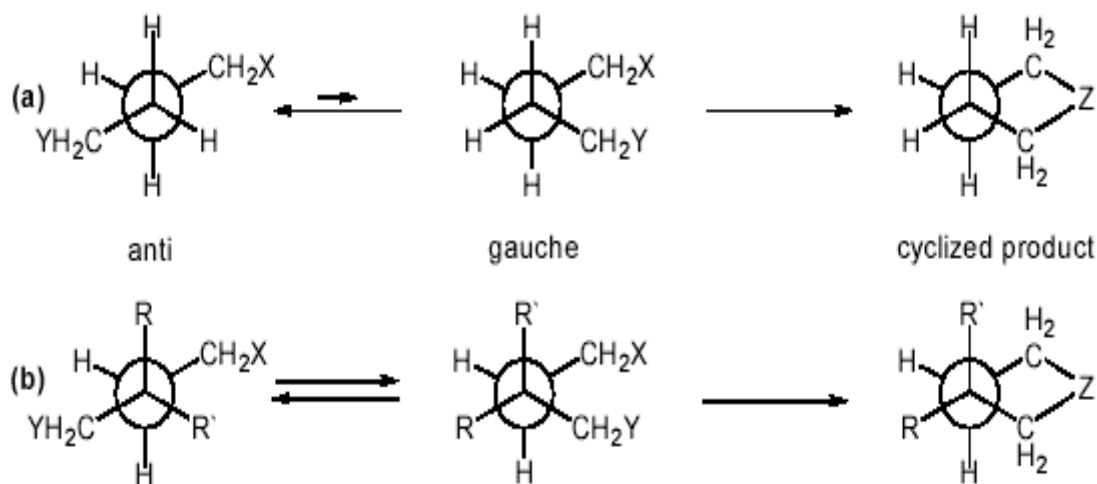


Figure 2.17. The reactive rotamer theory.

The most recent theory behind the gem-dialkyl effect proposes that the observed rate increase is a result of an overall decrease in the ΔH of the reaction. This facilitated transition hypothesis proposed by Dolata and co-workers is based largely on a variety of elegant computational experiments, and has been applied solely to systems where five member rings are formed. When the intramolecular Diels-Alder reaction and the lactonization reactions were studied using these computational methods, it was found that rate of the reaction corresponded linearly with the overall ΔH and that the various conformer populations of the starting materials did not play a significant role in the observed rate increase. This is rationalized additionally by examining the structure of the molecule in its ground state, and comparing it with its conformation in the transition-state. For instance, in the formation of five member rings, the transition-state conformation of the molecule is eclipsed (Figure 2.18). Any change in the structure of the molecule that results in the lowering of the barrier for rotation from a staggered resting-state to an eclipsed transition-state, will lead to an overall lowering of the ΔH . This, in turn, results in an overall decrease in the ΔG and thus the rate of product formation increases. Addition of alkyl groups to a carbon backbone, thereby lowering rotational barriers is not without precedent.

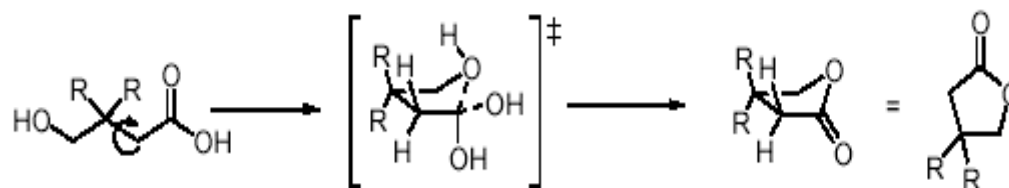


Figure 2.18. Facilitated Transition

2.6. Cram and Felkin-Anh Diastereoselectivity in Nucleophilic Addition to the Carbonyl Group [10]

Condensation of a nucleophile with a carbonyl compound, with concurrent carbon-carbon bond formation, has proven one of the most powerful reactions in organic synthesis, and many stereoselective condensations have been developed from this simple reaction. Thus, the need to control and predict the direction of attack for the nucleophilic species has spawned many models. The early rationalizations could be used in a predictive manner but suffered from errors due to the assumption of a perpendicular approach for the incoming nucleophile relative to the carbonyl plane. Calculations have shown that the trajectory of the nucleophile is at an angle, and closely relates to the model of Felkin. This model has become known as Felkin-Anh model.

The Felkin-Anh interpretation of the diastereoselectivity resulting from nucleophilic addition to the carbonyl group uses the model (A) shown in Figure 2.19 and makes the following assumptions: (a) the reactive conformation has the bonds to substituents L, M, S of disparate size (L= large, M= medium, S= small) staggered relative to the carbonyl group as in (A) (and (B)), with L located in the least sterically hindered site; (b) attack by the nucleophile takes place anti to the most bulky (L) or polar group. This does not take place perpendicular to the plane of the carbonyl group, but with an attack angle of about 109° . Formation of (C) via (A) is thus favored.

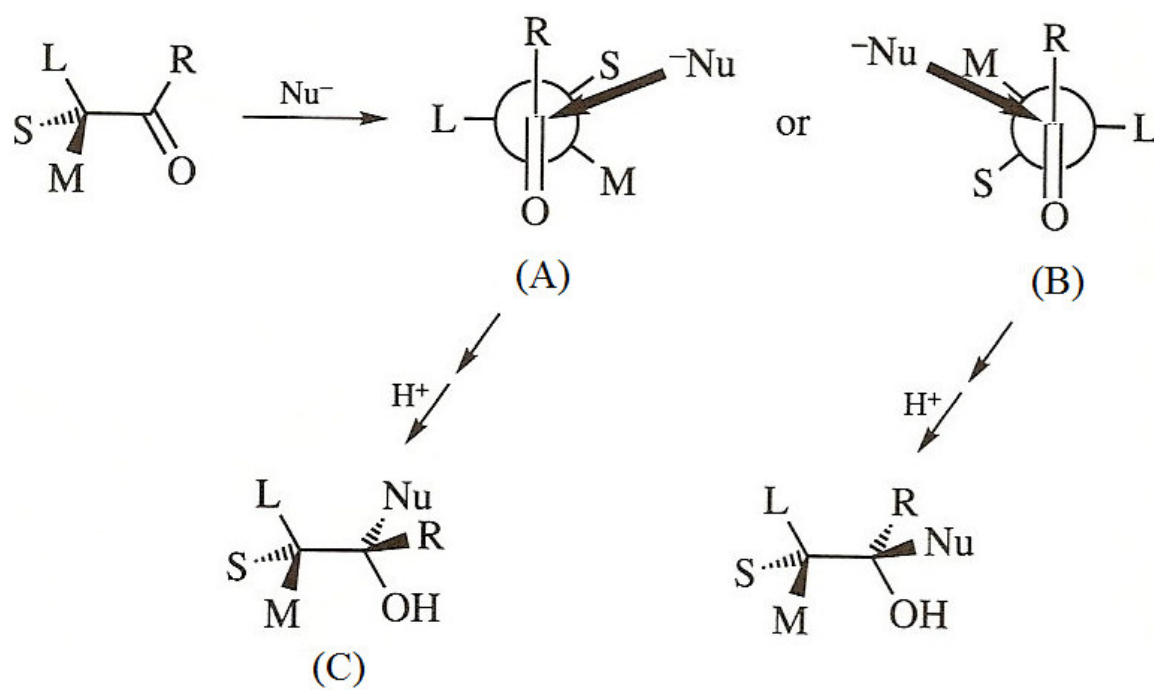


Figure 2.19. Felkin-Anh model

3. ORGANIC SYNTHESIS

3.1. The Synthesis of (5S)-methyl-3-(*o*-aryl)-2,4-oxazolidinediones

3.1.1. The General Procedure

The (5S)-methyl-3-(*o*-aryl)-2,4-oxazolidinediones were synthesized by the reaction of (S)-(-)-ethyl lactate and *o*-aryl isocyanates in the presence of sodium metal in toluene (Figure 3.1).

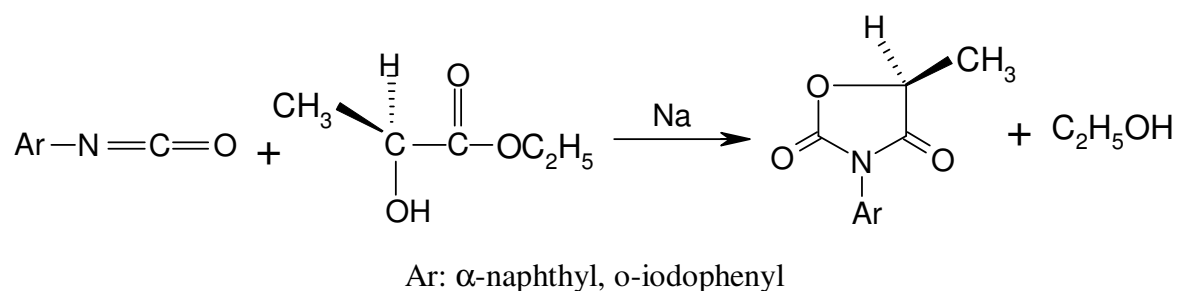


Figure 3.1. The synthesis of (5S)-methyl-3-(*o*-aryl)-2,4-oxazolidinediones

In a 100 ml three-necked flask, fitted with a thermometer and a reflux condenser, *o*-aryl isocyanate and S-(-)-ethyl lactate were mixed in toluene. Sodium metal was added prior to the heating in small pieces. After the addition of sodium, the mixture was heated for 10 hours at about 80 °C then the temperature was raised to 100-110 °C for one hour. At the end of this period, the reaction was stopped and the solvent was removed by evaporation in hood. (5S)-Methyl-3-(*o*-aryl)-2,4-oxazolidinediones were purified by recrystallization from ethanol.

3.1.1.1. (5S)-methyl-3-(α -naphthyl)-2,4-oxazolidinedione (2). The compound was prepared according to the general procedure using 0.012 mole α -naphthyl isocyanate, 0.012 mole S-(-)-ethyl lactate, 0.01 g sodium metal and 25 ml toluene. The white solid (1.51 g) was obtained with 52.5 per cent yield. Satisfactory ¹H NMR (Table 3.1), elemental analysis

(Table 3.2), melting point (130-132 °C) and FTIR (1752 cm⁻¹) data were used to confirm the purity and structure of compound **2**.

Table 3.1. ¹H NMR (400 MHz) data in CDCl₃ (Figure A.1).

	Chemical shifts (δ) in ppm
Methyl protons at C-5, (3H)	1.74 (d, J= 6.98 Hz), 1.81 (d, J= 6.98 Hz)
Methine proton at C-5, (1H)	5.1 (q, J= 6.98 Hz), 5.2 (q, J= 6.98 Hz)
Aromatic protons, (4H)	7.25-7.99 (m)

Table 3.2. Elemental analysis data for compound **2**

	Found, %	Calculated for C ₁₄ H ₁₁ O ₃ N, %
C	69.93	69.70
H	4.95	4.60
N	5.42	5.81

3.1.1.2. (5S)-methyl-3-(*o*-iodophenyl)-2,4-oxazolidinedione (**3**). The compound was prepared for the first time according to the general procedure using 0.018 mole *o*-iodophenyl isocyanate, 0.018 mole S-(-)-ethyl lactate, 0.0018 mole sodium metal and 15 ml toluene. The white solid (0.56 g) was obtained with 9.8 per cent yield. Satisfactory NMR (¹H and ¹³C) (Table 3.3), elemental analysis (Table 3.4), melting point (94.2-95.8 °C) and FTIR (1748 cm⁻¹) data were used to confirm the purity and structure of compound **3**.

Table 3.3. NMR data of compound **3**

	¹ H NMR Chemical shifts (δ) in ppm ^a	¹³ C NMR Chemical shifts (δ) in ppm ^b
C-5 methyls	1.74 (d, J= 7.02 Hz), (3H) 1.81 (d, J= 7.02 Hz), (3H)	17.2 and 16.8
C-5 Methines	5.06 (q, J= 7.02 Hz), (1H) 5.13 (q, J= 7.02 Hz), (1H)	77.10, 77.06
Aromatics	7.16-8.0 (m), (4H)	140.3, 133.8, 133.5, 131.9, 129.98, 129.90, 129.8, 129.7, 97.96
Carbonyls	-	171.9, 171.8, 153.1, 153.07
^a : ¹ H NMR (400 MHz) data in CDCl ₃ (Figure A.2)		
^b : ¹³ C NMR (100 MHz) data in CDCl ₃ (for two diastereomers) (Figure A. 47)		

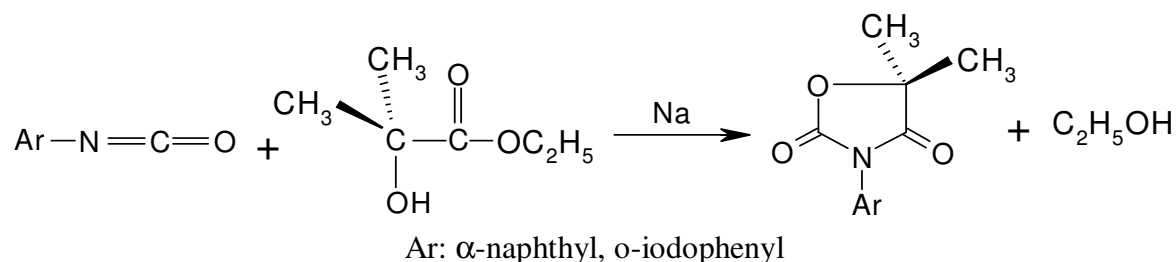
Table 3.4. Elemental analysis data for compound 3

	Found, %	Calculated for C ₁₀ H ₈ NO ₃ I, %
C	37.96	37.88
H	2.43	2.54
N	4.16	4.41

3.2. The Synthesis of 5,5-Dimethyl-3-(*o*-aryl)-2,4-oxazolidinediones

3.2.1. The General Procedure

The 5,5-dimethyl-3-(*o*-aryl)-2,4-oxazolidinediones were synthesized by the reaction of ethyl α -hydroxyisobutyrate and *o*-aryl isocyanates in the presence of sodium metal in toluene (Figure 3.2).

Figure 3.2. The synthesis of 5,5-dimethyl-3-(*o*-aryl)-2,4-oxazolidinediones

In a 100 ml three-necked flask, fitted with a thermometer and reflux condenser, *o*-aryl isocyanate and ethyl α -hydroxyisobutyrate were mixed in toluene. Sodium metal was added prior to heating in small pieces. After the addition of sodium, the mixture was heated for 10 hours at about 80 °C then the temperature was raised to 100-110 °C for one hour. At the end of this period, the reaction was stopped and the solvent was removed by evaporation in hood. The 5,5-dimethyl-3-(*o*-aryl)-2,4-oxazolidinediones were purified by recrystallization from ethanol.

3.2.1.1. 5,5-Dimethyl-3-(α -naphthyl)-2,4-oxazolidinedione (\pm 15). The compound was prepared according to the general procedure using 0.03 mole α -naphthyl isocyanate, 0.03 mole ethyl α -hydroxy isobutyrate, 0.003 mole sodium metal and 25 ml toluene. The white

solid (5.98 g) was obtained with 78 per cent yield. Satisfactory NMR (^1H and ^{13}C) (Table 3.5), elemental analysis (Table 3.6), melting point (142-143 $^{\circ}\text{C}$) data were used to confirm the purity and structure of compound **± 15** .

Table 3.5. NMR data of compound **± 15**

	^1H NMR Chemical shifts (δ) in ppm ^a	^{13}C NMR Chemical shifts (δ) in ppm ^b
Diastereotopic C-5 methyls	1.77 (s, 3H) 1.69 (s, 3H)	25 24
Aromatics	7.9-7.16 (m, 7H)	134-121
Carbonyls	-	176.6, 153.7
C-5		84
^a : ^1H NMR (400 MHz) data in CDCl_3 (Figure A.4)		
^b : ^{13}C NMR (100 MHz) data in CDCl_3		

Table 3.6. Elemental analysis data for compound **± 15**

	Found, %	Calculated for $\text{C}_{15}\text{H}_{13}\text{NO}_3$, %
C	69.96	70.59
H	4.81	5.09
N	5.22	5.49

3.2.1.2. 5,5-Dimethyl-3-(*o*-iodophenyl)-2,4-oxazolidinedione (**± 11**). The compound was prepared according to the general procedure using 1.59 g (6.5×10^{-3} mole) *o*-iodophenyl isocyanate, 0.86 g (6.5×10^{-3} mole) ethyl α -hydroxyisobutyrate, 0.015 g (6.5×10^{-4} mole) sodium metal and 15 ml xylene. The white solid (0.87 g) was obtained with 40.4 per cent yield. Satisfactory NMR (^1H and ^{13}C) (Table 3.7), elemental analysis (Table 3.8), melting point (118.2-119.2 $^{\circ}\text{C}$) and FTIR (3070, 2933, 2984, 1746 cm^{-1}) data were used to confirm the purity and structure of compound **± 11** .

Table 3.7. NMR data of compound (\pm 11)

	^1H NMR Chemical shifts (δ) in ppm ^a	^{13}C NMR Chemical shifts (δ) in ppm ^b
Diastereotopic C-5 methyls	1.2 (s, 3H) 1.4 (s, 3H)	21.8 22.4
Aromatics	6.4-7.4 (m, 4H)	127.7, 128.1, 129.5, 132.6, 138.2
Carbonyls	-	172.1, 150.3
C-5		82.4

^a: ^1H NMR (400 MHz) data in C_6D_6 (Figure A.3)
^b: ^{13}C NMR (100 MHz) data in C_6D_6 (for two diastereomers)

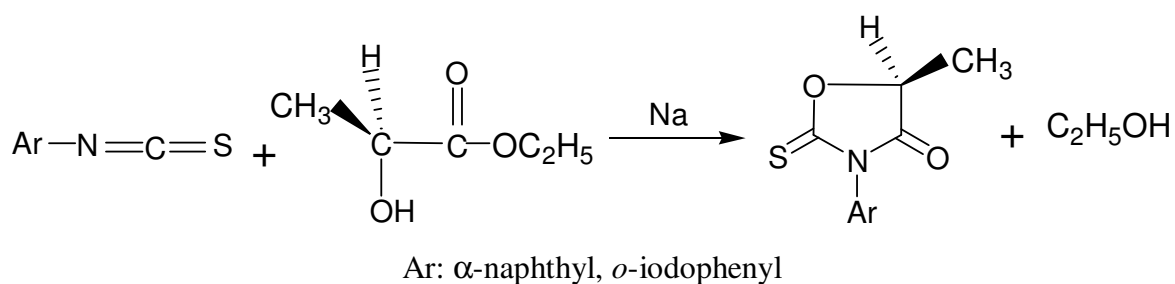
Table 3.8. Elemental analysis data for compound \pm 11

	Found, %	Calculated for $\text{C}_{11}\text{H}_{10}\text{O}_3\text{NBr}$, %
C	39.91	39.9
H	2.99	3.00
N	3.86	4.23

3.3. The Synthesis of (5S)-methyl-3-(*o*-aryl)-2-thioxo-4-oxazolidinones

3.3.1. The General Procedure

The (5S)-methyl-3-(*o*-aryl)-2-thioxo-4-oxazolidinones were synthesized by the reaction of (S)-(-)-ethyl lactate and *o*-aryl isothiocyanates in the presence of sodium metal in xylene (Figure 3.3).

Figure 3.3. The synthesis of (5S)-methyl-3-(*o*-aryl)-2-thioxo-4-oxazolidinones

In a 100 ml round-bottom flask, fitted with a reflux condenser, *o*-aryl isothiocyanate and S-(-)-ethyl lactate were mixed in xylene. Sodium metal was added prior to the heating in small pieces. After the addition of sodium, the mixture was refluxed for 11 hours. At the end of this period, the reaction was stopped and the solvent was removed by evaporation in hood. (5S)-Methyl-3-(*o*-aryl)-2-thioxo-4-oxazolidinones were purified by recrystallization from ethanol.

3.3.1.1. (5S)-methyl-3-(*o*-iodophenyl)-2-thioxo-4-oxazolidinone (58). The compound was prepared according to the general procedure using 0.01 mole *o*-iodophenyl thioisocyanate, 0.01 mole ethyl α -hydroxy isobutyrate, 0.001 mole sodium metal and 15 ml xylene. The white solid (1.98 g) was obtained with 62.1 per cent yield. Satisfactory ^1H NMR (Table 3.9) data were used to confirm the purity and structure of compound **58**.

Table 3.9. ^1H NMR (400 MHz) data of compound **58** in CDCl_3 (Figure A.42)

	^1H NMR Chemical shifts (δ) in ppm ^a
C-5 methyls	1.71 (d, 3H), 1.77 (d, 3H)
C-5 methines	5.14 (q, 1H), 5.08 (q, 1H)
Aromatics	7.14-7.92 (m, 4H)

3.4. The Ring Opening Reactions with Potassium Hydroxide [11]

3.4.1. General Procedure for the Formation of Amides

To the solution of the compounds in THF (0.5 M) at 0 $^{\circ}\text{C}$ was added 2 M, KOH solution prepared in distilled water. Reaction was followed by TLC. After completion, the reaction mixture was extracted three times by ethyl acetate. After evaporation of ethyl acetate, the products were obtained as oil or white solid and purified by ethyl acetate: hexane.

3.4.1.1. N-*o*-tolyl Lactamide (20). The compound was prepared according to the general procedure using 1 g (4.87 mmole) compound **1** in 9.75 ml THF (0.5 M), 1.09 g (19.5 mmole) potassium hydroxide in 9.75 ml water (2 M). After extraction with ethyl acetate,

the product was obtained as a colorless oil (0.044 g). Satisfactory NMR (^1H and ^{13}C) (Table 3.10) data were used to confirm the purity and structure of compound **20**.

Table 3.10. NMR data of compound **20**

	^1H NMR Chemical shifts (δ) in ppm ^a	^{13}C NMR Chemical shifts (δ) in ppm ^b
Methyl	1.41 (d, 3H, J= 7.2 Hz)	21.4
<i>o</i> -Methyl	2.15 (s, 3H)	17.7
Hydroxyl	3.70 (d, 1H, J= 2.7 Hz)	-
Methine	4.20-4.26 (m, 1H)	69.1
Aromatics	6.96-7.78 (m, 4H)	135.2, 130.7, 129.2, 127.0, 125.5, 122.6
Amide N-H	8.42 (s, br, 1H)	-
Carbonyl	-	173.3
^a : ^1H NMR (400 MHz) data in CDCl_3 (Figure A.7) ^b : ^{13}C NMR (100 MHz) data in CDCl_3 (Figure A. 48)		

3.4.1.2. N- α -naphthyl Lactamide (21). The compound was prepared according to the general procedure using 1 g (4.15 mmole) compound **2** in 8.3 ml THF (0.5 M), 0.99 g (17.66 mmole) potassium hydroxide in 8.3 ml water (2 M). After extraction with ethyl acetate, the product was obtained as a colorless oil (0.92 g). Satisfactory NMR (^1H and ^{13}C) (Table 3.11) data were used to confirm the purity and structure of compound **21**.

Table 3.11. NMR data of compound **21**

	^1H NMR Chemical shifts (δ) in ppm ^a	^{13}C NMR Chemical shifts (δ) in ppm ^b
Methyl	1.38 (d, 3H, j= 7.05 Hz)	18.7
Methine	4.84 (q, 1H, J= 7.05 Hz)	79.1
Aromatics	7.42.-8.17 (m, 4H)	134.9, 134.4, 128.9, 128.6, 128.3, 126.5, 126.2, 125.0, 123.7, 121.1
Amide N-H	9.46 (s, br, 1H)	-
Carbonyl	-	175.5
^a : ^1H NMR (400 MHz) data in DMSO (Figure A.8) ^b : ^{13}C NMR (100 MHz) data in CDCl_3		

3.4.1.3. N-*o*-fluorophenyl Lactamide (22). The compound was prepared according to the general procedure using 1.0 g (4.78 mmole) compound **6** in 9.56 ml THF (0.5 M), 1.08 g (19.12 mmole) potassium hydroxide in 9.56 ml water (2 M). After extraction with ethyl acetate, the product was obtained as a colorless oil (0.1022 g). Satisfactory NMR (^1H and ^{13}C) (Table 3.12) data were used to confirm the purity and structure of compound **22**.

Table 3.12. NMR data of compound **22**

	^1H NMR Chemical shifts (δ) in ppm ^a	^{13}C NMR Chemical shifts (δ) in ppm ^b
Methyl	1.41 (d, 3H, $j= 5.6$ Hz)	21.2
Hydroxyl	4.22 (s, br, 1H)	-
Methine	4.28 (q, 1H, $J= 5.6$ Hz)	69.1
Aromatics	6.75-8.15 (m, 4H)	125.8, 125.1, 124.7, 121.9, 115.2, 115.1
Amide N-H	8.76 (s, br, 1H)	-
Carbonyl	-	173.5
^a : ^1H NMR (400 MHz) data in CDCl_3 (Figure A.9) ^b : ^{13}C NMR (100 MHz) data in CDCl_3		

3.4.1.4. N-*o*-chlorophenyl Lactamide (23). The compound was prepared according to the general procedure using 1.0 g (4.43 mmole) compound **5** in 8.9 ml THF (0.5 M), 0.99 g (17.72 mmole) potassium hydroxide in 8.9 ml water (2 M). After extraction with ethyl acetate, the product was obtained as a colorless oil (0.12 g). Satisfactory NMR (^1H and ^{13}C) (Table 3.13) data were used to confirm the purity and structure of compound **23**.

Table 3.13. NMR data of compound **23**

	^1H NMR Chemical shifts (δ) in ppm ^a	^{13}C NMR Chemical shifts (δ) in ppm ^b
Methyl	1.41 (d, 3H, $j= 7.2$ Hz)	21.2
Methine	4.30 (q, 1H, $J= 7.2$ Hz)	69.2
Aromatics	6.73-8.27 (m, 4H)	134.3, 129.3, 127.8, 125.1, 123.6, 121.6
Amide N-H	9.09 (s, br, 1H)	-
Carbonyl	-	173.5
^a : ^1H NMR (400 MHz) data in CDCl_3 (Figure A.10) ^b : ^{13}C NMR (100 MHz) data in CDCl_3		

3.4.1.5. N-*o*-bromophenyl Lactamide (24). The compound was prepared according to the general procedure using 0.8 g (2.97 mmole) compound **4** in 5.9 ml THF (0.5 M), 0.67 g (11.89 mmole) potassium hydroxide in 5.9 ml water (2 M). After extraction with ethyl acetate, the product was obtained as a colorless oil (0.063 g). Satisfactory NMR (^1H and ^{13}C) (Table 3.14) data were used to confirm the purity and structure of compound **24**.

Table 3.14. NMR data of compound **24**

	^1H NMR Chemical shifts (δ) in ppm ^a	^{13}C NMR Chemical shifts (δ) in ppm ^b
Methyl	1.30 (d, 3H, $j=7.2$ Hz)	18.7
Methine	4.71 (q, 1H, $J=7.2$ Hz)	72.4
Aromatics	7.00-7.69 (m, 4H)	139.6, 133.2, 128.6, 126.5, 125.8, 117.2
Amide N-H	8.50 (s, br, 1H)	-
Carbonyl	-	173.0
^a : ^1H NMR (400 MHz) data in DMSO (Figure A.11) ^b : ^{13}C NMR (100 MHz) data in DMSO		

3.4.1.6. N-*o*-iodophenyl Lactamide (25). The compound was prepared according to the general procedure using 0.4 g (1.26 mmole) compound **3** in 2.5 ml THF (0.5 M), 0.28 g (5.05 mmole) potassium hydroxide in 2.5 ml water (2 M). After extraction with ethyl acetate, the product was obtained as a colorless oil (0.05 g). Satisfactory NMR (^1H and ^{13}C) (Table 3.15) data were used to confirm the purity and structure of compound **25**.

Table 3.15. NMR data of compound **25**

	^1H NMR Chemical shifts (δ) in ppm ^a	^{13}C NMR Chemical shifts (δ) in ppm ^b
Methyl	1.50 (d, 3H, $j=7.2$ Hz)	17.2
Hydroxyl	4.76 (s, br, 1H)	-
Methine	4.37 (q, 1H, $J=7.2$ Hz)	69.8
Aromatics	6.76-8.24 (m, 4H)	139.0, 131.9, 129.7, 128.8, 125.5, 122.6
Amide N-H	8.76 (s, br, 1H)	-
Carbonyl	-	171.8
^a : ^1H NMR (400 MHz) data in CDCl_3 ^b : ^{13}C NMR (100 MHz) data in CDCl_3		

3.4.1.7. *N*-*o*-tolyl- α -hydroxyisobutyramide (26). The compound was prepared according to the general procedure using 0.50 g (2.28 mmole) compound (\pm)**7** in 3.6 ml THF+1 ml MeOH (0.5 M), 0.51 g (9.12 mmole) potassium hydroxide in 4.6 ml water (2 M). After extraction with ethyl acetate, the product was obtained as a white solid (0.17 g). Satisfactory NMR (^1H and ^{13}C) (Table 3.16), melting point (66-68 $^{\circ}\text{C}$) and FTIR (3382, 3332, 3066, 2992, 2974, 1661 cm^{-1}) data were used to confirm the purity and structure of compound **26**.

Table 3.16. NMR data of compound **26**

	^1H NMR Chemical shifts (δ) in ppm ^a	^{13}C NMR Chemical shifts (δ) in ppm ^b
Methyls	1.46 (s, 6H)	28.2
<i>o</i> -Methyl	2.17 (s, 3H)	17.7
Hydroxyl	2.87(s, br, 1H)	-
Methine	-	74.6
Aromatics	6.94-7.85 (m, 4H)	135.7, 130.6, 128.6, 127.0, 125.1, 122.1
Amide N-H	8.57 (s, br, 1H)	-
Carbonyl	-	174.5
^a : ^1H NMR (400 MHz) data in CDCl_3 (Figure A.12) ^b : ^{13}C NMR (100 MHz) data in CDCl_3 (Figure A. 49)		

3.4.1.8. *N*- α -naphthyl- α -hydroxyisobutyramide (27). The compound was prepared according to the general procedure using 0.5 g (1.96 mmole) compound (\pm)**15** in 3.9 ml THF (0.5 M), 0.44 g (7.84 mmole) potassium hydroxide in 3.9 ml water (2 M). After extraction with ethyl acetate, the product was obtained as a white solid (0.17 g). Satisfactory NMR (^1H and ^{13}C) (Table 3.17) and FTIR (3347, 3305, 3055, 2980, 1652 cm^{-1}) data were used to confirm the purity and structure of compound **27**.

Table 3.17. NMR data of compound **27**

	¹ H NMR Chemical shifts (δ) in ppm ^a	¹³ C NMR Chemical shifts (δ) in ppm ^b
Methyls	1.54 (s, 6H)	28.3
Hydroxyl	2.60 (s, br, 1H)	-
Methine	-	74.8
Aromatics	7.18-8.03 (m, 7H)	134.3, 132.2, 129.0, 126.9, 126.4, 126.1, 126.0, 125.5, 120.5, 119.5
Amide N-H	9.17 (s, br, 1H)	-
Carbonyl	-	174.9
^a : ¹ H NMR (400 MHz) data in CDCl ₃ (Figure A.13) ^b : ¹³ C NMR (100 MHz) data in CDCl ₃		

3.4.1.9. *N*-*o*-fluorophenyl- α -hydroxyisobutyramide (**28**). The compound was prepared according to the general procedure using 0.50 g (2.24 mmole) compound (\pm)**8** in 4.5 ml THF (0.5 M), 0.50 g (8.96 mmole) potassium hydroxide in 4.5 ml water (2 M). After extraction with ethyl acetate, the product was obtained as a white solid (0.072 g). Satisfactory NMR (¹H and ¹³C) (Table 3.18), melting point (66-68 °C) and FTIR (3430, 3369, 3054, 2999, 2988, 1667 cm⁻¹) data were used to confirm the purity and structure of compound **28**.

Table 3.18. NMR data of compound **28**

	¹ H NMR Chemical shifts (δ) in ppm ^a	¹³ C NMR Chemical shifts (δ) in ppm ^b
Methyls	1.49 (s, 6H)	28.1
Hydroxyl	2.58 (s, br, 1H)	-
Methine	-	74.6
Aromatics	6.95-8.30 (m, 4H)	126.4, 126.3, 124.7, 121.6, 115.1, 114.9
Amide N-H	8.93 (s, br, 1H)	-
Carbonyl	-	174.7
^a : ¹ H NMR (400 MHz) data in CDCl ₃ (Figure A.14) ^b : ¹³ C NMR (100 MHz) data in CDCl ₃		

3.4.1.10. N-*o*-chlorophenyl- α -hydroxyisobutyramide (29). The compound was prepared according to the general procedure using 0.50 g (2.09 mmole) compound (\pm)**9** in 3.3 ml THF+1 ml MeOH (0.5 M), 0.47 g (8.35 mmole) potassium hydroxide in 4.3 ml water (2 M). After extraction with ethyl acetate, the product was obtained as a white solid (0.084 g). Satisfactory NMR (^1H and ^{13}C) (Table 3.19), melting point (78-80 $^{\circ}\text{C}$) and FTIR (3421, 3345, 3042, 2995, 2978, 1667 cm^{-1}) data were used to confirm the purity and structure of compound **29**.

Table 3.19. NMR data of compound **29**

	^1H NMR Chemical shifts (δ) in ppm ^a	^{13}C NMR Chemical shifts (δ) in ppm ^b
Methyls	1.49 (s, 6H)	28.1
Hydroxyl	2.57 (s, br, 1H)	-
Methine	-	74.7
Aromatics	6.94-8.36 (m, 4H)	134.7, 129.3, 127.9, 124.9, 123.5, 121.3
Amide N-H	9.24 (s, br, 1H)	-
Carbonyl	-	174.8
^a : ^1H NMR (400 MHz) data in CDCl_3 (Figure A.15) ^b : ^{13}C NMR (100 MHz) data in CDCl_3		

3.4.1.11. N-*o*-bromophenyl- α -hydroxyisobutyramide (30). The compound was prepared according to the general procedure using 0.50 g (1.76 mmole) compound (\pm)**10** in 2.5 ml THF+1 ml MeOH (0.5 M), 0.40 g (7.04 mmole) potassium hydroxide in 3.50 ml water (2 M). After extraction with ethyl acetate, the product was obtained as a white solid (0.081 g). Satisfactory NMR (^1H and ^{13}C) (Table 3.20), melting point (84-86 $^{\circ}\text{C}$) and FTIR (3310, 3272, 3065, 2995, 2968, 1668 cm^{-1}) data were used to confirm the purity and structure of compound **30**.

Table 3.20. NMR data of compound **30**

	¹ H NMR Chemical shifts (δ) in ppm ^a	¹³ C NMR Chemical shifts (δ) in ppm ^b
Methyls	1.58 (s, 6H)	28.2
Hydroxyl	2.47 (s, br, 1H)	-
Methine	-	74.7
Aromatics	6.96-8.42 (m, 4H)	135.8, 132.5, 128.6, 125.4, 121.6, 114.0
Amide N-H	9.29 (s, br, 1H)	-
Carbonyl	-	174.7
^a : ¹ H NMR (400 MHz) data in CDCl ₃ (Figure A.16)		
^b : ¹³ C NMR (100 MHz) data in CDCl ₃		

3.4.1.12. *N*-*o*-iodophenyl- α -hydroxyisobutyramide (**31**). The compound was prepared according to the general procedure using 1.0 g (3.02 mmole) compound (\pm)**11** in 6.0 ml THF (0.5 M), 0.68 g (12.1 mmole) potassium hydroxide in 6.0 ml water (2 M). After extraction with ethyl acetate, the product was obtained as a white solid (0.1765 g). Satisfactory NMR (¹H and ¹³C) (Table 3.21), melting point (48-50 °C) and FTIR (3373, 3280, 3055, 2992, 2969, 1651 cm⁻¹) data were used to confirm the purity and structure of compound **31**.

Table 3.21. NMR data of compound **31**

	¹ H NMR Chemical shifts (δ) in ppm ^a	¹³ C NMR Chemical shifts (δ) in ppm ^b
Methyls	1.51 (s, 6H)	26.9
Hydroxyl	2.51 (s, br, 1H)	-
Methine	-	73.4
Aromatics	6.75-8.24 (m, 4H)	137.9, 137.1, 128.2, 124.9, 120.5
Amide N-H	9.04 (s, br, 1H)	-
Carbonyl	-	173.6
^a : ¹ H NMR (400 MHz) data in CDCl ₃ (Figure A.17)		
^b : ¹³ C NMR (100 MHz) data in CDCl ₃		

3.4.2. General Procedure for the Formation of Carboxylic Acids [11]

To the solution of the compounds in THF (0.5 M) at 0 °C was added 2 M, KOH solution prepared in distilled water. Reaction was followed by TLC. After completion, the reaction mixture was extracted three times by ethyl acetate. The aqueous phase then acidified by 2M HCl to pH 6.2 at 0 °C. After extraction with ethyl acetate, the products were obtained as white solids.

3.4.2.1. N-(*o*-tolyl)-carbamoyloxy-lactic Acid (32). The compound was prepared according to the general procedure using 1 g (4.87 mmole) compound **1** in 9.75 ml THF (0.5 M), 1.09 g (19.5 mmole) potassium hydroxide in 9.75 ml water (2 M). After extraction the aqueous phase was acidified to pH 6.2. After extraction with ethyl acetate, compound **32** were obtained as white solid (0.18 g). Satisfactory NMR (¹H and ¹³C) (Table 3.22) data were used to confirm the purity and structure of compound **32**.

Table 3.22. NMR data of compound **32**

	¹ H NMR Chemical shifts (δ) in ppm ^a	¹³ C NMR Chemical shifts (δ) in ppm ^b
Methyl	1.57 (d, 3H, J= 6.8 Hz)	17.8
<i>o</i> -methyl	2.27 (s, 3H)	17.2
Methine	5.20 (q, 1H, J= 6.8 Hz)	69.1
Aromatics	6.65-7.21 (m, 4H)	135.5, 130.7, 127.1, 125.0
Carbamate N-H	7.71 (s, 1H)	-
Carbonyls	-	176.4, 154.0
^a : ¹ H NMR (400 MHz) data in CDCl ₃ (Figure A.18) ^b : ¹³ C NMR (100 MHz) data in CDCl ₃		

3.4.2.2. N-(α -naphthyl)-carbamoyloxy-lactic Acid (33). The compound was prepared according to the general procedure using 1 g (4.15 mmole) compound **2** in 8.3 ml THF (0.5 M), 0.99 g (17.66 mmole) potassium hydroxide in 8.3 ml water (2 M). After extraction the aqueous phase was acidified to pH 6.2. After extraction with ethyl acetate, compound **33** were obtained as white solid (0.20 g). Satisfactory NMR (¹H and ¹³C) (Table 3.23) and FTIR (3235, 3042-2544, 1697 cm⁻¹) data were used to confirm the purity and structure of compound **33**.

Table 3.23. NMR data of compound **33**

	¹ H NMR Chemical shifts (δ) in ppm ^a	¹³ C NMR Chemical shifts (δ) in ppm ^b
Methyl	1.46 (d, 3H, J= 6.8 Hz)	17.8
Methine	4.94 (q, 1H, J= 6.8 Hz)	69.9
Aromatics	7.45-8.10 (m, 7H)	134.4, 134.3, 128.7, 126.7, 126.5, 126.3, 125.8, 123.6, 122.0
Carbamate N-H	9.66 (s, br, 1H)	-
Carbonyls	-	173.9, 155.1
^a : ¹ H NMR (400 MHz) data in DMSO (Figure A.19)		
^b : ¹³ C NMR (100 MHz) data in DMSO		

3.4.2.3. *N*-(*o*-fluorophenyl)-carbamoyloxy-lactic Acid (**34**). The compound was prepared according to the general procedure using 1.0 g (4.78 mmole) compound **6** in 9.56 ml THF (0.5 M), 1.08 g (19.12 mmole) potassium hydroxide in 9.56 ml water (2 M). After extraction the aqueous phase was acidified to pH 6.2. After extraction with ethyl acetate, compound **34** were obtained as white solid (0.13 g). Satisfactory NMR (¹H and ¹³C) (Table 3.24), melting point (132-134 °C) and FTIR (3295, 2546-3295, 1706 cm⁻¹) data were used to confirm the purity and structure of compound **34**.

Table 3.24. NMR data of compound **34**

	¹ H NMR Chemical shifts (δ) in ppm ^a	¹³ C NMR Chemical shifts (δ) in ppm ^b
Methyl	1.41 (d, 3H, J= 6.8 Hz)	17.6
Methine	4.90 (q, 1H, J= 6.8 Hz)	69.5
Aromatics	7.10-7.62 (m, 4H)	126.6, 126.5, 126.0, 125.0, 116.4, 116.2
Carbamate N-H	9.54 (s, br, 1H)	-
Carboxylic acid OH	12.99 (s, br, 1H)	-
Carbonyls	-	173.2, 154.0
^a : ¹ H NMR (400 MHz) data in DMSO (Figure A.20)		
^b : ¹³ C NMR (100 MHz) data in DMSO		

3.4.2.4. N-(*o*-chlorophenyl)-carbamoyloxy-lactic Acid (35). The compound was prepared according to the general procedure using 1.00 g (4.43 mmole) compound **5** in 8.9 ml THF (0.33 M), 0.99 g (17.72 mmole) sodium borohydride in 8.9 ml water (4.05 M). After extraction the aqueous phase was acidified to pH 6.18. After extraction with ethyl acetate, compound **35** were obtained as white solid (0.16 g). Satisfactory NMR (^1H and ^{13}C) (Table 3.25) and FTIR (3310, 2541-3079, 1705 cm^{-1}) data were used to confirm the purity and structure of compound **35**.

Table 3.25. NMR data of compound **35**

	^1H NMR Chemical shifts (δ) in ppm ^a	^{13}C NMR Chemical shifts (δ) in ppm ^b
Methyl	1.41 (d, 3H, J= 6.8 Hz)	17.6
Methine	4.90 (q, 1H, J= 6.8 Hz)	69.6
Aromatics	7.14-7.55 (m, 4H)	135.5, 130.2, 128.2, 127.9, 126.9, 126.7
Carbamate N-H	9.19 (s, br, 1H)	-
Carboxylic acid OH	12.91 (s, br, 1H)	-
Carbonyls	-	173.1, 154.1
^a : ^1H NMR (400 MHz) data in DMSO (Figure A.21) ^b : ^{13}C NMR (100 MHz) data in DMSO (Figure A.52)		

3.4.2.5. N-(*o*-bromophenyl)-carbamoyloxy-lactic Acid (36). The compound was prepared according to the general procedure using 0.80 g (2.97 mmole) compound **4** in 5.94 ml THF (0.5 M), 0.67 g (11.89 mmole) potassium hydroxide in 5.94 ml water (2 M). After extraction the aqueous phase was acidified to pH 6.18. After extraction with ethyl acetate, compound **36** were obtained as white solid (0.095 g). Satisfactory NMR (^1H and ^{13}C) (Table 3.26), melting point (130-132 $^{\circ}\text{C}$) and FTIR (3297, 2524-3113, 1701 cm^{-1}) data were used to confirm the purity and structure of compound **36**.

Table 3.26. NMR data of compound **36**

	¹ H NMR Chemical shifts (δ) in ppm ^a	¹³ C NMR Chemical shifts (δ) in ppm ^b
Methyl	1.60 (d, 3H, J= 6.8 Hz)	17.2
Methine	5.19 (q, 1H, J= 6.8 Hz)	69.3
Aromatics	6.93-8.11 (m, 4H)	135.6, 132.6, 128.6, 124.9, 120.7, 113.1.7
Carbamate N-H	8.21 (s, br, 1H)	-
Carbonyls	-	176.6, 152.5
^a : ¹ H NMR (400 MHz) data in CDCl ₃ (Figure A.22)		
^b : ¹³ C NMR (100 MHz) data in CDCl ₃		

3.4.2.6. *N*-(*o*-tolyl)-carbamoyloxy-isobutyric Acid (**38**). The compound was prepared according to the general procedure using 0.5 g (2.28 mmole) compound (**±**)**7** in 4.6 ml THF (0.5 M), 0.51 g (9.12 mmole) potassium hydroxide in 4.6 ml water (2 M). After extraction the aqueous phase was acidified to pH 6.18. After extraction with ethyl acetate, compound **38** were obtained as white solid (0.16 g). Satisfactory NMR (¹H and ¹³C) (Table 3.27), melting point (130-132 °C) and FTIR (3234, 2575-3383, 1694 cm⁻¹) data were used to confirm the purity and structure of compound **38**.

Table 3.27. NMR data of compound **38**

	¹ H NMR Chemical shifts (δ) in ppm ^a	¹³ C NMR Chemical shifts (δ) in ppm ^b
Methyls	1.49 (s, 6H)	25.5
<i>o</i> -methyl	2.17 (s, 3H)	18.5
Methine	-	77.8
Aromatics	7.01-7.27 (m, 4H)	136.9, 132.6, 130.9, 126.9, 126.7, 125.6
Carbamate N-H	8.88 (s, 1H)	-
Carboxylic acid OH	12.66 (s, br, 1H)	
Carbonyls	-	174.9, 153.8
^a : ¹ H NMR (400 MHz) data in DMSO (Figure A.23)		
^b : ¹³ C NMR (100 MHz) data in DMSO		

3.4.2.7. N-(α -naphthyl)-carbamoyloxy-isobutyric Acid (39). The compound was prepared according to the general procedure using 0.5 g (1.96 mmole) compound (\pm)**15** in 3.9 ml THF (0.5 M), 0.44 g (7.84 mmole) potassium hydroxide in 3.9 ml water (2 M). After extraction the aqueous phase was acidified to pH 6.18. After extraction with ethyl acetate, compound **39** were obtained as white solid (0.25 g). Satisfactory NMR (^1H and ^{13}C) (Table 3.28) data were used to confirm the purity and structure of compound **39**.

Table 3.28. NMR data of compound **39**

	^1H NMR Chemical shifts (δ) in ppm ^a	^{13}C NMR Chemical shifts (δ) in ppm ^b
Methyls	1.51 (s, 6H)	28.3
Methine	-	74.9
Aromatics	7.32-8.00 (m, 7H)	134.3, 132.2, 129.0, 126.9, 126.5, 126.1, 126.0, 125.6, 120.5, 119.6
Carbamate N-H	9.16 (s, 1H)	-
Carbonyls	-	175.0, 156.7
^a : ^1H NMR (400 MHz) data in CDCl_3 (Figure A.24) ^b : ^{13}C NMR (100 MHz) data in CDCl_3		

3.4.2.8. N-(*o*-fluorophenyl)-carbamoyloxy-isobutyric Acid (40). The compound was prepared according to the general procedure using 0.5 g (2.24 mmole) compound (\pm)**8** in 4.5 ml THF (0.5 M), 0.50 g (8.96 mmole) potassium hydroxide in 4.5 ml water (2 M). After extraction the aqueous phase was acidified to pH 6.18. After extraction with ethyl acetate, compound **40** were obtained as white solid (0.12 g). Satisfactory NMR (^1H and ^{13}C) (Table 3.29), melting point (120-122 $^{\circ}\text{C}$) and FTIR (3243, 2569-3406, 1705 cm^{-1}) data were used to confirm the purity and structure of compound **40**.

Table 3.29. NMR data of compound **40**

	¹ H NMR Chemical shifts (δ) in ppm ^a	¹³ C NMR Chemical shifts (δ) in ppm ^b
Methyls	1.50 (s, 6H)	25.4
Methine	-	78.2
Aromatics	7.09-7.59 (m, 4H)	126.8, 126.6, 125.9, 125.0, 116.4, 116.2
Carbamate N-H	9.35 (s, 1H)	-
Carboxylic acid OH	12.75 (s, br, 1H)	-
Carbonyls	-	174.7, 153.7
^a : ¹ H NMR (400 MHz) data in DMSO (Figure A.25) ^b : ¹³ C NMR (100 MHz) data in DMSO		

3.4.2.9. *N*-(*o*-chlorophenyl)-carbamoyloxy-isobutyric Acid (**41**). The compound was prepared according to the general procedure using 0.5 g (2.09 mmole) compound (**±**)**9** in 4.3 ml THF (0.5 M), 0.47 g (8.35 mmole) potassium hydroxide in 4.3 ml water (2 M). After extraction the aqueous phase was acidified to pH 6.18. After extraction with ethyl acetate, compound **41** were obtained as white solid (0.12 g). Satisfactory NMR (¹H and ¹³C) (Table 3.30) and FTIR (3387, 2571-3024, 1715 cm⁻¹) data were used to confirm the purity and structure of compound **41**.

Table 3.30. NMR data of compound **41**

	¹ H NMR Chemical shifts (δ) in ppm ^a	¹³ C NMR Chemical shifts (δ) in ppm ^b
Methyls	1.56 (s, 6H)	25.0
Methine	-	79.4
Aromatics	7.01-8.43 (m, 4H)	134.7, 129.2, 127.9, 124.1, 122.5, 120.4
Carbamate N-H	9.34 (s, 1H)	-
Carbonyls	-	177.6, 152.2
^a : ¹ H NMR (400 MHz) data in CDCl ₃ (Figure A.26) ^b : ¹³ C NMR (100 MHz) data in CDCl ₃		

3.4.2.10. N-(*o*-bromophenyl)-carbamoyloxy-isobutyric Acid (**42**). The compound was prepared according to the general procedure using 0.50 g (1.76 mmole) compound (\pm)**10** in 3.5 ml THF (0.5 M), 0.4 g (7.04 mmole) potassium hydroxide in 3.5 ml water (2 M). After extraction the aqueous phase was acidified to pH 6.18. After extraction with ethyl acetate, compound **42** were obtained as white solid (0.12 g). Satisfactory NMR (^1H and ^{13}C) (Table 3.31), elemental analysis (Table 3.32) and FTIR (3375, 2569-3128, 1711 cm^{-1}) data were used to confirm the purity and structure of compound **42**.

Table 3.31. NMR data of compound **42**

	^1H NMR Chemical shifts (δ) in ppm ^a	^{13}C NMR Chemical shifts (δ) in ppm ^b
Methyls	1.50 (s, 6H)	25.4
Methine	-	78.4
Aromatics	7.06-7.66 (m, 4H)	136.9, 133.4, 128.7, 127.4, 127.3, 118.9
Carbamate N-H	8.89 (s, 1H)	-
Carboxylic acid OH	12.62 (s, br, 1H)	-
Carbonyls	-	174.6, 153.5
^a : ^1H NMR (400 MHz) data in DMSO (Figure A.27) ^b : ^{13}C NMR (100 MHz) data in DMSO (Figure A.53)		

Table 3.32. Elemental analysis data for compound **42**

	Found, %	Calculated for $\text{C}_{11}\text{H}_{10}\text{O}_3\text{NBr}$, %
C	43.73	44.12
H	4.00	, 4.05
N	4.64	4.47

3.4.2.11. N-(*o*-iodophenyl)-carbamoyloxy-isobutyric Acid (**43**). The compound was prepared according to the general procedure using 1.0 g (3.02 mmole) compound (\pm)**11** in 6.04 ml THF (0.5 M), 0.68 g (1.20 mmole) potassium hydroxide in 6.04 ml water (2 M). After extraction the aqueous phase was acidified to pH 6.18. After extraction with ethyl

acetate, compound **43** were obtained as white solid (0.23 g). Satisfactory NMR (^1H and ^{13}C) (Table 3.33) data were used to confirm the purity and structure of compound **43**.

Table 3.33. NMR data of compound **43**

	^1H NMR Chemical shifts (δ) in ppm ^a	^{13}C NMR Chemical shifts (δ) in ppm ^b
Methyls	1.61 (s, 6H)	25.1
Methine	-	74.6
Aromatics	6.73-7.94 (m, 4H)	140.3, 139.1, 138.4, 129.5, 125.5, 121.7
Carbamate N-H	9.09 (s, 1H)	-
Carbonyls	-	175.0, 152.7
^a : ^1H NMR (400 MHz) data in DMSO ^b : ^{13}C NMR (100 MHz) data in DMSO		

3.5. The Reduction Reactions with Sodium Borohydride

3.5.1. General Procedure [12]

To a mixture of the starting material (1 eq.) in THF was added a solution of sodium borohydride (4 eq.) in water at a rate to maintain the internal temperature at 20-25°C. the mixture was stirred at room temperature for 1-4 h, and the completion of the reaction was monitored by TLC. To the reaction mixture was added 2 M HCl (5 eq.) at a rate to maintain the internal temperature at 20-25°C. The reaction mixture was extracted with ethyl acetate. The combined organic layers were washed with brine, and purified by ethyl acetate-hexane.

3.5.1.1. 1-Hydroxypropan-2-yl-*o*-tolylcarbamate ((\pm) **44).** The compound was prepared according to the general procedure using 0.41 g (2.01 mmole) compound **1** in 6.3 ml THF (0,33 M), 0.30 g (8,02 mmole) sodium borohydride in 2.0 ml water (4,05 M). After extraction with ethyl acetate, the product was obtained as a white solid (0.37 g). Satisfactory NMR (^1H and ^{13}C) (Table 3.34) data were used to confirm the purity and structure of compound (\pm) **44**.

Table 3.34. NMR data of compound (\pm) **44**

	¹ H NMR Chemical shifts (δ) in ppm ^a	¹³ C NMR Chemical shifts (δ) in ppm ^b
Methyl	1.25 (d, 3H, J= 6.24 Hz)	16.6
<i>o</i> -methyl	2.21 (s, 3H)	17.8
Hydroxyl proton	3.05 (s, br, 1H)	-
methylene	δ 3.58 and 3.65, 3.57 and 3.64 (2 AB quartets, 1 H each, J= 12.09 Hz)	66.0
Methine	4.88-4.96 (m, 1H)	73.5
Carbamate N-H	6.69 (s, br, 1H)	-
Aromatics	7.00-7.66 (m, 4H)	135.9, 133.8, 130.7, 128.8, 126.8, 124.8
Carbonyl	-	154.7
^a : ¹ H NMR (400 MHz) data in CDCl ₃ (Figure A.28)		
^b : ¹³ C NMR (100 MHz) data in CDCl ₃		

3.5.1.2. 1-Hydroxypropan-2-yl- α -naphthylcarbamate ((\pm) **45).** The compound was prepared according to the general procedure using 1.00 g (4.15 mmole) compound **2** in 13 ml THF (0,33 M), 0.63 g (16.58 mmole) sodium borohydride in 4,0 ml water (4,05 M). After extraction with ethyl acetate, the product was obtained as a white solid (0.86 g). Satisfactory NMR (¹H and ¹³C) (Table 3.35), melting point (73-75 °C) and FTIR (3358, 3262, 3063, 2969, 2930, 1689 cm⁻¹) data were used to confirm the purity and structure of compound (\pm) **45**.

Table 3.35. NMR data of compound (\pm) **45**

	^1H NMR Chemical shifts (δ) in ppm ^a	^{13}C NMR Chemical shifts (δ) in ppm ^b
Methyl	1.28 (s, 3H)	16.6
Hydroxyl proton	2.68 (s, br, 1H)	-
methylene	3.64-3.70, (m, 2H)	65.9
Methine	4.98-5.06 (m, 1H)	73.4
Carbamate N-H	7.23 (s, br, 1H)	-
Aromatics	7.41-7.87 (m, 7H)	134.3, 132.8, 128.8, 127.4, 126.6, 126.4, 126.2, 125.9, 125.5, 121.2
Carbonyl	-	155.2
^a : ^1H NMR (400 MHz) data in CDCl_3 (Figure A.29) ^b : ^{13}C NMR (100 MHz) data in CDCl_3		

3.5.1.3. 1-Hydroxypropan-2-yl-*o*-fluorophenylcarbamate ((\pm) **46).** The compound was prepared according to the general procedure using 0.5 g (2.39 mmole) compound **6** in 7.5 ml THF (0.33 M), 0.36 g (9.56 mmole) sodium borohydride in 2.3 ml water (4.05 M). After extraction with ethyl acetate, the product was obtained as a white solid (0.45 g). Satisfactory NMR (^1H and ^{13}C) (Table 3.36), melting point (40-42 $^\circ\text{C}$) and FTIR (3381, 3295, 3070, 2984, 2936, 1728 cm^{-1}) data were used to confirm the purity and structure of compound (\pm) **46**.

Table 3.36. NMR data of compound (\pm) **46**

	^1H NMR Chemical shifts (δ) in ppm ^a	^{13}C NMR Chemical shifts (δ) in ppm ^b
Methyl	1.32 (d, 3H, $J = 6.63$ Hz)	16.6
Hydroxyl proton	2.12 (s, br, 1H)	-
methylene	δ 3.67 and 3.76, 3.68 and 3.75 (2 AB quartets, 1 H each, $J = 12.09$ Hz)	66.3
Methine	4.98-5.06 (m, 1H)	73.7
Carbamate N-H	6.91 (s, br, 1H)	-
Aromatics	6.97-8.06 (m, 4H)	126.5, 124.8, 123.8, 120.5, 115.2, 115.0
Carbonyl	-	153.7
^a : ^1H NMR (400 MHz) data in CDCl_3 (Figure A.30) ^b : ^{13}C NMR (100 MHz) data in CDCl_3		

3.5.1.4. 1-Hydroxypropan-2-yl-*o*-chlorophenylcarbamate ((±) 47). The compound was prepared according to the general procedure using 0.5 g (2.22 mmole) compound **5** in 7.0 ml THF (0,33 M), 0.34 g (8.86 mmole) sodium borohydride in 2.2 ml water (4,0 M). After extraction with ethyl acetate, the product was obtained as an oil (0.49 g). Satisfactory NMR (^1H and ^{13}C) (Table 3.37) and FTIR (3411, 3304, 3066, 2980, 1713 cm^{-1}) data were used to confirm the purity and structure of compound (\pm) **47**.

Table 3.37. NMR data of compound (\pm) **47**

	^1H NMR Chemical shifts (δ) in ppm ^a	^{13}C NMR Chemical shifts (δ) in ppm ^b
Methyl	1.26 (d, 3H, J= 6.00 Hz)	16.6
Hydroxyl proton	3.45 (s, br, 1H)	-
methylene	δ 3.62 and 3. 69, 3.63 and 3. 68 (2 AB quartets, 1 H each, J= 12.40 and 12.00 Hz)	65.8
Methine	4.93-5.00 (m, 1H)	73.5
Carbamate N-H	7.29 (s, br, 1H)	-
Aromatics	6.92-8.08 (m, 4H)	134.8, 129.3, 127.9, 124.2, 122.6, 120.5
Carbonyl	-	153.6
^a : ^1H NMR (400 MHz) data in CDCl_3 (Figure A.31)		
^b : ^{13}C NMR (100 MHz) data in CDCl_3		

3.5.1.5. 1-Hydroxypropan-2-yl-*o*-bromophenylcarbamate ((±) 48). The compound was prepared according to the general procedure using 0.5 g (1.85 mmole) compound **4** in 6 ml THF (0,33 M), 0.28 g (7.40 mmole) sodium borohydride in 1.85 ml water (4,05 M). After extraction with ethyl acetate, the product was obtained as an oil (0.49 g). Satisfactory NMR (^1H and ^{13}C) (Table 3.38) and FTIR (3400, 3339, 3067, 2977, 2936, 1712 cm^{-1}) data were used to confirm the purity and structure of compound (\pm) **48**.

Table 3.38. NMR data of compound (\pm) 48

	^1H NMR Chemical shifts (δ) in ppm ^a	^{13}C NMR Chemical shifts (δ) in ppm ^b
Methyl	1.28 (d, 3H, J= 6.24 Hz)	16.6
Hydroxyl proton	3.14 (s, br, 1H)	-
methylene	δ 3.65 and 3.71, 3.64 and 3.70 (2 AB quartets, 1H each, J= 12.09 Hz)	65.6
Methine	4.94-5.02 (m, 1H)	73.5
Carbamate N-H	7.22 (s, br, 1H)	-
Aromatics	6.87-8.08 (m, 4H)	136.0, 132.6, 128.5, 124.8, 121.0, 113.3
Carbonyl	-	153.6
^a : ^1H NMR (400 MHz) data in CDCl_3 (Figure A.32) ^b : ^{13}C NMR (100 MHz) data in CDCl_3		

3.5.1.6. 1-Hydroxypropan-2-yl-*o*-iodophenylcarbamate (\pm) 49. The compound was prepared according to the general procedure using 1.00 g (3.15 mmole) compound **3** in 9.9 ml THF (0.33 M), 0.48 g (12.62 mmole) sodium borohydride in 9.2 ml water (4.05 M). After extraction with ethyl acetate, the product was obtained as an oil (0.94 g). Satisfactory NMR (^1H and ^{13}C) (Table 3.39) and FTIR (3427, 3379, 3067, 2979, 2934, 1708 cm^{-1}) data were used to confirm the purity and structure of compound (\pm) **49**.

Table 3.39. NMR data of compound (\pm) 49

	^1H NMR Chemical shifts (δ) in ppm ^a	^{13}C NMR Chemical shifts (δ) in ppm ^b
Methyl	1.18 (d, 3H, J= 6.63 Hz)	16.8
Hydroxyl proton	3.90 (s, br, 1H)	-
methylene	δ 3.55 and 3.61, 3.57 and 3.58 (2 AB quartets, 1 H each, J= 12.09 Hz)	65.7
Methine	4.85-4.92 (m, 1H)	73.5
Carbamate N-H	7.00 (s, br, 1H)	-
Aromatics	6.64-7.87 (m, 4H)	139.2, 138.6, 129.4, 125.7, 121.3, 90.0
Carbonyl	-	153.8
^a : ^1H NMR (400 MHz) data in CDCl_3 (Figure A.33) ^b : ^{13}C NMR (100 MHz) data in CDCl_3		

3.5.1.7. 4-Hydroxy-5,5-dimethyl-3-(*o*-tolyl)-2-oxazolidinone (50). The compound was prepared according to the general procedure using 1.00 g (4,56 mmole) compound (\pm)**7** in 14 ml THF (0,33 M), 0.69 g (18,25 mmole) sodium borohydride in 4,5 ml water (4,05 M). The white solid (1.00 g) was obtained with 99.11 per cent yield. Satisfactory NMR (^1H and ^{13}C) (Table 3.40), melting point (96-98 $^{\circ}\text{C}$) and FTIR (3262, 3017, 2988, 2868, 1714 cm^{-1}) data were used to confirm the purity and structure of compound **50**.

Table 3.40. NMR data of compound **50**

	^1H NMR Chemical shifts (δ) in ppm ^a	^{13}C NMR Chemical shifts (δ) in ppm ^b
Diastereotopic methyls	1,40 and 1,48 (ss, 6H)	22.9, 17.0
<i>o</i> -methyl	2,23 (s, 3H)	14.3
Hydroxyl proton	3,32 (d, OH, $j=7.4$ Hz)	-
C-5 methine	-	78.8
C-4 methine	4,90 (d, 1 H, $j=7.4$ Hz)	84.3
Aromatics	7,17-7.29 (m, 4H)	132.9, 130.2, 127.4, 25.4, 124.9, 123.1
Carbonyl	-	151.8
^a : ^1H NMR (400 MHz) data in CDCl_3 (Figure A.34) ^b : ^{13}C NMR (100 MHz) data in CDCl_3		

3.5.1.8. 4-Hydroxy-5,5-dimethyl-3-(α -naphthyl)-2-oxazolidinone (51). The compound was prepared according to the general procedure using 0.50 g (1.96 mmole) compound (\pm)**15** in 6 ml THF (0,33 M), 0.30 g (7.84 mmole) sodium borohydride in 1.8 ml water (4,35 M). The white solid (0.36 g) was obtained with 71,43 per cent yield. Satisfactory NMR (^1H and ^{13}C) (Table 3.41) and melting point (124-126 $^{\circ}\text{C}$) data were used to confirm the purity and structure of compound **51**.

Table 3.41. NMR data of compound **51**

	¹ H NMR Chemical shifts (δ) in ppm ^a	¹³ C NMR Chemical shifts (δ) in ppm ^b
Diastereotopic methyls	1,48 and 1,64 (ss, 6H)	27.2, 21.1
Hydroxyl proton	3,80 (s, br, 1H)	-
C-5 methine	-	82.9
C-4 methine	5,02 (s, 1 H)	88.5
Aromatics	7,40-8.00 (m, 7H)	134.8, 131.5, 130.9, 129.4, 128.9, 127.5, 127.3, 126.7, 125.8, 122.4
Carbonyl	-	156.3
^a : ¹ H NMR (400 MHz) data in CDCl ₃ (Figure A.35) ^b : ¹³ C NMR (100 MHz) data in CDCl ₃		

3.5.1.9. 4-Hydroxy-5,5-dimethyl-3-(*o*-fluorophenyl)-2-oxazolidinone (52**).** The compound was prepared according to the general procedure using 0.25 g (1.12 mmole) compound (**±**)**8** in 3.5 ml THF (0,32 M), 0.17 g (4.48 mmole) sodium borohydride in 1.1 ml water (4,00 M). The white solid (0.25 g) was obtained with 64,87 per cent yield. Satisfactory NMR (¹H and ¹³C) (Table 3.42) and FTIR (3367, 3055, 2984, 2938, 1752 cm⁻¹) data were used to confirm the purity and structure of compound **52**.

Table 3.42. NMR data of compound **52**

	¹ H NMR Chemical shifts (δ) in ppm ^a	¹³ C NMR Chemical shifts (δ) in ppm ^b
Diastereotopic methyls	1,48 and 1,55 (ss, 6H)	25.8, 20.2
Hydroxyl proton	3,32 (s, br, 1H)	-
C-5 methine	-	82.8
C-4 methine	5,15 (s, 1 H)	88.0
Aromatics	7,16-8.57 (m, 4H)	130.3, 124.3, 116.1, 115.9
Carbonyl	-	155.3
^a : ¹ H NMR (400 MHz) data in CDCl ₃ (Figure A.36) ^b : ¹³ C NMR (100 MHz) data in toluene-d ₈		

3.5.1.10. 4-Hydroxy-5,5-dimethyl-3-(*o*-chlorophenyl)-2-oxazolidinone (53). The compound was prepared according to the general procedure using 0.20 g (0.84 mmole) compound (\pm)**9** in 2.6 ml THF (0,32 M), 0.13 g (3.34 mmole) sodium borohydride in 0,8 ml water (4,00 M). The white solid (0.19 g) was obtained with 92,71 per cent yield. Satisfactory NMR (^1H and ^{13}C) (Table 3.43) data were used to confirm the purity and structure of compound **53**.

Table 3.43. NMR data of compound **53**

	^1H NMR Chemical shifts (δ) in ppm ^a	^{13}C NMR Chemical shifts (δ) in ppm ^b
Diastereotopic methyls	1,40 and 1,53 (ss, 6H)	26.6, 20.9
Hydroxyl proton	3,63 (s, br, 1H)	-
C-5 methine	-	83.9
C-4 methine	5,04 (s, 1 H)	87.7
Aromatics	7,22-7.46 (m, 4H)	133.0, 132.7, 131.9, 130.4, 130.0, 127.9
Carbonyl	-	156.0
^a : ^1H NMR (400 MHz) data in CDCl_3 (Figure A.37) ^b : ^{13}C NMR (100 MHz) data in CDCl_3		

3.5.1.11. 4-Hydroxy-5,5-dimethyl-3-(*o*-bromophenyl)-2-oxazolidinone (54). The compound was prepared according to the general procedure using 0.30 g (1.06 mmole) compound (\pm)**10** in 3.5 ml THF (0,30 M), 0.16 g (4.22 mmole) sodium borohydride in 1.0 ml water (4,22 M). The white solid (0.24 g) was obtained with 79.40 per cent yield. Satisfactory NMR (^1H and ^{13}C) (Table 3.44), melting point (154-156 $^{\circ}\text{C}$) and FTIR (3342, 3097, 2978, 2963, 1708 cm^{-1}) data were used to confirm the purity and structure of compound **54**.

Table 3.44. NMR data of compound **54**

	¹ H NMR Chemical shifts (δ) in ppm ^a	¹³ C NMR Chemical shifts (δ) in ppm ^b
Diastereotopic methyls	1,42 and 1,56 (ss, 6H)	26.7, 21.0
Hydroxyl proton	3,42 (d, OH, J= 8.0 Hz)	-
C-5 methine	-	83.5
C-4 methine	5,09 (d, 1 H, J= 8.0 Hz)	87.5
Aromatics	7,16-7.60 (m, 4H)	134.2, 133.6, 132.2, 130.3, 128.6, 123.4
Carbonyl	-	155.6
^a : ¹ H NMR (400 MHz) data in CDCl ₃ (Figure A.38) ^b : ¹³ C NMR (100 MHz) data in CDCl ₃		

3.5.1.12. 4-Hydroxy-5,5-dimethyl-3-(*o*-iodophenyl)-2-oxazolidinone (55**).** The compound was prepared according to the general procedure using 0.20 g (0.60 mmole) compound (**±**)**11** in 1.9 ml THF (0,32 M), 0.091 g (2.42 mmole) sodium borohydride in 0.6 ml water (4,00 M). The white solid (0.13 g) was obtained with 65.53 per cent yield. Satisfactory NMR (¹H and ¹³C) (Table 3.45) and FTIR (3334, 3044, 2997, 2929, 1709 cm⁻¹) data were used to confirm the purity and structure of compound **55**.

Table 3.45. NMR data of compound **55**

	¹ H NMR Chemical shifts (δ) in ppm ^a	¹³ C NMR Chemical shifts (δ) in ppm ^b
Diastereotopic methyls	1,42 and 1,56 (ss, 6H)	27.0, 21.2
Hydroxyl proton	3,42 (d, OH, J= 8.0 Hz)	-
C-5 methine	-	83.6
C-4 methine	5,09 (d, 1 H, J= 8.0 Hz)	87.5
Aromatics	7,16-7.60 (m, 4H)	140.0, 137.3, 131.9, 130.6, 130.5, 129.6
Carbonyl	-	155.6
^a : ¹ H NMR (400 MHz) data in CDCl ₃ (Figure A.39) ^b : ¹³ C NMR (100 MHz) data in CDCl ₃ (Figure A.56)		

3.6. Asymmetric Alkylation and Aldol Reactions

3.6.1. General Procedure [13]

Reactions were carried out in a septum-capped, oven dried flask under nitrogen. To the solution of 5-Methyl-3-(*o*-aryl)-2,4-oxazolidinediones and 5-Methyl-3-(*o*-aryl)-2-thioxo-4-oxazolidinedione (0.16 M) in dry THF at -78°C was added lithium diisopropylamide (LDA) (2 M, 1.2 equivalent based on the oxazolidinedione). The reaction mixture was stirred for 1 hour for the enolate formation. Benzyl bromide, allyl bromide or benzaldehyde (2.0 equivalent based on oxazolidinedione) was added neat, and the reaction was quenched after completion by adding saturated ammonium chloride solution at 0°C (2 ml/ mmol of oxazolidinedione used). The solution was extracted with diethyl ether three times. The organic layer was dried (MgSO_4) and after evaporation of diethyl ether, the crude product was recrystallized by ethanol or ethyl acetate-hexane.

3.6.1.1. 5-Benzyl-5-methyl-3-(*o*-tolyl)-2,4-oxazolidinedione (**56**). The compound was prepared according to the general procedure using 0.30 g (1.46 mmole) compound **1** in 9.14 ml THF, (1.75 mmole) 0.88 ml LDA, 0.35 ml (2.92 mmole) benzyl bromide. After extraction with diethyl ether, compound **56** were obtained as white solid (0.22 g). Satisfactory NMR (^1H and ^{13}C) (Table 3.46) and FTIR (3030, 2930, 1815, 1740 cm^{-1}) data were used to confirm the purity and structure of compound **56**.

Table 3.46. NMR data of compound **56**

	^1H NMR Chemical shifts (δ) in ppm ^a	^{13}C NMR Chemical shifts (δ) in ppm ^b
C-5 methyls	1.80 (s, 3H), 1.29 (s, 3H)	23.8, 22.8
<i>o</i> -Methyls	2.13 (s, 3H), 1.80 (s, 3H)	17.5, 16.5
Methylenes	3.2-3.3 (2 AB quartets, 4H)	43.3, 42.7
Methines	-	87.0, 86.9
Aromatics	6.00-7.36 ppm (m), (18H)	136.5, 135.9, 133.4, 133.3, 131.5, 131.2, 130.8, 130.6, 130.10, 130.05, 129.6, 129.5, 129.1, 129.0, 128.2, 128.1, 127.9, 127.8, 127.2, 127.0
Carbonyls	-	174.1, 173.9, 153.30, 153.26
^a : ^1H NMR (400 MHz) data in CDCl_3 (for two diastereomers) (Figure A.40)		
^b : ^{13}C NMR (100 MHz) data in CDCl_3 (for two diastereomers) (Figure A. 57)		

3.6.1.2. 5-Benzyl-5-methyl-3-(*o*-iodophenyl)-2,4-oxazolidinedione (57). The compound was prepared according to the general procedure using 0.30 g (0.95 mmole) compound **3** in 5.9 ml THF, 0.57 ml (1.14 mmole) LDA, 0.23 ml (1.89 mmole) benzyl bromide. After extraction with diethyl ether, compound **57** were obtained as white solid (0.24 g). Satisfactory NMR (^1H and ^{13}C) (Table 3.47) and FTIR (3058, 3033, 2986, 2919, 1812, 1743 cm^{-1}) data were used to confirm the purity and structure of compound **57**.

Table 3.47. NMR data of compound **57**

	^1H NMR Chemical shifts (δ) in ppm ^a	^{13}C NMR Chemical shifts (δ) in ppm ^b
C-5 methyls	0.93 (s, 3H), 1.20 (s, 3H)	23.1, 22.6
Methylenes	2.86 and 2.63, 2.53 and 2.43 (2 AB quartets, 2 H each, J= 14.43 and 14.04 Hz)	43.3, 42.6
Methines	-	87.5
Aromatics	5.088-7.07 (m), (18H)	140.5, 139.9, 133.5, 133.3, 131.6, 131.3, 130.6, 129.7, 129.6, 129.4, 129.2, 128.97, 128.1, 97.9
Carbonyls	-	172.94, 172.88, 152.3
^a : ^1H NMR (400 MHz) data in C_6D_6 (for two diastereomers) (Figure A.41)		
^b : ^{13}C NMR (100 MHz) data in CDCl_3 (for two diastereomers) (Figure A. 58)		

3.6.1.3. 5-Benzyl-5-methyl-3-(*o*-iodophenyl)-2-thioxo-4-oxazolidinone (59). The compound was prepared according to the general procedure using 0.31 g (0.94 mole) compound **58** in 5.9 ml THF, 0.56 ml (1.13 mmole) LDA, 0.22 ml (1.88 mmole) benzyl bromide. After extraction with diethyl ether, compound **59** were obtained as white solid (0.28 g). Satisfactory NMR (^1H and ^{13}C) (Table 3.48) and FTIR (3083, 3031, 2987, 2923, 1768 cm^{-1}) data were used to confirm the purity and structure of compound **59**.

Table 3.48. NMR data of compound **59**

	¹ H NMR Chemical shifts (δ) in ppm ^a	¹³ C NMR Chemical shifts (δ) in ppm ^b
C-5 methyl	1.82 (s, 3H)	22.5
Methylenes	3.26 and 3.18 (1 AB quartet, 2H, J= 14.40)	43.6
Methine	-	90.8
Aromatics	5.93-7.80 ppm (m), (9H)	139.96, 135.3, 133.0, 131.6, 130.7, 129.8, 129.4, 128.96, 128.2, 97.9
Carbonyl	-	173.3
Thiocarbonyl	-	187.2
^a : ¹ H NMR (400 MHz) data in CDCl ₃ (for one diastereomer) (Figure A.43)		
^b : ¹³ C NMR (100 MHz) data in CDCl ₃ (for one diastereomer)		

3.6.1.4. 5-Allyl-5-methyl-3-(*o*-iodophenyl)-2-thioxo-4-oxazolidinone (**60**). The compound was prepared according to the general procedure using 0.34 g (1.0 mmole) compound **58** in 6.4 ml THF, 0.61 ml (1.23 mmole) LDA, 0.18 ml (2.0) allyl bromide. After extraction with diethyl ether, compound **60** were obtained as white solid (0.30 g). Satisfactory NMR (¹H and ¹³C) (Table 3.49) data were used to confirm the purity and structure of compound **60**.

Table 3.49. NMR data of compound **60**

	¹ H NMR Chemical shifts (δ) in ppm ^a	¹³ C NMR Chemical shifts (δ) in ppm ^b
C-5 methyl	1.73 (s, 3H)	22.4
Diastereotopic methylenes	2.64- 2.75 (m, 2H)	41.3
C-5 methine	-	89.8
Vynilic methylene	5.26 (d, 2H, J= 12 Hz)	122. 5
Vynilic methine	5.72-5.82 (m, 1H)	129.1
Aromatics	7.10-7.91 ppm (m), (4H)	140.3, 135.6, 131.8, 129.98, 129.95, 98.1
Carbonyl	-	173.8
Thiocarbonyl	-	187.6
^a : ¹ H NMR (400 MHz) data in CDCl ₃ (for one diastereomer) (Figure A.44)		
^b : ¹³ C NMR (100 MHz) data in CDCl ₃ (for one diastereomer) (Figure A.60)		

3.6.1.5. 5-(1-Hydroxybenzyl)-5-methyl-3-(*o*-iodophenyl)-2,4-oxazolidinedione (61). The compound was prepared according to the general procedure using 0.61 g (1.91 mmole) compound **3** in 11.96 ml THF, 1.15 (2.30 mole) LDA, 0.39 ml g (3.83 mmole) benzaldehyde. After extraction with diethyl ether, compound **61** were obtained as white solid (0.52 g). Satisfactory NMR (^1H and ^{13}C) (Table 3.50) and FTIR (3564, 3065, 2990, 2934, 2897, 1812, 1743 cm^{-1}) data were used to confirm the purity and structure of compound **61**.

Table 3.50. NMR data of compound **61**

	^1H NMR Chemical shifts (δ) in ppm ^a	^{13}C NMR Chemical shifts (δ) in ppm ^b
C-5 methyls	1.89 (s, 3H) and 1.71 (s, 3H)	19.5, 19.3
Hydroxyl proton	2.68 (s, br, 2H)	-
Benzylic methines	5.17 (s, 1H) and 5.02(s, 1H)	76.7, 75.9
C-5 methines	-	89.1, 87.8
Aromatics	6.24-7.93 ppm (m), (18H)	140.6, 140.1, 139.98, 137.0, 136.9, 136.6, 133.8, 133.7, 133.3, 131.8, 129.98, 129.8, 129.7, 129.6, 129.5, 129.4, 129.2, 128.95, 128.4, 128.3, 127.98, 127.8, 97.9, 97.3
Carbonyls	-	173.8, 171.97, 152.6, 152.4
^a : ^1H NMR (400 MHz) data in CDCl_3 (for two diastereomers) (Figure A.45)		
^b : ^{13}C NMR (100 MHz) data in CDCl_3 (for two diastereomers) (Figure A.61)		

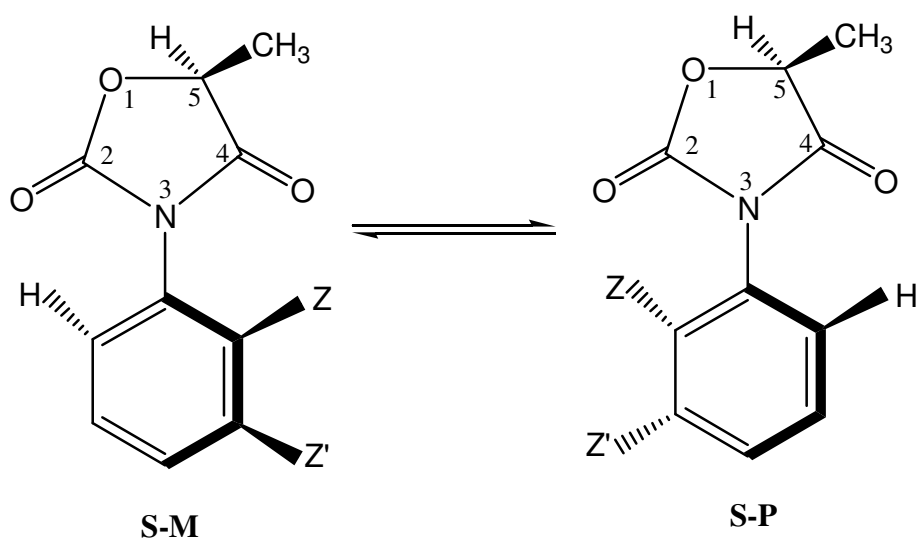
3.6.1.7. 5-(1-Hydroxybenzyl)-5-methyl-3-(*o*-iodophenyl)-2-thioxo-4-oxazolidinone (62). The compound was prepared according to the general procedure using 0.4 g (1.20 mmole) compound **58** in 7.5 ml THF, 0.72 ml (1.44 mmole) LDA, 0.24 ml (2.40 mmole) benzaldehyde. After extraction with diethyl ether, compound **62** were obtained as white solid (0.36 g). Satisfactory NMR (^1H and ^{13}C) (Table 3.51) and FTIR (3400, 3060, 2979, 1769 cm^{-1}) data were used to confirm the purity and structure of compound **62**.

Table 3.51. NMR data of compound **62**

	¹ H NMR Chemical shifts (δ) in ppm ^a	¹³ C NMR Chemical shifts (δ) in ppm ^b
C-5 methyls	1.86 (s, 3H) and 1.54 (s, 3H)	19.4, 19.3
Hydroxyl proton	2.56 (s, br, 2H)	-
Benzylic methines	4.96 (s, 2H)	76.7, 75.9
C-5 methines	-	92.2, 90.98
Aromatics	6.11-7.90 ppm (m), (18H)	140.1, 140.0, 136.8, 136.7, 135.7, 135.2, 134.6, 131.8, 131.7, 129.96, 129.8, 129.7, 129.6, 129.4, 129.2, 129.0, 128.9, 128.6, 128.5, 128.4, 128.2, 127.9, 98.1, 97.9
Carbonyls	-	173.7, 172.3
Thiocarbonyls	-	188.0, 187.2
^a : ¹ H NMR (400 MHz) data in CDCl ₃ (for two diastereomers) (Figure A.46) ^b : ¹³ C NMR (100 MHz) data in CDCl ₃ (for two diastereomers)		

4. RESULTS AND DISCUSSION

4.1. Conformational Preferences in Diastereomeric (5*S*)-Methyl-3-(*o*-aryl)-2,4-oxazolidinediones [14]



- 1, Z= CH₃, Z' = H
- 2, Z, Z' = benzo
- 3, Z= I, Z' = H
- 4, Z=Br, Z' = H
- 5, Z= Cl, Z' = H
- 6, Z= F, Z' = H

Figure 4.1. Diastereomeric (5*S*)-methyl-3-(*o*-aryl)-2,4-oxazolidinediones

4.1.1. ¹H NMR

Compounds **1**, **2**, **3**, **4** and **5** have been obtained as mixtures of unequal composition of two diastereomers which were differentiated by their ¹H NMR spectra. It has been observed that ratios of the produced diastereomers were 43.0 %:57.0 %, 46.8 %:53.2 %, 77.0 %:23.0 %, 31.4 %: 68.6 %, 41.2 %:58.8 % for compounds **1**, **2**, **3**, **4** and **5**, respectively.

For all these compounds, it has been observed that at equilibrium the minor diastereomer had its C-5 proton signal (quartet) at a lower field, whereas its C-5 methyl proton signal (doublet) at a higher field than that of the major component (Figure 4.2, Table 4.1). The diastereomers of compound **6** were only observable in CD₃OD at 30 °C which were also present in unequal amounts. Since the only difference between the diastereomers **S-M** and **S-P** (Figure 4.1) is the position of the aryl ring with respect to the heterocyclic ring, it was thought that NMR could be used to determine the stereostructures of the major and the minor components. In these stereostructures, the anisotropy of the *o*-halo substituents has different effects on magnetic environments of C-5 methyl and C-5 hydrogen. Thus, the lower intensity of the quartets and the higher intensity of the doublets are more deshielded with respect to the other one. Due to the increasing atomic radius in the Cl, Br, I series, the dihedral angle between the two rings also increases which makes the halogen atom approach closer to the methyl or methine hydrogen giving rise to a greater diamagnetic shift [15]. Thus, the largest difference has been observed for the *o*-iodine and the smallest in *o*-chlorine derivative among compounds **3**, **4** and **5** (Figure 4.2 and Table 4.1)

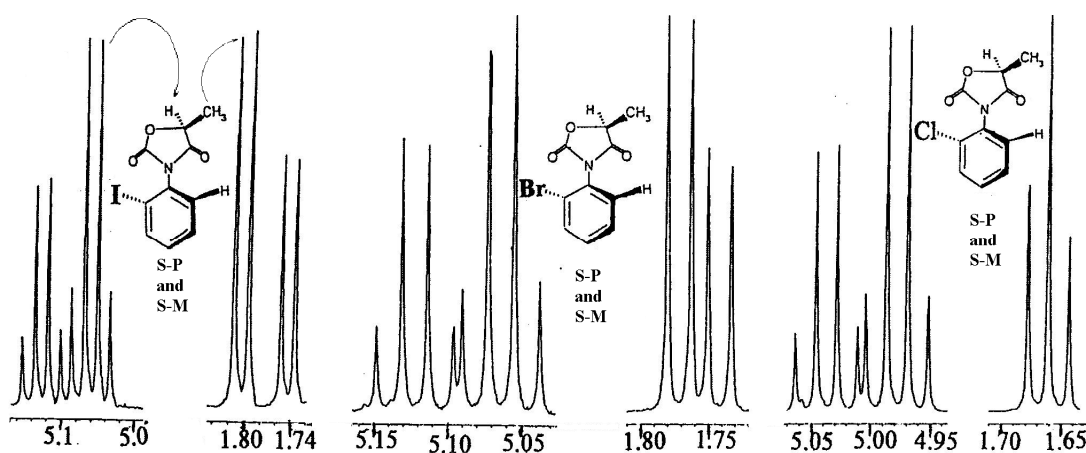


Figure 4.2. 400 MHz ¹H NMR signals of C-5 hydrogen and methyl protons of diastereomers of compounds a) **3**, b) **4**, c) **5**, in CDCl₃ at 30 °C, at equilibrium

Table 4.1. The 400 MHz ^1H NMR chemical shift values of the compounds in different solvents at 30 °C

	δ , (ppm) C-5 methyl ^a	δ , (ppm) C-5 methine ^a	δ , (ppm) aromatics	δ , (ppm) <i>o</i> -methyl ^a
1				
CDCl_3	1.72	5.05 and 5.08	7.1-7.4	2.1 and 2.3
Pyridine- d_5	0.31 and 0.33	4.02 and 4.20	5.8-6.3	0.90 and 0.92
2				
CDCl_3	1.75 and 1.80	5.10 and 5.20	7.4-8.0	
DMSO-d_6	1.65 and 1.75	5.30 and 5.50	7.5-8.1	
3				
CDCl_3	1.74 and 1.81	5.06 and 5.13	7.16-8.0	
Pyridine- d_5	0.32 and 0.43	4.05 and 4.25	5.7-6.8	
4				
CDCl_3	1.74 and 1.77	5.06 and 5.12	7.2-7.8	
Pyridine- d_5	0.43 and 0.49	4.18 and 4.39	5.9-6.6	
C_6D_6	0.77 and 0.89	3.85 and 3.95	6.2-6.9	
CD_3OD	1.56 and 1.57	5.1 and 5.2	7.3-7.7	
5				
CDCl_3	1.65 and 1.67	4.98 and 5.04	7.2-7.5	
Pyridine- d_5	0.49 and 0.52	4.25 and 4.46	6.0-6.6	
DMSO-d_6	1.63 and 1.68	5.36 and 5.56	7.5-7.8	
C_6D_6	0.7 and 0.9	3.85 and 3.95	6.3-6.8	
CD_3OD	1.67 and 1.69	5.22 and 5.32	7.4-7.7	
6				
CDCl_3	1.73 ^b	5.08 ^b	7.2-7.5	
CD_3OD	1.40 and 1.54	4.96 and 5.11	6.9-7.7	
Acetone- d_6	1.60 ^b	5.25 ^b	7.25-7.60	
^a : Two values refer to two diastereomers				
^b : Only one doublet and quartet were observed				

This kind of shift difference was also found to show a solvent dependence. In Table 4.1 the ^1H NMR chemical shift values are reported. Compared to CDCl_3 , aromatic solvents (C_6D_6 and pyridine- d_5) give rise to a larger chemical shift difference for the quartets and the doublets. The difference for $\text{DMSO-}d_6$ is also greater than that of CDCl_3 . This may be resulting from the carbonyl-solvent or phenyl ring-solvent π - π interactions. Depending on the orientation of the solvent brought about by these groups, C-5 methyl and methine hydrogens may be affected differently. For compound **6**, the chemical shift difference between the diastereomers was observable only in CD_3OD probably because of the deuterium-fluorine association.

Compound **1** has two hardly resolved doublets due to the methyl protons at C-5, two singlets due to two *ortho* methyl protons and two quartets due to the proton at C-5 of the heterocyclic ring. The diastereomer ratio at equilibrium is 57.0 % to 43.0 %. The more deshielded of the *ortho* methyl singlets, the more deshielded of the C-5 proton quartets and the slightly more shielded of the doublets belong to the diastereomer with lower concentration.

The NOESY spectrum of this compound shows that (Figure 4.3) the lower intensity *ortho* methyl has a cross peak (a) with the lower intensity C-5 methyl. The higher intensity *ortho* methyl on the other hand shows NOE relationships only to aromatic protons as (b). The lower and the higher intensity quartets at 5.0 and 5.2 ppm due to the C-5 protons have the expected cross peaks with the lower and higher intensity doublets respectively at around 1 ppm (c). Because the higher intensity C-5 methyl signal has a cross peak with a proton in the aromatic region (d) (probably the *ortho* proton), the major component is assigned to **S-P** and the minor to **S-M** isomer (Figure 4.3).

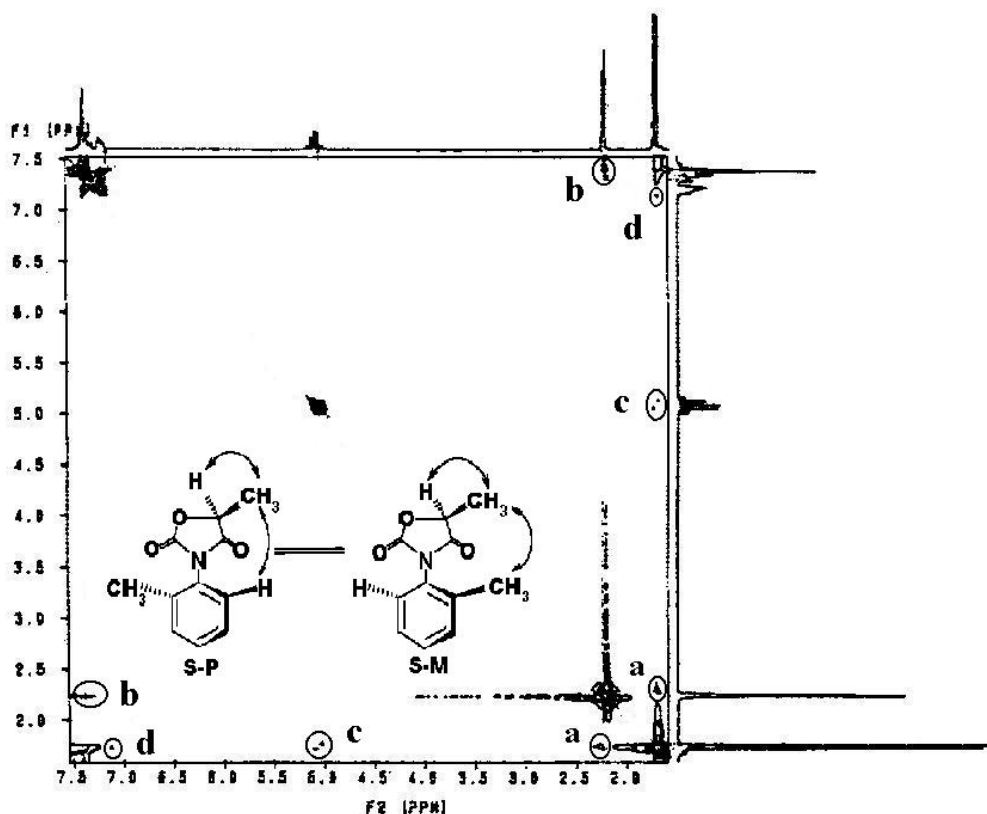


Figure 4.3. The 2D NOESY spectrum of compound 1

From the ¹H NMR spectrum of compound 2, diastereomeric yield was found as 46.8 % and 53.2 %. In order to determine the conformation of the excess conformer 2D NOESY experiment was used. We expected to see a through-space proximity between C-5 methyl and C-8 naphthyl proton. The 2D NOESY spectrum (Figure 4.4) showed that the low-intensity doublet at 1.78 ppm has a cross peak with the signal at 7.53 ppm. In order to prove that the signal at 7.53 ppm corresponds to the C-8 naphthyl proton the HMQC spectrum was used (Figure 4.5). In ¹H NMR of 2, between 7.4 ppm and 8.0 ppm there are fourteen protons corresponding to naphthyl protons of the two diastereomers. The doublet at 7.97 ppm, the doublet of doublets at 7.92 ppm, the multiplet at 7.62 ppm, the multiplet at 7.50-7.58 ppm and the multiplet at 7.43 ppm correspond to two, two, one, seven and two protons, respectively. It was thought that the signal at 7.62 ppm might be the C-8 naphthyl proton of one diastereomer and the other C-8 naphthyl proton signal was under the multiplet that appeared between 7.50 and 7.58 ppm. These two protons can be observed separately and not the others because these are the protons whose magnetic environments are most affected by the hindered rotation. Furthermore, two different carbon signals for C-8 of each

diastereomer were observed in the HMQC spectrum (Figure 4.5) at 121.9 and 121.5 ppm which correlated to signals at 7.53 ppm within the multiplet at 7.50-7.58 ppm and 7.62 ppm. Again due to the hindered rotation magnetic environment of the diastereomeric C-8 carbons can be observed separately.

The crosspeaks corresponding to the low intensity doublet and the C-8 naphthyl proton gave a conclusive proof of the **S-M** conformation produced in lower amount. **S-P** conformer is slightly more preferred than **S-M** conformation.

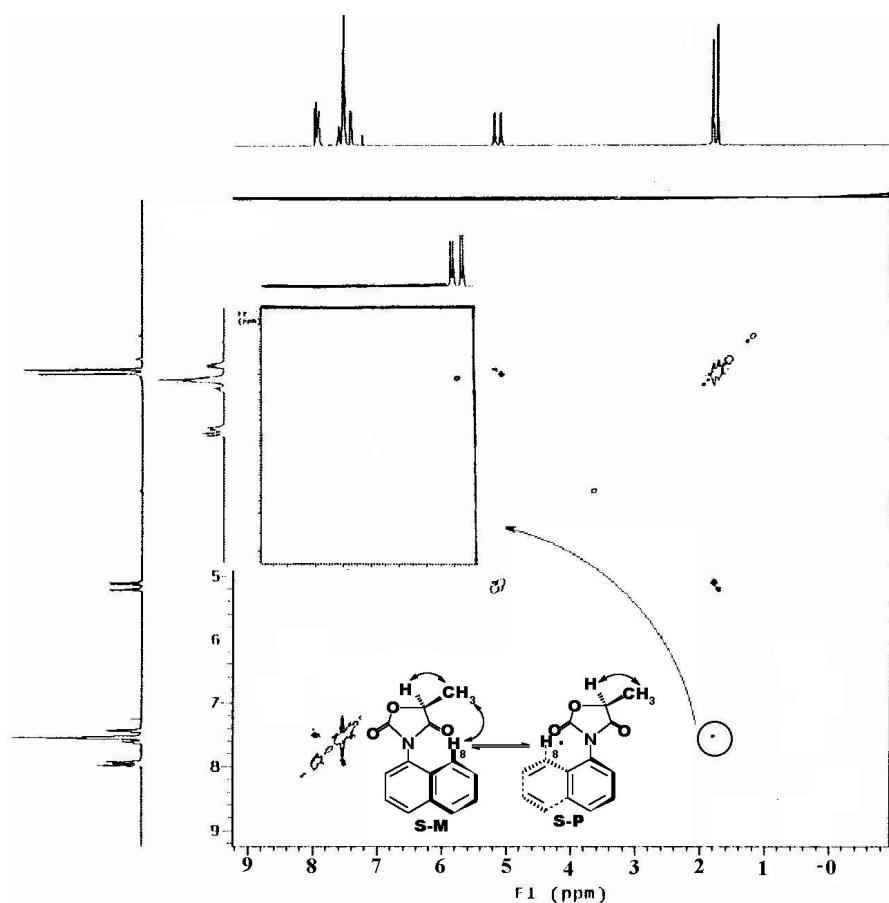


Figure 4.4. The 2D NOESY spectrum of compound **2**. The inset shows the partly enlarged spectrum where the correlation of C-8 proton at 7.53 ppm with the lower intensity C-5 methyl at 1.78 ppm is seen

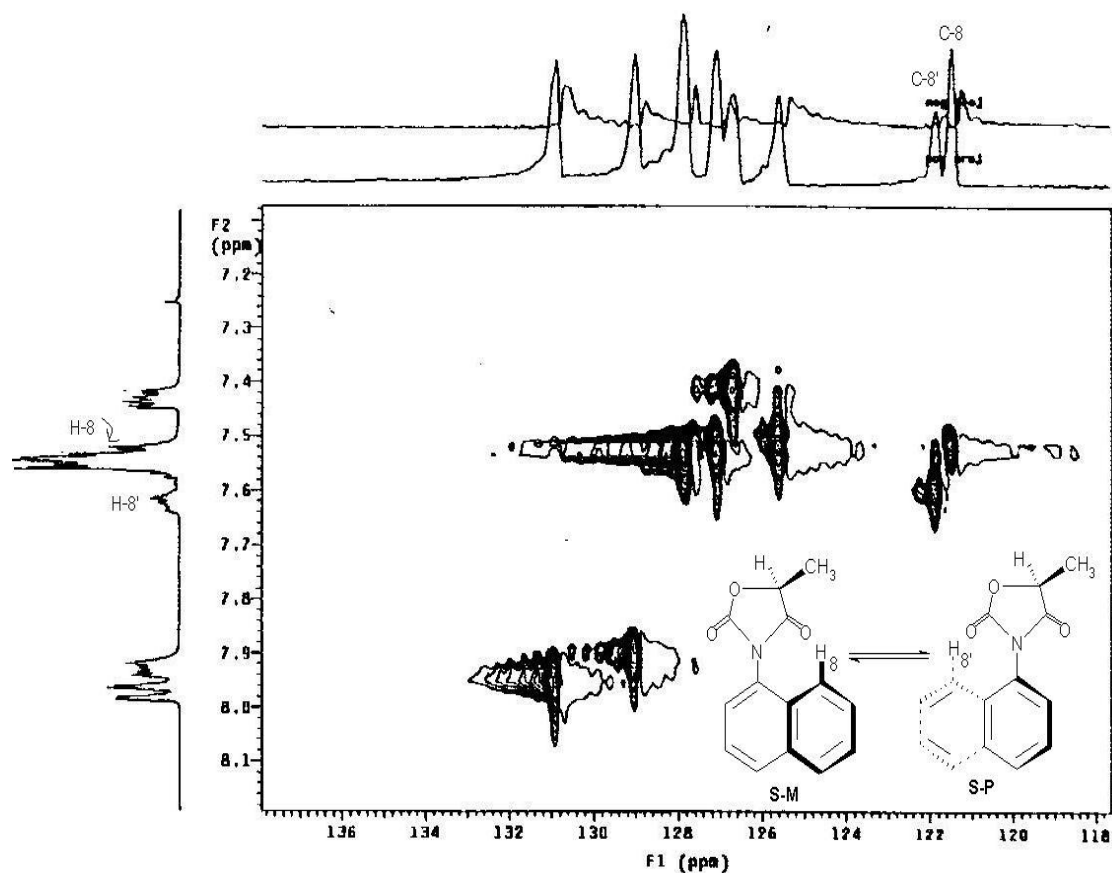


Figure 4.5. The HMQC spectrum of compound **2**

Compound **3** was also obtained as an unequal isomer composition of the two diastereomers. From the intensity values in ^1H NMR spectrum, the percentage values at equilibrium were found as 63.65 % and 36.35 %. An examination of the cross peaks at 6.33 ppm and 0.5 ppm in 2D NOESY diagram (Figure 4.6) indicates the spatial proximity of the *ortho* proton and C-5 methyl protons of the higher intensity diastereomer. This is consistent with the structure of **S-P** conformation. It was thought that the signals at 6.33 and 6.26 ppm which appeared as doublet of doublets belong to the aromatic *ortho* protons of the two diastereomers because during the kinetic study we observed a change in the intensity values of these signals (Figure 4.7). The equilibrium ratio of these signals was also 63.65% to 36.35%.

Based on these results, it was concluded that at equilibrium the higher intensity signals which appeared at 6.33 and 0.5 ppm belong to the **S-P** conformer.

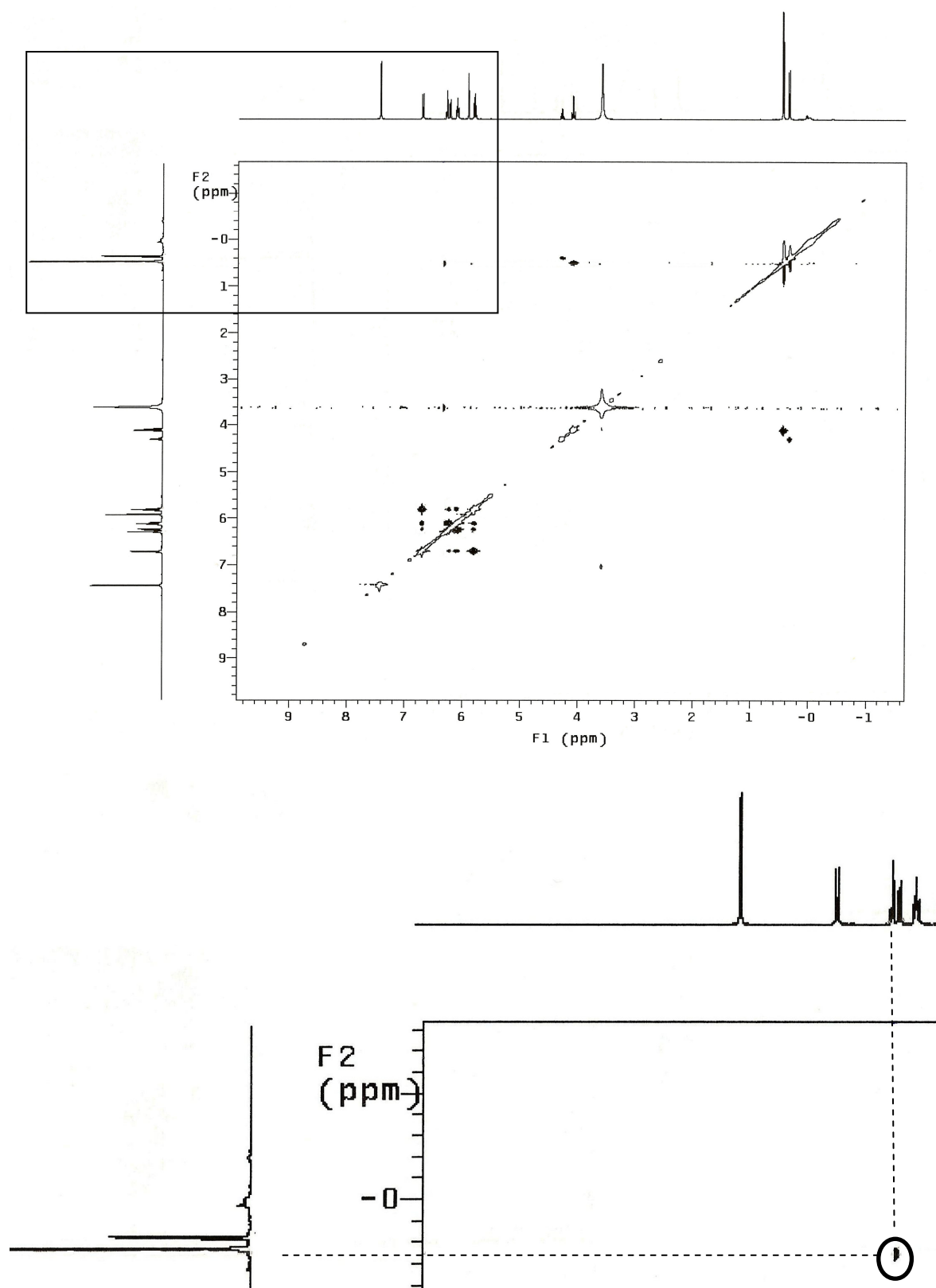


Figure 4.6. The 2D NOESY spectrum of compound **3**. The inset shows the partly enlarged spectrum where the correlation of *ortho* proton at 6.33 ppm with the higher intensity C-5 methyl at 0.5 ppm is seen

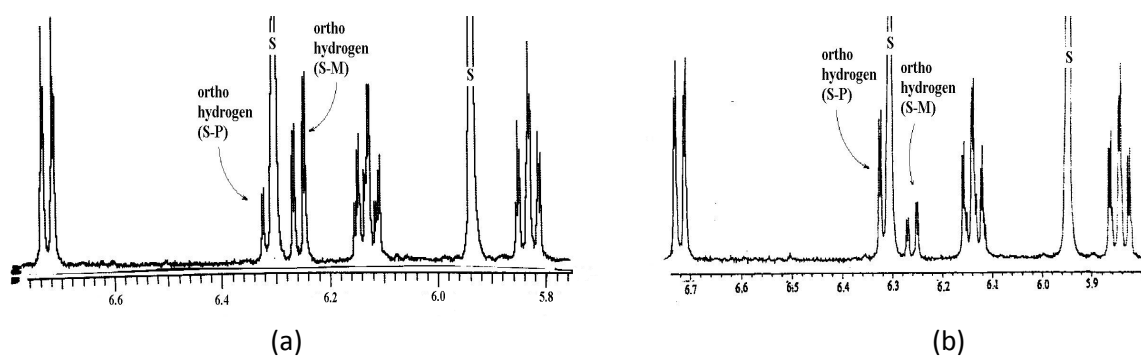


Figure 4.7. The partial ^1H NMR spectrum of the aromatic region of compound **3** a) before equilibrium, b) at equilibrium, S= solvent= pyridine- d_5

4.1.2. The Thermal Interconversion Process of the Diastereomers of **3**, **4** and **6** by NMR

The work-up procedures of compounds **3** and **4** produced products with diastereomeric yields of 23.0 % (**S-P**), 77.0 % (**S-M**) and 68.6 % (probably **S-P**), 31.4 % (probably **S-M**), respectively determined by ^1H NMR in CDCl_3 . When the solutions prepared in CDCl_3 were kept at constant probe temperatures (30 °C for **3** and 15 °C for **4**) a thermal interconversion of conformer **S-M** to **S-P** was observed until equilibrium (thermal enrichment of **S-P**). This reversible first order process is followed by taking ^1H NMR spectra at certain time intervals. The slope of first order plots of $\ln ([A]_t - [A]_{\text{eq}} / [A]_0 - [A]_{\text{eq}})$ versus time [16] yielded the rate constants ($k_f + k_r$), where $[A]_t$ = the concentration of one isomer at time t , $[A]_{\text{eq}}$ = the equilibrium concentration, $[A]_0$ = the starting concentration, k_f = the rate constant for the forward reaction, k_r = the rate constant for the reverse reaction (Equation 4.1). When this data was combined with that calculated from equilibrium constant $K = k_f/k_r$, the values for the rate constants were obtained. The free energy of activation (the energy barrier for interconversion in Figure 4.1) was calculated using the Eyring Equation (Equation 4.2), where $R = 8.3143 \text{ J/mol.K}$, T = temperature (Kelvin) at which the interconversion took place, k_b (Boltzmann constant) = $1.3805 \cdot 10^{-23} \text{ J/K}$, h (Planck constant) = $6.6256 \cdot 10^{-34} \text{ J.s}$, k_f = the rate constant for the forward reaction. The kinetic data are given in Table II.

$$\ln ([A] - [A]_{\text{eq}} / [A]_0 - [A]_{\text{eq}}) = -(k_f + k_r)t \quad (4.1)$$

$$\Delta G_{\text{,forward}}^{\#} = RT \ln(k_b \cdot T / k_f \cdot h) \quad (4.2)$$

The ^1H NMR spectrum of **6** taken in CDCl_3 showed only one quartet (5.08 ppm) and one doublet (1.73 ppm) due to fast rotation. However, in methanol- d_4 , two quartets and two doublets were observed with a ratio of 52.6 % to 47.4% at 30 $^\circ\text{C}$. After kept at constant temperature of 15 $^\circ\text{C}$, one diastereomer was converted to the other one. This process was followed by taking the ^1H NMR spectra in methanol- d_4 at constant probe temperature (15 $^\circ\text{C}$). The kinetic data are given in Table 4.2. The methanol- d_4 probably formed an association complex with the fluorine which increased the barrier to rotation to make the diastereomers observable separately by NMR.

The diastereomers of *ortho*-chloro derivative (**5**) were found to be already at equilibrium in CD_3OD observed by NMR ($K= 1.82$ at 15 $^\circ\text{C}$).

Table 4.2. The kinetic data of the interconversion process (**S-M** \rightleftharpoons **S-P**) of compounds **3**, **4**, **6**

Compound No	3 ^a	4 ^a	6 ^b
Starting Composition, %	23.0, 77.0	68.6, 31.4	52.6, 47.4
Equilibrium composition, %	63.6, 36.4	57.2, 42.8	36.5, 63.5
K^c	1.8	1.3	1.7
k_f , (s^{-1})	$5.7 \cdot 10^{-4}$	$4.0 \cdot 10^{-4}$	$5.1 \cdot 10^{-4}$
k_r , (s^{-1})	$3.3 \cdot 10^{-4}$	$2.99 \cdot 10^{-4}$	$2.9 \cdot 10^{-4}$
ΔG_f , (kJ/mol)	93.1	89.2	88.6
ΔG_r , (kJ/mol)	94.5	89.9	89.9
^a : solvent= CDCl_3 , ^b : solvent= CD_3OD , ^c : $K= [\text{S-P}]/[\text{S-M}]$			

4.1.3. Determination of Activation Barriers by Temperature Dependent NMR

Activation barriers to hindered rotation about C-N single bond of compounds **1**, **2** and **6** were determined using the Eyring equation [17,18] for the unequal intensity diastereomers (Equation 4.3), where Δn is the difference in mole fractions of the two diastereomers at equilibrium. The data of **1** is in good agreement with the previously found value [3] of 76.6 kJ/mol which reported an average value of rate constant and the barrier, whereas we report the values for forward and reverse processes for interconversion of **S-M**

to **S-P** as 74 and 75.2 kJ/mol, respectively. The barrier found for the α -naphthyl derivative (**2**) as 91.4 and 91.8 kJ/mol (Table 4.3) is higher than the average value found for the same compound in reference 3 as 79.5 kJ/mol in pyridine- d_5 . The difference may be due to the solvent effect. Figure 4.8 shows the temperature dependent NMR spectrum of compound **6** which yielded a barrier of 54.7 kJ/mol in acetone- d_6 (Table 4.3). The rate constants and the barriers found have been summarized in Table 4.3.

$$k_A = (1 + \Delta n) \text{ and } k_B = (1 - \Delta n) \quad (4.3)$$

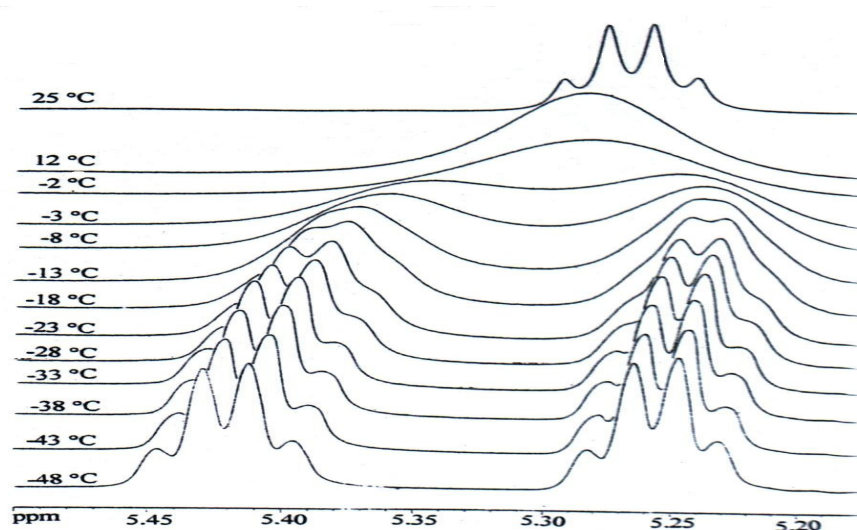


Figure 4.8. The temperature dependent NMR spectra of **6** in acetone- d_6

Table 4.3. The data for the determination of activation barriers

Compound	1 in pyridine- d_5	2 in DMSO- d_6	6 in acetone- d_6
T, (K)	338	408	270
Δn	0.2	0.06	0
k_f , (s^{-1})	24.9	16.4	145.17 ^a
k_r , (s^{-1})	16.6	14.6	
ΔG_f , (kJ/mol)	74.0	91.4	54.7 ^b
ΔG_r , (kJ/mol)	75.2	91.8	
^a : Average rate constant at coalescence			
^b : Average free energy of activation			

4.1.4. The Thermal Interconversion of the Diastereomers of **4** by HPLC

The synthesis of (5*S*)-methyl-3-(*o*-bromophenyl)-2,4-oxazolidinedione (**4**) yielded a 37.5 %:62.5 % mixture of **S-P** to **S-M** diastereomers as determined by HPLC on Chiralcel OD-H in ethanol. When this mixture was kept in a constant temperature bath, it was observed that the **S-M** gradually converted to **S-P** until equilibrium (Figure 4.9). For compound **4** a direct NOE effect could not be observed between substituents at C-5 and the *ortho* hydrogen. However, **S-M** and **S-P** conformers were assigned to the diastereomers of **3** by the NOESY experiment. By analogy, we assigned **S-P** to the higher equilibrium concentration diastereomer of **4**. The dihedral angle between the two rings may be affecting the NOESY experiments of compounds **3** and **4**. The thermal interconversion of the diastereomers was followed by taking samples from a solution of non-equilibrium composition kept in a constant temperature bath at certain time intervals and injecting to HPLC. The chromatograms taken on Chiralcel OD-H column using UV detection at 240 nm gave the subsequent ratios of the diastereomers. At equilibrium, it has been observed that **S-P** concentration exceeded that of **S-M** with **S-M** to **S-P** ratio of 30.92%:69.08%, 23.7%:76.3% and 18.2%:81.8% at 40 °C, 50 °C and 60 °C, respectively (Figure 4.9).

Based on these observations, we concluded that the **S-M** conformation that was formed dominantly during the reaction was the less stable conformer and it could be formed via a kinetically controlled pathway (Figure 4.10). Since a thermal interconversion of **S-M** to **S-P**, via rotation about C-N single bond was observed, the **S-P** conformation was considered more stable which led to its thermodynamic enrichment.

The thermodynamic enrichment of **S-P** of **4** was also observed by NMR in CDCl₃. In ethanol by HPLC, it was found that at the beginning the concentration of **S-M** exceeded that of **S-P** and but at equilibrium the **S-P** concentration was higher. However in CDCl₃ observed by NMR, the **S-P** conformer which already was greater than the **S-M** initially kept increasing until equilibrium. Infact a lower barrier (89 kJ/mol) was determined for that compound in CDCl₃ by NMR whereas 100 kJ/mol has been observed by HPLC in ethanol. Apparently, during the acquisition period when taking the ¹H NMR spectrum, some **S-M** had been converted to the **S-P** due to the faster rotation of this compound with respect to that in ethanol solution. Hydrogen bonding between ethanol and **4** may have

increased the barrier up to about 100 kJ/mol and made the diastereomers stable at room temperature. This indicates a large solvent dependence of the barriers to rotation of these compounds as far as hydrogen bonding solvents are concerned

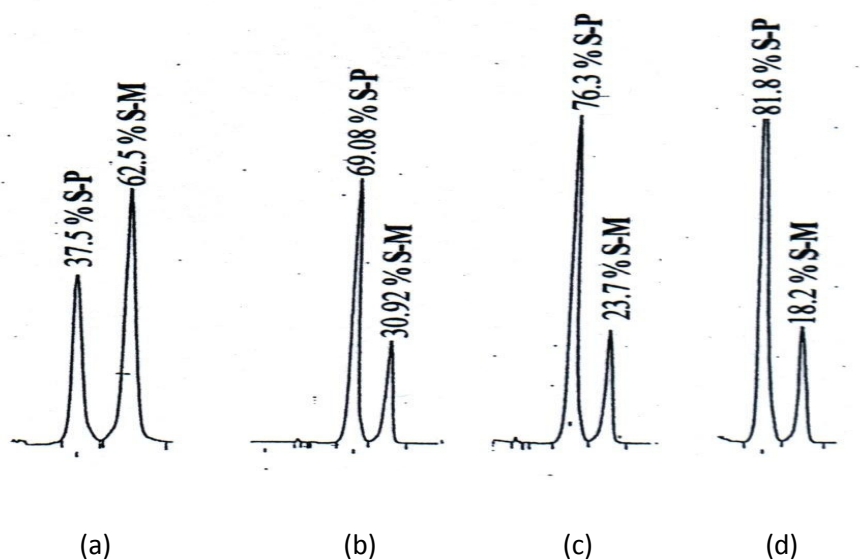


Figure 4.9. HPLC chromatograms of compound **4** on chiralcel OD-H column. Eluent: Hexane: ethanol (80:20) (v:v), UV detection at 240nm. Numbers written on the peaks show the percentages of the **S-P** or **S-M** conformations of the two diastereomers a) initial composition obtained from the synthesis, b) equilibrium composition at 40 °C, c) equilibrium composition at 50 °C, d) equilibrium composition at 60 °C

In order to explain the kinetically controlled pathway, a diastereoselective π -facial addition to the carbonyl was considered. During the ring closure step, the carbonyl group of the molecule (Figure 4.10) has two diastereotopic faces. The nucleophilic nitrogen was thought to approach the ester carbonyl preferentially from the less hindered face to minimize the steric repulsion of the C-5 methyl group, thus forming preferentially the **S-M** conformation.

Compounds **1**, **2**, **3**, **5** and **6** were also studied by HPLC. The diastereomers of **1**, **2** and **5** could be separated when the eluent was ethanol, ethanol-hexane or 2-propanol-hexane mixtures. Due to the lower activation barriers of compounds **1**, **2** and **5**, it was observed that they were already in equilibrium, ie. the kinetic product **S-M** was already interconverted to thermodynamic product **S-P** during work-up procedure. Therefore the

thermodynamic enrichment of **S-P** from **S-M** could not be observed. Compound **3** could be observed as two separate diastereomers both in ethanol-hexane and 2-propanol-hexane mixtures. However due to its reaction with ethanol under reflux, the activation barrier could not be determined. The diastereomers of compound **6** were observable in 2-propanol-hexane mixtures, however since the ratio was found as 1:1.

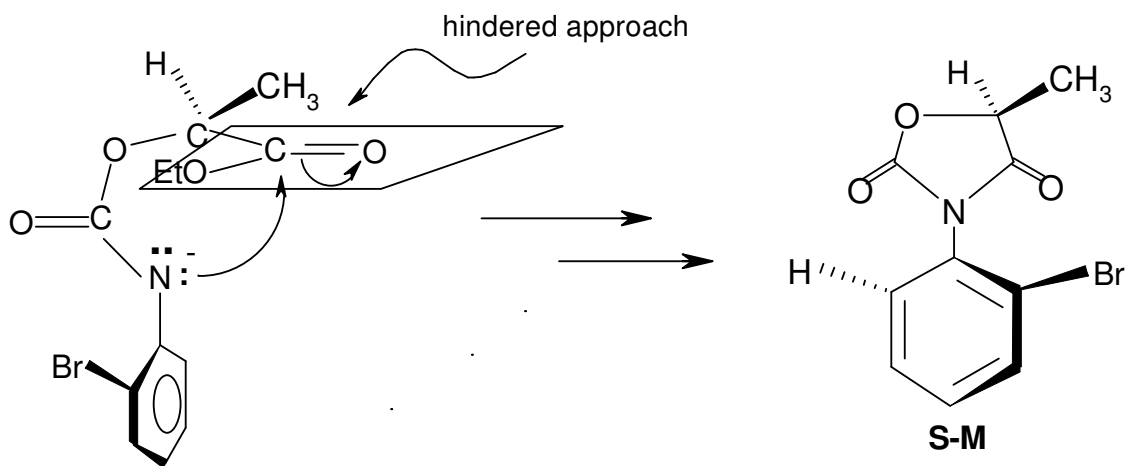


Figure 4.10. The ring closure leading to the **S-M** conformation

4.1.5. Kinetic and Thermodynamic Constants of **4**

The forward and reverse rate constants (k_f and k_r) and equilibrium constants ($K = k_f / k_r$) were determined for the interconversion of **S-M** to **S-P** at three different temperatures (40 °C, 50 °C, 60 °C) (Table 4.4). ΔG° , the free energy difference between the diastereomers, was calculated using the equilibrium constant values (Equation 4.4).

$$\Delta G^\circ = -RT \ln K = \Delta H^\circ - T \Delta S^\circ \quad (4.4)$$

The standard enthalpy change, ΔH° and the standard entropy change, ΔS° were determined from the slope and the intercept respectively, of the plot of $\ln K$ versus $1/T$, assuming that ΔH° and ΔS° are constant in the temperature range studied (Equation 4.5).

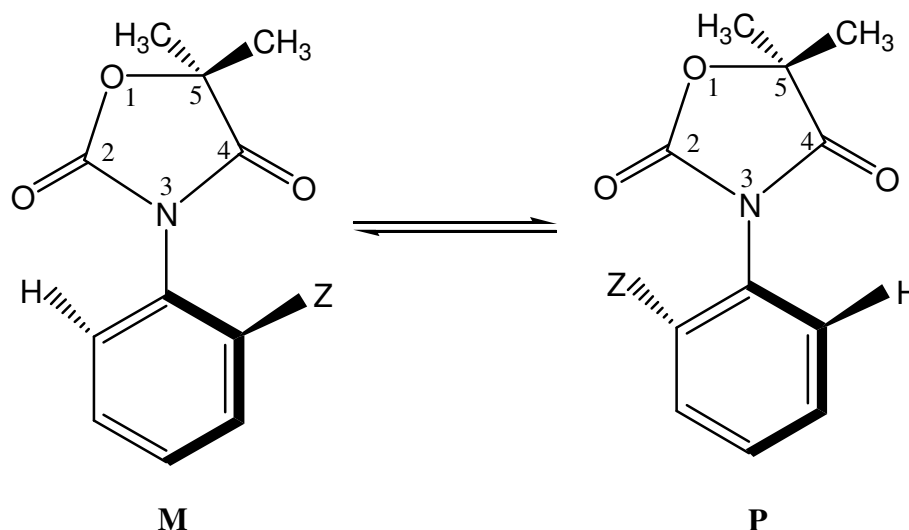
$$\ln K = -\Delta H^\circ / RT + \Delta S^\circ / R \quad (4.5)$$

The samples were kept in a constant temperature bath and HPLC chromatograms with UV detection were taken at several time intervals. The integration of the UV signals in HPLC chromatograms yielded the ratio of the diastereomers. The rate constants were obtained using the ratios of the diastereomers taken at certain time intervals at a constant temperature, based on reversible first order reaction kinetics [16]. ΔG^\ddagger for the interconversion between the rotational isomers has been determined using the values of the rate constants in the Eyring equation and it was found around 100 kJ/mol at 40 °C and 50 °C, which enabled the rotational isomers of compound **4** to be separable at room temperature. The results are presented in Table 4.4.

Table 4.4. Kinetic and thermodynamic constants of the internal rotation in compound **4**

kinetic/thermodynamic constants for $M \rightleftharpoons P$	40 °C	50 °C	60 °C
$k_f, (s^{-1})$	$6.9 \cdot 10^{-5}$	$2.3 \cdot 10^{-4}$	-
$k_r, (s^{-1})$	$3.1 \cdot 10^{-5}$	$7.1 \cdot 10^{-5}$	-
$\Delta G^\ddagger, (kJ/mol)^a$	101.7	101.8	-
$\Delta G^\ddagger, (kJ/mol)^b$	103.8	105	-
$\Delta G^o, (kJ/mol)$	-2.1	-3.1	-
K	2.2	3.2	4.5
$\Delta H^o, (kJ/mol)$	30.5	-	-
$\Delta S^o, (J/K.mol)$	104.2	-	-
^a : Forward direction; ^b : reverse direction			

4.2. Determination of Energy Barriers to Rotation and Absolute Conformations of Thermally Interconvertible 5,5-Dimethyl-3-(*o*-aryl)-2,4-oxazolidinedione Enantiomers [19]



(±) **7**, Z= CH₃

(±) **8**, Z= F

(±) **9**, Z= Cl

(±) **10**, Z= Br

(±) **11**, Z= I

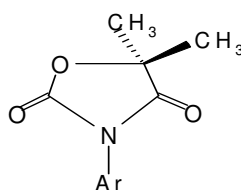
Figure 4.11. Enantiomeric 5,5-dimethyl-3-(*o*-aryl)-2,4-oxazolidinediones

4.2.1. ¹H and ¹³C NMR

The rotational isomers of 5,5-Dimethyl-3-(*o*-aryl)-2,4-oxazolidinediones (Figure 4.11) are enantiomeric and expected to exhibit identical NMR spectra in an achiral solvent. However, the methyl protons on the C-5 position of the heterocyclic ring, because of the presence of a C_{aryl}-N_{sp2} chiral axis, are diastereotopically related, and should be, in principle, magnetically non-equivalent provided that the rate of internal rotation is slow on the NMR time scale. Analysis of the ¹H NMR spectra did indicate the existence of diastereotopic protons. The two methyl groups on the C-5 of the heterocyclic moiety in compounds (±) **7**, (±) **9**, (±) **10** and (±) **11** gave two separate singlets with chemical shift

differences of 0.02 ppm, 0.09 ppm, 0.12 ppm and 0.2 ppm, respectively in C₆D₆ (Table 4.). The diastereotopic methyl groups also exhibited unequal shifts of ¹³C nuclei in C₆D₆, the shift differences being equal to, 0.7 ppm, 0.9 ppm, 0.9 ppm and 0.5 ppm, respectively (Table 4.5).

Table 4.5 ¹H and ¹³C NMR spectral data for the synthesized compounds in the presence and absence of the optically active auxiliary, (S)-TFAE at 30 °C



Entry	Ar	Medium	¹ H NMR, ppm, C-5 methyl	¹ H NMR, ppm, <i>o</i> -methyl	¹³ C NMR, ppm, C-5 methyl
(±) 7	<i>o</i> -tolyl	C ₆ D ₆ C ₆ D ₆ +(S)-TFAE ^a	1.15 and 1.17 ^c 1.06, 1.08, 1.09 ^c	1.97 1.88, 1.89 ^c	23.0, 23.7
(±) 8	<i>o</i> - fluorophenyl	C ₆ D ₆ Acetone-d ₆ C ₆ D ₆ +(S)-TFAE ^b	1.11 ^c 1.68 and 1.69 ^{d,e} 1.05 and 1.06 ^c	- - -	23.3 - -
(±) 9	<i>o</i> - chlorophenyl	C ₆ D ₆ DMSO C ₆ D ₆ +(S)-TFAE ^b	1.16 and 1.25 ^c 1.64 and 1.69 ^c 1.10, 1.11, 1.20, 1.21 ^c	- - -	22.9, 23.8 - -
(±) 10	<i>o</i> - bromophenyl	C ₆ D ₆ DMSO C ₆ D ₆ +(S)-TFAE ^b	1.19 and 1.31 ^c 1.71 and 1.75 ^d 1.12, 1.13, 1.26 ^{c,f}	- - -	22.9, 23.8 - -
(±) 11	<i>o</i> - iodophenyl	C ₆ D ₆ DMSO CDCl ₃ CDCl ₂ CDCl ₂ C ₆ D ₆ +(S)-TFAE ^a CDCl ₃ +TFAE ^a	1.21 and 1.41 ^d 1.76 ^d 1.72 and 1.80 ^d 2.27 and 2.32 ^d 0.20, 0.21, 0.39, 0.40 ^d 1.68, 1.69, 1.76, 1.77 ^d	- - - - - -	21.8, 22.3 - 24.1, 24.4 -

^a: 1:8 equivalents of (S)-TFAE were used.
^b: 1:6 equivalents of (S)-TFAE were used.
^c: 200 MHz ¹H NMR spectral data.
^d: 400 MHz ¹H NMR spectral data.
^e: At - 55 °C.
^f: A shoulder was observed for the signal at 1.26 ppm.

These findings show that the rates of internal rotation are slow on the NMR time scale and confirm the chirality of the compounds in their ground states. For compound (±) 8, the *ortho*-fluoro derivative, on the other hand, anisochronous carbon and proton nuclei

for the diastereotopic methyl groups were not detected at ordinary probe temperature (30 °C) by NMR. Lowering the probe temperature to – 55 °C enabled the observation of these diastereotopic methyl protons.

4.2.2. Barriers to Rotation

4.2.2.1. Temperature Dependent NMR. Activation parameters to hindered rotation around C-N single bond were determined by temperature dependent NMR spectroscopy for all the synthesized compounds except for (\pm) **11** (for which thermal racemization after micropreparative enrichment of the enantiomers has been applied). The two magnetically nonequivalent C-5 methyl protons which were distinguished by NMR at room temperature became equivalent at higher temperatures (Figure 4.11) The kinetic data of the interconversion process were determined using Eyring equation [16] and the results are listed in Table 4.6.

Comparison of the energy barriers of the studied compounds revealed the influence of the relative sizes of the substituents on hindered rotation. As can be seen from Table 4.6, the ΔG^\ddagger values for the *ortho*-halogen substituted compounds (\pm) **8**, (\pm) **9**, (\pm) **10** and (\pm) **11** were found to increase linearly with the van der Waals radii of the halogens (Figure 4.12).

Compound (\pm) **9** bearing an *o*-chlorine substituent showed a barrier greater than compound (\pm) **7** having an *o*-methyl group although the van der Waals radius of chlorine is smaller than that for methyl group. Thus, this difference can not be explained by consideration of the relative sizes in the planar transition states (Figure 2.2). Electrostatic repulsion between the lone pairs of carbonyl oxygen and chlorine atom can be expected to make the rotation around C-N single bond more hindered and thus causing a larger barrier for this compound.

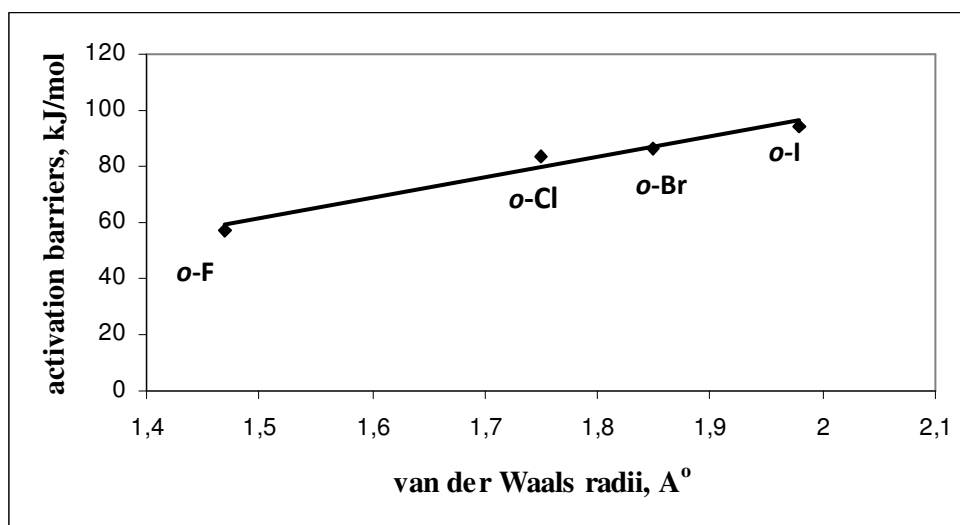


Figure 4.12. The plot of activation barriers vs. Van der Waals radii of the *o*-substituted halogens

4.2.2.2. HPLC. The racemic mixtures of interconverting enantiomers were tried to be resolved by Chiralcel OD-H and Chiralpak AD columns, packed with cellulose tris-(3,5-dimethyl)-carbamate and amylose tris-(3,5-dimethyl)-carbamate as chiral stationary phases, respectively. On both columns at room temperature, separation of enantiomers were not achieved except for (\pm) **10** and (\pm) **11** due to the fact that the barrier to rotation was not sufficiently high to allow the resolution of the compounds into enantiomers. The resolution of enantiomeric peaks were found to be better on the AD column where (\pm) **10** was separated analytically and (\pm) **11** micropreparatively in ethanol: hexane (9:1,v/v) as eluent.

In the chromatographic separation of interconverting enantiomers of (\pm) **11** on chiral OD-H column, the solvent was found to have an effect on the barrier as has been observed before [14]. When the eluent was 80:20 (v/v) hexane: ethanol a series of flow-rate and temperature dependent plateaus [20-22] resulting from on-column racemization were observed (Figure 4.13). The interfering “plateau” originated from molecules for which slow racemization took place during elution on the column, whereas the two terminal peaks essentially resulted from molecules that kept their conformation as **M** or **P** during the whole resolution process. Increasing the ratio of ethanol in the ethanol/hexane eluent resulted in the disappearance of the plateaus, but decreased the difference between the

retention times. A series of flow rate and temperature dependent plateaus were also observed on AD column for compound (\pm) **9** and (\pm) **10** with eluent composition of ethanol:hexane (1:1,v/v) at a flow rate of 0.3 ml/min, at 7 ± 2 °C. On column racemization can, in fact, be expected for interconvertible enantiomers having barriers about these magnitudes (Table 4.6) as has been observed before [21].

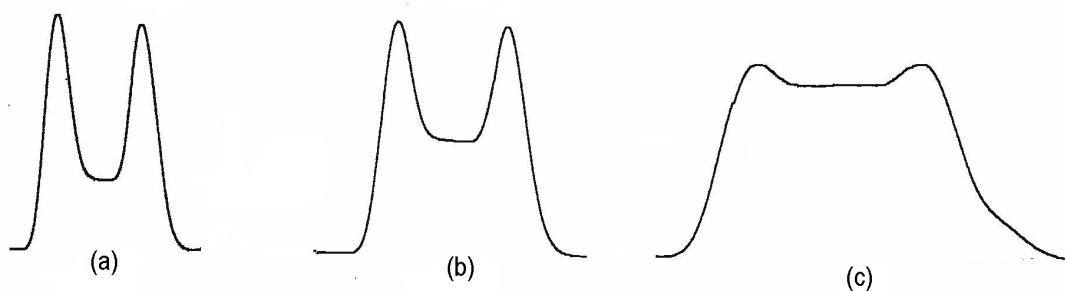


Figure 4.13. The flow-rate dependent plateaus observed for (\pm) **11** on OD-H column, (a), flow-rate= 0,3 ml/min, (b), flow-rate= 0,2 ml/min, (c), flow-rate= 0,1 ml/min. Eluent composition: 80:20, v/v, hexane-ethanol

For (\pm) **11** the micropreparative enrichment of the first eluted enantiomer using 90 % ethanol: 10 % hexane as eluent was done for two purposes: to follow the interconversion between enantiomers in order to obtain the kinetic data (Table 4.6) of the interconversion process (thermal racemization) which led to the determination of the activation barrier and second to determine the absolute conformations of the enantiomers using (*S*)-TFAE as optically active auxiliary by NMR as will be described later.

The ethanol solution containing the enriched enantiomer of (\pm) **11** was kept at a constant temperature (20 °C, 298 K) and its thermal racemization was followed by UV detection at 240 nm (Figure 4.14). The barrier to rotation for the first-order interconversion process was determined using the rate constant and Eyring equation [16] and found as 94,16 kJ/mol. Data pertinent to the chromatographic separation of the enantiomers of compound (\pm) **11** on Chiralpak AD column are shown in Figure 4.14.

Table 4.6 The kinetic and thermodynamic data for the interconversion process shown in Figure 4.11.

Compound No	solvent	T, K	k, s ⁻¹	$\Delta G^{\ddagger, e}$, kJ/mol
(±) 7	C ₆ D ₆	321 ^c	6.91 ^d	73.49±0.05 ^a
(±) 8	Acetone-d ₆	247 ^c	3.64 ^d	57.33±0.05 ^b
(±) 9	DMSO- d ₆	377 ^c	22.97 ^d	83.24±0.05 ^a
(±) 10	DMSO- d ₆	395 ^c	28.82 ^d	86.62±0.05 ^b
(±) 11	Ethanol:hexane (9:1, v/v)	293 ^f	1.10 ^{-4 g}	94,16±1.31

^a: determined by 200 MHz NMR instrument.
^b: determined by 400 MHz NMR instrument.
^c: the coalescence temperature.
^d: rate constant at coalescence temperature.
^e: free energy of activation.
^f: the temperature at which the HPLC analysis has been done.
^g: the rate constant of interconversion.

We have previously found that the diastereomers of 5S-methyl-3-(*o*-aryl)-2,4-oxazolidinediones were obtained in unequal compositions [14]. The conformations of the major and the minor diastereomers were deduced from the analysis of ¹H NMR, NOESY and HMQC spectra, and it was found that the major diastereomer had a **P** conformation. When (5S)-methyl-3-(*o*-iodophenyl)-2,4-oxazolidinedione which is analogous to the compound (±) **11**, was injected onto the Chiralpak AD column it was observed that the minor **M** conformer eluted first with eluent composition of ethanol:hexane (9:1, v/v) at a flow rate of 0.3 ml/min, at 240 nm. Since hydrogen bonding between racemic compounds and the carbamate residues of Chiralpak AD column plays an important role in chiral recognition [23] and provided that these interactions are the same for the enantiomers of 5,5-dimethyl-3-(*o*-iodophenyl)-2,4-oxazolidinedione, (±) **11**, and the diastereomers of (5S)-methyl-3-(*o*-iodophenyl)-2,4-oxazolidinedione, the elution order of these compounds may be expected to be the same on the AD column, thus the first eluted enantiomer of the compound (±) **11** may correspond to the **M** conformer and the second to the **P**.

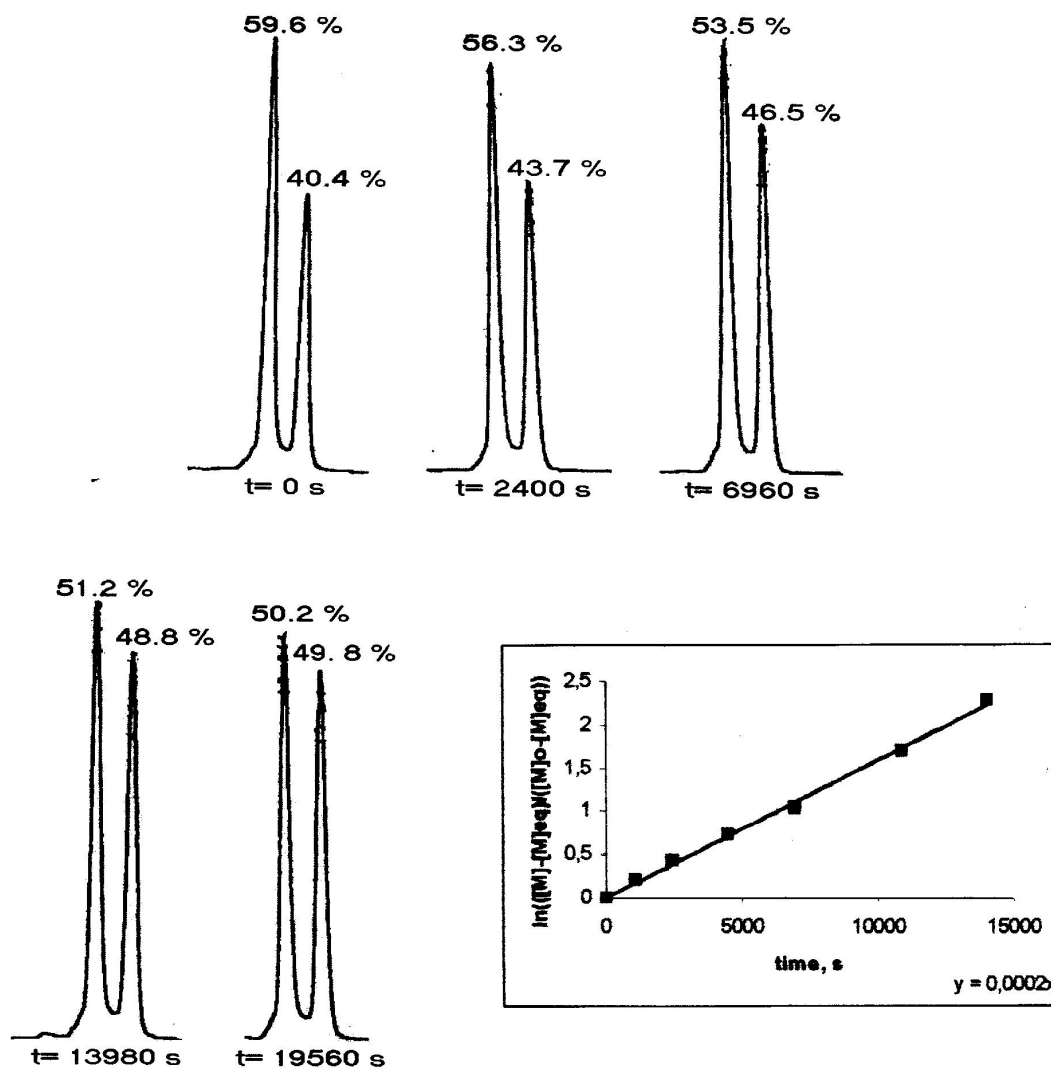


Figure 4.14. The change in enantiomer composition versus time for compound (±) **11** after micropreparative enrichment of the first eluted enantiomer followed by HPLC at 293 K, Eluent: ethanol: hexane (9:1, v/v), flow rate: 0,3 ml/min, t_1 : 12,85 min, t_2 : 13,89, k_1 : 0.33, k_2 : 0.44, α : 1.33, detection: UV at 240 nm. Inset: The plot of $\ln\left(\frac{[M] - [M]_{eq}}{[M]_0 - [M]_{eq}}\right)$ versus time

4.2.2.3. ^1H NMR in the Presence of Chiral Auxiliary. The chirality of compounds (±) **7-11** was also confirmed by ^1H NMR spectroscopy in the presence of the chiral auxiliary (S)-(+)-1-(9-anthryl)-2,2,2-trifluoro ethanol ((S)-TFAE) (Table 4.5). Noncovalent interactions between the chiral auxiliary, (S)-TFAE, and the enantiomeric solute molecules led to the formation of diastereomeric association complexes. Hydrogen bonding between hydroxyl group of (S)-TFAE and oxygen atoms of the heterocyclic ring and π - π interaction between

anthryl group and benzene ring have been thought to be responsible for the formation of these association complexes [24]. A special type of complex formation has been proposed between lactones and (S)-TFAE where (S)-TFAE hydrogen bonds to the exocyclic oxygen with the hydroxyl proton and to the ring oxygen with the methine hydrogen [6, 7, 25]. The proposed structure of the complex led to the assignment of the absolute configuration of the furanone based on the consideration of different shielding effects of the anthryl group on the lactone protons [7, 25].

In the ^1H NMR spectra of (\pm) **7**, **9-11**, the expected four singlets were observed in the presence of (S)-TFAE. The peaks observed with a chemical shift difference of 0.02 ppm, 0.09 ppm, 0.12 ppm and 0.2 ppm, respectively, due to the diastereotopic methyl groups in the absence of the optically active auxiliary were found to further split by a chemical shift difference of 0.01 ppm (Table 4.5). Only three singlets (like triplet in appearance) were observed however for (\pm) **7**, resulting from an accidental overlapping of two inner singlets having the same chemical shifts. *O*-methyl protons of the two diastereomeric complexes were also observed for (\pm) **7** with a chemical shift difference of 0.01 ppm.

In the spectrum of (\pm) **8** taken in the presence of six equivalents of (S)-TFAE, two singlets were observed with a chemical shift difference of 0.01 ppm due to the overlapping of two singlets because of the fast rotation around C-N single bond. In fact, when the temperature was lowered to $-55\text{ }^\circ\text{C}$, the expected four singlets were observed.

Determination of absolute stereochemistry of certain enantiomers can be done on the basis of interactions between enantiomers and (S)-TFAE [25]. In order to get a solvation model for our compounds, all the ^1H NMR signals of pure (S)-TFAE were compared with those of the diastereomeric association complex. It has been observed that all of the signals of the complexed anthryl, except for the hydroxyl proton, have been shielded with respect to pure (S)-TFAE. The downfield shift (0.1-0.2 ppm) noted for O-H proton was thought to result from a hydrogen bonding with oxygens of the heterocyclic ring. Among these groups, the stronger hydrogen bonding was expected to occur between C-4 and C-2 carbonyl oxygens and the anthryl hydroxyl due to the greater basicity of these groups compared to the ring oxygen. When ^1H NMR signals of enantiomers of (\pm) **11** in the

presence of (S)-TFAE were examined in C_6D_6 , all protons were shifted upfield, probably due to the anisotropic effect of the anthryl ring. The upfield shift was also observed in $CDCl_3$ (Table 4.5) ruling out the shielding effect of the solvent C_6D_6 . An increase in the amount of (S)-TFAE also resulted in an enhancement of the shielding effect. Since an upfield shift was observed for both C-5 methyl protons of the enantiomers of (\pm) **11**, the two-point lactone model [6, 7, 25] alone can not account for the upfield shift of both C-5 methyl protons. A weaker π - π interaction between anthryl and the *ortho*-substituted phenyl rings and a hydrogen bond between anthryl hydroxyl and the amide carbonyl oxygen might be the other possible interactions [6,7]. With the knowledge of the stereostructure of (S)-TFAE, in which the hydroxyl group and the carbinyl hydrogen are aligned to the same face [26,27] we proposed a solvation model represented in Figure 4.21. In this model, while one of the phenyl rings of the anthryl system could interact with the *ortho*-substituted phenyl ring of the compounds studied the other two rings of the anthryl could not (Figure 4.15).

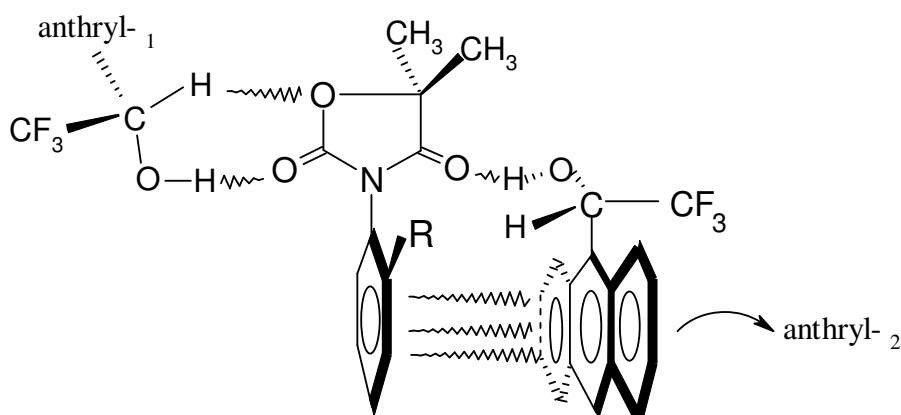


Figure 4.15. The proposed solvation model for (M,S) compounds (\pm)-**7-11** (R= CH₃, F, Cl, Br, I) and (S)-TFAE

In order to gain further insight for the solvation model, NOESY spectra of compound (\pm) **11** (Figure 4.16) was taken in the presence of two equivalents of (S)-TFAE. Close inspection of the NOESY spectra revealed the presence of the through space π - π interactions of two of the aromatic protons of compound (\pm) **11** and two of the anthryl protons (either protons 2,3 or 6,7) of (S)-TFAE.

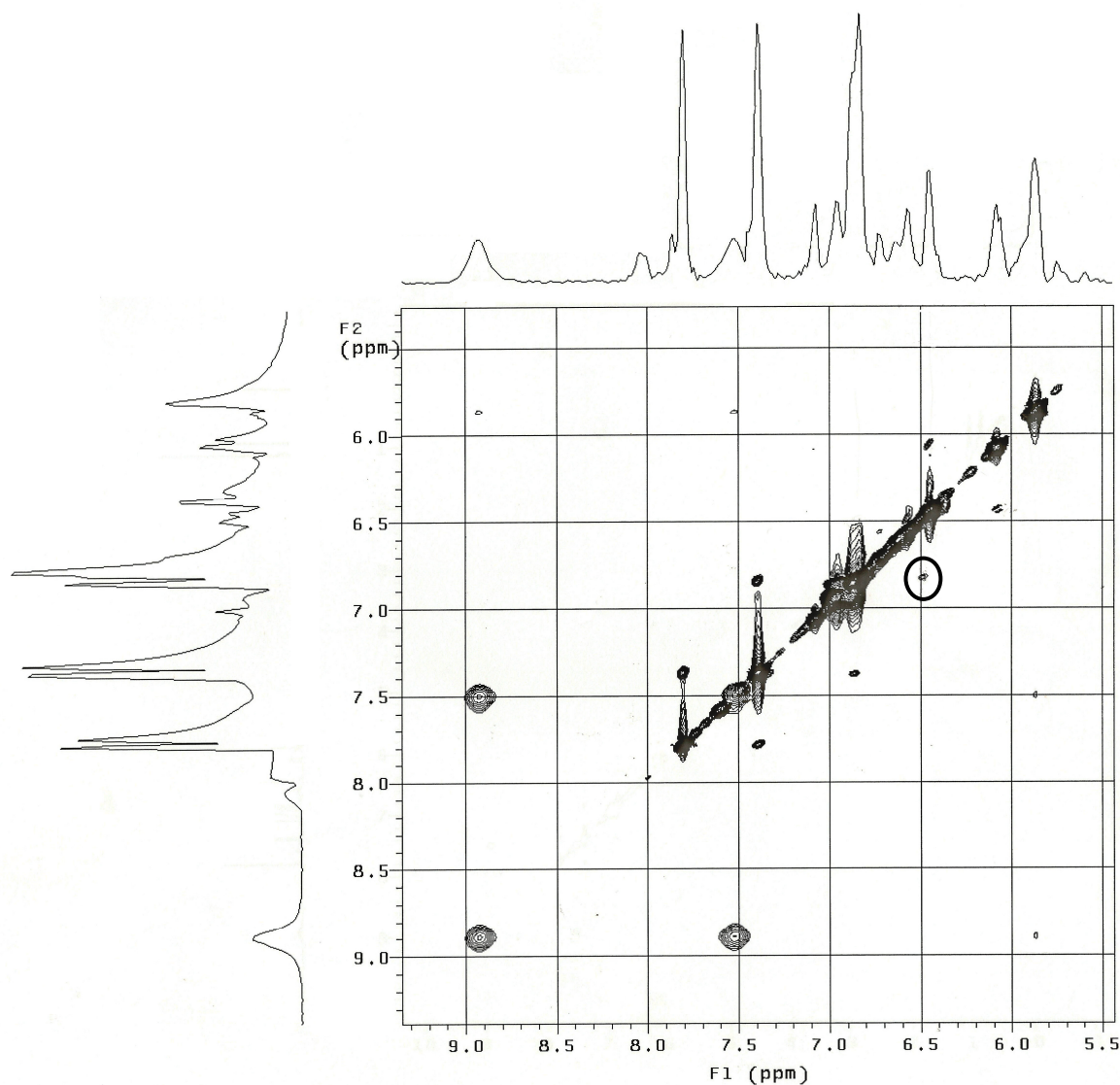


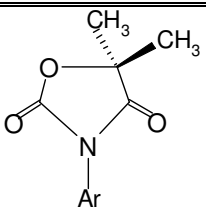
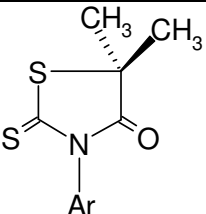
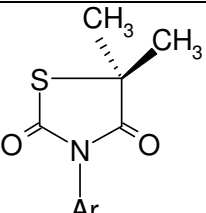
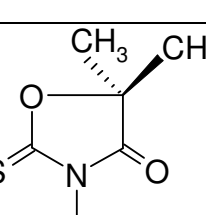
Figure 4.16. The NOESY spectrum of compound (\pm)-**11** taken in the presence of (S)-TFAE. The cross-peak between the phenyl and the anthryl rings is shown in circle.

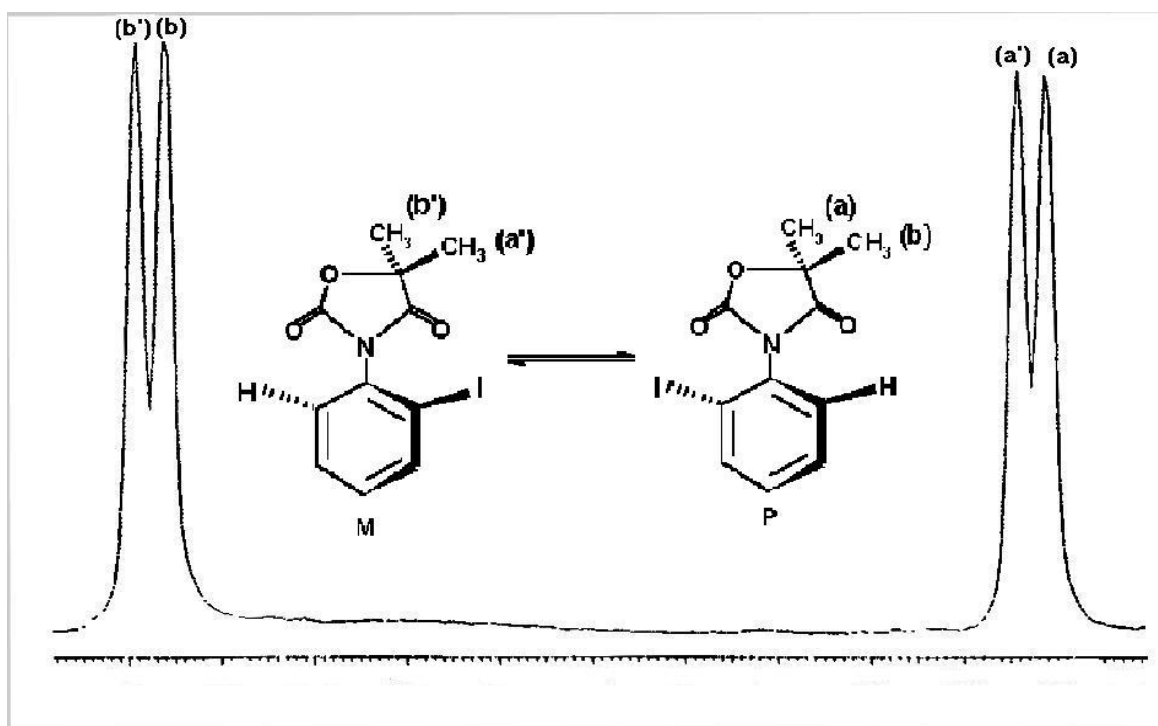
The 5,5-dimethyl-3-(*o*-aryl)-2,4-oxazolidinedione enantiomers studied here are thus thought to interact with (S)-TFAE in three ways: 1) A two-point interaction complex is formed with the lactone part of the ring, 2) an association of the (S)-TFAE hydroxyl proton with the amide carbonyl oxygen and 3) π - π interactions exist between the aromatic rings of the two. These interactions are schematically shown in Figure 4.15. The importance of the two-point lactone model in differentiation of C-5 methyl protons by NMR in the presence of (S)-TFAE might be confirmed when the ^1H spectrum of (\pm) **7** together with (S)-TFAE was compared with those of 5,5-dimethyl-3-(*o*-tolyl)-rhodanine ((\pm) **12**) [24] 5,5-dimethyl-3-(*o*-tolyl)-2,4-thiazolidinedione ((\pm) **13**) [28] and 5,5-dimethyl-3-(*o*-tolyl)-

oxazolidinone-2-thione ((\pm) **13**) [24] in the presence of (S)-TFAE (Table 4.7). While differentiation of the C-5 methyl groups of the enantiomers of (\pm) **7** was achieved, for (\pm) **12** and (\pm) **14** only one pair of the previously enantiotopic protons was distinguished in the presence of (S)-TFAE. The upfield pair was resolved with a chemical shift difference of 0.01 ppm whereas the downfield pair appeared as one singlet. On the other hand, for (\pm) **13** [28] only two singlets were observed instead of four. Of the *o*-methyl groups of compounds (\pm) **7**, **12**, **13**, **14**, only those of (\pm) **7** could be differentiated ($\Delta\delta= 0.01$ ppm) in NMR. It can be deduced from these results that the oxygen atoms in the oxazolidinone ring play an important role for enantiomeric discrimination in the presence of (S)-TFAE. As a result of lactone type of association [6,7,25] with (S)-TFAE, together with association from the C-4 carbonyl oxygen and the π - π interactions (Figure 4.15), enantiotopic groups of the enantiomers (\pm) **7-11** became anisochronous, thus 5,5-dimethyl protons displayed four distinct ^1H NMR signals.

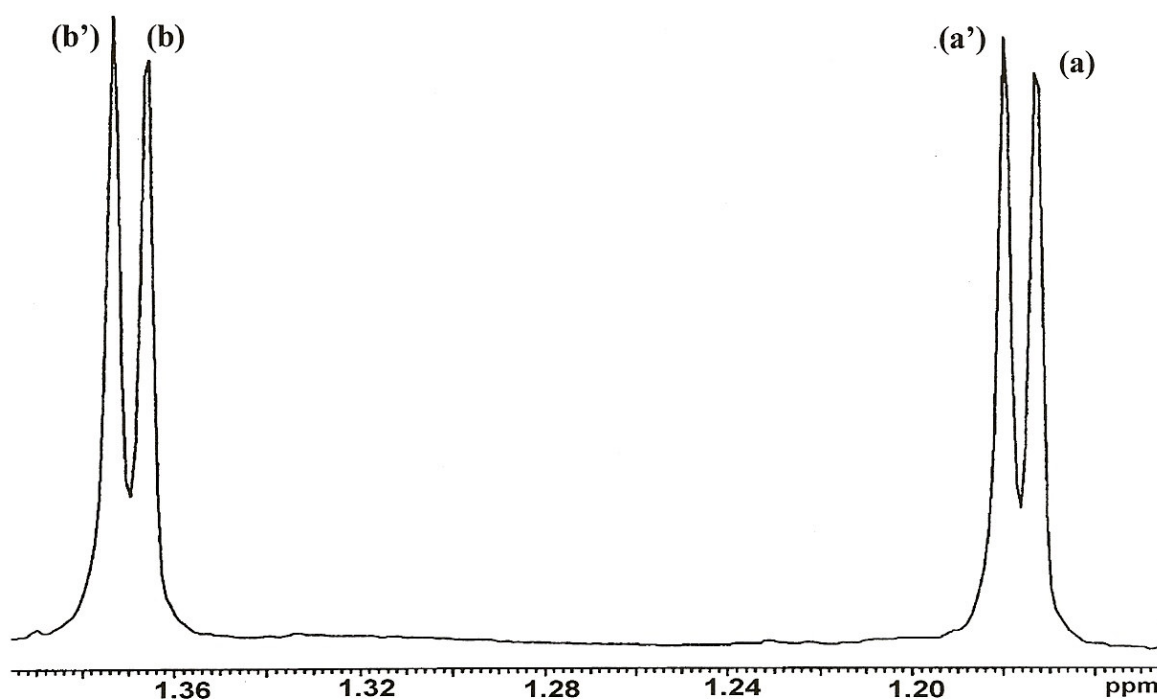
When ^1H NMR spectrum of a mixture enriched in the **M** conformer of compound (\pm) **11** was taken in the presence of (S)-TFAE, the chemical shifts of the diastereotopic 5,5-dimethyl protons ((a') and (b')) in Figure 4.17-(A)) of the (M,S) solvate was observed downfield to that of the (P,S) solvate ((a) and (b) in Figure 4.17-(A)). Thus, the diastereotopic protons of the **M** conformer were both deshielded while those of P conformer were shielded in the presence of (S)-TFAE. That observation could be explained when the proposed solvate model (Figure 4.15) was taken into account. Since the chemical shift differences of the diastereotopic protons ((a)-(b) and (a')-(b')) of (\pm) **5** was the same before and after the complex formation, it was thought that the difference resulted from the position of iodine atom with respect to the C-5 methyl protons. In the previous work [14] we had determined by NOESY and HMQC experiments, that iodine, naphthyl and the other *ortho* substituents, due to their anisotropy, caused a shielding effect on the protons which had a close proximity. Therefore the protons in the upfield pair may be the ones indicated as (a) and (a'), since they were close to iodine in the **P** and **M** conformations, respectively. The discriminations of (a)-(a') and (b)-(b') were achieved via analysis of disposition of anthryl groups. It was thought that the two anthryl groups might have slightly different anisotropic shielding effects with the closer one having the larger shielding effect.

Table 4.7. ^1H NMR chemical shifts of N-*o*-tolyl substituted O, S, N containing five membered heterocyclic systems in the presence of (S)-TFAE. Ar= *o*-tolyl

Compound-no and structure	^1H NMR, ppm C-5 methyl	^1H NMR, ppm <i>ortho</i> -methyl	Experimental Conditions
 <p>(±) 7</p>	0.80 0.79 0.78	1.59 1.60	8 equivalents (S)-TFAE, C_6D_6 , 400 MHz ^a
 <p>(±) 12</p>	0.99 1.00 1.01	1.67	8 equivalents (S)-TFAE, C_6D_6 , 400 MHz
 <p>(±) 13</p>	1.27 1.28	1.90	8 equivalents (S)-TFAE, C_6D_6 , 200 MHz
 <p>(±) 14</p>	0.80 0.79 0.78	1.62	8 equivalents (S)-TFAE, C_6D_6 , 400 MHz
^a : Similar spectrum with 200 MHz NMR			



(A)



(B)

Figure 4.17. The ^1H NMR signals in the presence of eight equivalents of (S)-TFAE in C_6D_6 for the 5,5-dimethyl protons of the enantiomers (\pm) **11**, (A) At 30 °C, (B) At 22 °C, enriched in **M** conformer.

Protons (a) and (b') were exposed to the same shielding effect by the anthryl-₁ (Figure 4.15) and they were directly included in the shielding region of this anthryl (Figures 4.15 and 4.17). Since proton (a) unlike (b') was also shielded by the *o*-iodine it appeared as the most shielded proton. The anthryl₂ might have an important role in the shielding of (a') and (b). This anthryl group may have had a tighter approach for the (P,S) solvate than for the (M,S) solvate [29] owing to the steric interaction of the lone pair electrons of the *o*-iodine in the **M** conformer and the π electrons of the anthryl group [7] which prevented the two rings to be close to each other. Therefore, by virtue of the greater proximity of the proton (b) to anthryl₂ group than the proton (b') to anthryl-₁, the proton (b) of the **P** conformer may experience a stronger shielding effect than the proton (b') of **M** conformer. The proton (a') was affected by *o*-iodine together with anthryl₂, therefore it was shielded to the upfield region. On the other hand, shielding of (a') by anthryl₂ was not as strong as that of (a) by anthryl-₁ because of the prevention of a tight complex by *o*-iodine in the **M** conformer.

Since the *ortho*-substituents are known to have a shielding effect on the syn-substituent at C-5 [14] it can be argued that of all the compounds studied, (\pm) **7-11**, in the presence of (S)-TFAE the more deshielded of the diastereotopic 5-methyl pairs can be assigned to the complexed **M** conformer and the more shielded to complexed **P**.

4.3. Determination of the Absolute Stereochemistry and the Activation Barriers of Thermally Interconvertible Oxazolidinone Heterocycles Bearing Naphthyl Substituent [30]

Supramolecular interactions like hydrogen bonding and π -stacking between aromatic rings play an important role in diverse areas such as stereochemistry of organic reactions [31] and host-guest chemistry [32,33]. Dependence of spectral properties on these type of interactions has been used for the determinations of absolute stereochemistry for many years [7,25]. Diastereometric association complexes formed through these kind of interactions of chiral molecules show nonidentical spectral behavior on the NMR time scale. With the knowledge of the structures of the solvates and on the basis of sense of nonequivalence, absolute stereochemistries can be achieved.

The importance of π - π interaction between the *o*-substituted phenyl of the studied compounds [19] and the anthryl ring of the chiral auxiliary led us to synthesize a series of axially chiral heterocyclic compounds bearing naphthyl ring (Compounds (\pm)-**15-17**, Figure 4.18) that can be involved in enhanced π stacking interactions with the anthryl ring of the (S)-TFAE. In these compounds, axial chirality arises from the hindered rotation around C_{sp^2} - N_{sp^2} single bond and makes the compounds enantiomers [24]. In this study, with the aim of finding a solvation model for determination of the absolute stereochemistry, 1H NMR signals of compounds (\pm)-**15-17** (Figure 4.18, Table 4.8) were compared with those of compounds (\pm)-**18-19** (Figure 4.19, Table 4.9).

4.3.1. 1H and ^{13}C NMR

The naphthyl bearing heterocyclic compounds exist as two enantiomeric **M** and **P** atropisomers (Figure 4.18) that exhibit identical NMR spectra in an achiral solvent. However, due to the hindered rotation around C_{sp^2} - N_{sp^2} single bond, the C-5 methyl protons of the compounds 5,5-dimethyl-3-(α -naphthyl)-2,4-oxazolidinedione ((\pm)-**15**) and 5,5-dimethyl-3-(α -naphthyl)-2-thioxo-4-oxazolidinone ((\pm)-**16**) and the C-5 protons of the compounds 3-(α -naphthyl)-2,4-oxazolidinedione ((\pm)-**17**) are diastereotopically related and should have unequal chemical shifts if the barrier to rotation is slow on the NMR time scale. Analysis of the 1H and ^{13}C NMR spectra of the synthesized compounds did show these magnetically nonequivalent protons (Table 4.8). The two methyl groups on C-5 in compounds (\pm)-**15** and (\pm)-**16** gave two separate singlets in toluene- d_8 with the same chemical shift difference of 0.04 ppm. The protons at C-5 of (\pm)-**17** on the other hand, showed AB type splittings, the chemical shift differences being equal to 0.06 ppm. The anisochronous ^{13}C nuclei of the C-5 methyl groups in compounds (\pm)-**15** and (\pm)-**16** gave also two distinct singlets in toluene- d_8 , with the same chemical shift difference of 0.6 ppm. These results proved the restricted rotation around C_{sp^2} - N_{sp^2} , making this bond a chiral axis.

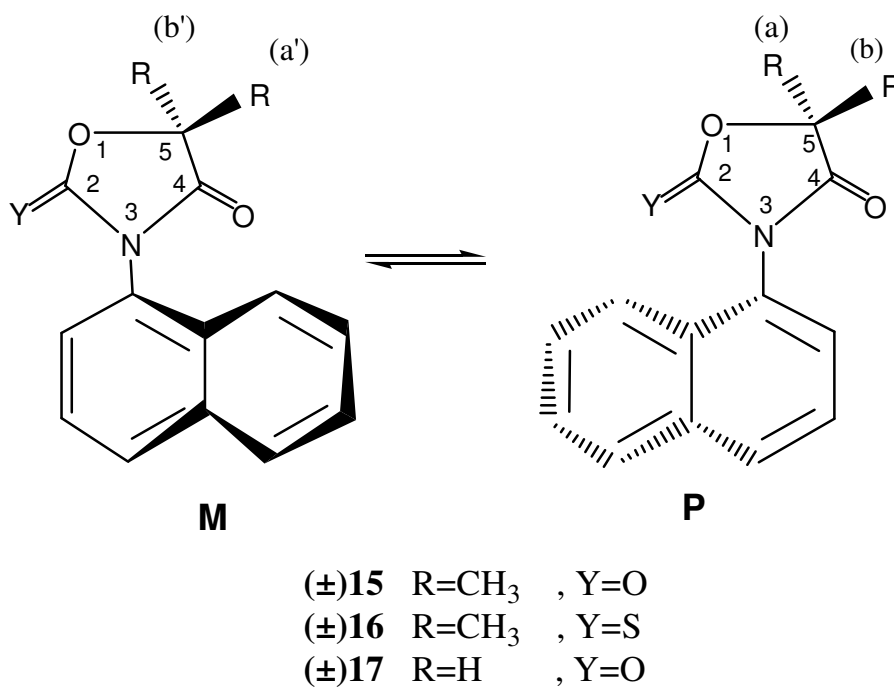


Figure 4.18. The naphthyl substituted oxazolidinone derivatives

Table 4.8. ¹H and ¹³C NMR spectral data for compounds (±)**15-17** in the presence and absence of the optically active auxiliary, (S)-TFAE at 30 °C

Compound no	Medium	¹ H NMR, ppm, C-5 methyl	¹ H NMR, ppm, C-5 protons	¹³ C NMR, ppm, C-5 methyl
(±) 15	toluene-d ₈	1.28 and 1.24	-	28.9 and 28.3
	toluene-d ₈ +(S)-TFAE ^a	1.35, 1.33, 1.30, 1.29	-	-
(±) 16	toluene-d ₈	1.27 and 1.23	-	28,6 and 28.0
	toluene-d ₈ +(S)-TFAE ^a	1.37, 1.36 and 1.31	-	-
(±) 17	toluene-d ₈	-	3.07 and 3.01	-
	toluene-d ₈ +(S)-TFAE ^a	-	3.06, 3.04, 2.98, 2.97	-

^a: 1:6 equivalents of (S)-TFAE were used

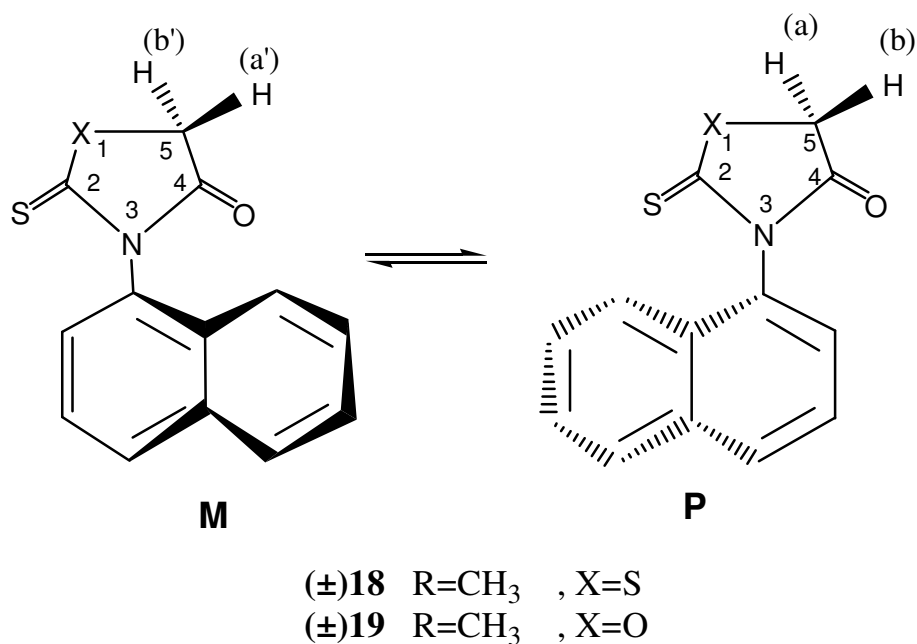


Figure 4.19. The naphthyl substituted rhodanine and thiazolidine derivatives

Table 4.9. ¹H and ¹³C NMR spectral data for compounds (±)**18-19** in the presence and absence of the optically active auxiliary, (S)-TFAE at 30 °C

Compound no	Medium	¹ H NMR, ppm, C-5 methyl	¹ H NMR, ppm, C-5 protons	¹³ C NMR, ppm, C-5 methyl
(±)- 18	toluene-d ₈	-	3.04 and 2.97	-
	toluene-d ₈ +(S)-TFAE ^a	-	2.88, 2.86, 2.79, 2.78	-
(±)- 19	toluene-d ₈	-	3.08 and 3.02	-
	toluene-d ₈ +(S)-TFAE ^a	-	3.08, 3.06, 2.99, 2.98	-

^a: 1:6 equivalents of (S)-TFAE were used

4.3.2. ¹H NMR in the Presence of a Chiral Auxiliary

The existence of the two enantiomeric forms for compounds (±)-**15-19** was also proved by ¹H NMR spectroscopy in the presence of six equivalents of (S)-(+)-2,2,2-trifluoroanthryl ethanol, (S)-TFAE. Enantiomeric groups become diastereotopic by

nonequivalent interactions with (S)-TFAE as proposed previously [19] and thus display unequal ^1H NMR chemical shifts.

In the ^1H NMR spectra of (\pm)-**15** the expected four singlets of C-5 methyl groups were observed in the presence of (S)-TFAE with a chemical shift difference of 0.01 ppm for the upfield and 0.02 ppm for the downfield pair of the signals in toluene- d_8 (Figure 4.20). For compound (\pm)-**16** however only one enantiomeric pair for C-5 methyl groups was distinguished under the same conditions. The two separated singlets appeared downfield with a chemical shift difference of 0.01 ppm in toluene- d_8 (Figure 4.20).

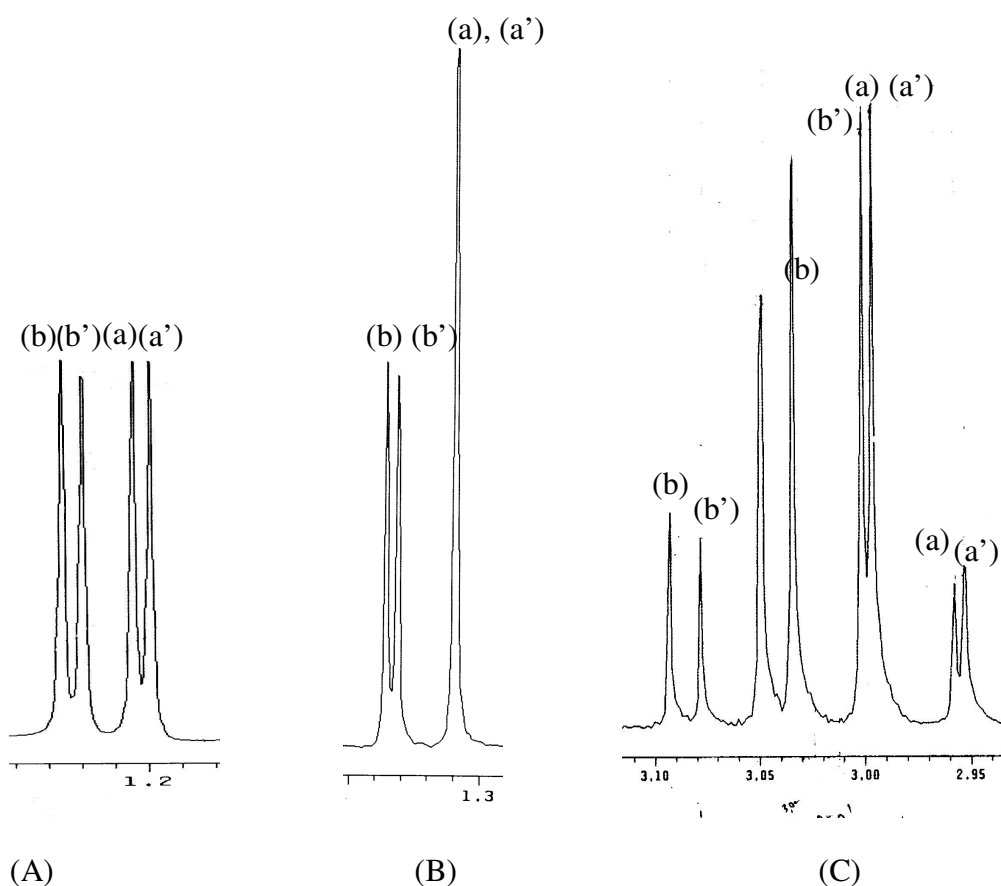


Figure 4.20. The ^1H NMR spectra of the compounds (\pm)-**15-17** taken in the presence of six equivalents of (S)-TFAE in toluene- d_8 , A= (\pm)-**15**, B= (\pm)-**16**, C= (\pm)-**17**

In the presence of (S)-TFAE, the two expected AB splittings were differentiated on the NMR time scale for C-5 methylene protons of the compounds (\pm)-**17** and (\pm)-**19**, chemical shift difference being equal to 0.02 ppm for the downfield and 0.01 ppm for

upfield pair of the signals (Figures 4.20 and 4.21). The two AB splittings for C-5 methylene protons of the compound (\pm)-**18** were also observed with a chemical shift difference of 0.02 ppm for the downfield signals however the upfield part of the spectrum could not be resolved (Figure 4.21, A).

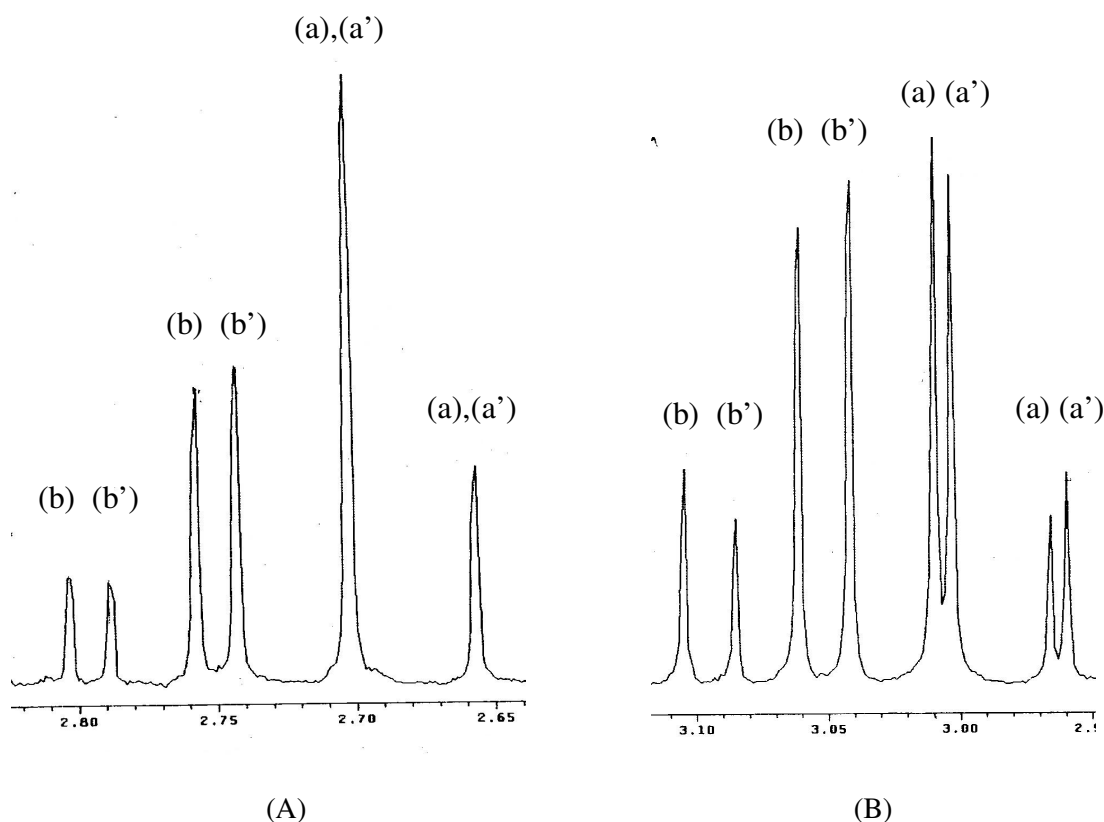


Figure 4.21. The ^1H NMR spectra of the compounds (\pm)-**18** and **19** taken in the presence of six equivalents of (S)-TFAE in toluene- d_8 , A= (\pm)-**18**, B= (\pm)-**19**

Having these results, it may be concluded that the existence of the $-\text{C}=\text{S}$ group on C-2 (Compounds (\pm)-**16** and (\pm)-**18**) decreases the resolution of the enantiomeric pairs of these compounds compared to the $-\text{C}=\text{O}$ analogs. The observed decrease in resolution for the enantiomeric upfield signals may arise from a structural change in the solvation model that will be discussed later.

4.3.3. Determination of Absolute Stereochemistry

The resolution of the enantiomeric resonances of 5,5-dimethyl-3-(*o*-aryl)-2,4-oxazolidinediones could be accomplished through interaction of the enantiomers with the chiral auxiliary (S)-TFAE [19]. For 5,5-dimethyl-3-(*o*-iodophenyl)-2,4-oxazolidinedione studied in a previous work [19] four singlets corresponding to the C-5 methyl groups of **M** and **P** rotational isomers could be distinguished by ¹H NMR in the presence of (S)-TFAE. For this compound the chemical shift difference between the diastereotopic C-5 methyl protons (0.19 ppm in C₆D₆) did not change with the addition of (S)-TFAE and cooling a toluene-d₈ solution in probe from 30 °C to -70 °C did not result in a significant difference in chemical shifts. Contrary to this, for compound (±)-**15** it was observed that the chemical shift difference between the diastereotopic C-5 methyl protons were found to be slightly different in the absence (0.040 ppm, in toluene-d₈) and in the presence (0.046 ppm, in toluene-d₈) of (S)-TFAE. Moreover the ¹H NMR of this compound in toluene-d₈ unlike the 5,5-dimethyl-3-(*o*-iodophenyl)-2,4-oxazolidinedione showed a strong temperature dependence [34,35] in the 30-(-70) °C range (Figure 4.22). We presume that this fact may arise from the enforced existence of a naphthyl group and hence π-stacking. Therefore to relate these results to a solvation model we have studied sterically congested, axially chiral heterocyclic compounds (Figure 4.18 and Figure 4.19) bearing naphthyl ring that would facilitate studies of intermolecular interactions between stacked aromatic groups. We surmise that stacking propensity of naphthyl ring with anthryl group of (S)-TFAE would be higher than that of the *o*-iodo substituted phenyl ring due to the high surface area of naphthyl [36,37].

Among these compounds ((±)-**15-19**) the enantiomers of 2,4-oxazolidinedione ((±)-**15, 17**) and 2,4-thiazolidinedione ((±)-**19**) derivatives could be differentiated well by ¹H NMR spectroscopy in the presence of (S)-TFAE (Figures 4.20 and 4.21). The better resolution of the 2,4-oxazolidinediones ((±)-**15, 17**) led us consider that the origin of this resolution was much the same as it was in our previous work done for 5,5-dimethyl-3-(*o*-aryl)-2,4-oxazolidinediones. However on lowering the temperature, the C-5 methyl and C-5 methylene ¹H NMR signals of the complexed enantiomers of the α-naphthyl derivatives showed a different shielding behaviour as will be discussed below from that had been

observed for the *o*-iodophenyl derivative. It is also interesting to note that the ^1H NMR spectra of all comparable signals through the series showed close similarities. The C-5 methyl groups of the compounds (\pm)-**15** (Figure 4.22) and (\pm)-**16** (Figure 4.23) were shielded in the same way upon cooling and the signals of C-5 methylene for compounds (\pm)-**17** (Figure 4.24), **18**, **19** were shielded in a similar way on cooling. The fact that the temperature dependence of the C-5 methylene signals for compounds (\pm)-**18** and (\pm)-**19** was similar with that of compound (\pm)-**17** led us think that all of these compounds could have the same solvation model, although the enantiomers of (\pm)-**16** and (\pm)-**18** could not be completely resolved.

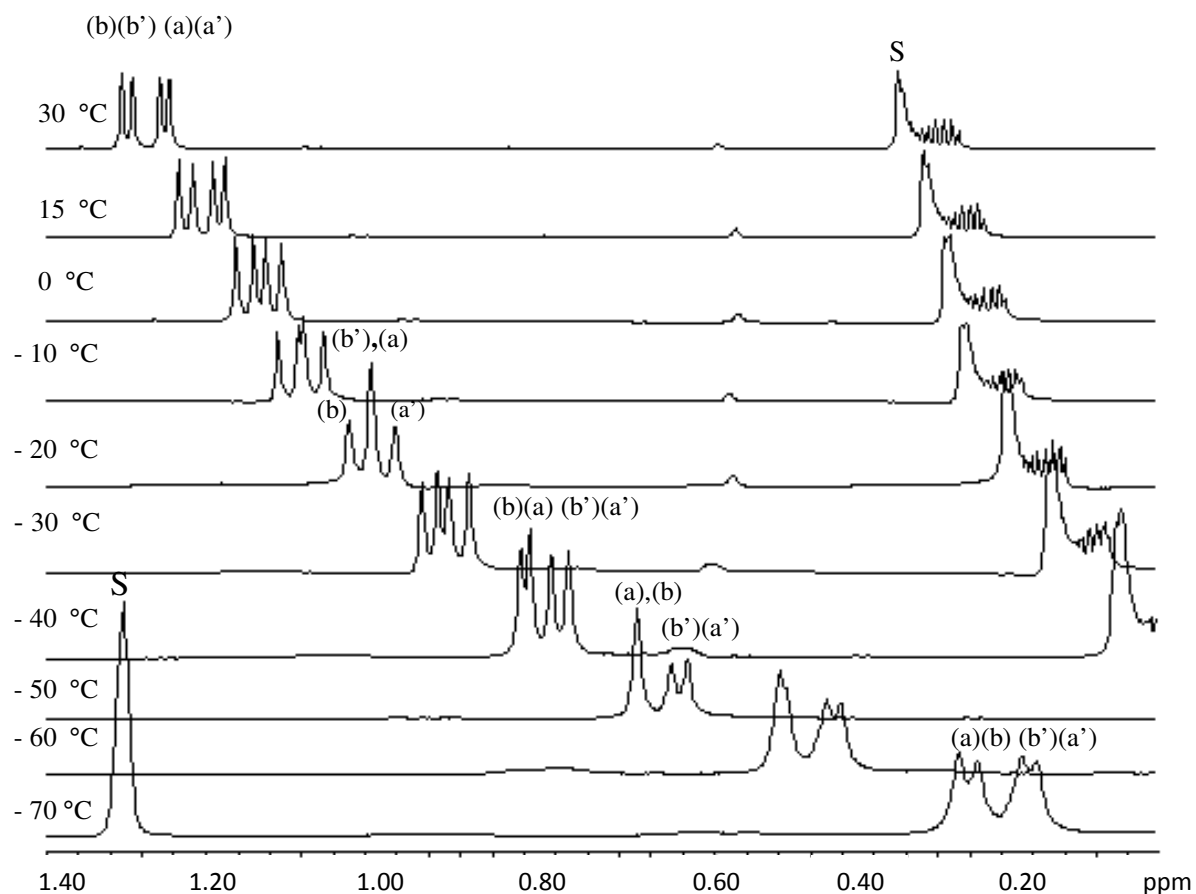


Figure 4.22. The temperature dependence of the ^1H NMR signals of the methyl groups on C-5 of the compound (\pm)-**15** upon cooling from 30 °C to -70 °C, S: Solvent

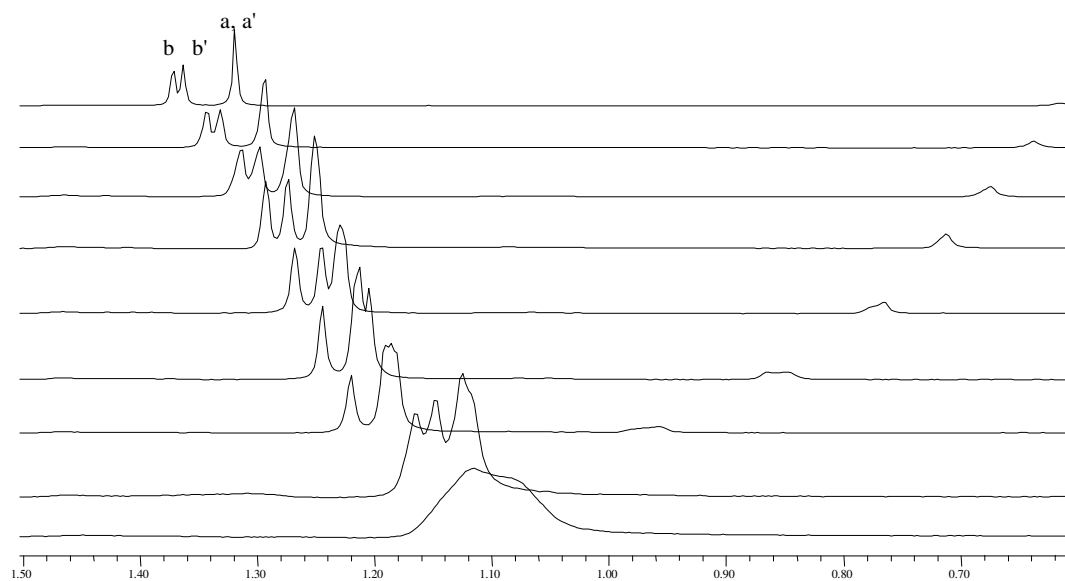


Figure 4.23. The temperature dependence of the ^1H NMR signals of the methyl protons on C-5 of the compound (\pm)-**16** upon cooling from 30 °C to -70 °C, S: Solvent

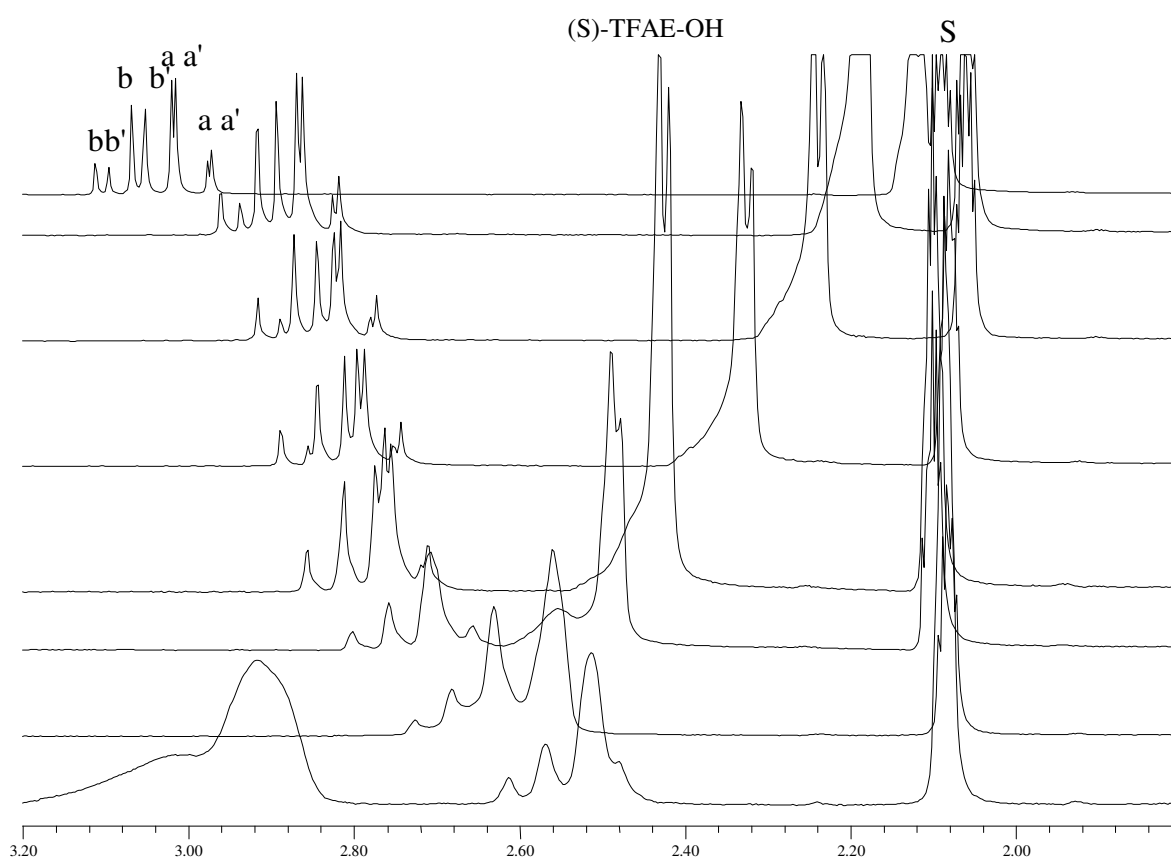


Figure 4.24. The temperature dependence of the ^1H NMR signals of the methylene protons on C-5 of the compound (\pm)-**17** upon cooling from 30 °C to -70 °C, S: Solvent

By considering these results it can be said that the solvation model for all of these compounds ((\pm)-**15-19**) should be the same within the series and very similar to that proposed for 5,5-dimethyl-3-(*o*-aryl)-2,4-oxazolidinediones [19]. However there must be a difference from the previously proposed model to account for the different temperature dependence of the signals.

In order to get a solvation model for our compounds all ^1H NMR signals of pure (S)-TFAE and each of the racemates were compared with those of the diastereomeric association complex. It has been observed that all of the signals of complexed (S)-TFAE and the enantiomers, except for the hydroxyl group of the (S)-TFAE, have been shielded with respect to the corresponding pure compounds and these observed upfield shifts and the dowfield shift increased with decreasing temperature [35].

The downfield shift observed for the hydroxyl proton was thought to result from hydrogen bonding with the racemates [37]. The upfield changes in chemical shifts observed for the aromatic naphthyl and anthryl groups may arise from ring current effects and suggest a face-to-face π stacked geometry (Figure 4.25) [36,38]. Also consistent with the face-to-face π stacking, crosspeaks between some of the protons of naphthyl and anthryl ring of (S)-TFAE were observed in the NOESY spectrum (Figure 4.25). The π stacking tendency of the naphthyl substituent in a π - π interaction as a π -base [32] was thought to be higher [36,37] and hence these compounds ((\pm)-**15-19**) would form tighter complexes with (S)-TFAE than that of the *o*-iodo substituted phenyl ring. The change in chemical shift difference of the diastereotopic C-5 protons of compound (\pm)-**15** from 0,040 ppm to 0,046 ppm upon complex formation might be an additional indication for an increase in anisotropic shielding effect as a result of enhanced π stacking between the aromatics. In order to find out whether the observed shielding was instrumental and/or by the effect of the solvent used or by enforced π - π interaction, the toluene- d_8 solution of the compound (\pm)-**15** was cooled to 0 °C in the absence of (S)-TFAE. The fact that none of the protons of compound (\pm)-**15** indicated any shielding effect on cooling to 0 °C revealed the enhanced π - π interaction between the anthryl group of the (S)-TFAE and the naphthyl substituent of the enantiomers.

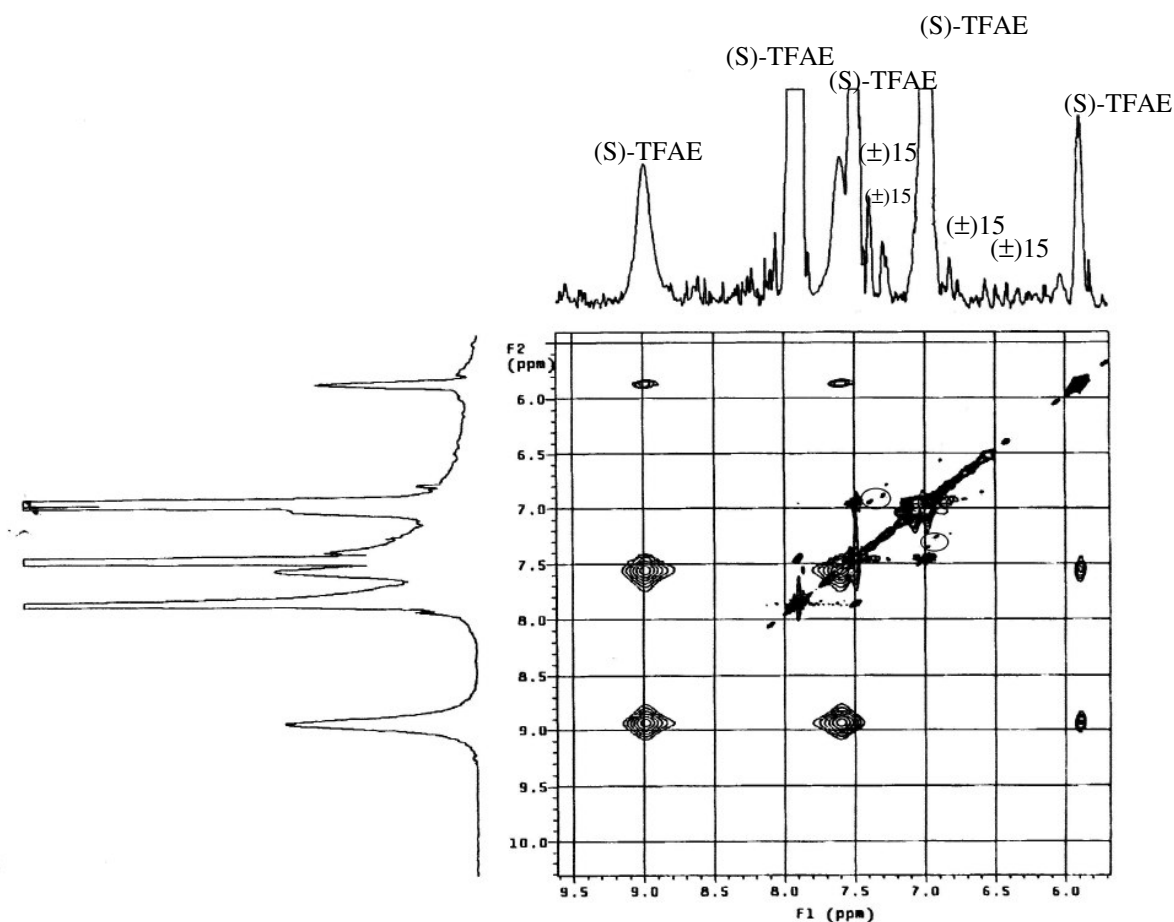


Figure 4.25. The NOESY spectrum of compound (\pm)-**15** taken in the presence of (*S*)-TFAE. The cross-peaks between the naphthyl and the anthryl rings are shown in circles.

In our previous work done for diastereomeric (*S*)-methyl-3(*o*-aryl)-2,4-oxazolidinediones it has been found that the naphthyl substituent exerted a similar shielding effect as the iodine [14] on the C-5 methyl group that is on the same side with the naphthyl or iodine. Similarly the enantiomers of the compounds ((\pm)-**15-17**) studied in this work in the absence of (*S*)-TFAE could be differentiated on the NMR time scale via the diastereotopic groups on C-5 (a-b or a'-b')¹ (Figure 4.20) depending the position of naphthyl substituent. In the presence of (*S*)-TFAE however, the discrimination of the enantiotopic groups (a-a' and b-b') was also possible.

¹ Notations a, b, a', b' refer to the C-5 methyl protons for the compounds (\pm) **1-2** and the C-5 methylene protons the compounds (\pm) **3-5**

For the **M** and **P** conformations the hydroxyl group of (S)-TFAE formed hydrogen bonding with the carbonyl or thiocarbonyl groups, carbinyl hydrogen of (S)-TFAE involved in carbinyl hydrogen bonding with the oxygen or sulphur atoms of the heterocycle formed a chelate-like structure and the anthryl group of (S)-TFAE formed π - π interaction with the naphthyl substituent of the enantiomers (Figure 4.26, models A and C). As can be seen in Figure 4.26 during the interaction of compound (\pm)-**15** with (S)-TFAE, two more different solvation models (B and D in Figure 4.26) are possible for both conformers. In our basic models (A and C in Figure 4.26) (S)-TFAE forms a chelate via a carbinyl hydrogen bonding between the C-H proton of the (S)-TFAE and the ring oxygen and a hydrogen bond between the -OH group of the (S)-TFAE and the -C=O on C-2. However, a π - π interaction would also be possible between the anthryl and the naphthyl rings, destroying the chelate structure without cleavage of the hydrogen bonding with the C-2 carbonyl group. In these models (B and D in Figure 4.26), anthryl₂ can not approach the naphthyl due to the presence of anthryl₃ and the weak basicity of naphthyl. Therefore, either carbinyl hydrogen bonding (A and C) or π - π interaction (B and D) should be preferred at a given time, one being more populated than the other. The models B and D were thought to be less populated than the models A and C since they have less number of interactions. Compared to model D, model B would be even less populated due to the weaker π - π interaction. Therefore, it was thought that the model B may have little or no effect on the observed chemical shifts. The observed ¹H NMR signals should be consistent with the time-averaged structure of these solvates.

In order to assign the pairs (a-b or a'-b') corresponding to the signals of the diastereotopic methyl or methylene protons, the second eluted enantiomers of (\pm)-**16** resolved by HPLC on a Chiralpak AD-H was added into a toluene-d₈ solution containing racemic compound and (S)-TFAE. Taking the NMR spectrum, it was observed that the intensity of the signals belonging to this enantiomer which were the more shielded of the C-5 methyl or methylene proton signals (Figures 4.20, B) increased. For the compound (\pm)-**17** the splitting patterns of the AB spectra enabled us to distinguish between the signals of **M** and **P** conformers.

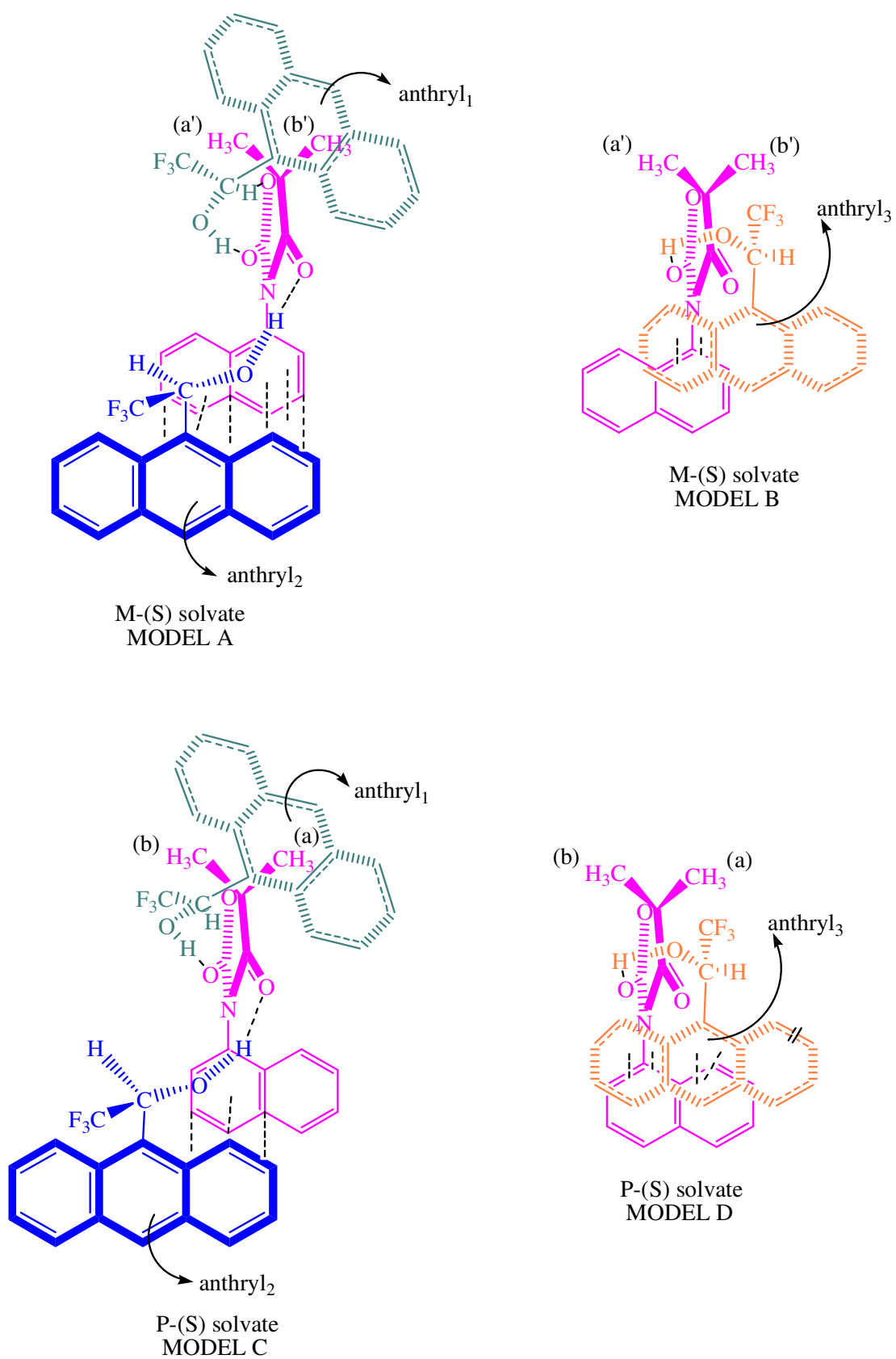


Figure 4.26. The proposed solvation models for the **M** and the **P** enantiomers of (\pm)-**15**

The assignments of the four peaks to the four methyl groups (Figures 4.20 and 4.26) as a, a', b, b' has been done in the following way: The protons (a) and (a') both were affected by the shielding zone of the naphthyl group, giving the signals in the upfield region compared to (b), (b'). Additionally, the proton (a) of the **P** conformer was affected by shielding zone of anthryl₃ (Figure 4.26, model D) and anthryl₁ (Figure 4.26, model C), whereas the proton (a') was shielded by anthryl₂ (Figure 4.26, model A). Since anthryl₂ was closer to the proton (a') and **M** conformation could form a tighter complex [29] this proton should be shielded more with respect to the proton (a) of the **P** conformer.

The protons (b) and (b') were not affected by the naphthyl (Figure 4.26). The proton (b) was part of the time in the shielding zone of the anthryl₂ (Figure 4.26, model C), part of the time not (Figure 4.26, model D) whereas the proton (b') was always affected by anthryl₁ (Figure 4.26, model A). Since (b') experiences a stronger shielding effect than the proton (b) of the **P** conformer it appeared more shielded than b. Therefore it can be argued that for all the compounds studied ((±)-**15-17**), in the presence of (S)-TFAE the more deshielded of the diastereotopic C-5 methyl and the methylene protons (Figure 4.20) can be assigned to the complexed **P** conformer and the more shielded to complexed **M** (Figure 4.20). Thus, second eluted enantiomer of (±)-**16** have been assigned to **M** conformation.

The model also accounts for the difference in chemical shifts between the a and a' (upfield, 0.01 ppm) and the b-b' (downfield, 0.02 ppm) pairs (Figure 4.20, C) which was absent for *o*-iodo derivative [19]. Since the a and a' protons are subjected to similar anisotropy effects the chemical shift difference between them was smaller than that of b and b'.

The nonresolved (a) and (a') protons of the compounds (±)-**16** (Figure 4.20) may be explained on the basis of the ring size of the chelate structure formed between the (S)-TFAE and the ring oxygen or sulphur and the C=O or C=S groups of the heterocycle (Figure 4.26), changing the geometry of the ring formed on chelation. In compound (±)-**16**, although anthryl₁ was closer to the proton (a) than (±)-**15, 17**, anthryl₃ was far away from it (model D). This causes a similar shielding effect on protons (a) and (a'), giving the same chemical shift values for these compounds.

On cooling it was observed that the upfield chemical shift differences of the ^1H NMR signals of the C-5 methyl groups of the compounds (\pm)-**15** and (\pm)-**16** increased in the following order, (b')>(b)>(a')>(a)ⁱⁱ, (Figures 4.22 and 4.23). However the signals of C-5 methylene protons of the compound (\pm)-**17** had a shift pattern that was in the following order, (b')>(a')>(a)>(b) (Figure 4.24). The observed chemical shift behaviour on cooling could be explained on the basis of the proposed solvation model (Figure 4.26). The fact that the aromatic protons of the naphthyl and the anthryl rings were shielded more and the hydroxyl proton was deshielded more compared to the values at 30 °C pointed that all of the intermolecular interactions were getting stronger upon cooling. This result may be attributed to the slower rotation of the molecules at lower temperatures. The conformation might even have been frozen at -70 °C. For example, the aromatic groups of the enantiomers and (S)-TFAE could be positioned well parallel to each other enhancing the intermolecular interactions. In compounds (\pm)-**15** and (\pm)-**16** as the temperature was lowered the change in chemical shift values of proton (b') of the **M** conformer was the most affected one and it was strongly shielded. As a matter of fact based on our model this proton was already strongly affected by an average anisotropy of the anthryl₁ at 30 °C where its rotation was fast around C_{sp2}-C_{sp3} single bond of (S)-TFAE. However decreasing the temperature made this rotation slower, making the anthryl₁ adopt a conformation where the hydroxyl group and the carbonyl hydrogen were alligned on the same side and -CF₃ positioned nearly orthogonal to the plane of the anthryl group [26]. In this conformation the anthryl₁ would be closer to the proton (b') thus shielding it more.

At 30 °C both of the solvation models (C and D in Figure 4.26) are possible for the **P** conformer, model C being more populated. The proton (b) was only affected by the anisotropy of anthryl₂ during solvation C as shown in Figure 4.26. Therefore its shielding was only explained on the basis of Model C. Upon cooling the change in the solvation model from D to C (Figure 4.26) increased the anisotropy effect on this proton, making it more shielded.

ⁱⁱ For compound (\pm)-**2** and (\pm)-**4** the chemical shift values of (a) and (a') were the same.

In model A there was a strong π - π interaction between the aromatic rings, affecting the proton (a'). This intermolecular interaction was getting stronger upon cooling making this proton more shielded.

The proton (a) was affected by the average shielding effect of both anthryl₁ and anthryl₂ at 30 °C. However on cooling the **P** enantiomer may prefer the model C where the proton (a) was only affected by anthryl₁. This proton although can be expected to be less shielded due to the same reason noted for proton (b), shielding by the anthryl₁ had a compensating effect thus the chemical shift of this proton did not change much on cooling.

Having these results it can be said that the diastereotopic methyl signals of **M** conformer forming a tighter complex with (S)-TFAE was shielded more compared to that of **P** conformer. These results are also consistent with what we observed for 5,5-dimethyl-3-(*o*-iodophenyl)-2,4-oxazolidinedione on cooling. For this compound, although the chemical shift of the signals did not change significantly, the signals of **P** conformer which formed a tighter complex with (S)-TFAE was the most shielded ones upon cooling.

The different shift pattern observed for the compound (\pm)-**3** upon cooling may arise from the difference in the van der Waals radii of C-5 methyl and methylene protons. Since methyl protons are exposed into space more, these protons may experience a different anisotropy effect. Even if a different shift pattern was observed for these compounds on cooling, the diastereotopic methyl signals of the **M** conformer (a'-b') was the most shielded ones as observed in the compounds (\pm)-**15**, **16**.

4.3.4. Activation Barriers to Hindered Rotation

Activation barriers to hindered rotation of the compounds studied were determined either by temperature dependent NMR or by enantioresolution on a chiral sorbent via HPLC. If the barrier to restricted rotation about C_{sp2}-N_{sp2} chiral axis is sufficiently high separation of enantiomeric rotational isomers would be possible by HPLC.

Dynamic NMR studies of all the compounds, except the compound (\pm)-**15**, indicated no coalescence for the diastereotopic protons up to 110 °C due to the high activation barrier

for restricted rotation. Therefore thermal racemization after micropreparative enrichment of these enantiomers was applied to calculate the barriers. Enantioresolution of the racemic mixtures was performed on Chiralpak AD-H column packed with amylose tris-(3,5-dimethyl)-carbamate as chiral stationary phase and thermal racemization process was followed by UV at 254 nm. To obtain a better resolution of the enantiomers, all chromatographic separations were conducted at 7 ± 2 °C. The same procedure described in our previous work [19] was followed for thermal racemization (Figures 4.27 and 4.28). The activation parameters of compounds (\pm)-**16**, (\pm)-**17** are listed in Table 4.10 and data pertinent to the chromatographic separations of the enantiomers on Chiralpak AD-H are shown in Table 4.11.

Table 4.10. The kinetic and thermodynamic data for the interconversion process shown in Figure 4.18

Compound No	solvent	T, K	k, s^{-1}	$\Delta G^\ddagger, kJ/mol$
(\pm)-15	DMSO- d_6	398 ^a	54,52 ^b	85,01 \pm 0.05 ^c
	Toluene- d_8	378 ^a	36,62 ^b	81,83 \pm 0.05 ^c
(\pm)-16	Ethanol:hexane (20%:80%, v/v)	333 ^d	4.10 ⁻⁵ . ^e	109,9 \pm 0.07 ^f
(\pm)-17	Ethanol:hexane (60%:40%, v/v)	313 ^d	3.10 ⁻⁵ . ^e	103,8 \pm 0.07 ^f

^a: the coalescence temperature
^b: rate constant at coalescence temperature
^c: free energy of activation determined by 400 MHz NMR instrument.
^d: the temperature at which the thermal racemization has been done.
^e: the rate constant of interconversion
^f: free energy of activation determined by HPLC

Table 4.11. Chromatographic parameters for the separation of enantiomers by HPLC on Chiralpak AD-H at 7 ± 2 °C

Compound No	Eluent composition	Retention times, t_1, t_2, min	Capacity Factors, k_1, k_2	Selectivity, α	Flow rate, ml/min
(\pm)-16	Ethanol:hexane (20%:80%, v/v)	12,96	1,23	1,30	0,5
		15,08	1,60		
(\pm)-17	Ethanol:hexane (60%:40%, v/v)	19,71	2,40	1,79	0,5
		30,78	4,31		

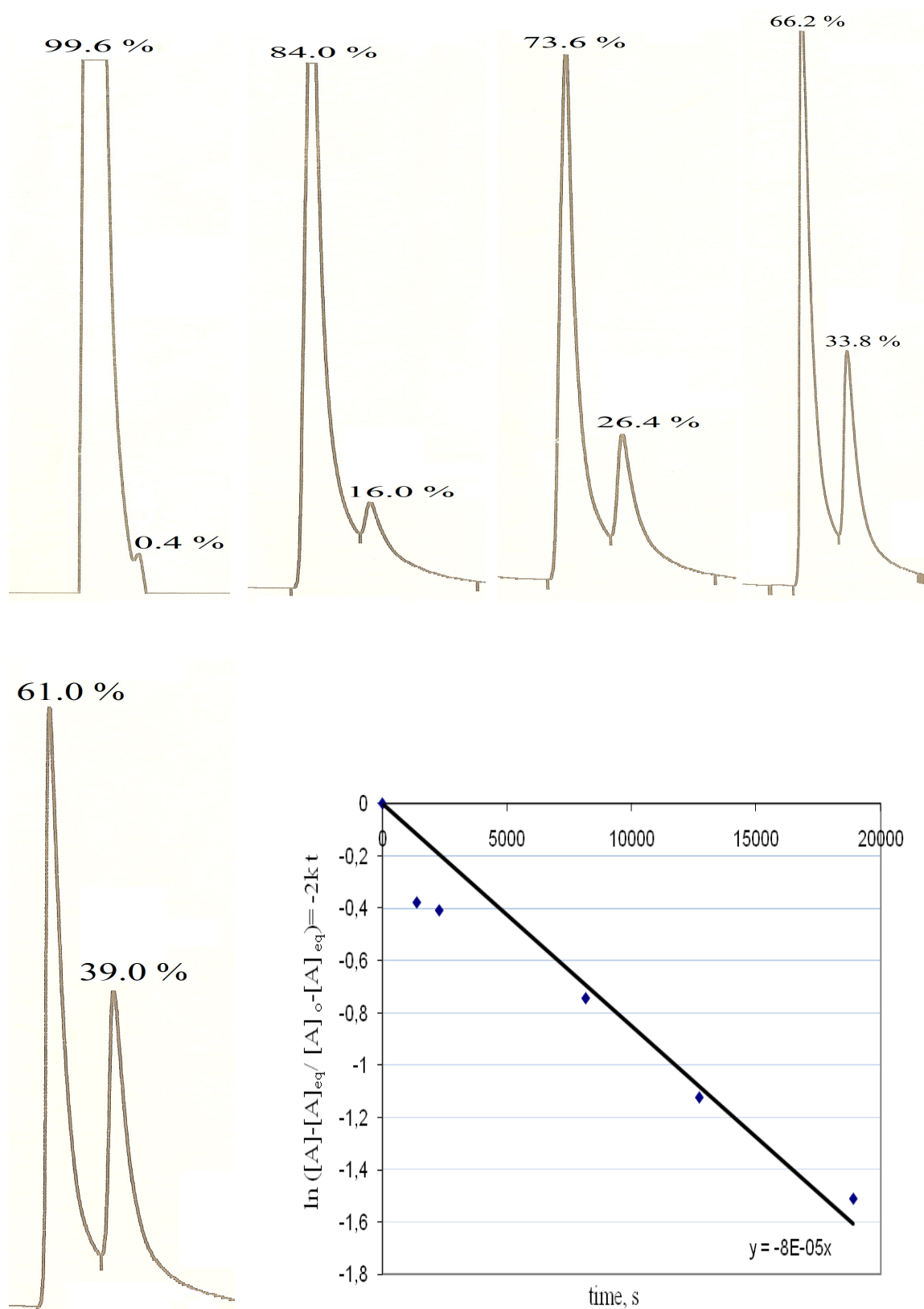


Figure 4.27. The change in enantiomer composition versus time for compound (\pm) **16** after micropreparative enrichment of the first eluted enantiomer followed by HPLC at 293 K, detection: UV at 240 nm. Inset: The plot of $\ln([A]-[A]_{eq}/[A]_0-[A]_{eq})$ versus time

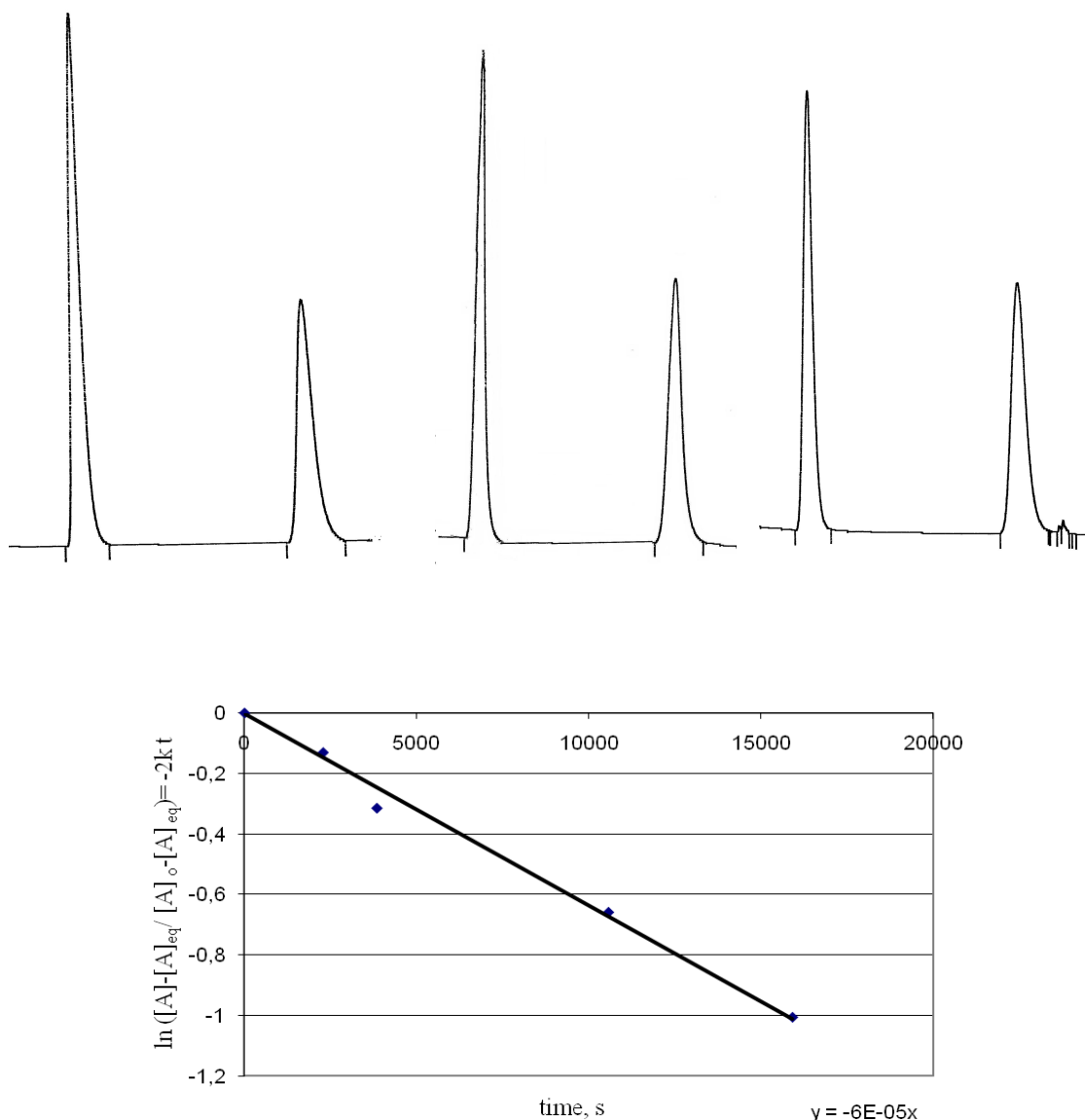


Figure 4.28. The change in enantiomer composition versus time for compound (\pm) **17** after micropreparative enrichment of the first eluted enantiomer followed by HPLC at 293 K, detection: UV at 240 nm. Inset: The plot of $\ln([A]-[A]_{eq}/[A]_0-[A]_{eq})$ versus time

Activation parameters of (\pm)-**15** were found by dynamic NMR spectroscopy. The two singlets of the diastereotopic C-5 methyl protons that were distinguishable at 30 °C coalesced into one peak at higher temperatures due to the fast rotation. The kinetic data of the interconversion process were determined by the Eyring equation [16] and it was apparent that the barrier (85,01 kJ/mol in DMSO- d_6 , Table 4.10) was not high enough to allow the resolution of the compound (\pm)-**15** into enantiomers on Chiralpak AD-H.

The barriers of 2,4-oxazolidinedione (compounds (\pm)-**15**, (\pm)-**17**, Y=O, Figure 4.18) derivatives were found to be lower than that of 2-thioxo-4-oxazolidinone (compound (\pm)-**16**, Y=S) derivatives. This difference was interpreted by means of the higher standard bond length of the C=S double bond (1,71 Å) than that of the C=O (1,22 Å) and the larger van der Waals radius of sulphur (1,85 Å) than that of the oxygen atom (1,40 Å). In compound (\pm)-**16** repulsion between thiocarbonyl sulphur atom and the peri hydrogen of the naphthyl group in the transition state serves as a steric impediment to the enantiomer interconversion and makes the passage of the peri hydrogen more difficult and, in turn, increases the barrier to hindered rotation.

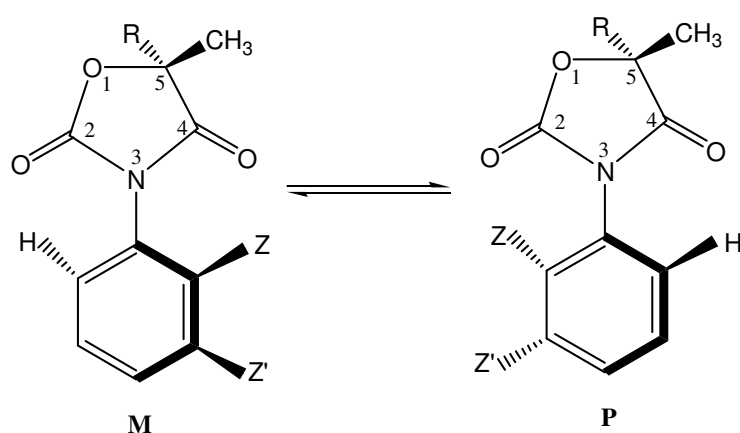
Comparison of the energy barriers of compounds (\pm)-**15** and (\pm)-**17** revealed the influence of the solvent used (Table 4.10). Compound (\pm)-**17** unexpectedly exerted a higher barrier than compound (\pm)-**15** (Figure 4.18). This result may be attributed to the solvent effect [14] of ethanol that may form hydrogen bonds with the C=O groups on position 2 and 4 and makes the rotation around the C_{sp2}-N_{sp2} bond more hindered.

4.4. Ring Opening and Asymmetric Reduction Reactions of 2,4-Oxazolidinedione Derivatives

There has been a great interest in the oxazolidine ring containing compounds because of their potential biological activity [39] pharmaceutical significance [40] and their utility as directing groups in asymmetric synthesis [8,41]. The oxazolidinedione ring is present in some antidiabetic drugs [40], anticonvulsants [2] and herbicides. Introducing an *ortho* substituted phenyl ring to the oxazolidinedione ring on the nitrogen atom brings dissymmetry to these compounds and makes them axially chiral due to the restricted rotation around the C_{aryl}-N_{sp2} single bond, which gives rise to a pair of atropisomers (Figure 4.29) [14,19].

Since compounds bearing oxazolidine ring have found wide-spread use in a number of biologically active synthetic products and in asymmetric synthesis, the stability of the heterocyclic ring in various conditions must be investigated to increase the yield of their synthesis, to predict the structure of the reaction products and the reaction route followed.

Although ring opening reactions of oxazolidinones have been studied by Evans [11] there are only a few reports on 2,4-oxazolidinedione derivatives [2]. In this project, we report our results of a comprehensive study of basic and reductive ring opening reactions of diastereomeric (5*S*)-methyl-*N*-(*o*-aryl)-2,4-oxazolidinediones [14] and enantiomeric 5,5-dimethyl-*N*-(*o*-aryl)-2,4-oxazolidinediones [19] (Figure 4.29) to examine the stability of the ring and to synthesize various organic compounds (Figure 4.30) such as chiral α -hydroxyamides, carbamoyloxyacids, chiral diols via ring opening. Chiral α -hydroxyamides have anticonvulsant activity and could be converted to β -amino alcohols that can be further utilized in the synthesis of biologically active products or as a chiral auxiliary in asymmetric syntheses. Chiral diols are synthetic intermediates and can be used in the determination of the enantiomer composition [8].



- 1**, R=H, Z= CH₃, Z'=H
2, R=H, Z=Z'=benzo
3, R=H, Z= I, Z'=H
4, R=H, Z= Br, Z'=H
5, R=H, Z= Cl, Z'=H
6, R=H, Z= F, Z'=H
(±)7, R= CH₃, Z= CH₃, Z'=H
(±)8, R= CH₃, Z= F, Z'=H
(±)9, R= CH₃, Z= Cl, Z'=H
(±)10, R= CH₃, Z= Br, Z'=H
(±)11, R= CH₃, Z= I, Z'=H
(±)15, R= CH₃, Z=Z'=benzo

Figure 4.29. The compounds studied

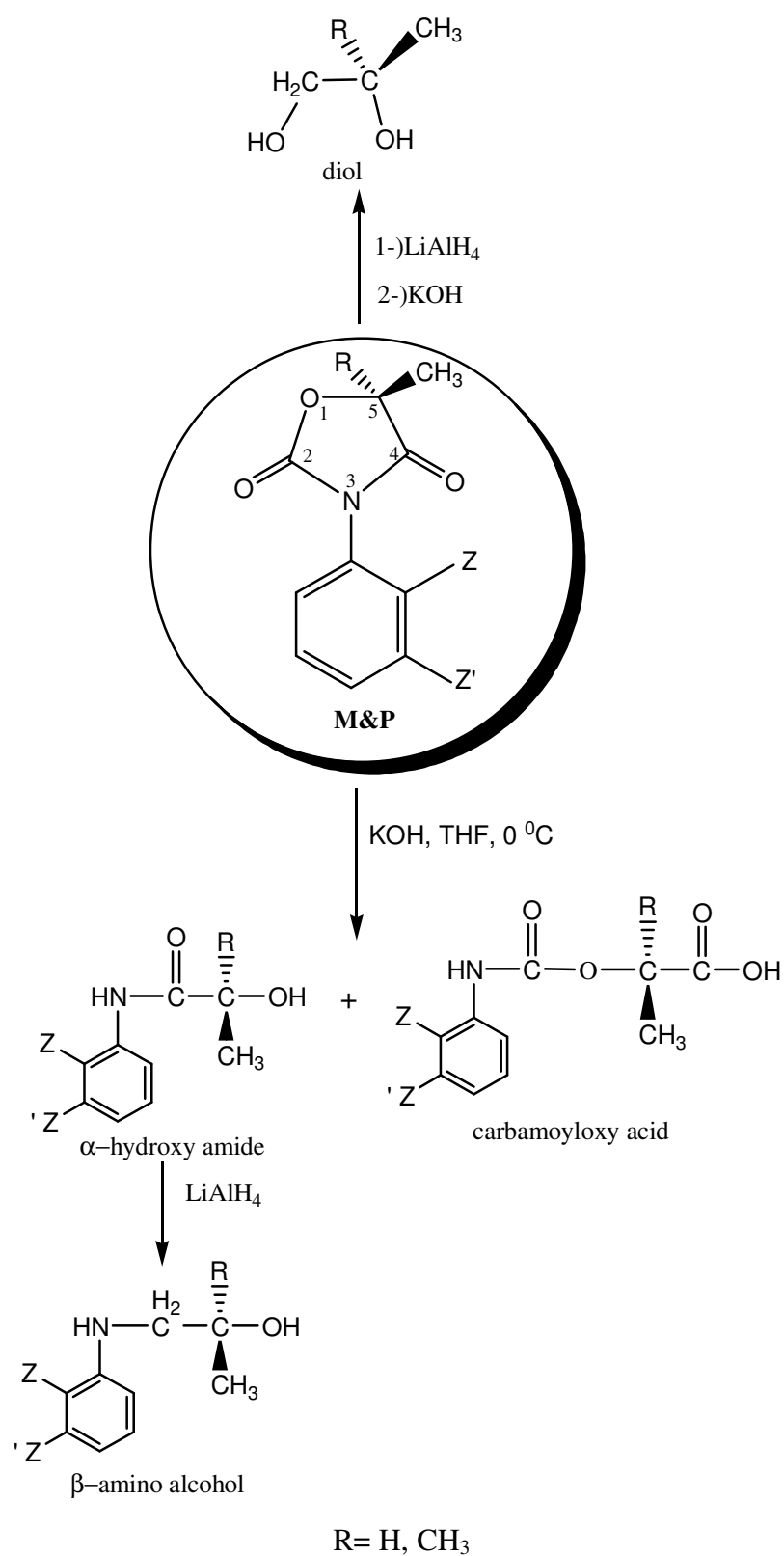


Figure 4.30. Ring opening reactions

The synthesized (5*S*)-methyl-3-(*o*-aryl)-2,4-oxazolidinedione (Compounds **1-6** and 5,5-dimethyl-*N*-(*o*-aryl)-2,4-oxazolidinediones (Compounds (\pm)**7-11**, **15**) have been shown [14,19] to have thermally interconvertible conformations, **M** and **P** stereoisomers (Figure 4.29), corresponding to the ground states for the internal rotation about the chiral C-N bond axis. Due to the chiral center with “*S*” configuration at C-5 and the hindered rotation around the C_{aryl}-N_{sp2} single bond compounds **1-6** exists as a pair of diastereomers, whereas compounds (\pm)**7-11**, **15** bearing only a chiral axis are obtained as a pair of enantiomers.

4.4.1. Reaction with Ethanol

During an experiment done for the determination of the activation barrier for Compound **3**, it has been observed that this compound reacted with the solvent ethanol at 70 °C. During the interconversion process which was followed by HPLC it has been observed that a new peak whose intensity increased with time was formed. That product was then collected micropreparatively and its structure was found to be the ring opening product at the N-C₄ bond (amide part of the ring) by ¹H NMR identification. Refluxing compound **3** with ethanol for one day yielded the same product.

Moreover, when the synthetic yields of compounds **1-6** and (\pm)**7-11**, **15** was compared it was found that the yield of diastereomeric compounds was lower than that of enantiomeric ones [14,19]. Together with geminal dimethyl effect (Thorpe-Ingold effect) [42-43], this might be attributed to the reaction of the compounds with ethanol being produced during the synthesis [44].

All these results led us to study the stability of the heterocyclic ring in the presence of different nucleophiles.

4.4.2. Reaction with KOH

To study the stability of the oxazolidinedione ring to nucleophilic attack, first the reaction of compounds **1-11**, **15** with KOH, which is a more powerful nucleophile than ethanol, was examined in THF-methanol at 0 °C [11]. THF was used to increase the

solubility of the compounds studied and it was seen that the presence of even 1 ml of methanol decreased the reaction times.

Since there are two carbonyl groups in the structure, there are two possibilities for nucleophilic attack of hydroxide ion. Both of these attacks resulted in a ring opening product arising from the endocyclic cleavage pathway. While attack to C-2 carbonyl yielded a α -hydroxy amide (N-aryl- α -hydroxyisobutyramide and N-aryl-lactamides) after the removal of CO₂ from the molecule (Figure 4.31), a potassium salt of carbamoyloxy acid was obtained as a result of attack to C-4 carbonyl (Figure 4.31). Acidification of the aqueous phase containing the potassium salt to pH 2 directly did not give the corresponding acids instead the reformation of the oxazolidinedione ring was found to occur (Figure 4.32). Therefore the aqueous solution was acidified in a more controlled way to pH 6.2 to obtain the carbamoyloxy acid as the only product. (Figure 4.31) Acidification to pH < 6.2 gave rise to the formation of oxazolidinedione ring together with carbamoyloxy acid. (Figure 4.31). Further acidification to below pH 6 resulted the reformation of the ring.

When the yields of the α -hydroxy amide and carbamoyloxy acid products were compared it was observed that the hydroxide ion preferred mostly to attack C-4 carbonyl carbon resulting in the formation of carbamoyloxy acid salts. This regioselectivity was attributed to the fact that C-4 carbonyl carbon of the heterocycle is more electron deficient revealed by a more deshielded signal at around 170 ppm by ¹³C NMR vs. 150 ppm signal of the C-2 carbonyl. Moreover, C-4 carbonyl carbon that could be considered as a part of an amide group can be expected to be more sensitive to basic hydrolysis than the C-2 carbonyl carbon that is a part of a secondary carbamate unit.

While the yields of the α -hydroxy amide to that of the carbamoyloxy acid salt was close to each other for the compounds (**±**)**7-11**, **15**, the difference between them was much more pronounced for the compounds **1-6**. The reaction with hydroxide ion favored mostly the carbamoyloxy acid product for these compounds. That might be explained by the fact that the less hindered C-5 in compounds **1-6** resulted in a more preferred attack to neighbouring C-4 carbon.

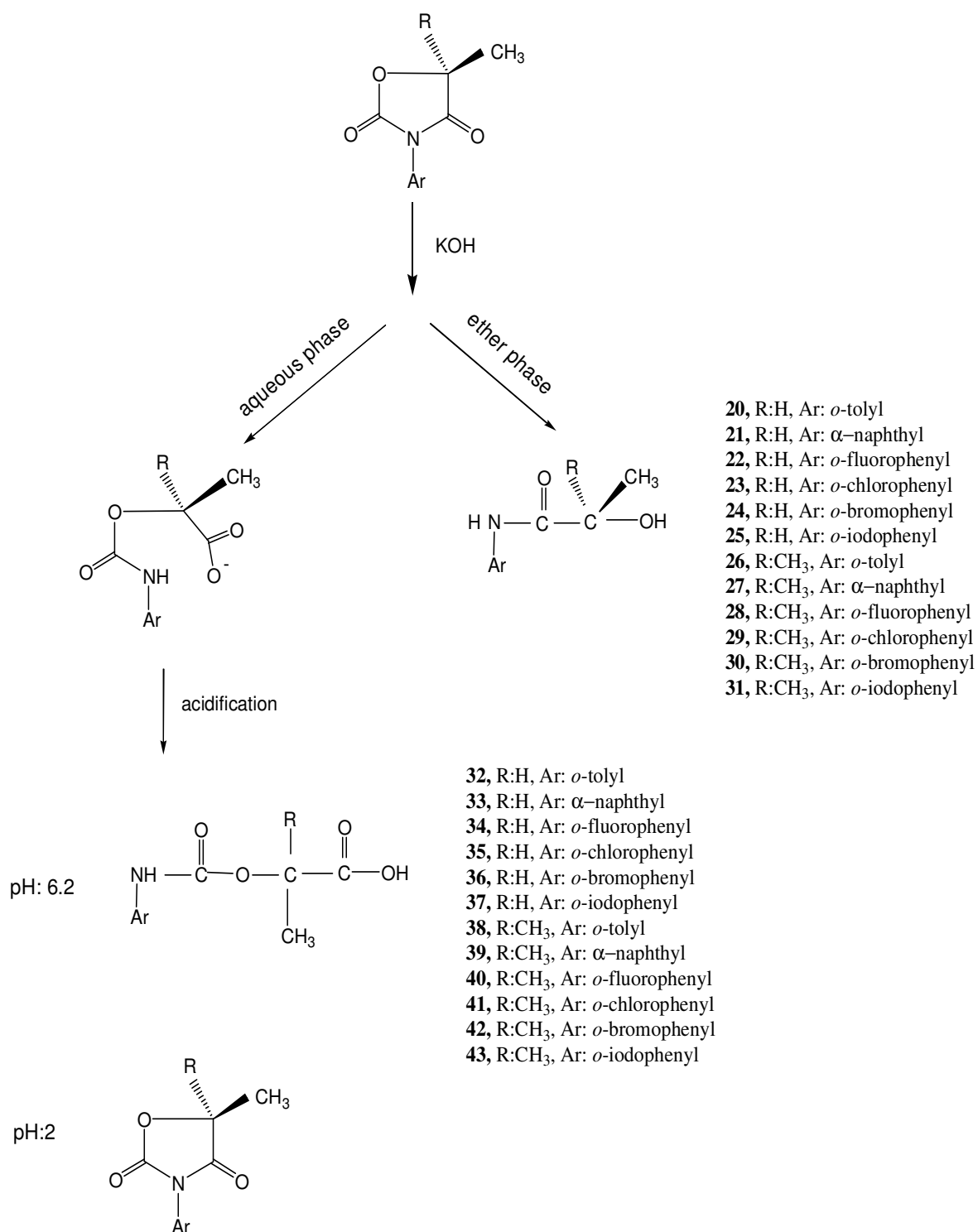


Figure 4.31. The reaction of the compounds studied with KOH and controlled acidification of aq. phase

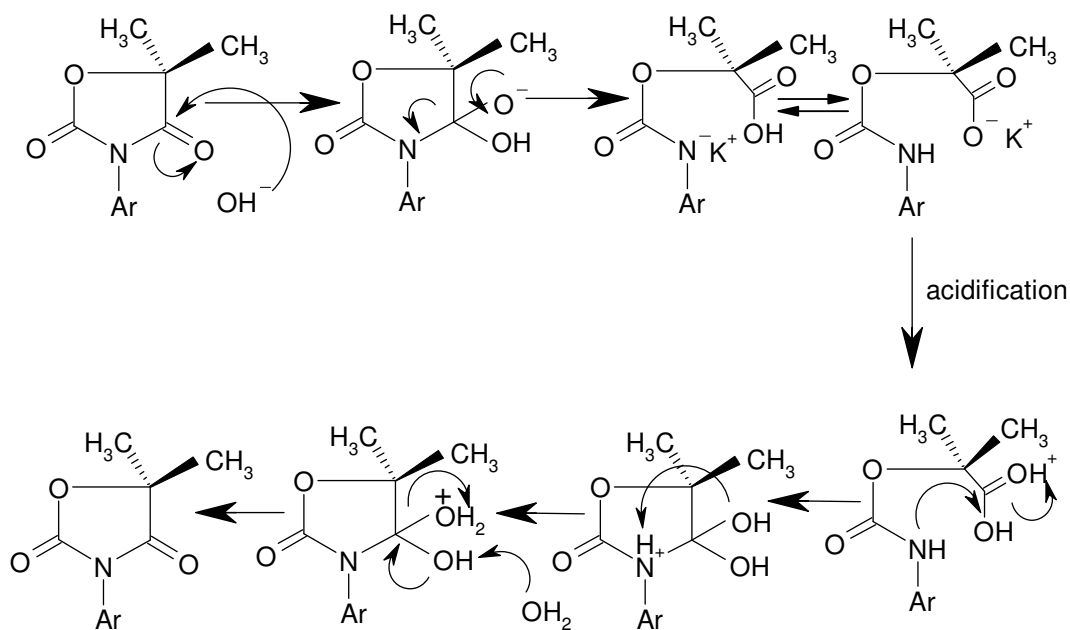


Figure 4.32. Regeneration of the heterocyclic ring at pH 2 for compounds (\pm)7-11, 15)

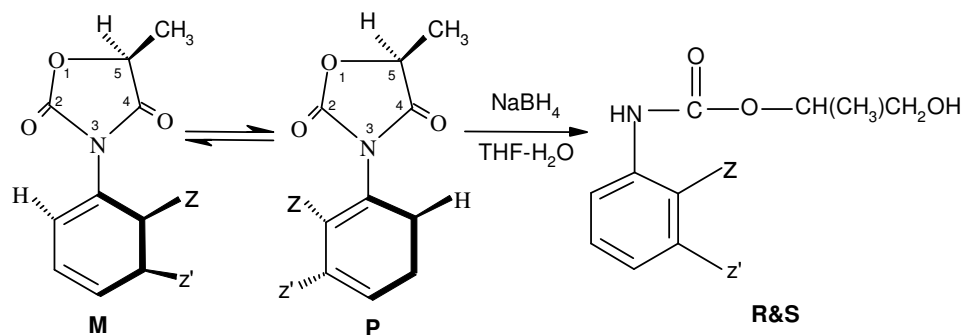
It was observed that there is a correlation between the reaction times and the activation barriers of compounds (\pm)7-11, 15. Increasing the barrier increased the reaction time. However the reaction of compounds 1-6 with hydroxide ion took place immediately after mixing. No correlation could be determined due to an easy access to C-4 carbonyl carbon resulting in a very fast reaction at 0 °C.

4.4.3. Reaction with NaBH₄

The reduction reactions of compounds 1-6 and (\pm)7-11, 15 with NaBH₄ took place regioselectively affecting only the C-4 carbonyl carbon instead of C-2 which could be considered as a part of an urethane unit.

Compounds 1-6 was reacted with 4 equivalents of NaBH₄ at room temperature yielding a primary alcohol as a consequence of a complete reduction of C-4 carbonyl carbon (Figure 4.33). In order to understand whether reductive ring opening reaction took place without racemization, the product was analyzed on a chiralpak AD-H column. The observation of two peaks (81.3:18.7) showed that racemization has occurred partially during the reaction probably due to the enolization of the acidic hydrogen on C-5. Repeating this

reaction at 0 °C to avoid racemization failed. Although this procedure is known as a racemization free method [12] the existence of a C-5 hydrogen neighbouring to both a carbonyl and an oxygen facilitated the enolization for the compounds **1-6**.



(±)**44**, Z= CH₃, Z'=H

(±)**45**, Z=Z'=benzo

(±)**46**, Z= F, Z'=H

(±)**47**, Z= Cl, Z'=H

(±)**48**, Z= Br, Z'=H

(±)**49**, Z= I, Z'=H

Figure 4.33. Reductive ring opening reactions of compounds **1-6**

Due to the presence of the C-5 chiral center in products of **1-6** the newly formed CH₂ is expected to be diastereotopic. Analysis of the proton NMR spectra (Figure 4.34) did indicate the existence of diastereotopic protons giving an AB type splitting. The C-H proton on the chiral center splitted by both diastereotopic protons and the methyl protons gave the expected multiplet.

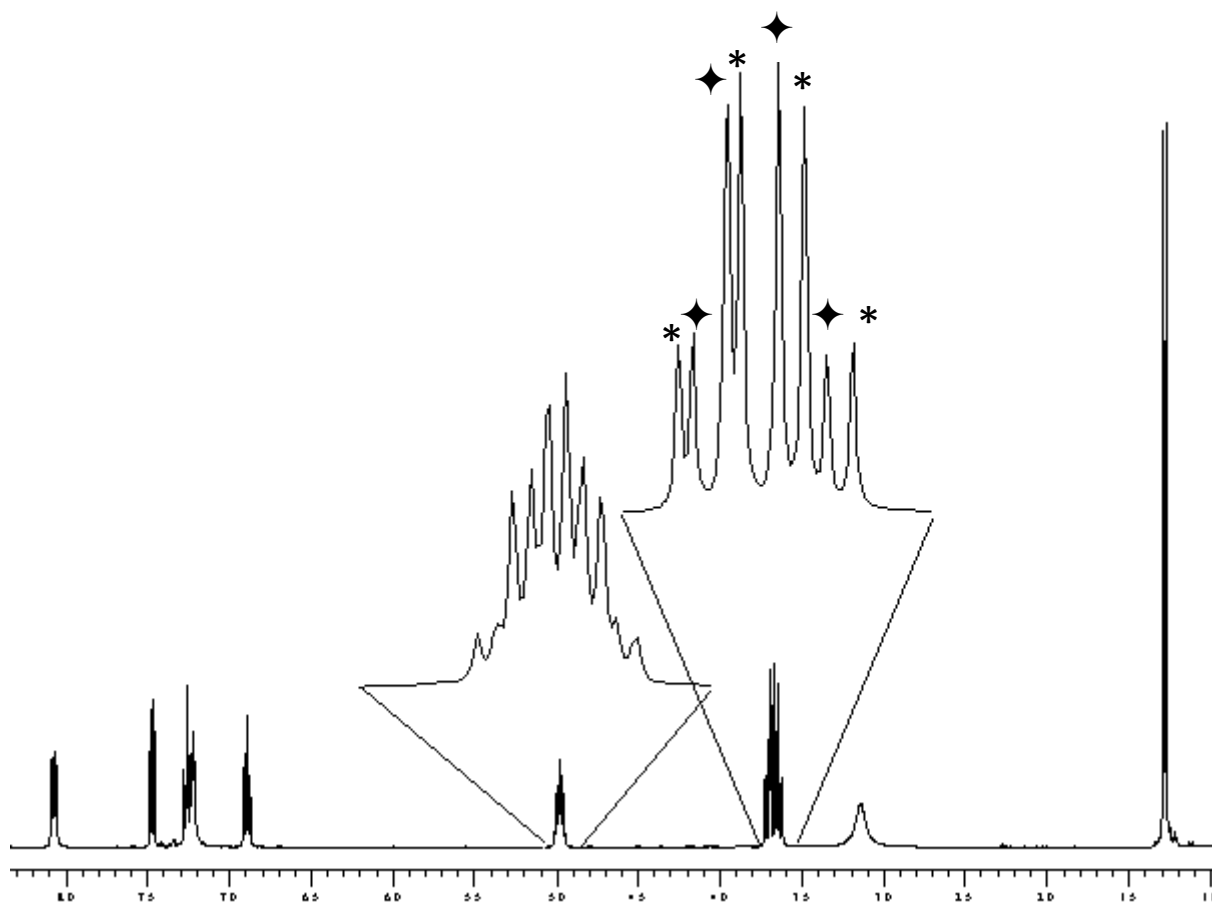
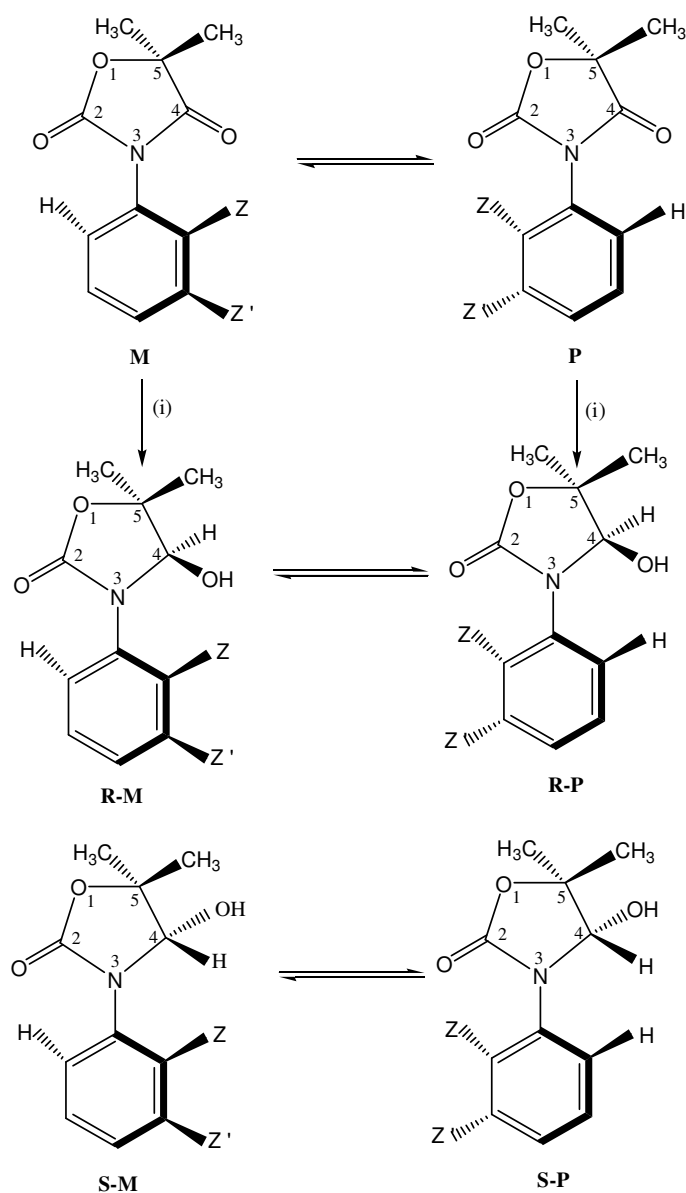


Figure 4.34. The 400 MHz ^1H NMR spectrum of compound (\pm)**48** in CDCl_3 .

The reaction of compounds (\pm)**7-11**, **15** with NaBH_4 did not result in a ring opening product. A secondary alcohol functionality was obtained at C-4 carbon as a result of only one hydride transfer (Figure 4.35). This might be explained by a steric hindrance of 5,5-dimethyl groups that hindered the approach of the second hydride. An attempt to get a primary alcohol functionality by increasing the reaction time failed. An increase in temperature to $60\text{ }^\circ\text{C}$ together with an increase with the amount of NaBH_4 did not cause a complete reduction. Since the reductions of compounds (\pm)**7-11**, **15** are sensitive to steric hindrance around the carbonyl, instead of using NaBH_4 , more powerful reducing agents LiAlH_4 and LiBH_4 were also used, however the reaction still gave the same reduction product and did not a primary alcohol unit at $0\text{ }^\circ\text{C}$ or upon heating for 2 days.



50, Z= CH₃, Z'=H

51, Z=Z'=benzo

52, Z= F, Z'=H

53, Z= Cl, Z'=H

54, Z= Br, Z'=H

55, Z= I, Z'=H

Figure 4.35. The reaction of compounds (\pm)**7-11**, **15** with NaBH₄, (i) NaBH₄, THF-H₂O, room temperature

Due to the formation of a new chiral center on C-4 the chemical shift difference between the diastereotopic geminal dimethyl protons increased for compounds **50-54**.

Comparing the reduction times revealed that compounds **1-6** reacted faster than compounds (\pm)**7-11, 15** probably due to the steric hinderance caused by the presence of 5,5 dimethyl groups. One another reason may be the stability of the ring of compounds (\pm)**7-11, 15** having geminal dimethyl groups which is resistant to opening (Thorpe-Ingold effect).

4.4.3.1. Stereoselective (Diastereoselective) Reduction of Compounds (\pm)**7-11, 15**. The reaction of NaBH₄ with compounds (\pm)**7-11, 15** is expected to form four stereoisomers due to the formation of a new chiral center on C-4: two enantiomeric (**S-M/ R-P, S-P/ R-M**) and two diastereomeric pairs (**S-M/S-P, R-M/R-P**) (Figure 4.35). The two expected diastereomeric pairs were not be observed by NMR. When the product mixture was injected to the chiral OD-H column at 7 °C, only one enantiomeric pair was observed for compounds (\pm)**50, 51, 53-55**. In contrast, compound (\pm)**52** could not be resolved by changing the eluent composition or even using different columns (Table 4.12).

The observation of only one enantiomeric pair for compounds (\pm)**50, 51, 53-55** led us consider the possibility of stereoselective reduction. Since boron is tetracoordinated, in the attack of the hydride the Felkin-Anh model is usually invoked [45]. The attack of the hydride takes place anti to the most bulky or polar group. ie. the *ortho* substituent in our case, resulting in a facial selectivity for a carbonyl group. The attack of a hydride on prochiral C-4 carbonyl group can be accomplished either on the *Re* or *Si* face of the carbonyl. Due to the presence of an *ortho* substituent that was very close to the reaction site we expected to observe a selectivity for that attack from the opposite side of the *ortho* substituent (Figure 4.36).

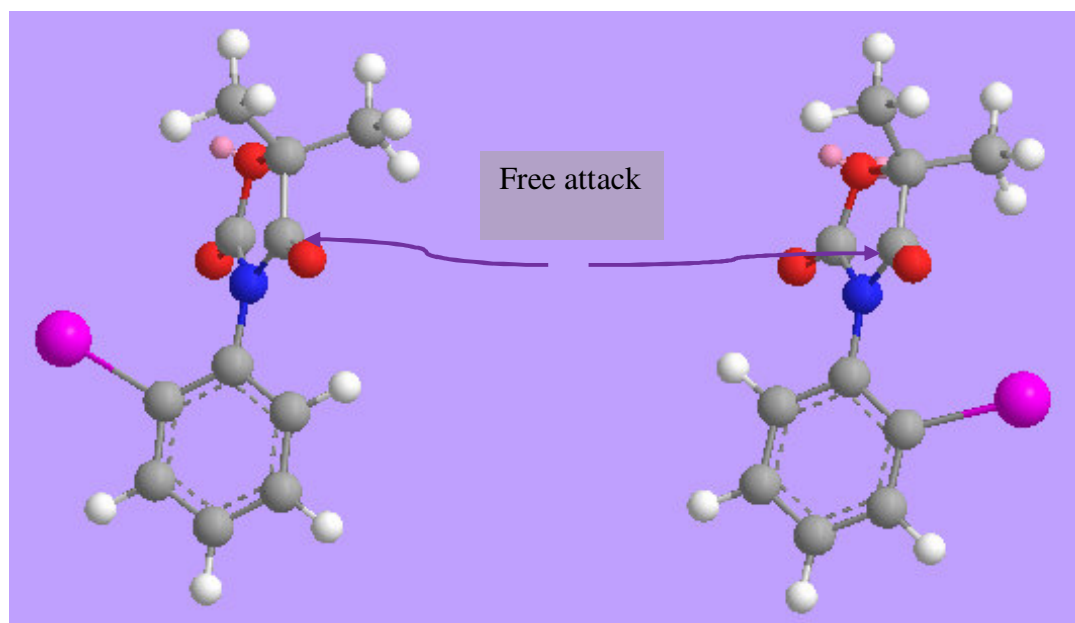


Figure 4.36. Selective approach of hydride to the compound (\pm)**52** from the less hindered sites

Table 4.12. Chromatographic parameters for the separation of enantiomers by HPLC at 7 ± 2 °C

Entries	Diastereomer ratio, %	Column	Eluent composition, % (hexane:ethanol)	Flow, ml/min
50	38,8:61,2 ^a	Chiralpak IB	80:20	0,6
51	100 ^b	Chiralpak IB	70:30	0,5
52	100 ^c	Chiralcel OD-H	70:30	0,4
	100 ^c	Chiralpak IB	80:20	0,6
53	100 ^b	Chiralpak IB	80:20	0,6
54	100 ^b	Chiralcel OD-H	80:20	0,6
55	100 ^b	Chiralpak IB	60:40	0,4

^a: Diastereomer ratio, % obtained upon cooling
^b: only one enantiomeric pair could be seen
^c: Only one peak was seen for the four isomers

When the product (\pm)**55** (Figure 4.38) was injected to the chiral OD-H column only two isomers (50% each) which were interpreted as enantiomers of each other were detected (Table 4.12, Figure 4.35). Attempts to observe the other enantiomeric pair failed when different columns and eluent compositions were used. After heating the solution of (\pm)**55** for 105.5 hours at 78 °C the other pair (minor in amount in thermodynamic equilibrium) could be observed. The observation of the newly formed enantiomeric pair in small amount revealed that they were the kinetic products. Since iodine is the most bulky in the series, the hydride atom may favor only the attack that is opposite to iodine. Therefore, **S-P** and **R-M** were the kinetically produced isomers, however the presence of hydroxyl group and the iodide atom on the same side made these isomers very unstable. Since the hydroxyl on C-4 and the *ortho* substituent were on opposite sites the **S-M** and its enantiomer **R-P** were expected to be the thermodynamically stable isomers (Figure 4.37).

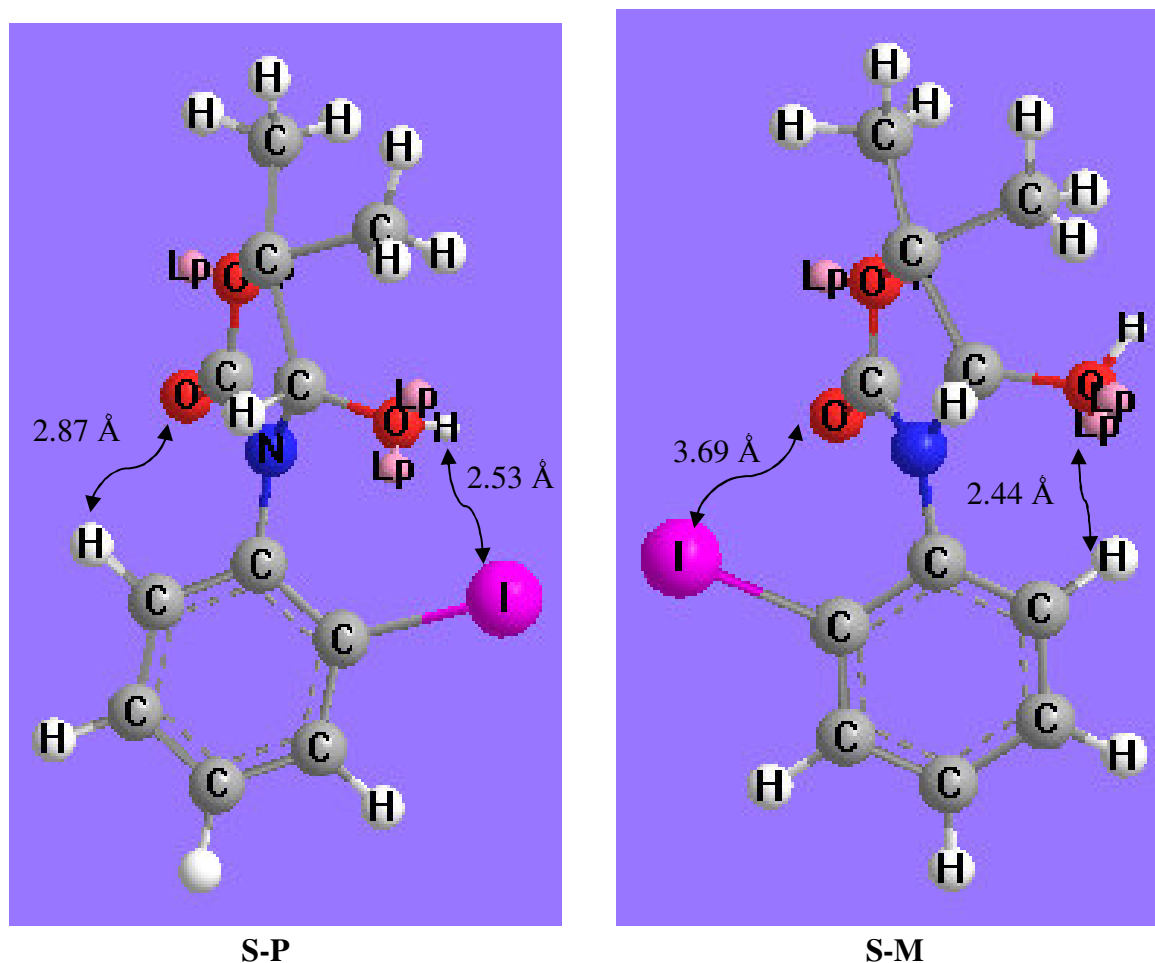


Figure 4.37. Molecular models of compound (\pm)**55** showing the spatial proximity of the selected groups in Å (Lp: lone pairs)

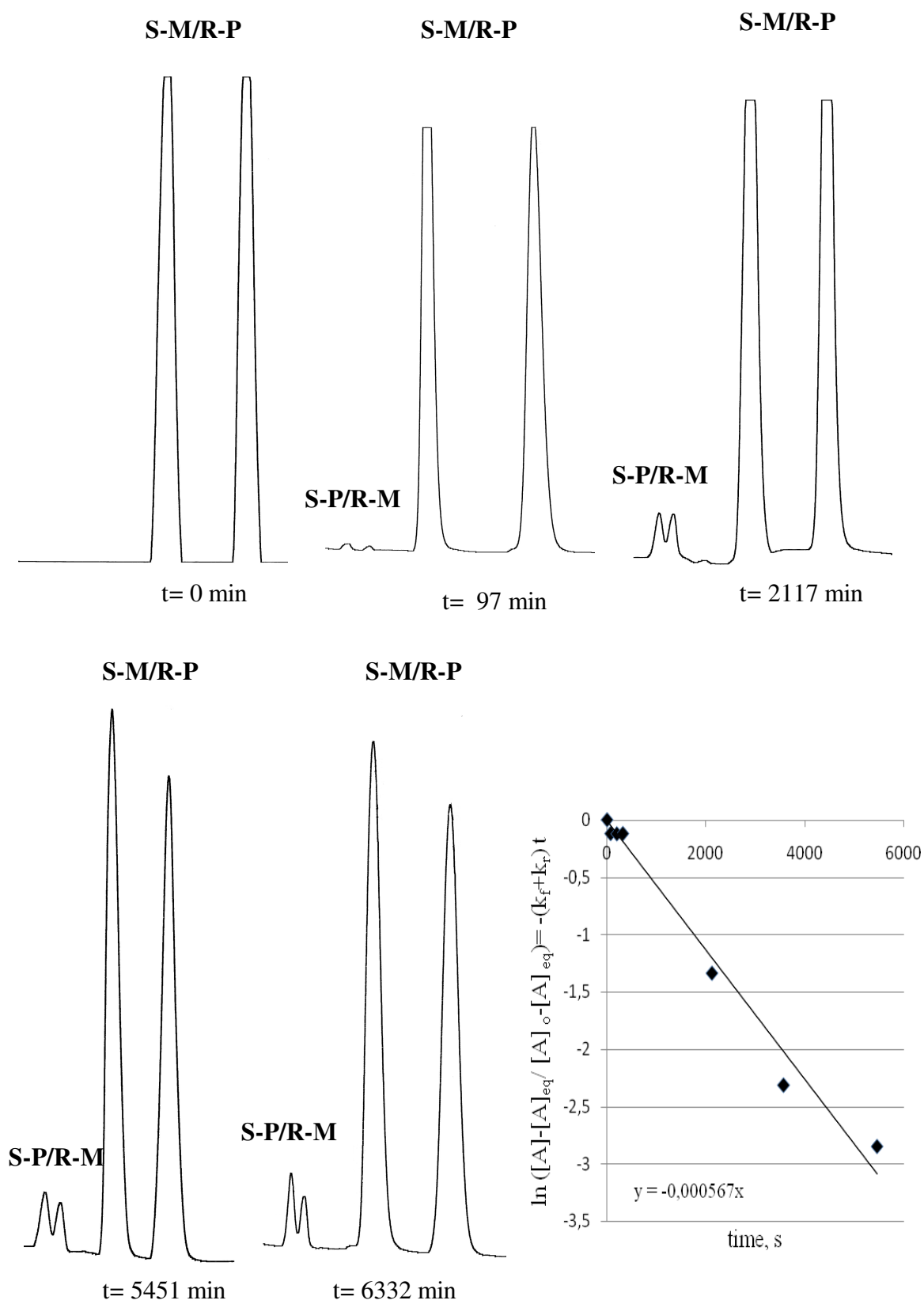


Figure 4.38. The chromatograms taken to follow the thermal equilibration of the rotational isomers of (\pm)55

In order to prove this hypothesis, the selective reduction reactions of compounds (\pm)**7**, **11**, **15** at room temperature with Chiralpak IB column were followed by HPLC. The reduction of compound (\pm)**7** yielded a peak at 11.7 min (first enantiomeric pair that could not be resolved) and two peaks having a ratio of 1:1 at 16.3 and 18.3 min. (second enantiomeric pair) (Figure 4.39). The ratio of these diastereomeric pairs was 31.97: 68.03 % after quenching but after solution was kept at room temperature for several days it was 13.53: 86.47 %. Therefore it was concluded that the first enantiomeric pair corresponded to the kinetic product, the others to thermodynamic ones and due to the low activation barrier of this compound in extracting solvent ethyl acetate or reaction mixture containing THF, the observation of selective formation of first enantiomeric pair could not be achieved because as soon as they were formed they rapidly interconverted to the other pair.

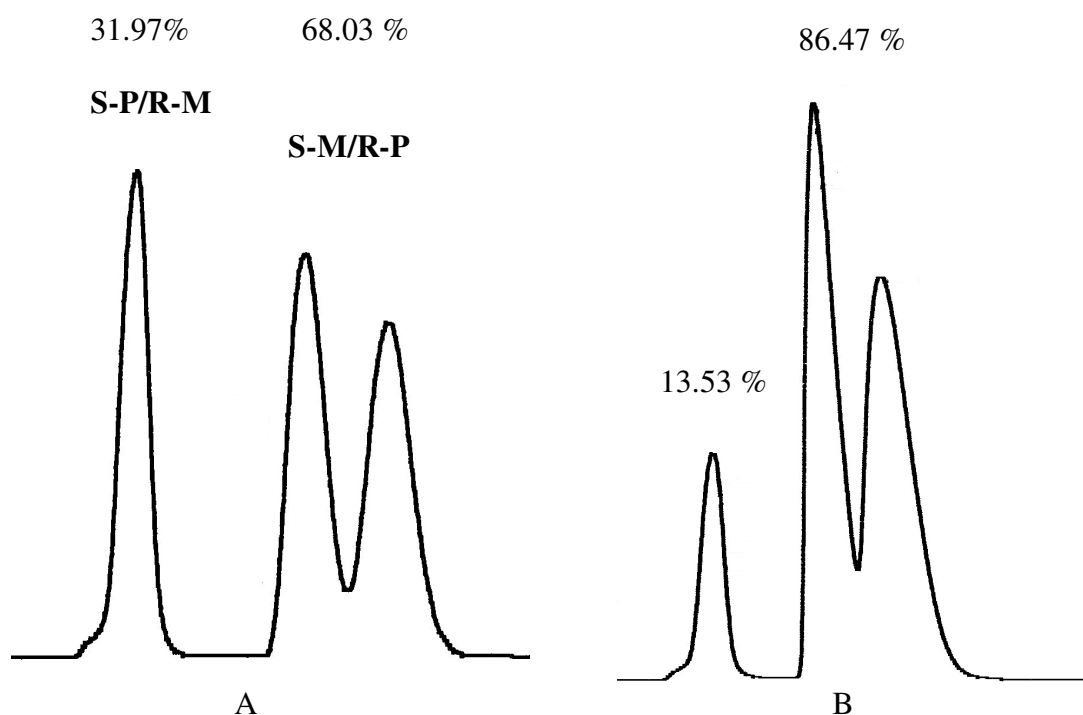


Figure 4.39. The stereoisomers of compound (\pm)**7**, A: upon cooling, B, ethanol solution was kept for several days at RT

NOESY spectra for compounds (\pm)**50** and **55** were taken in order to elucidate the stereochemistry of the thermodynamic isomers (Figures 4.40 and 4.41). The observed crosspeaks between the C-4 carbinyl hydrogen and the *ortho* methyl protons of compound (\pm)**50** revealed that in the structure of the stable isomers, these protons are on the same side

(**S-M** and **R-P**) (Figure 4.40). The spatial proximity between the carbonyl hydrogen and one of the C-5 methyl group could also be seen in this spectrum. Similarly, in the NOESY spectrum of compound (\pm)**55**, the crosspeaks observed between *ortho* hydrogen and C-4 hydroxyl group showed that the stable isomers have conformations where C-4 hydroxyl group and iodine atom are on opposite sides (**S-M** and **R-P**) (Figure 4.41).

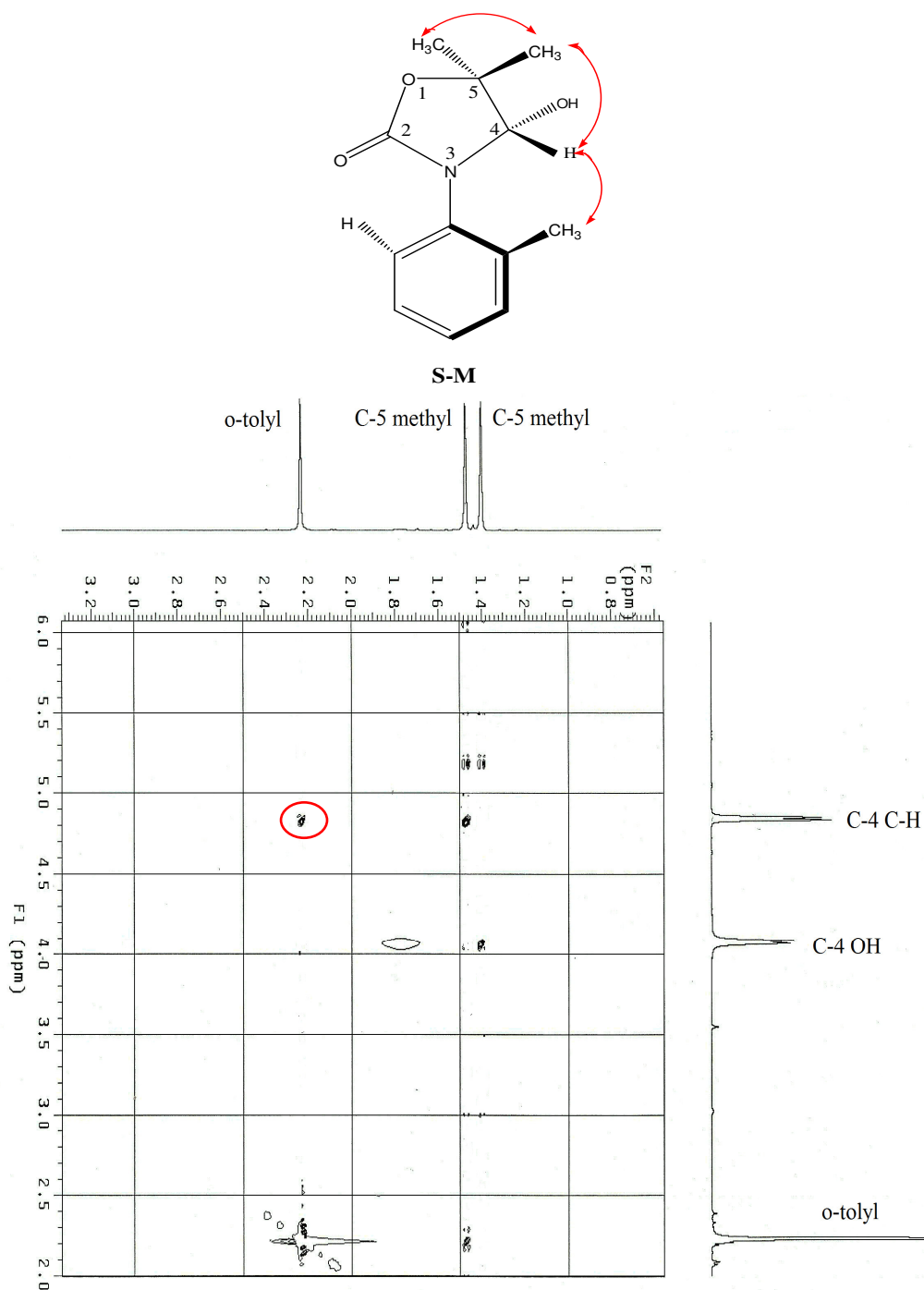
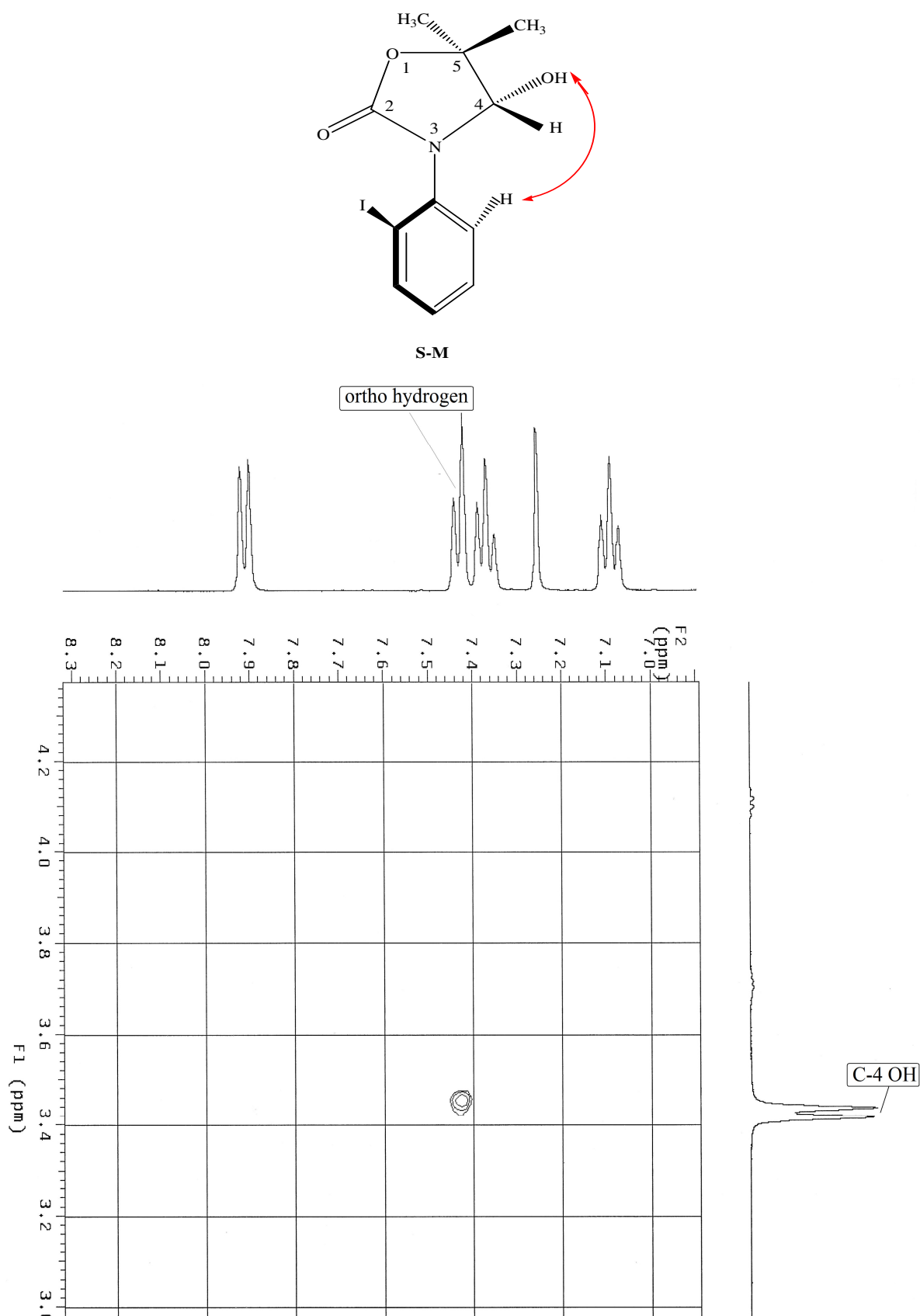


Figure 4.40. The NOESY spectrum of compound (\pm)**50** in CDCl_3

Figure 4.41. The NOESY spectrum of compound (\pm)**55** in CDCl_3

4.4.4. Determination of Activation Barriers

The reduction of compound (\pm)**11** yielded a diastereomeric ratio of 100:0 determined by HPLC on chiralPak IB in ethanol, due to the selective reduction. When this mixture was kept in a constant temperature bath, it was observed that the **S-M** and **R-P** gradually converted to **R-M** and its enantiomer **S-P** until equilibrium (Figure 4.38). The thermal interconversion of the diastereomers was followed by HPLC on chiralPak IB at 85 °C in ethanol. The activation barrier for the interconversion of **S-M** to **S-P** (or **R-P** to **R-M**) was found as 116.5 kJ/mol for the forward reaction and 108.4 for the reverse reaction in ethanol. These barriers are both greater than that of compound (\pm)**11** which could arise from the change in geometry of C-4 from sp^2 to sp^3 hybridized carbon. Although the angle of an sp^3 hybridized carbon is 109.5° , the lone pair of oxygen (also sp^3 hybridized) is more exposed in space (Figures 4.37 and 4.42).

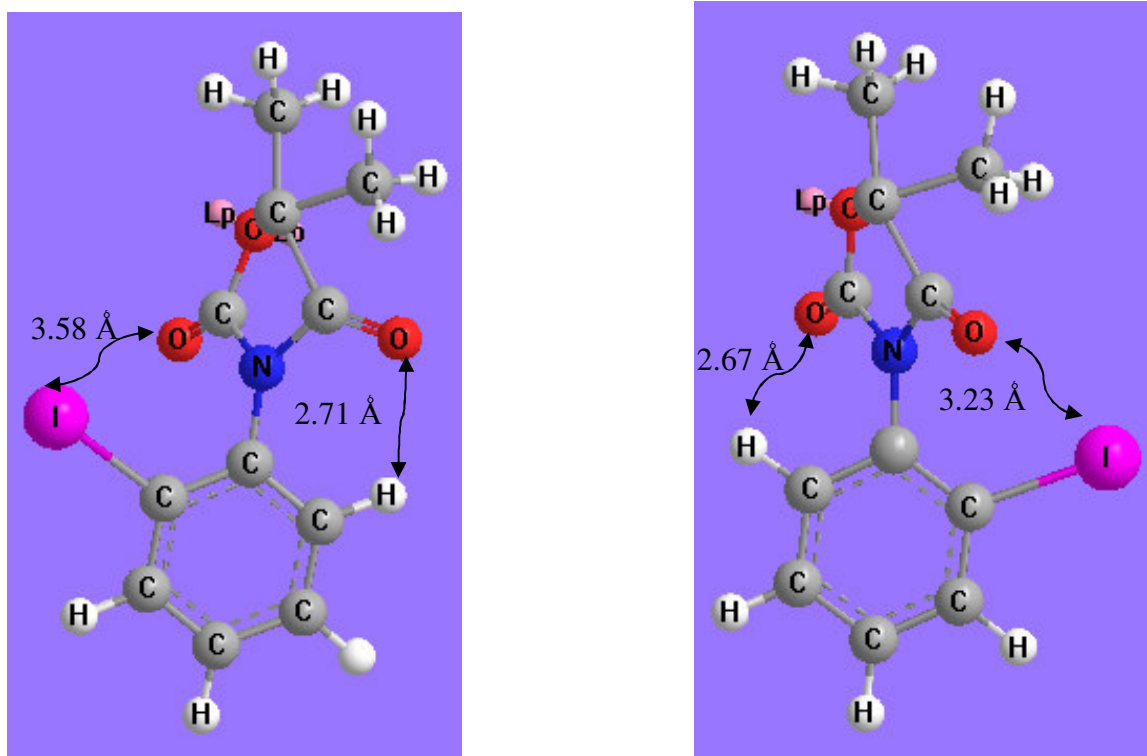


Figure 4.42. Molecular models of compound (\pm)**11** showing the spatial proximity of the selected groups in Å (Lp: lone pairs)

The stereoisomers of compound **52** could not be resolved both by chiral HPLC and NMR. It was thought that the activation barrier was slow that preventing the formation of chiral axis around C-N single bond. Due to the presence of only one stereogenic center which was in **R** and **S** configuration the resultant isomers were enantiomeric and could not be resolved without a chiral medium. The observation of diastereomers could only be possible if the rotation was slow on the NMR time scale. Therefore, the activation barrier corresponding to the interconversion of one diastereomer to another was found by low temperature dependent NMR in toluene- d_8 in the range of 30 to -70 °C (Figure 4.43). The separation in Hertz between the signals in the absence of rapid rotation could be achieved at -53 °C (220 K) and found as 12 Hz for 400 MHz NMR instrument. The coalescence of the signals took place at -53 °C. By using the Eyring Equation, the activation barrier to hindered rotation was found as 47.3 kJ/mol which was lower than that of compound (\pm)**8** (57.3 kJ/mol). The decrease in activation barrier was explained in terms of the stability of the transition state (Figure 2.2). Since the hydroxyl and *ortho* fluorine groups are very close to each other in space (Figure 4.44), they should be capable of forming hydrogen bond that will stabilize the transition state. In Figure 4.43 it could be seen that the OH proton signal shifted to downfield remarkably upon cooling that proved the hydrogen bond formation. Therefore, it was concluded that below -50 °C the rotation was so slow that enabled the observation of two diastereomers (**S-M/S-P** or **R-M/R-P**). In the structures of **S-M** or **R-P**, the fluorine and OH groups having lone pair electrons are on opposite sides, whereas in **R-M** or **S-P**, they are on the same side involved in hydrogen bond formation that stabilizing the conformations. The observation of two signals having 1:1 ratio at -53 °C interpreted as **R-M/R-P** or **S-M/S-P** had equal stability.

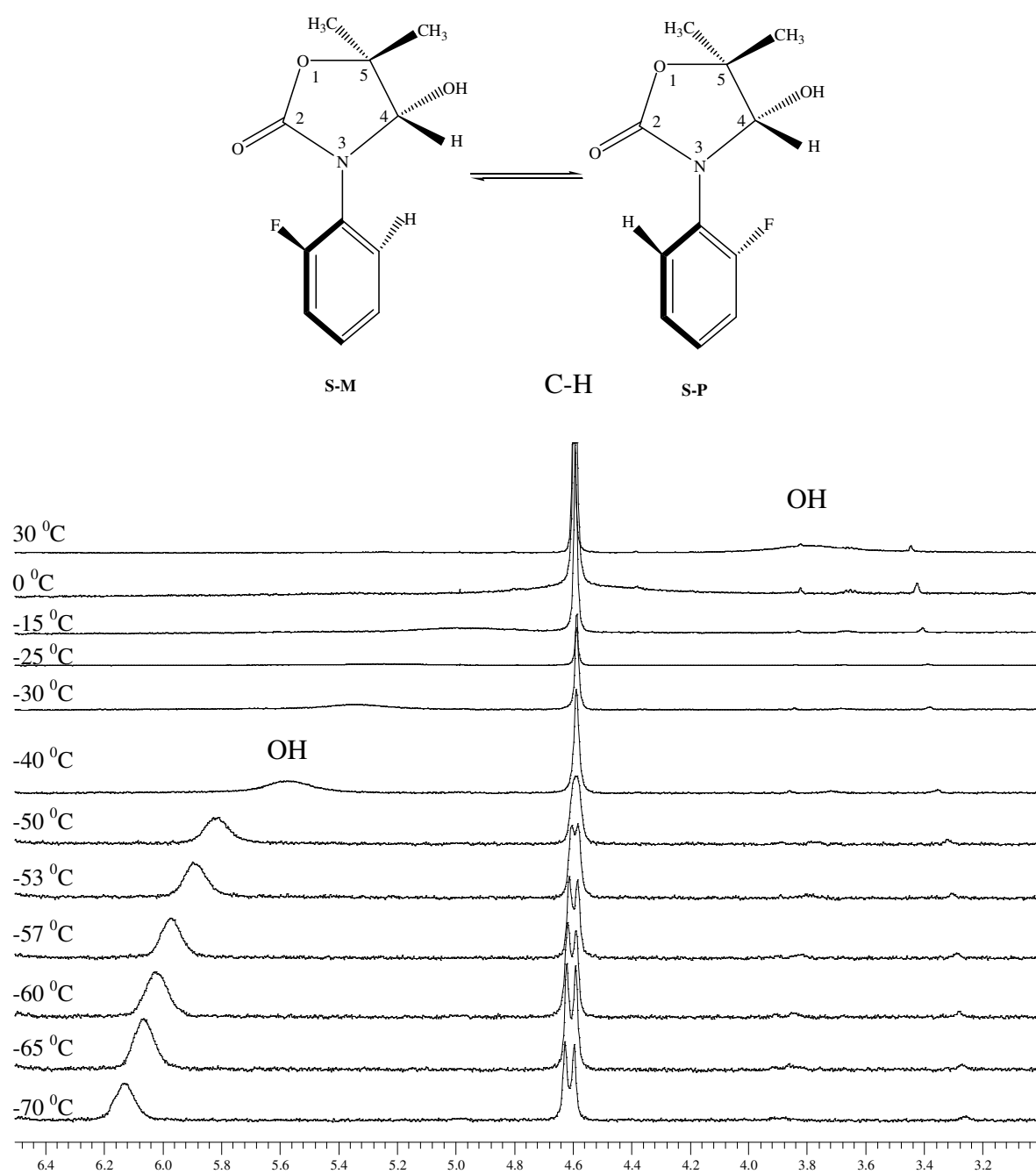


Figure 4.43. Low temperature dynamic NMR study of compound **52**

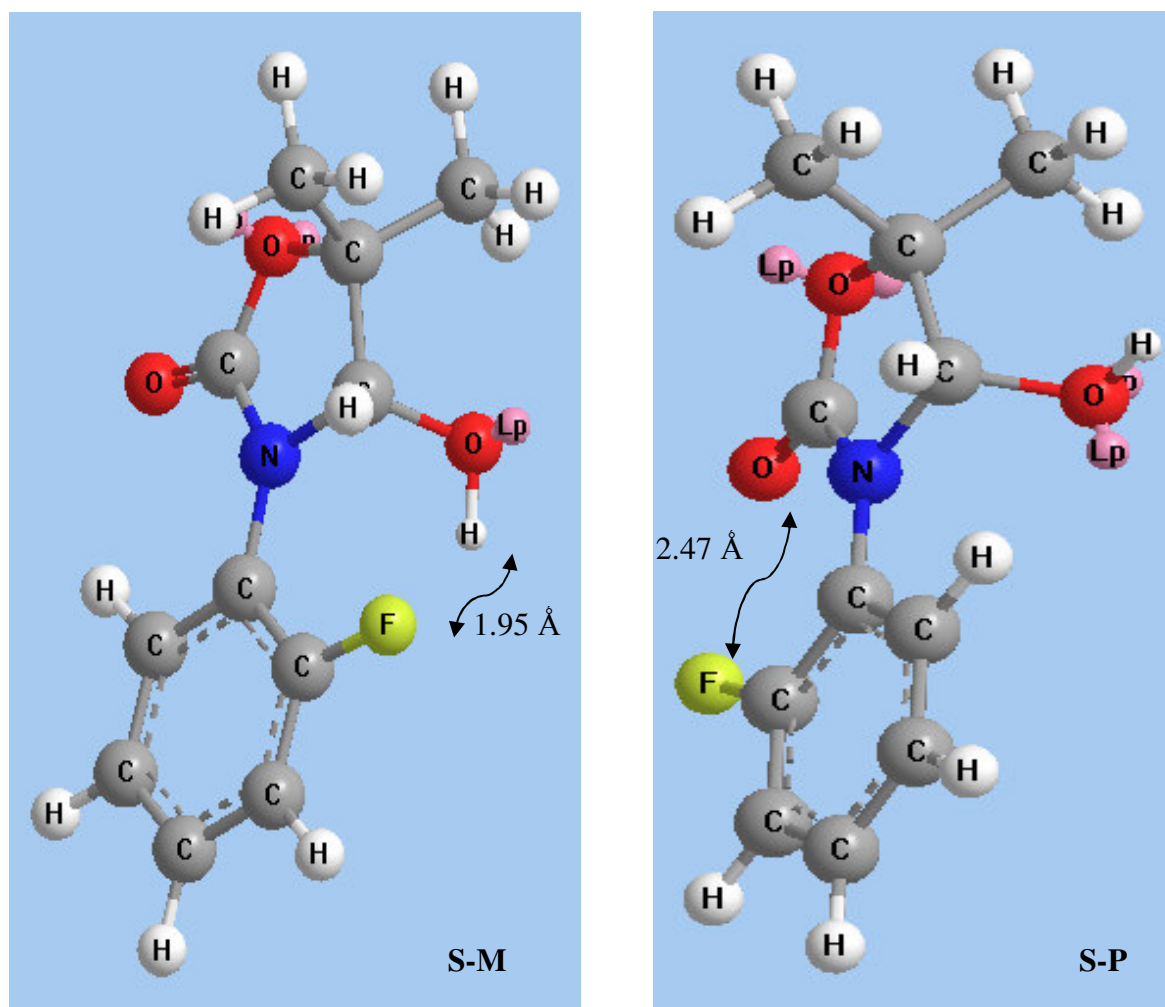


Figure 4.44. The models representing the **S-M** and **S-P** conformations of compound **52**

4.5. Asymmetric Alkylation and Aldol Reactions

In our previous work done for diastereomeric (5*S*)-methyl-3-(*o*-aryl)-2,4-oxazolidinedione derivatives [14] it was found that the stable isomer conformation was **S-P** where the C-5 methyl and *ortho* substitution was on opposite sites. This was proved by NOESY in which for compound **1** the crosspeaks between *ortho* methyl and C-5 methyl signals, for compounds **2** and **3** that C-5 methyl with peri hydrogen and *ortho* hydrogen signals, respectively, were seen (Figures 4.3, 4.4, 4.6). The observation of crosspeaks between the groups on C-5 and *ortho* position revealed that these sites were close to each other ($< 4\text{\AA}$) so that the *o*-aryl substituents may have a stereodirecting effect on the reactions taking place at C-5 of the ring. Therefore the single enantiomers of (**M** or **P**) may be expected to cause chiral induction at C-5 upon aldol and alkylation reactions over the

enolate forms. Enolate formation of the compounds took place at -78°C with lithium diisopropyl amide (LDA). Due to the cyclic nature of the oxazolidine ring E enolate must be formed [6,8,9].

With this thought, (5*S*)-methyl-3-(*o*-tolyl)-2,4-oxazolidinedione, **1** was chosen as a first candidate in order to see whether asymmetric alkylation reaction with benzyl bromide would result in high asymmetry (Figure 4.45). In this first trial, a mixture of diastereomers (**S-M** and **S-P**) (Compound **1**) having a composition of 40%:60% was used. For **S-M** conformation, the formed enolate is expected to attack from less hindered *Re* face, forming the **R*-M** conformation as major product (Compound **56**) (Figure 4.45). Similarly, **S-P** would approach BnBr from the less hindered side *Si* face, yielding **S*-P** majorly. The newly formed stereoisomers which are still diastereomeric (**S*-M/R*-P** or **R*-M/S*-P**) were found to form by 40% to 60%, respectively. This corresponded to a poor diastereoselectivity of 20% diastereomeric excess (de).

Diastereomer ratio did not change upon heating showing that it was the ratio of thermodynamic equilibrium. This might be due to the low activation barrier to hindered rotation (expected to be similar to that of compound **1** which amounted to 78 kJ/mol), meaning that the stereoisomers were not stable at room temperature. Although reaction was carried out at -78°C at which the rotation around the C-N single bond could be considered as being frozen, during work-up the stereoisomers could be interconverted rapidly at room temperature.

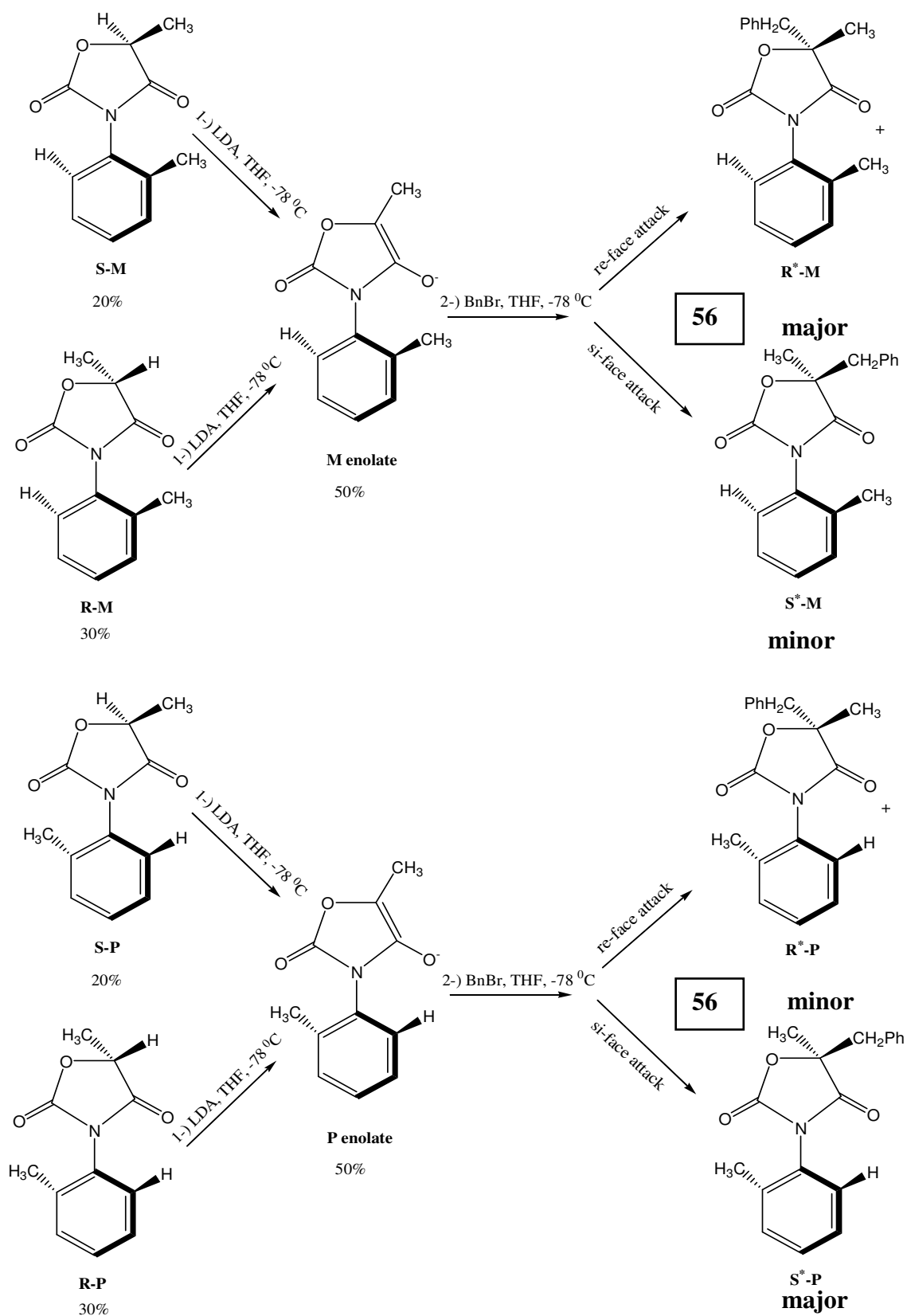


Figure 4.45. Asymmetric alkylation reaction of compound **1** with benzyl bromide (BnBr).

Figure represents that if reaction done by only **S-M** or **S-P** the major products would be

R*-M and **S*-P**.

Having this result, asymmetric alkylation reaction was performed with compound **3** (Figure 4.46) having an activation barrier of approximately 100 kJ/mol [14]. In order to determine the de (or ee) value, the reaction was followed by HPLC on chiralpak IB column (Figure 4.47). In Figure 4.47, peaks A and A' had a ratio of 1:1 so were peaks B and B' revealing that they belong to enantiomers. Therefore the ee value for this reaction was zero. Peaks A-A' and B-B' belong to diastereomeric isomers (compound **57**) having a ratio of 78%:22%, de being equal to 56%, which was better than that obtained with alkylation of compound **1**. The major products having conformations **R*-M/ S*-P** were the kinetic products which were formed by the attack of enolates from the less hindered side. It was found that for compound **3** the **S-P** conformation was the more stable isomer in which the bulky methyl group and iodine atom were on opposite sides. Therefore, it was expected that for compound **57** the major products that were formed kinetically would also thermodynamically stable due to the fact that bulky benzyl and iodine were on opposite sides. After purification, the composition of major diastereomer increased to 95% as a result of interconversion around C-N single bond. Therefore it was concluded that the major diastereomer was both kinetic and thermodynamic product (Probably **S*P** and **R*-M**) (Figures 4.46 and 4.48).

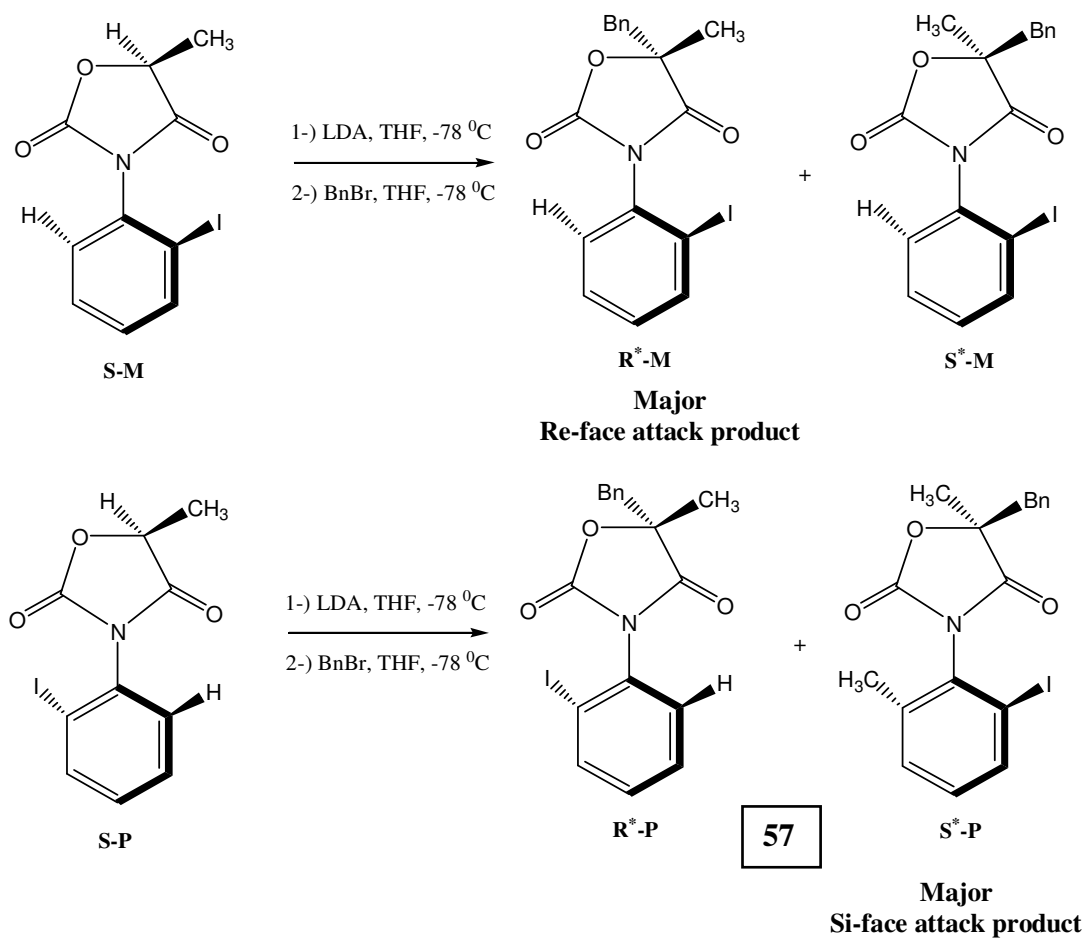


Figure 4.46. Asymmetric alkylation reaction of compound **3** with benzyl bromide (BnBr).

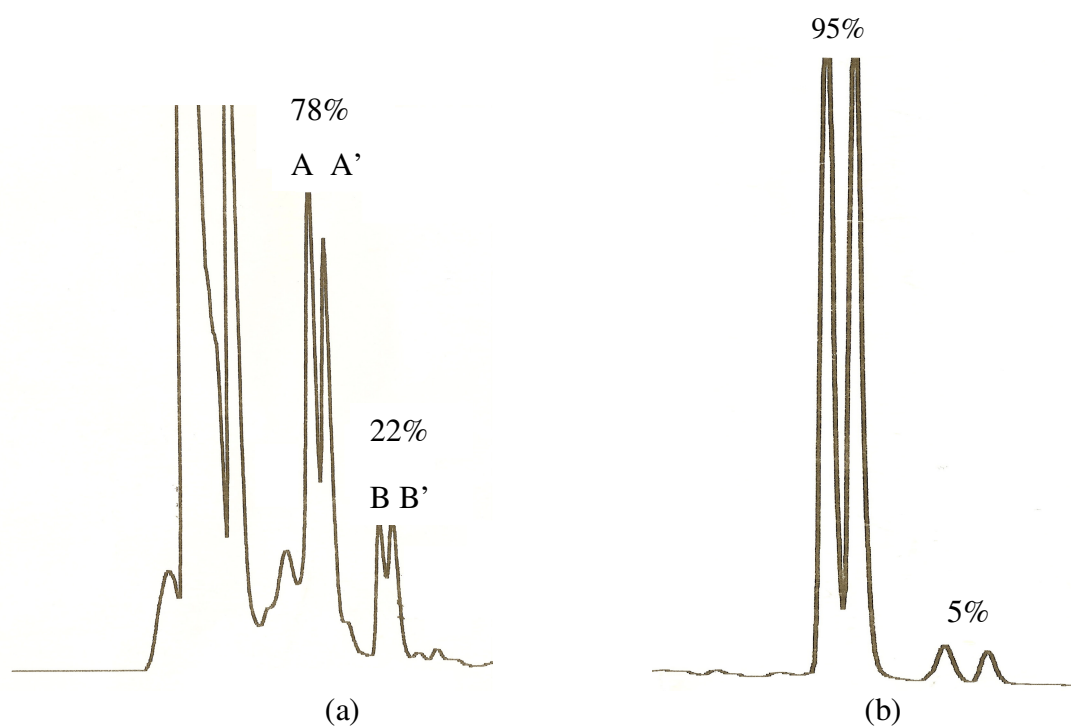


Figure 4.47. Isomer composition of compound **57** (a), during reaction, (b) after work-up

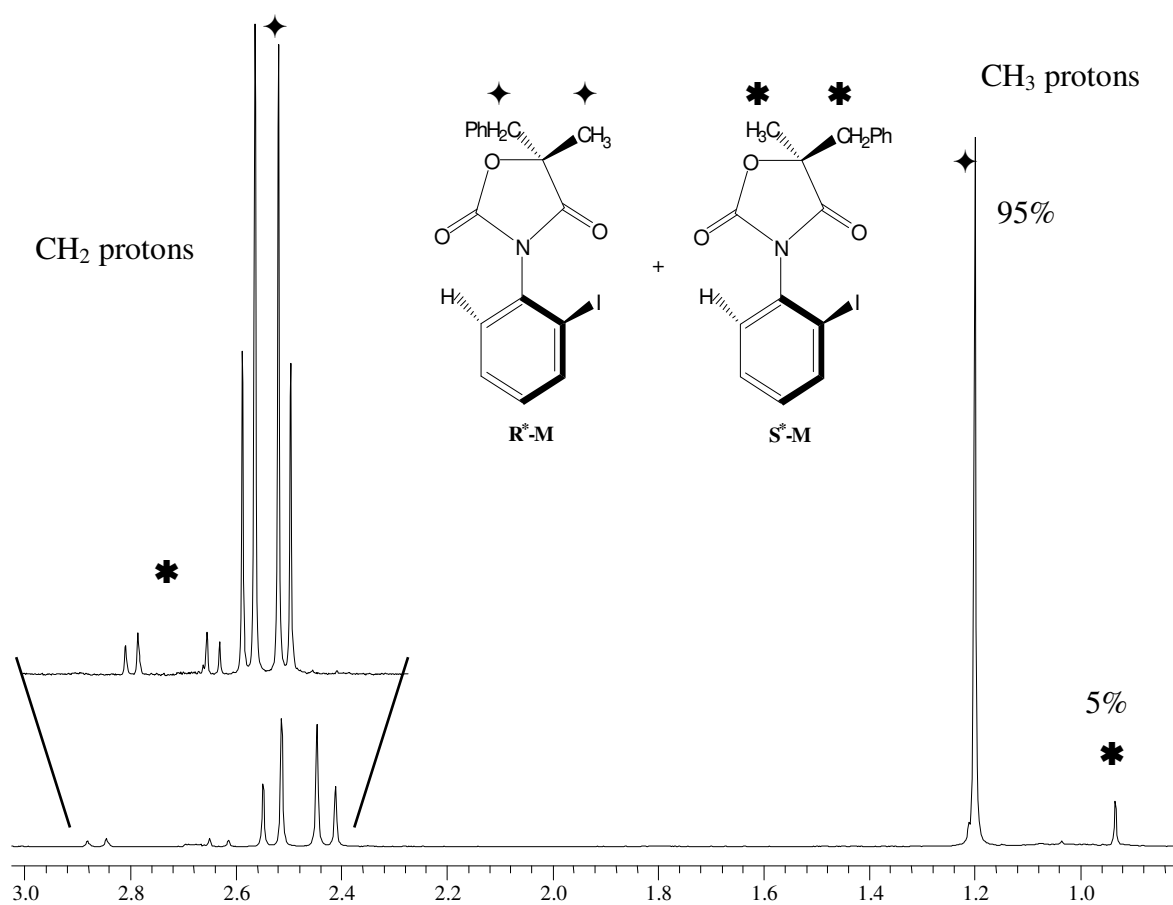


Figure 4.48. 400 MHz ^1H NMR spectrum of compound **57**

The presence of the enantiomeric pairs was also proved by ^1H NMR in the presence of chiral auxiliary (S)-TFAE (Figure 4.49). It was again found that ee was zero but it was not understood that why it was so at that time.

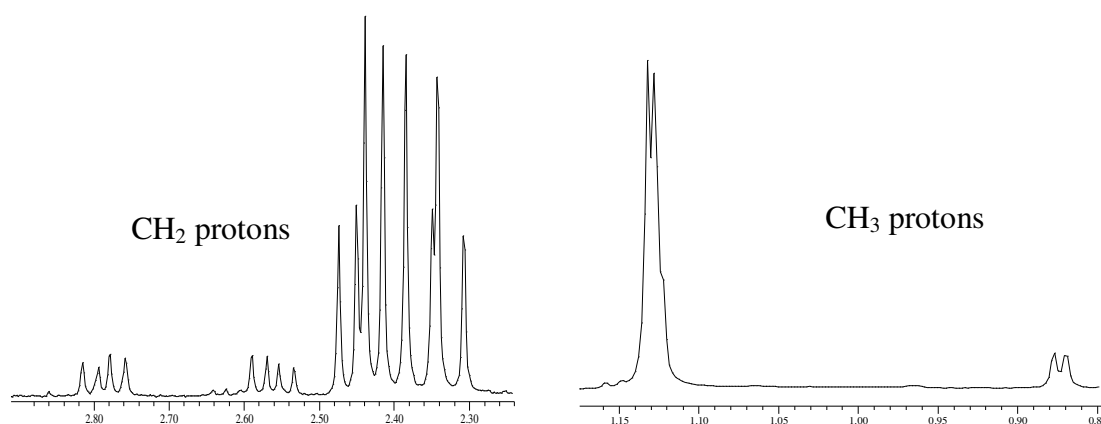


Figure 4.49. 400 MHz ^1H NMR spectrum of compound **57** in the presence of chiral auxiliary (S)-TFAE

In order to get more stable stereoisomers, that is, the isomers whose activation barrier for interconversion was slow, compound **58** was synthesized (Figure 4.51). The activation barrier was expected to be around 124 kJ/mol. Compound **58**, similar to compounds **1** and **3**, was expected to exist in two diastereomeric forms (**S-P** and **S-M**). However, when it was analyzed by HPLC on chiralpak IB, it was found that there were four isomers: two enantiomeric and two diastereomeric pairs (Figure 4.50). Therefore it was clarified that starting with a racemate resulted in zero ee value. Only two HPLC peaks were seen for *o*-iodo derivative (compound **3**) on Chiralpak AD and chiralcel OD which had been interpreted in terms of the presence of **S-M** and **S-P** diastereomers only. However after the alkylation reactions it became evident that actually four isomers existed (**S*-M**, **S*-P**, **R*-M**, **R*-P**). As can be seen in Figure 4.51, starting composition of compound **58** does not have any effect on ee or de. Ee has to be zero at each time but de could be affected by the position of *ortho* substituent.

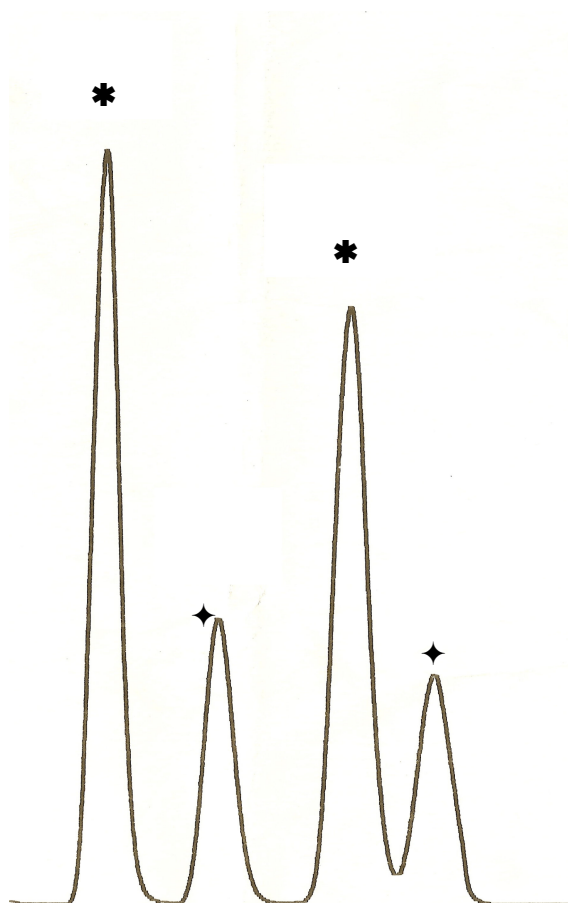
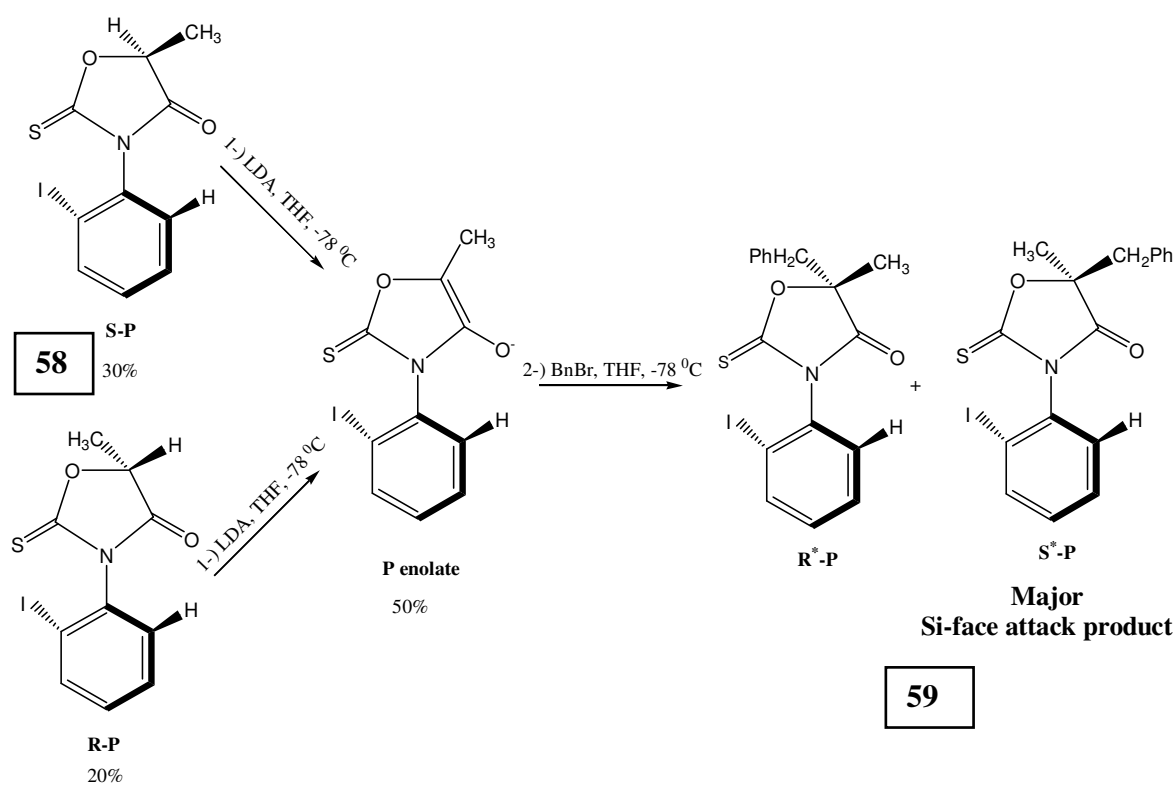
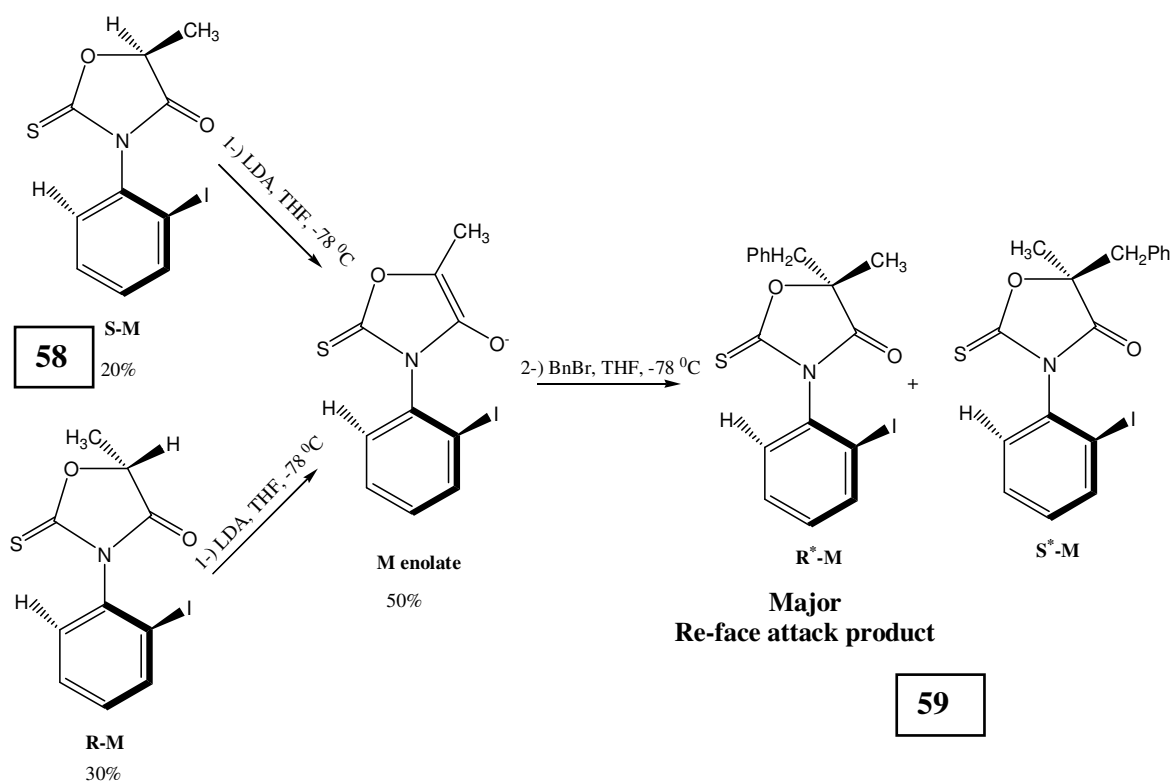


Figure 4.50. HPLC chromatogram of compound **58** showing the presence of four isomers.

Column:OD-H, eluent: 70:30 (Hexane:ethanol), λ : 254 nm, Flow: 0.4 ml/min

Figure 4.51. Alkylation reaction of compound **58** with BnBr

The formation of a racemic compound was explained by the fact that the presence of sodium metal which was used in catalytic amount to deprotonate the hydroxyl group of S-ethyl lactate (Figures 3.1 and 3.3) might cause enolization of acidic C-5 methine proton. In order to get a nonracemic mixture, reaction was done without sodium. Synthesis of nonracemic compound **1** could be achieved without sodium with one and a half day-reflux in xylene. The reaction taking place for two and a half day to synthesize compound **58** (Figure 4.51) yielded again a racemic form. The synthesis of compound **3** without sodium resulted in a mixture containing compound **3** and the uncyclic compound before ring closure. Therefore, the procedure followed to synthesize the compounds could not be used to synthesize the non-racemic forms. Therefore we decided to carry out the reactions with compound **3** and **58** in racemic form in order to see whether the deposition of *ortho* substitution would result in high de value.

Alkylation of compound **58** with benzyl bromide (BnBr) (Figure 4.51) yielded a diastereomer composition of 72%:28% (de: 44) after completion of the reaction (Figure 4.52) which is close to that obtained at the end of the reaction of compound **3** with BnBr. Reaction was followed taking samples from the reaction mixture at certain time intervals

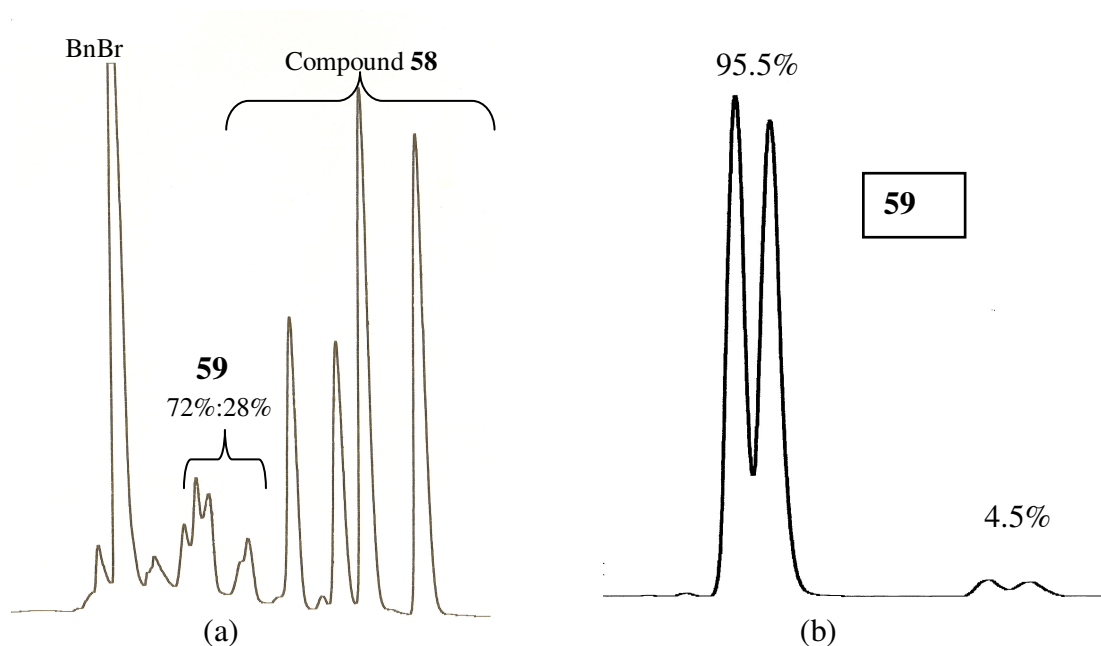


Figure 4.52. Alkylation reaction of compound **58** with BnBr. The composition of compound **59** was obtained (a) during reaction after one and a half hour at -78°C , (b) after purification

Reaction of compound **58** with allyl bromide yielded a diastereomer composition (compound **60**) of 87%:13% (de:74) (Figure 4.53) which is better than that obtained at the end of the reaction of compound **58** with BnBr. The major products **R^{*}-M** and **S^{*}-P** were formed by the approach of **M** and **P** enolates from the less hindered side to allyl bromide (Figure 4.54). After purification, the diastereomer composition changed to 78%:22. This equilibrium composition again revealed that the kinetic products were also thermodynamically stable (probably the conformations of **S^{*}-P/R^{*}-M** in Figure 4.54 due to the fact that allyl and iodine groups are on opposite sides).

Compound **60** (Figure 4.54) bears a chiral center on C-5. Due to this chiral center the allylic CH₂ protons is expected to be diastereotopic giving an AB type splitting. These AB signals were further splitted by the neighbouring C-H. However, as a result of overlapping of the inner signals it was observed as a multiplet at around 2.7 ppm (Figure 4.55).

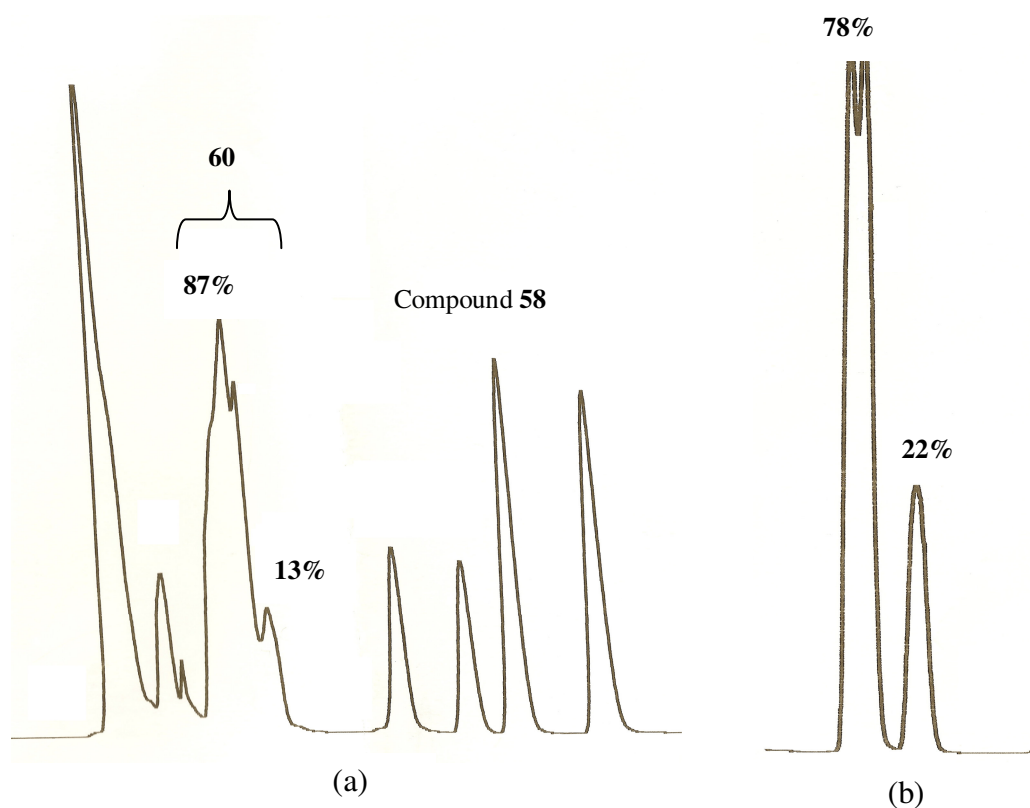


Figure 4.53. Reaction of compound **58** with allyl bromide (Product **60**) (a) after half an hour, (b) after purification

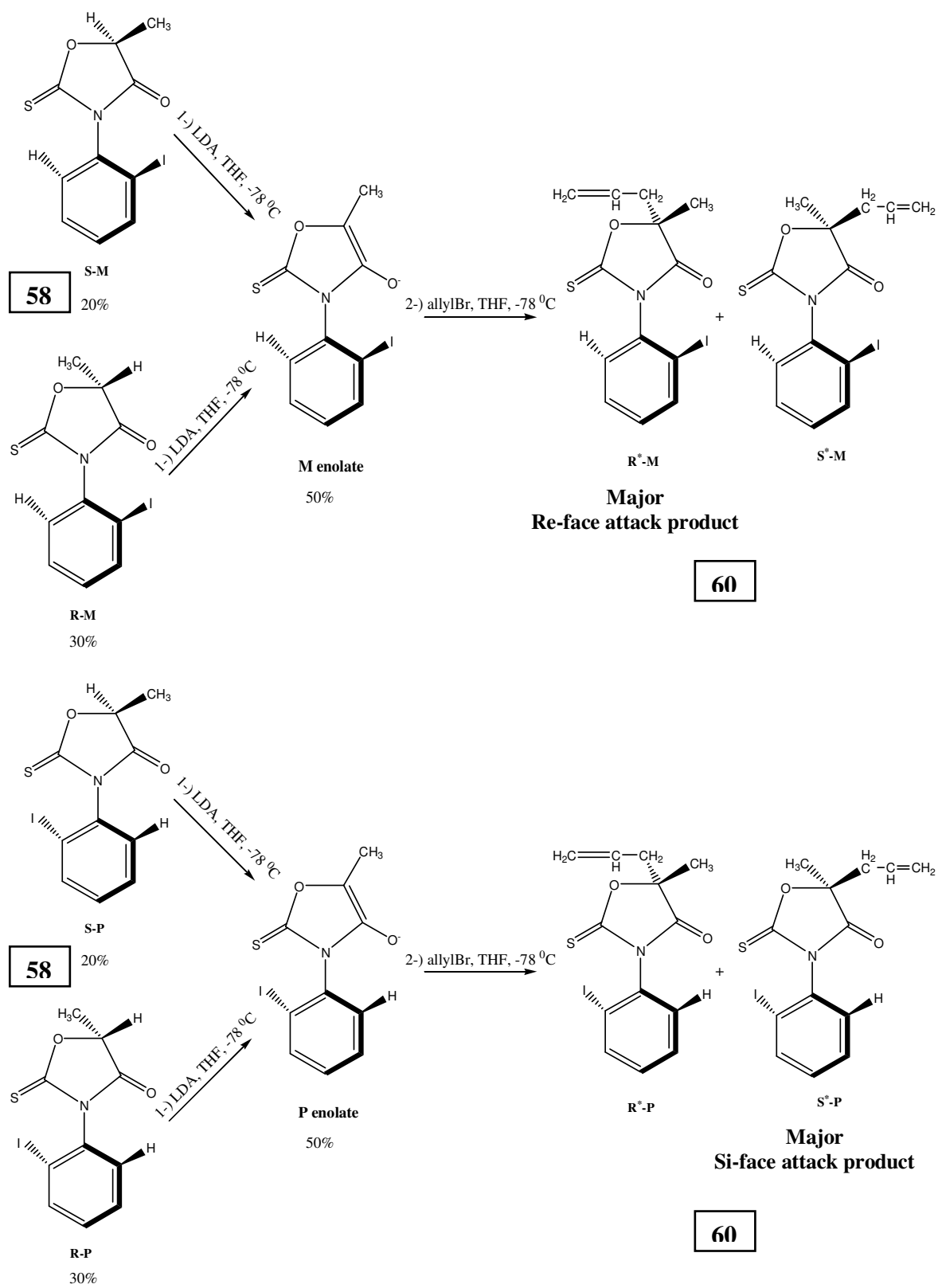


Figure 4.54. Reaction of **58** with allyl bromide and formation of stereoisomers of compound **60**

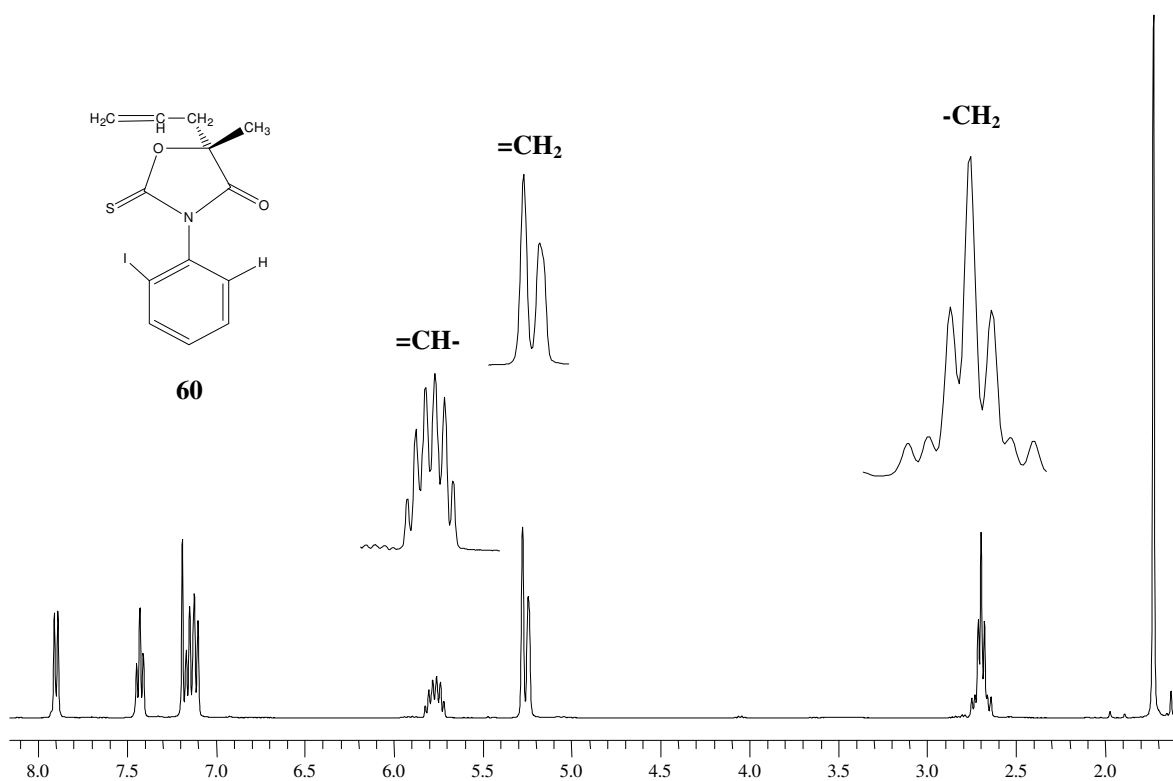


Figure 4.55. 400 MHz ^1H NMR spectrum of compound **60** in CDCl_3

Aldol reaction of compound **3** with benzaldehyde yielded a diastereomer composition of 78%: 21% of compound **61** (Figures 4.56, 4.57 and 4.58). This ratio was similar to those of alkylation reactions of compound **3** and **58**. As can be seen in Figure 4.56 one of the enantiomeric pairs could be resolved by Chiralpak IB column with eluent composition of 80%.20% (v/v). The reaction was followed by HPLC taking samples at certain time intervals and it was seen that reaction was complete after half an hour. **M** enolate would preferentially approach benzaldehyde from re-face and form a stable Zimmermann-Traxler transition state depicted in Figure 4.57. Since **E** enolate forms anti aldol product its configuration must be that in Figure 4.57. Similarly, the **P** enolate would form the **S*-P** as a major product passing through a stable transition state.

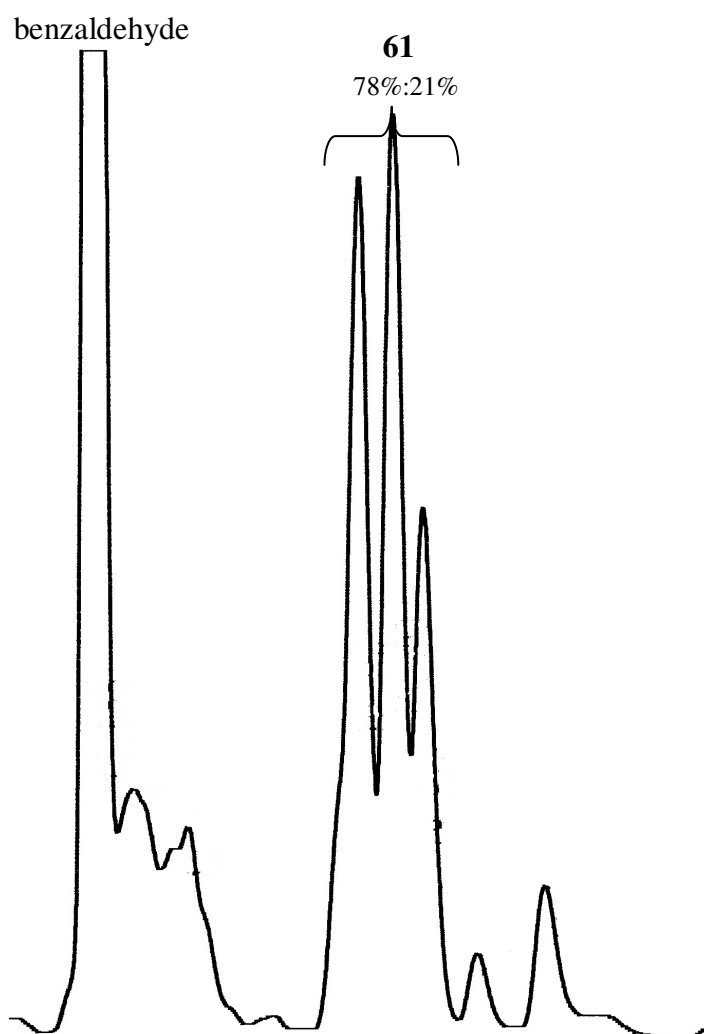


Figure 4.56. Aldol reaction of compound **3** after completion of reaction

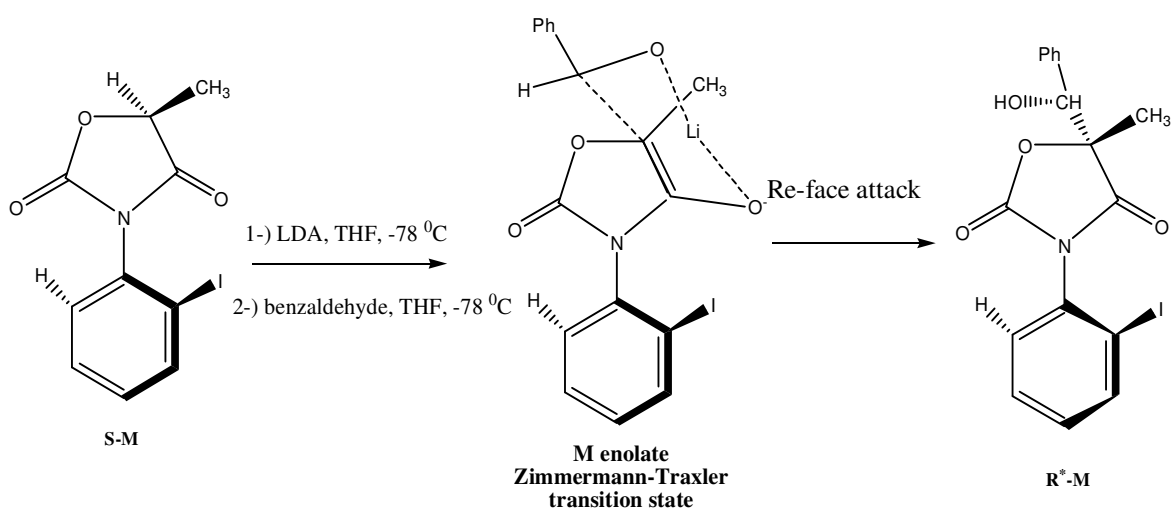


Figure 4.57. The formation of $\text{R}^*\text{-M}$ of compound **61** through M enolate

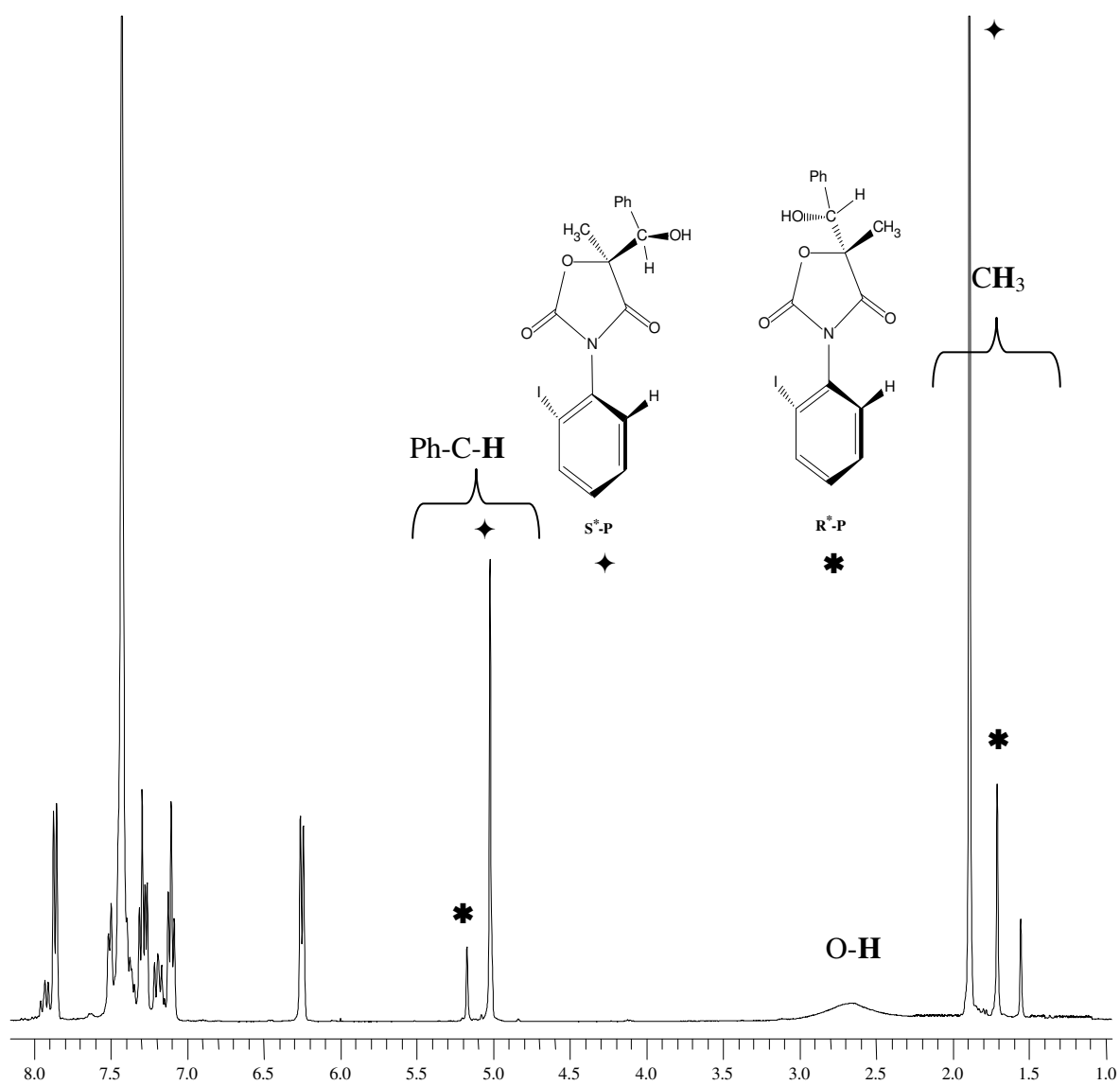
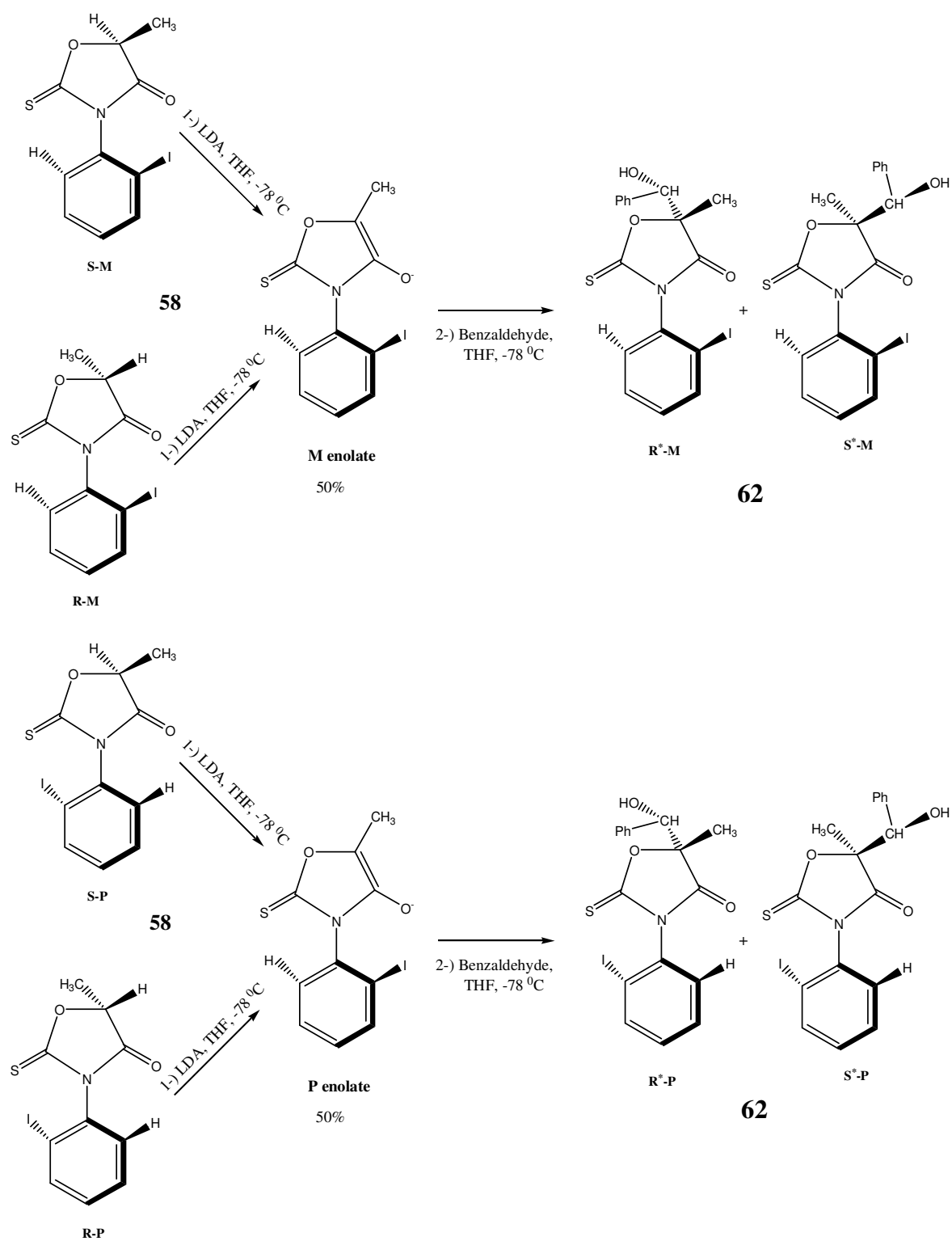


Figure 4.58. 400 MHz ^1H NMR spectrum of compound **61** in CDCl_3

The diastereomer composition was found as 34%:66% after completion of the aldol reaction of compound **58** with benzaldehyde after 20 minutes (Figures 4.59 and 4.60).

Figure 4.59. Aldol reaction of **58** with benzaldehyde

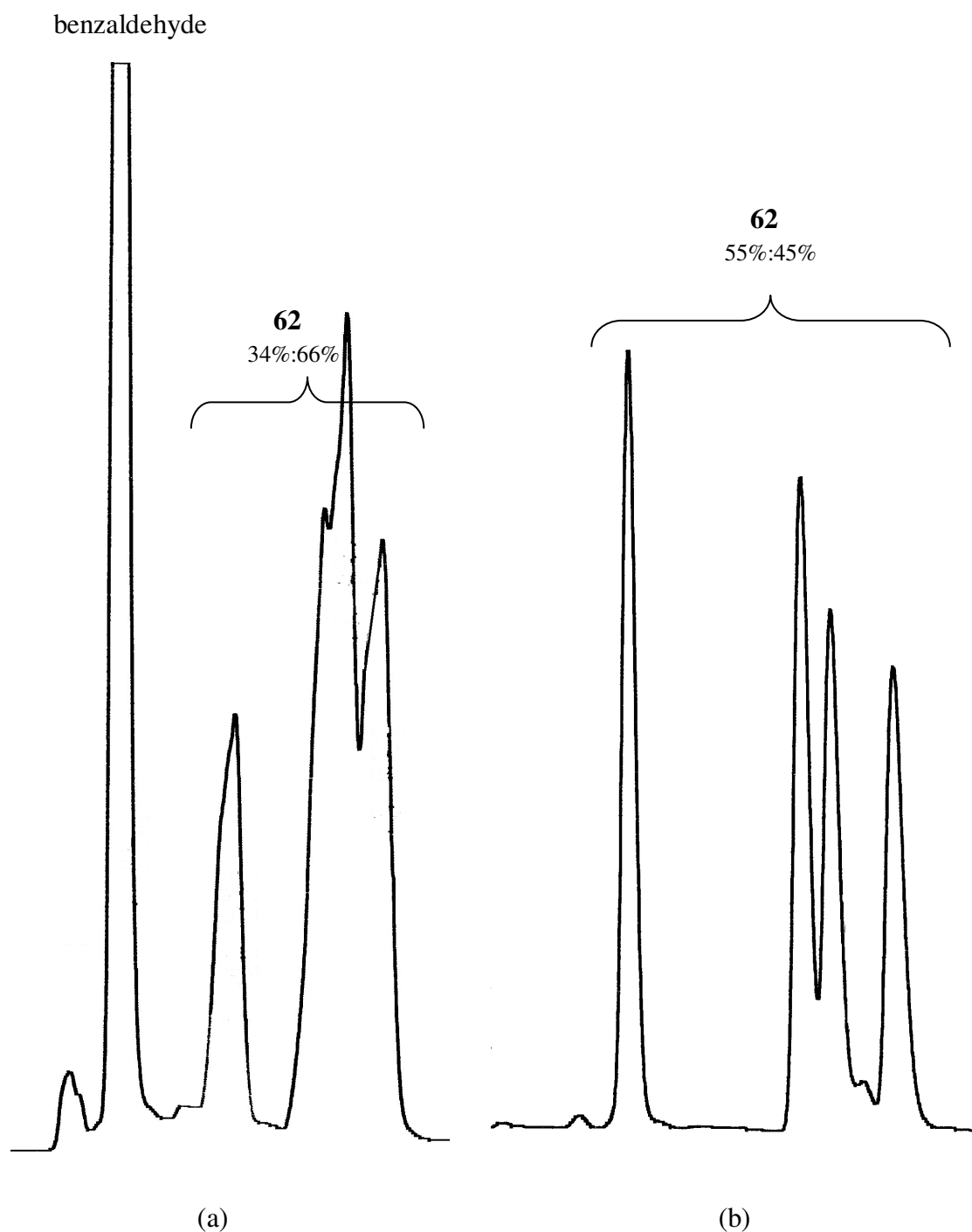


Figure 4.60. Aldol reaction of compound **58** (a), after completion of reaction, (b), after purification before equilibrium

With these results in hand, compound **58** (Figure 4.59) was collected semipreparatively (2.5 mg) and one of the stable isomers (**S-P** or **R-M**) was used for asymmetric aldol reaction. However, it was seen that the collected isomer partly interconverted the other isomer. Actually the reaction was carried out with a pair of

diastereomers having a ratio of 69%:31%. The diastereomer composition of the products was similar to that of the starting ratio. The composition of **S*-P** and **R*-P** (or the other pair) was found to be 96.4%:3.6%, ee being equal to 92.8% (Figures 4.61 and 4.62). The obtained de value showed that compound **58** could be used effectively to direct an asymmetric reaction.

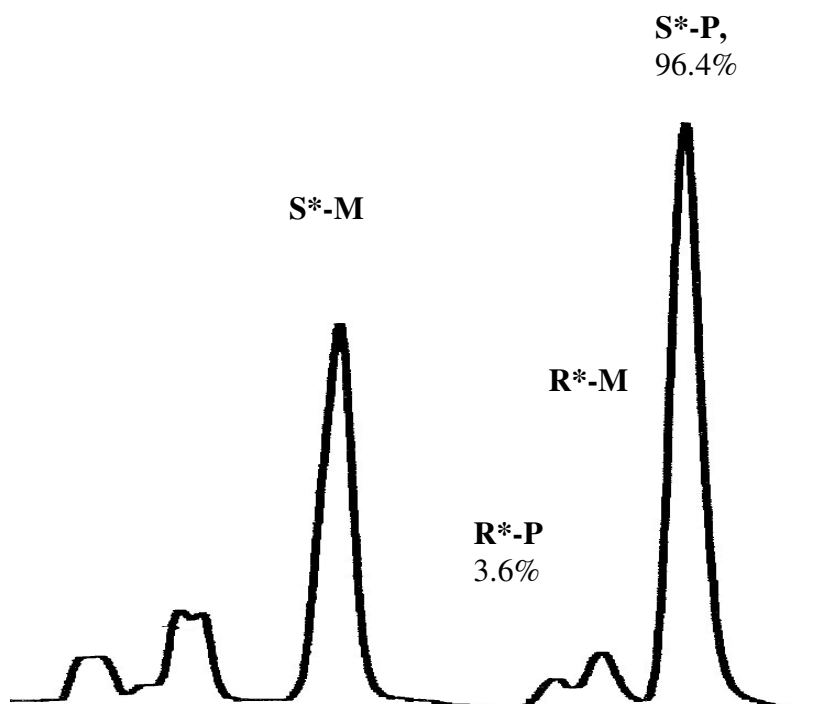


Figure 4.61. Asymmetric aldol reaction

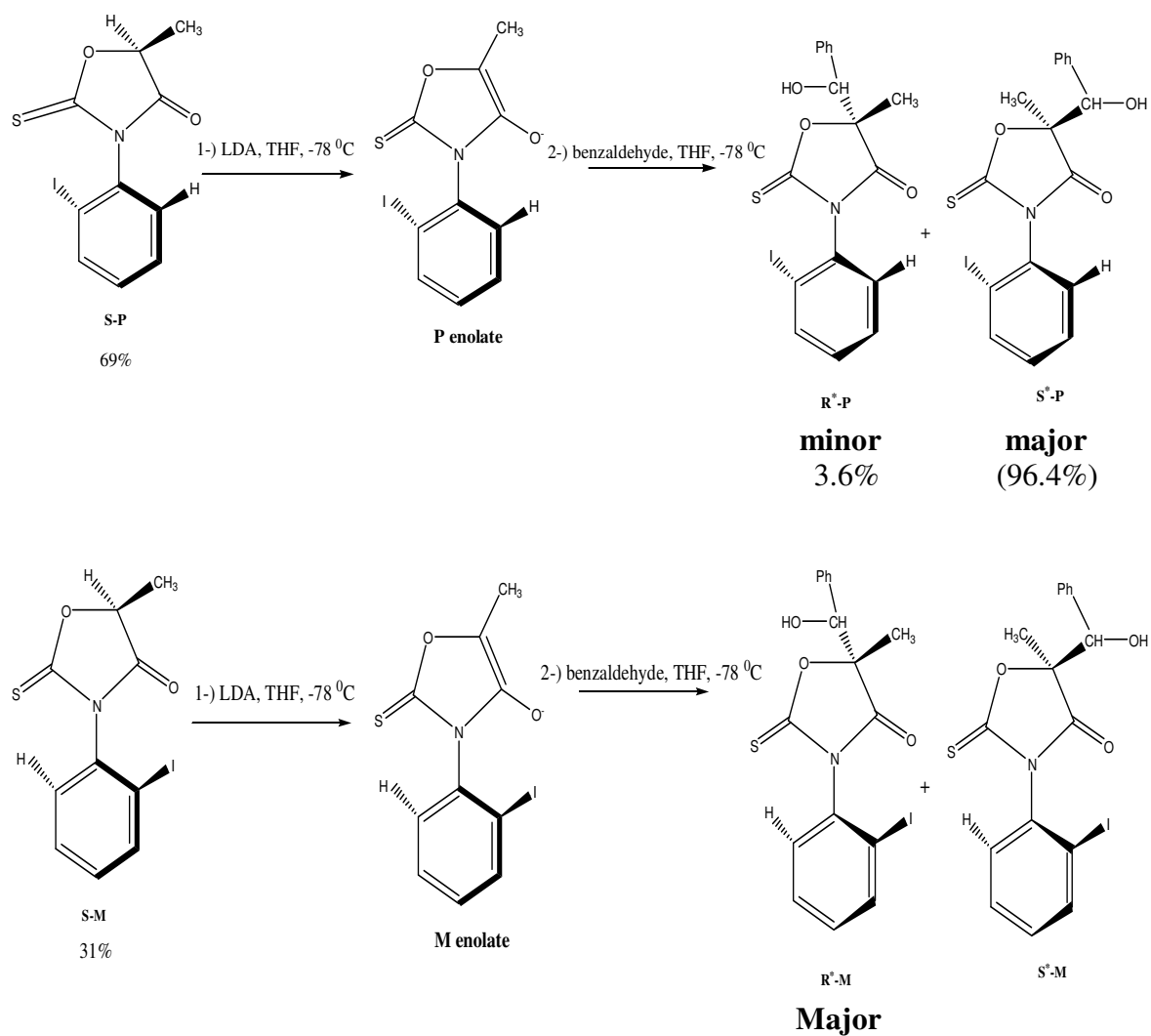


Figure 4.62. Asymmetric aldol reaction of **58** collected semipreparatively.

5. CONCLUSIONS

In this project, axially chiral 5-methyl-3-(*o*-aryl)-2,4-oxazolidinediones, 5-methyl-3-(*o*-iodophenyl)-2-thioxo-4-oxazolidinedione and 5,5-dimethyl-3-(*o*-aryl)-2,4-oxazolidinediones have been synthesized.

Diastereomeric isomers of the 5-methyl-3-(*o*-aryl)-2,4-oxazolidinediones and 5-methyl-3-(*o*-iodophenyl)-2-thioxo-4-oxazolidinedione have been found to form diastereoselectively yielding the **S-M/R-P** conformations in major amount. However this conformation where the C-5 methyl and the *ortho* substituent were on the same side was found to be kinetic product and during the work-up they were converted to the more stable isomers **S-P/R-M**. The stereostructures of the conformations were identified by using two dimensional NMR spectroscopy.

Activation barriers to hindered rotation around the C-N single bond of the diastereomeric isomers have been determined by using temperature dependent NMR and/or by thermal racemization on chiral sorbents by HPLC.

The activation barriers for the interconversion between enantiomers of 5,5-dimethyl-3-(*o*-aryl)-2,4-oxazolidinediones ($M \rightleftharpoons P$) have been determined by temperature dependent NMR and by enantioresolution on chiral sorbents via HPLC. The activation barriers were found to increase linearly with the size of the van der Waals radii of the *ortho*-halogen substituents. The enantiomers of the *o*-iodo-oxazolidinedione derivative were micropreparatively enriched on Chiralpak AD column, leading to the determination of its barrier to rotation via thermal racemization and resulting in the assignments of conformations in the presence of the optically active chiral auxiliary (S)-(+)-1-(9-anthryl)-2,2,2-trifluoro ethanol ((S)-TFAE).

Absolute conformations of 5,5-dimethyl-3-(*o*-aryl)-2,4-oxazolidinediones have been determined by one and two dimensional ^1H NMR in the presence of a chiral auxiliary (S)-(+)-1-(9-anthryl)-2,2,2-trifluoro ethanol ((S)-TFAE). A solvation model has been proposed

for the determination absolute stereochemistry on the basis of interactions between the enantiomers and (S)-TFAE.

The enantiotopic methyl signals of the 5,5-dimethyl-3-(α -naphthyl)-oxazolidinediones could be resolved in the presence of the optically active chiral auxiliary (S)-(+)-2,2,2-trifluoroanthryl ethanol, (S)-TFAE via complex formation between (S)-TFAE and the compounds. Two different solvation models were proposed for both **M** and **P** conformations leading to the assignments of the ^1H NMR signals and thus absolute conformations. The proposed solvation models also explained the strong temperature dependence of the ^1H NMR signals upon cooling. The activation barriers for the interconversion between the enantiomers of the compounds studied have been determined by either temperature dependent NMR or by enantioresolution on a chiral sorbent via HPLC.

Asymmetric alkylation and aldol reactions have been carried out on 5-methyl-3-(*o*-tolyl)-2,4-oxazolidinedione, 5-methyl-3-(*o*-iodophenyl)-2,4-oxazolidinedione and 5-methyl-3-(*o*-iodophenyl)-2-thioxo-4-oxazolidinedione over the lithium enolates formed by lithium diisopropylamide at $-78\text{ }^\circ\text{C}$ under nitrogen. The formed enolates then reacted with benzyl bromide, allyl bromide and benzaldehyde. It was found that the *o*-aryl substituents had a stereodirecting effect on the reactions taking place at C-5 of the ring.

One of the stereoisomers of 5-methyl-3-(*o*-iodophenyl)-2-thioxo-4-oxazolidinedione has been collected semipreparatively and used in an asymmetric aldol reaction with benzaldehyde. The obtained high ee value was promising and revealed that the chiral axis, that is the disposition of the iodine atom, could be used in an asymmetric reaction as a stereodirecting group.

Basic and reductive ring opening reactions of diastereomeric 5-methyl-N-(*o*-aryl)-2,4-oxazolidinediones and enantiomeric 5,5-dimethyl-N-(*o*-aryl)-2,4-oxazolidinediones have been done to examine the stability of the ring and to synthesize various organic compounds such as chiral α -hydroxyamides, carbamoyloxyacids and carbamate derivatives via ring opening. It was observed that 5-methyl-2,4-oxazolidinedione ring cleaved more easily than 5,5-dimethyl-2,4-oxazolidinedione ring by the reaction of KOH

and reduced by sodium borohydride. 5-methyl-2,4-oxazolidinedione ring was reduced to a primary alcohol, whereas the reduction of 5,5-dimethyl-2,4-oxazolidinedione ring yielded a secondary alcohol. A second hydride transfer resulting in ring opening did not happen due to the steric hindrance of the 5,5-dimethyl groups. The reduction of enantiomeric 5,5-dimethyl-N-(*o*-aryl)-2,4-oxazolidinediones by sodium borohydride has been also found to take place asymmetrically. The orientation of the *ortho* substituent was found to be very effective in selective reduction reactions taking place on C-4 which was very close to the chiral axis.

APPENDIX A: SPECTROSCOPY DATA

^1H and ^{13}C NMR data for the synthesized compounds are given. Required regions of NMR data are expanded.

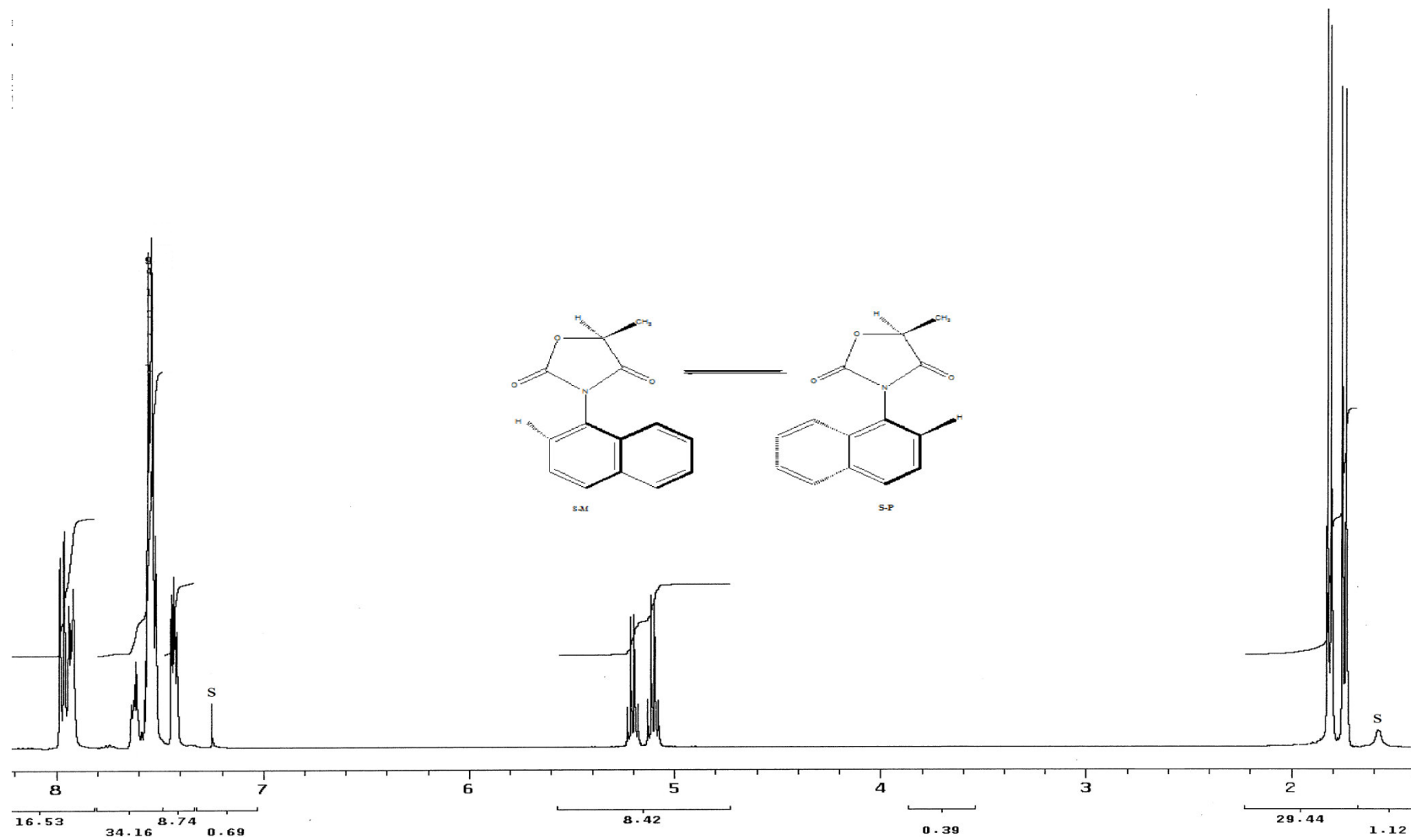


Figure A.1. 400 MHz ^1H NMR spectrum of compound **2** in CDCl_3 . S: Solvent

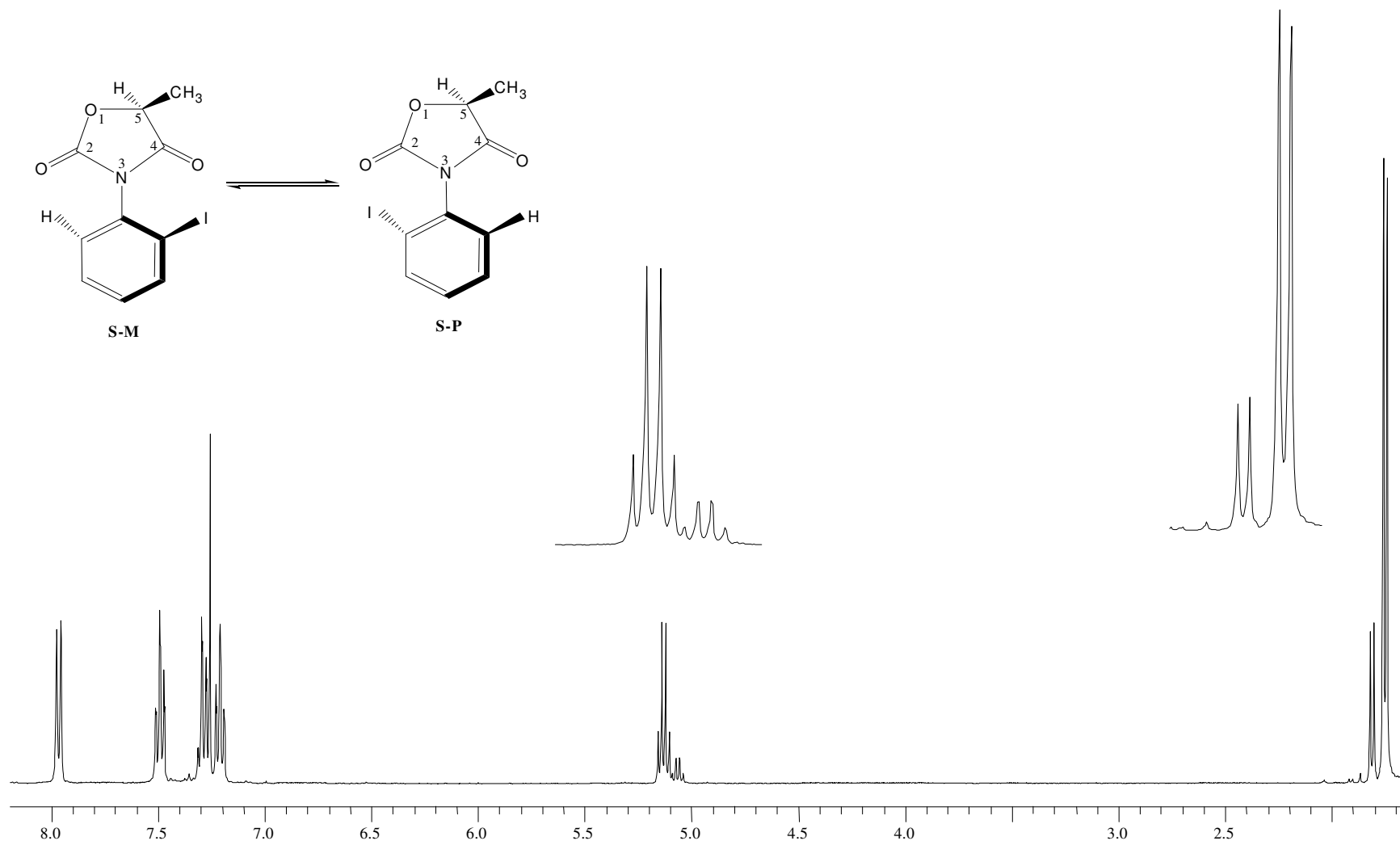


Figure A.2. 400 MHz ¹H NMR spectrum of compound 3 in CDCl₃

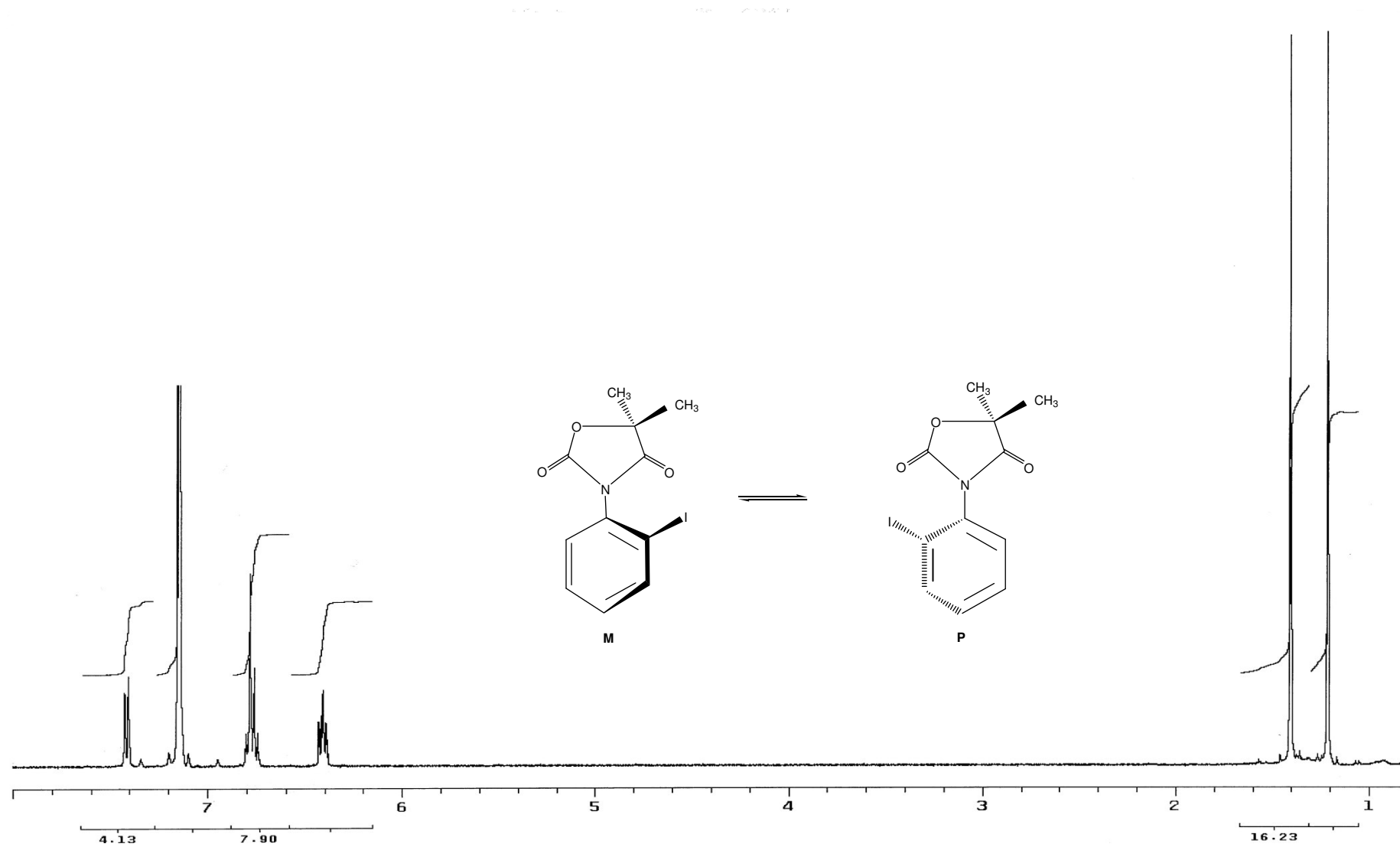


Figure A.3. 400 MHz ^1H NMR spectrum of compound (\pm)**11** in C_6D_6

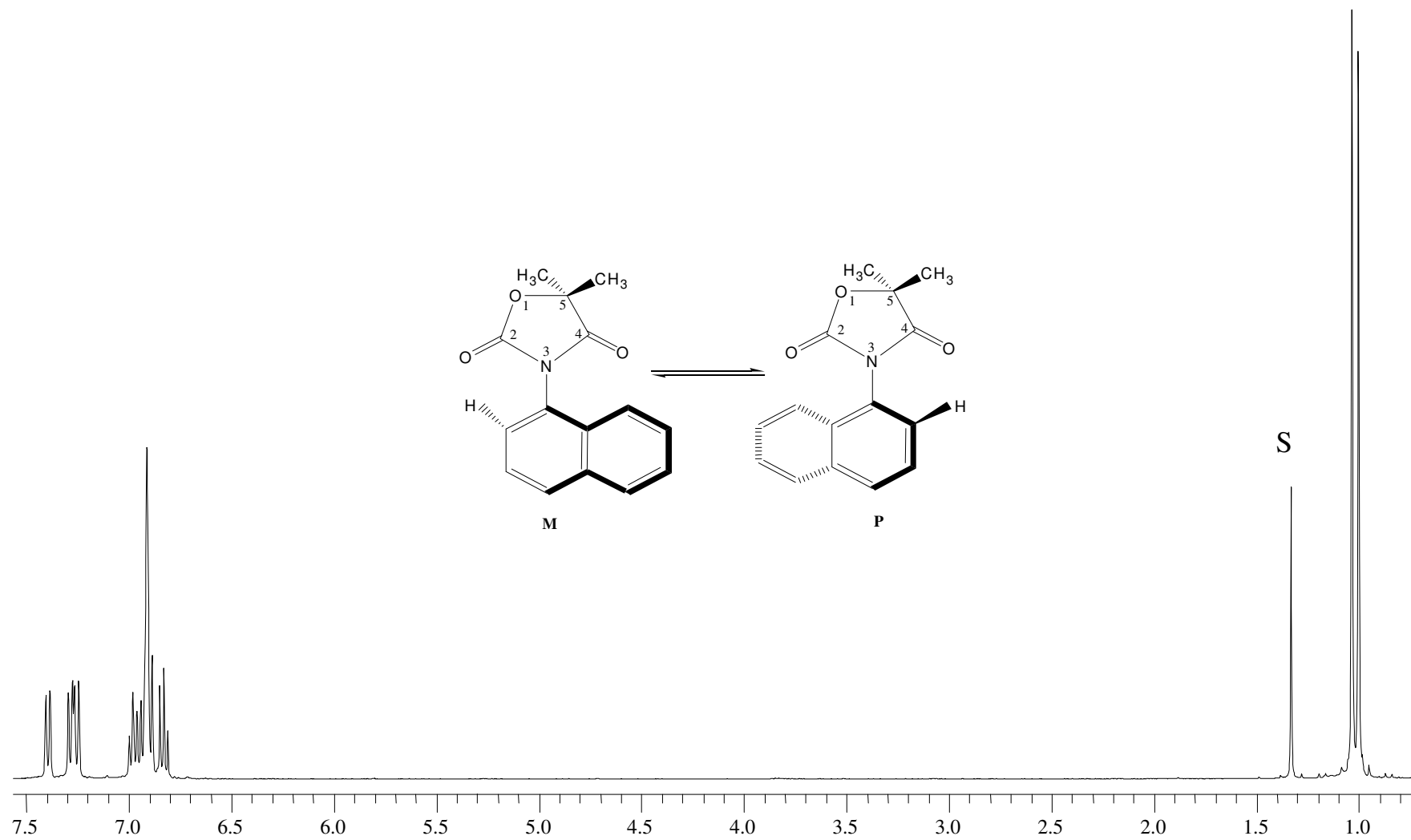


Figure A.4. 400 MHz ^1H NMR spectrum of compound (\pm)**15** in C_6D_6 . S: Solvent

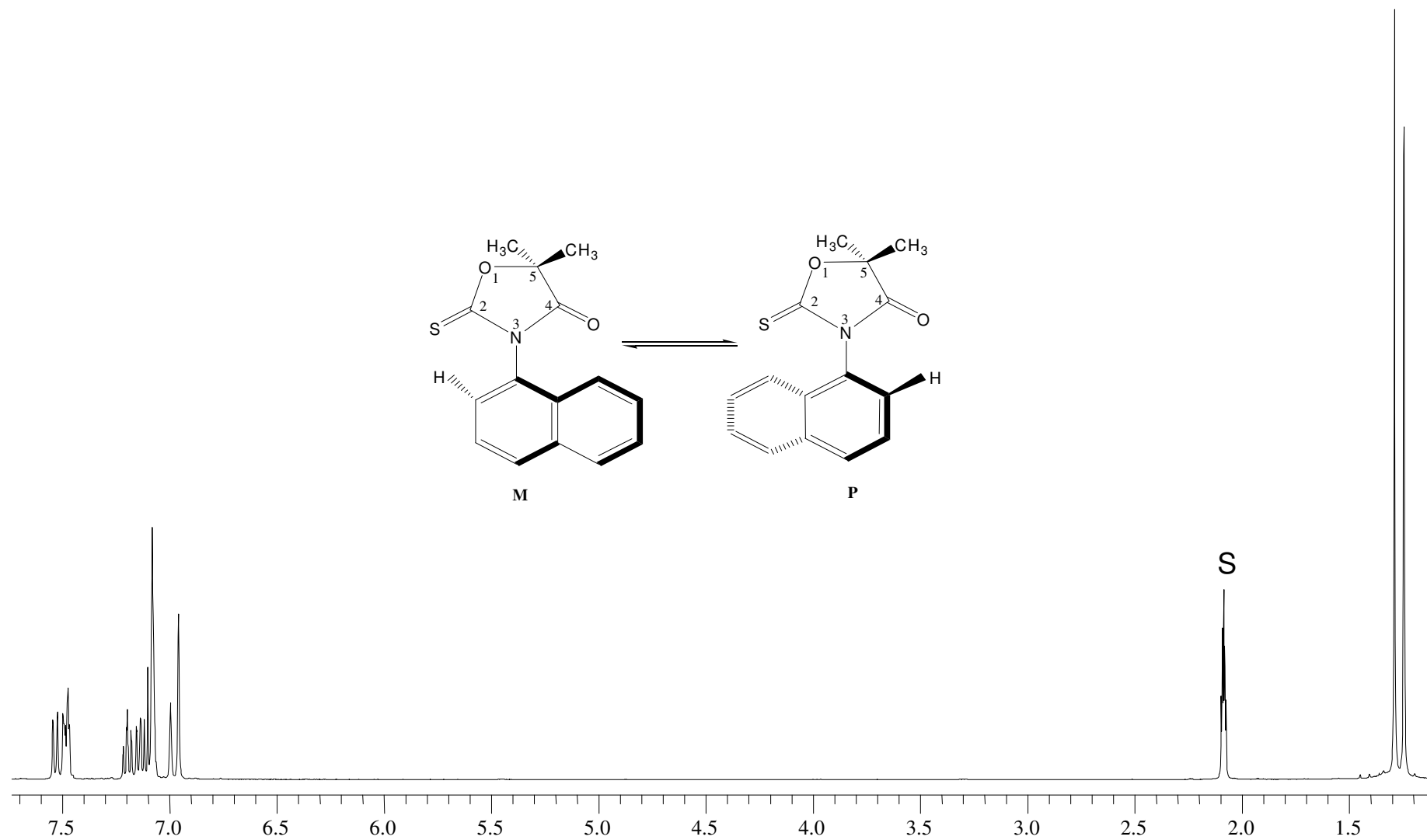


Figure A.5. 400 MHz ^1H NMR spectrum of compound **16** in toluene-d_8 . S: Solvent

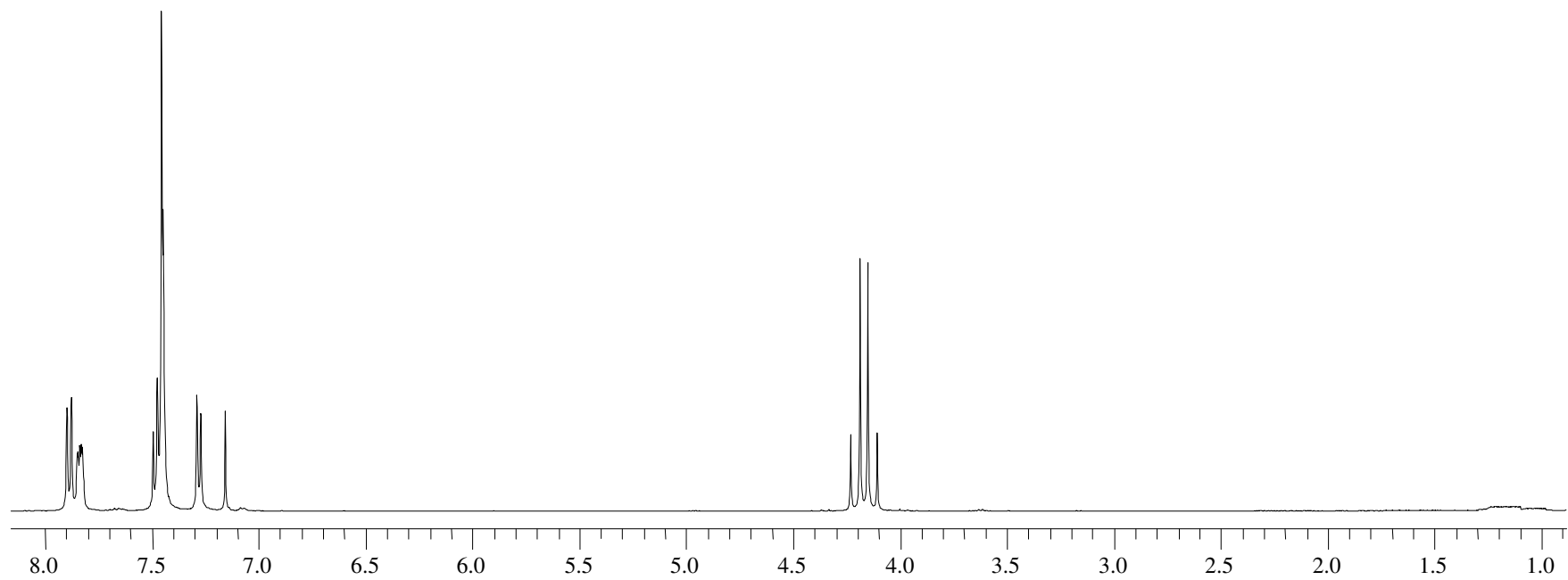
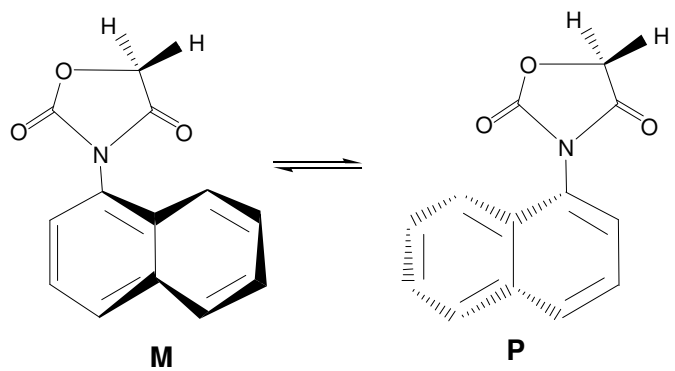


Figure A.6. 400 MHz ^1H NMR spectrum of compound **17** in CDCl_3

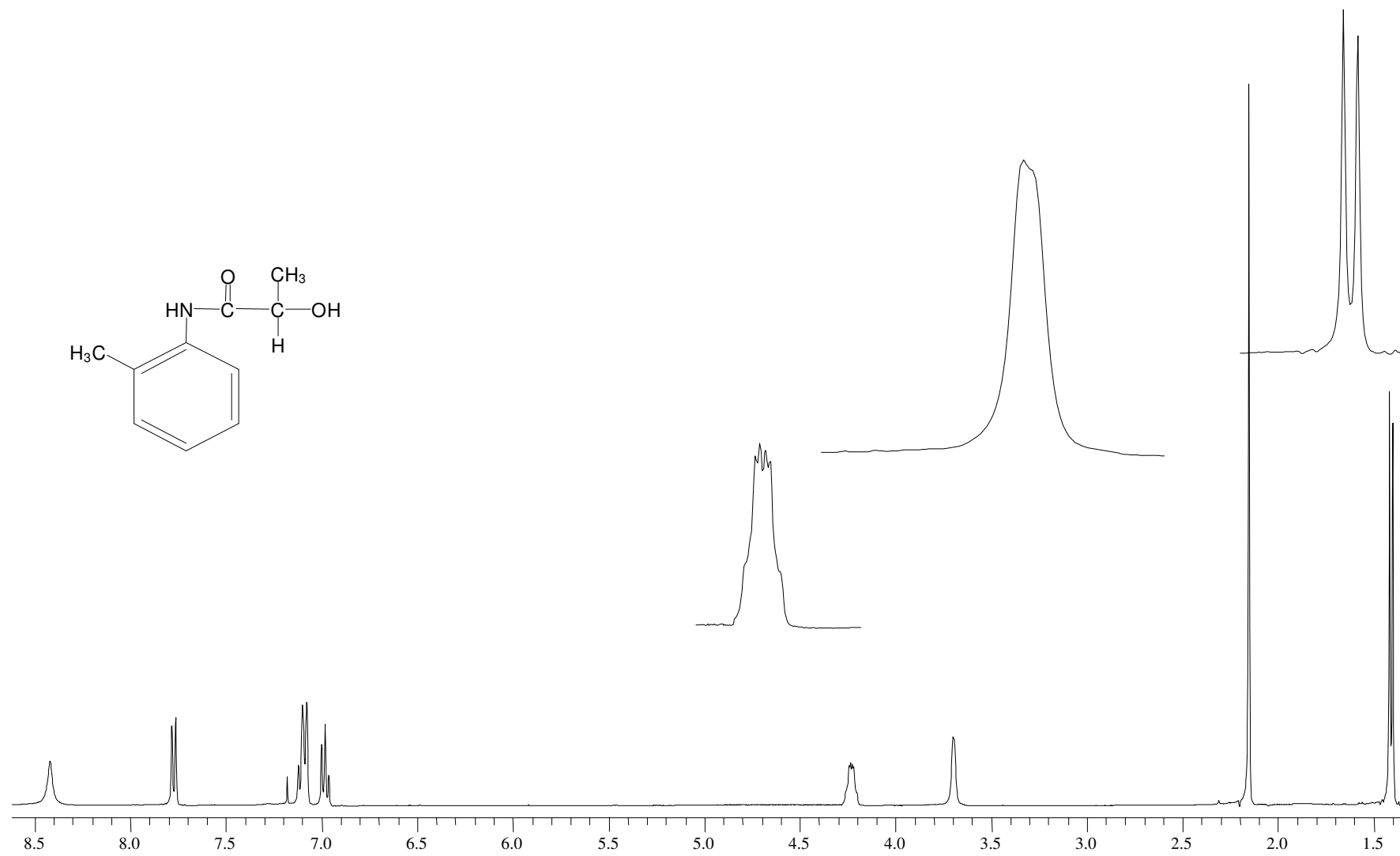


Figure A.7. 400 MHz ^1H NMR spectrum of compound **20** in CDCl_3

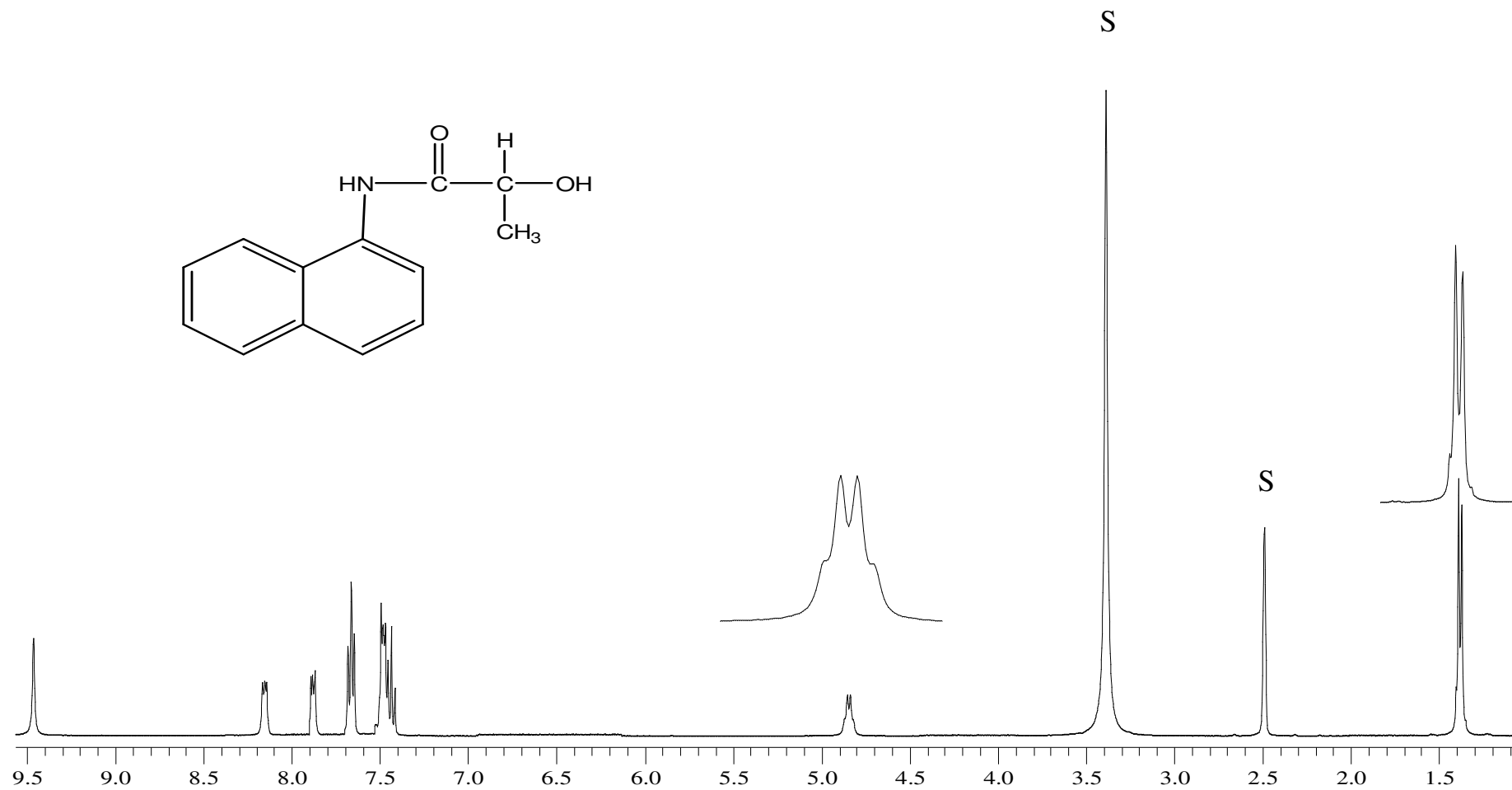


Figure A.8. 400 MHz ¹H NMR spectrum of compound **21** in DMSO. S:Solvent

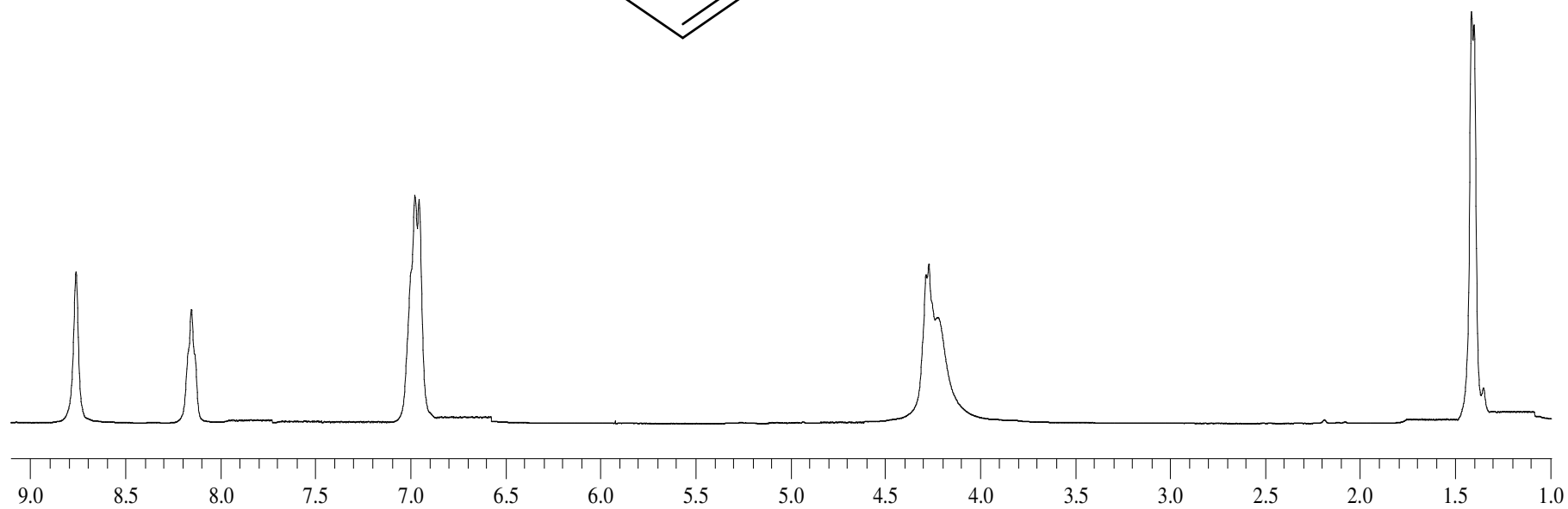
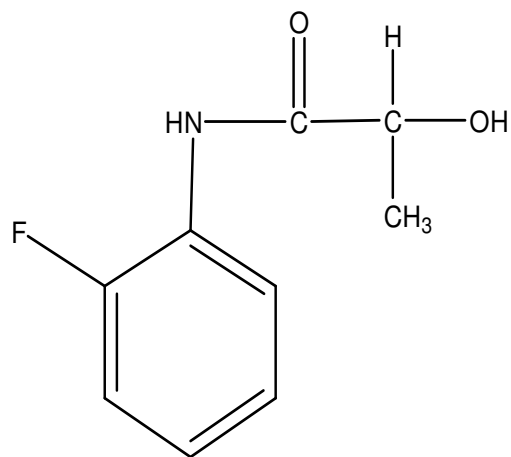


Figure A.9. 400 MHz ¹H NMR spectrum of compound **22** in CDCl₃

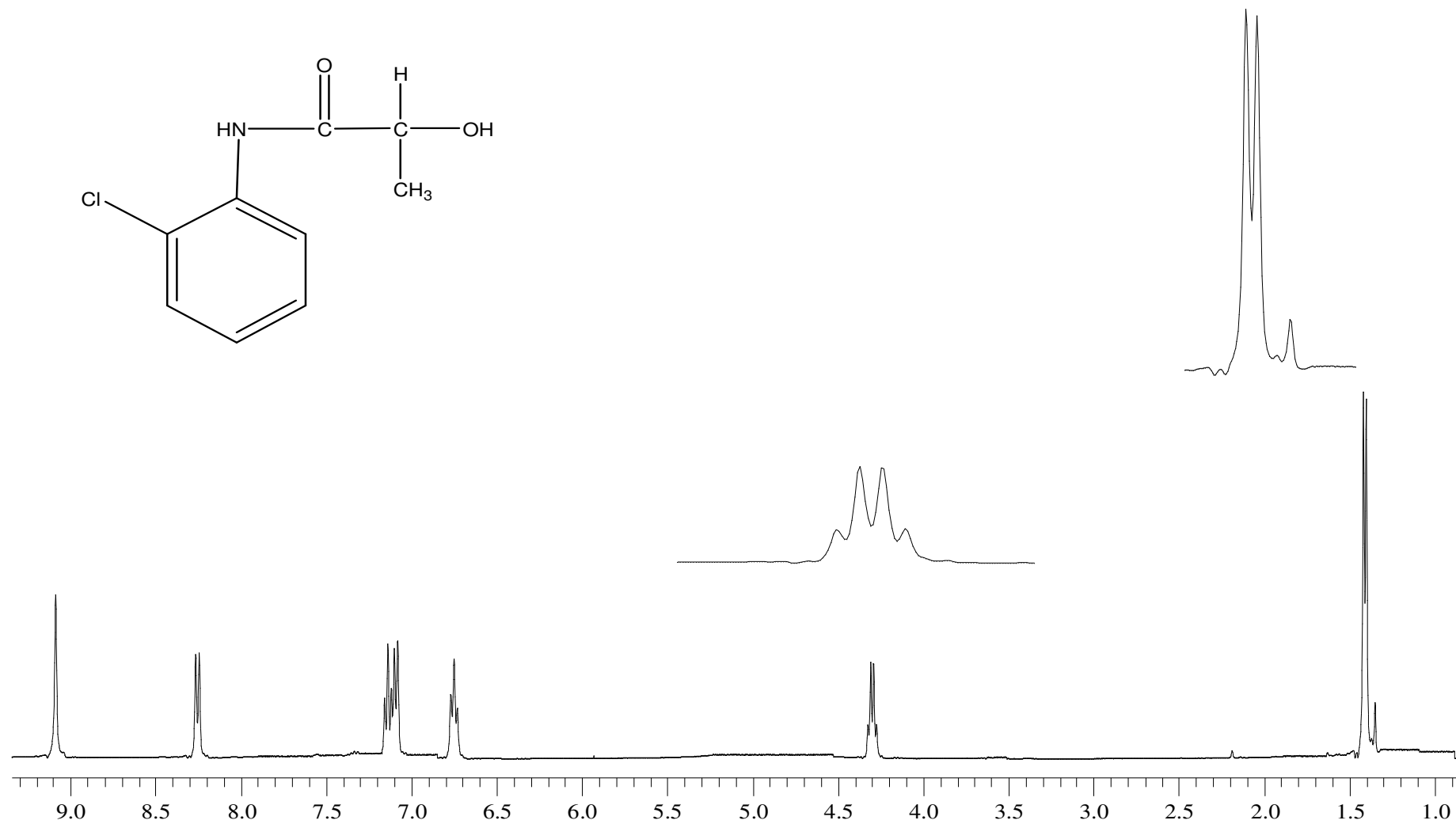


Figure A.10. 400 MHz ¹H NMR spectrum of compound **23** in CDCl₃

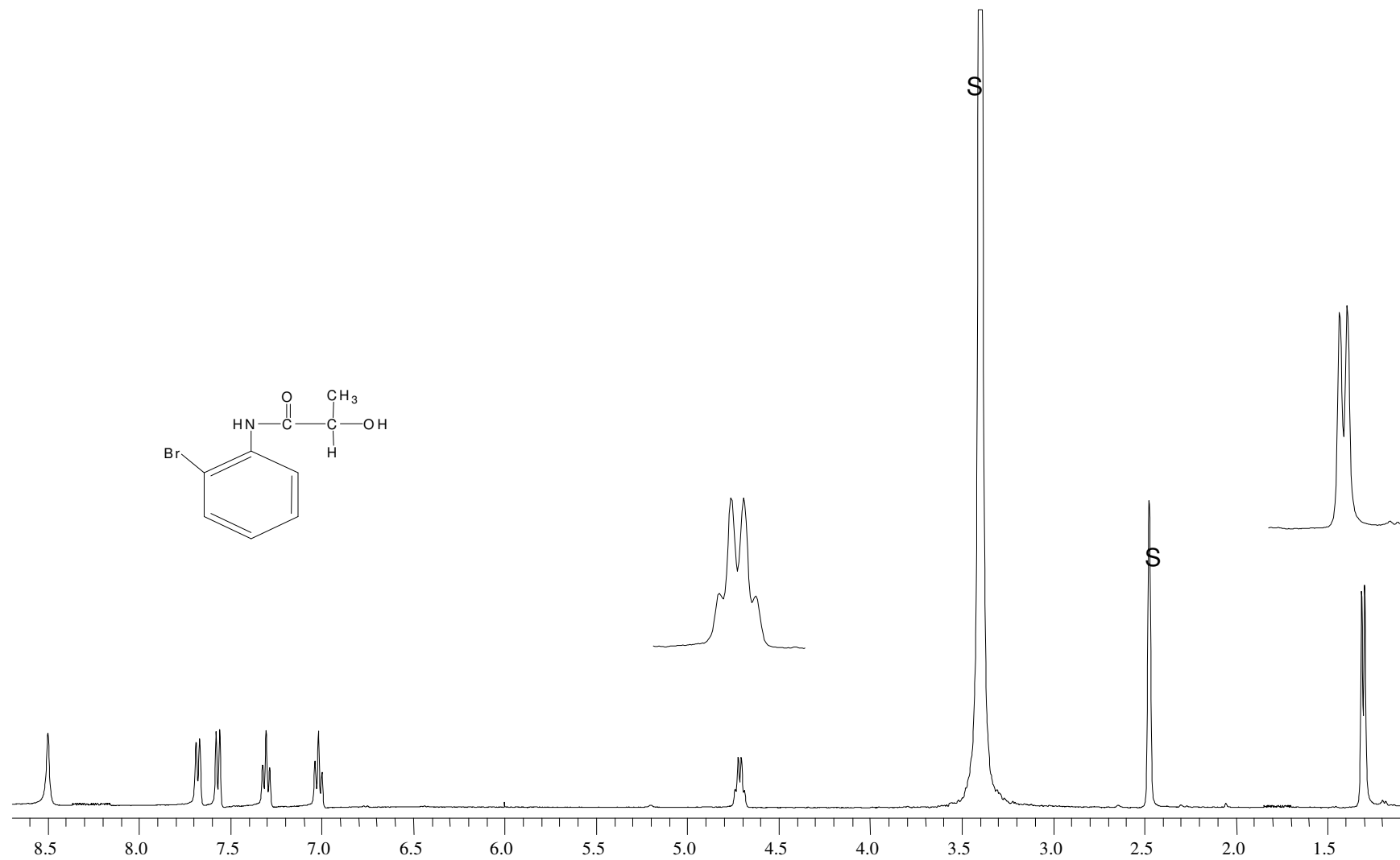


Figure A.11. 400 MHz ^1H NMR spectrum of compound **24** in DMSO. S: Solvent

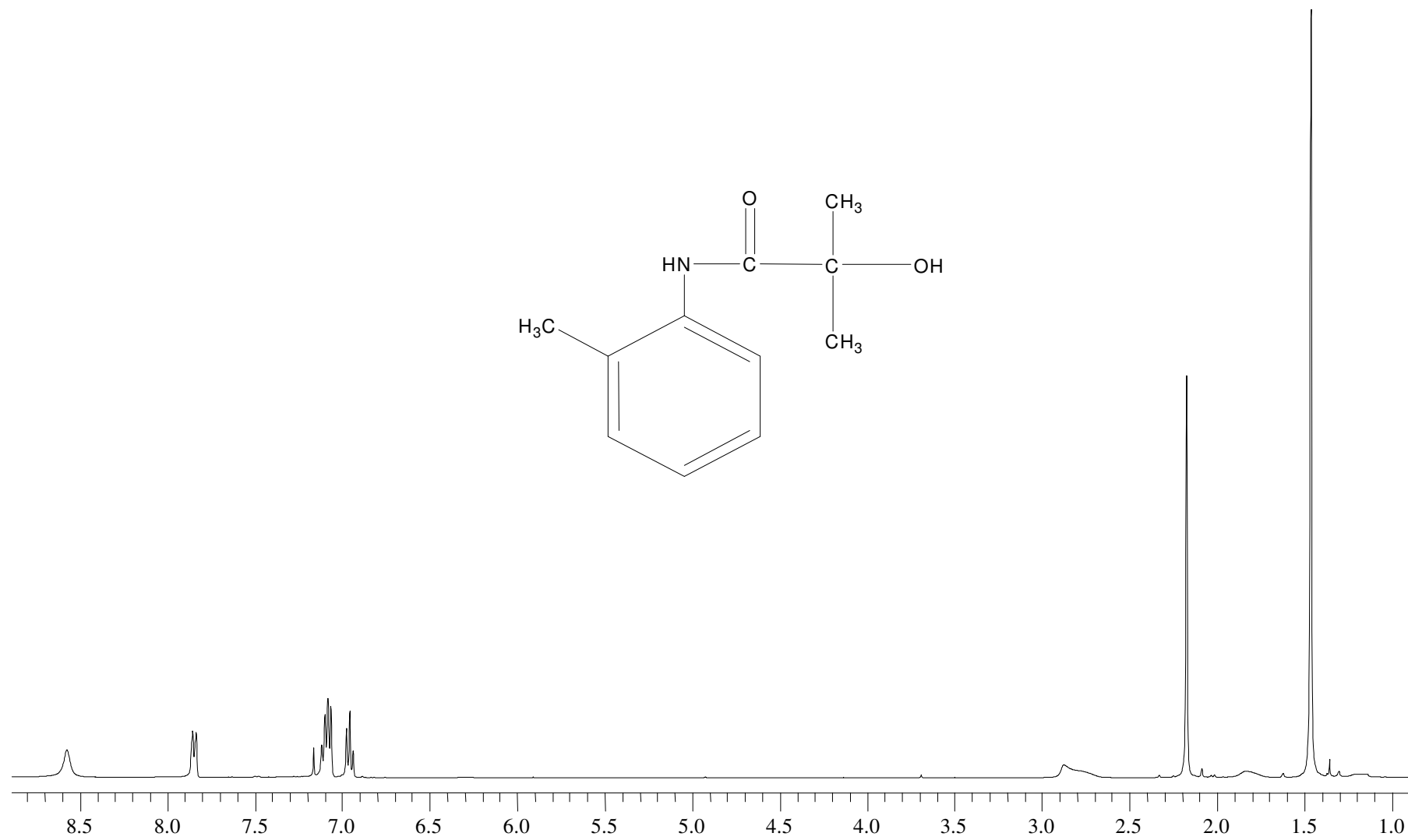


Figure A.12. 400 MHz ¹H NMR spectrum of compound **26** in CDCl₃.

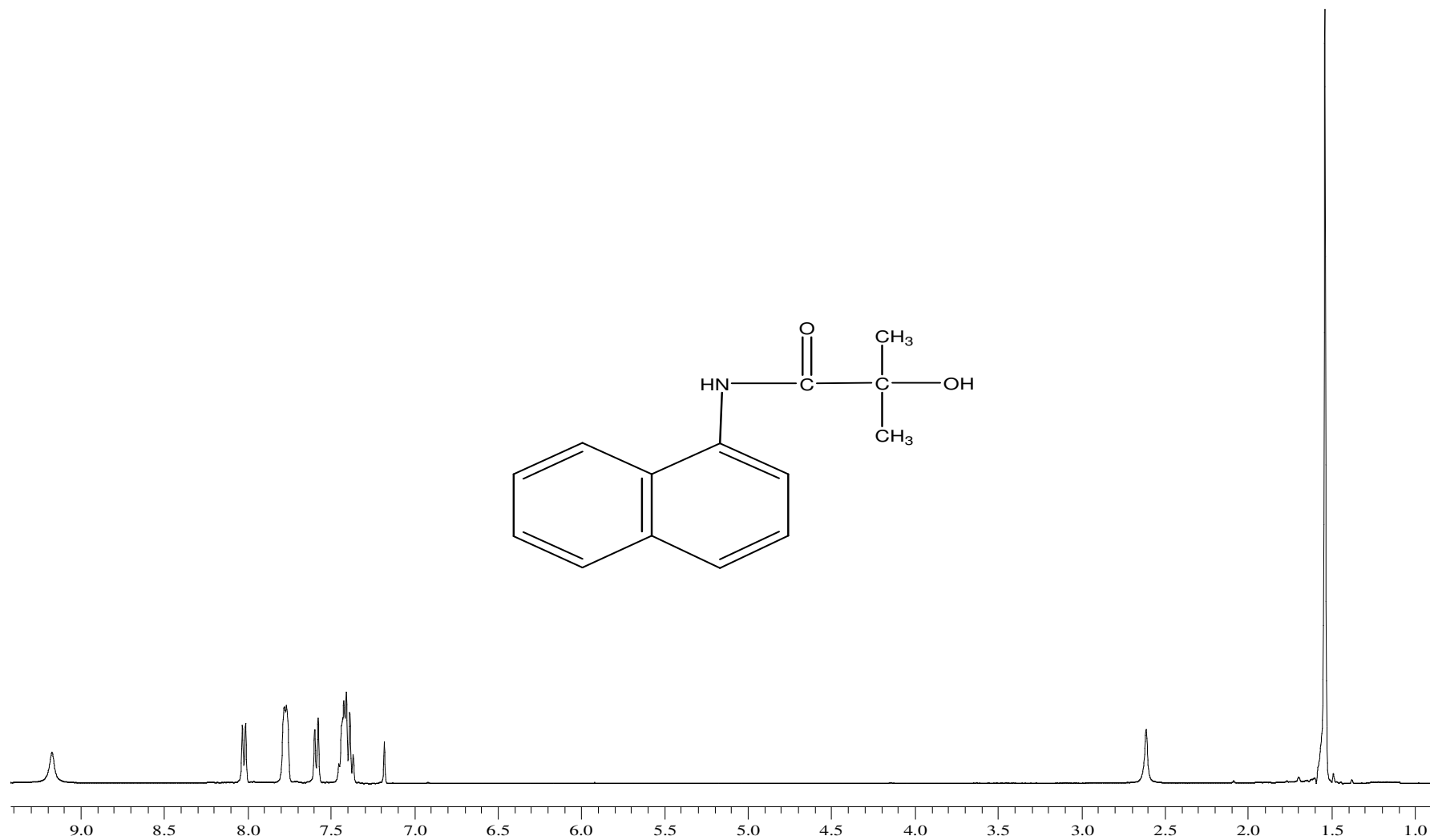


Figure A.13. 400 MHz ¹H NMR spectrum of compound **27** in CDCl₃

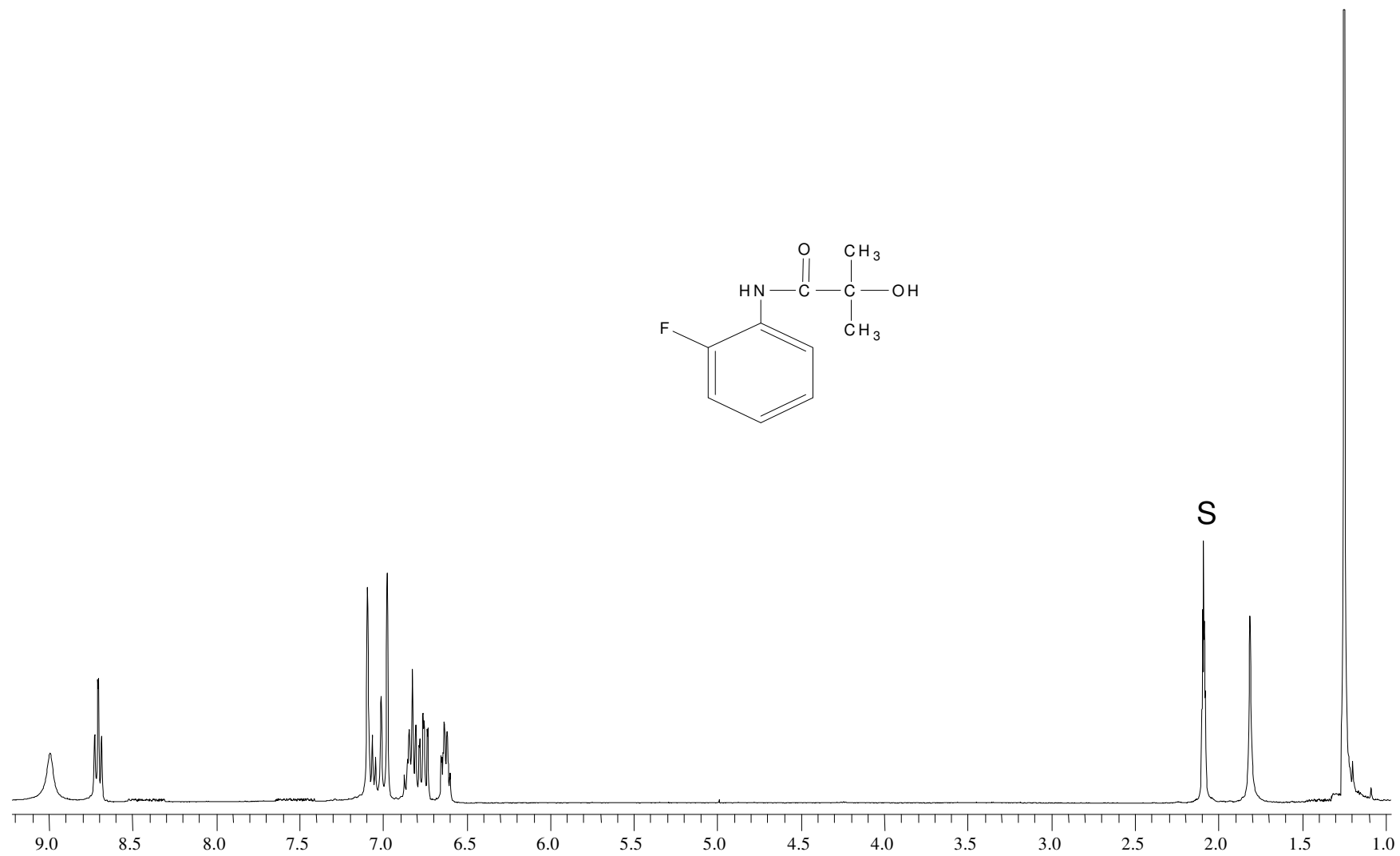


Figure A.14. 400 MHz ^1H NMR spectrum of compound **28** in toluene-d_8 . S=solvent.

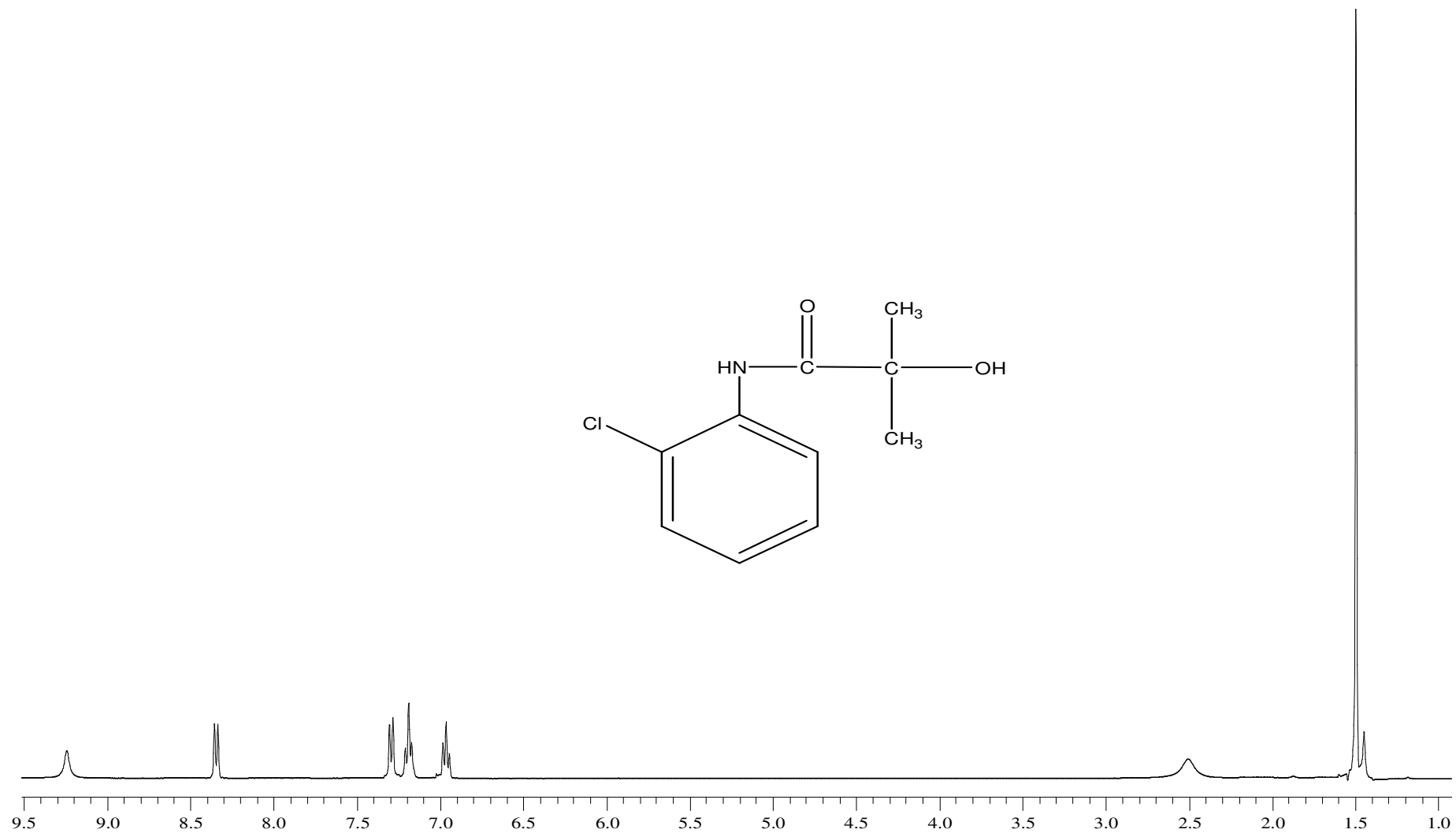


Figure A.15. 400 MHz ¹H NMR spectrum of compound **29** in CDCl₃

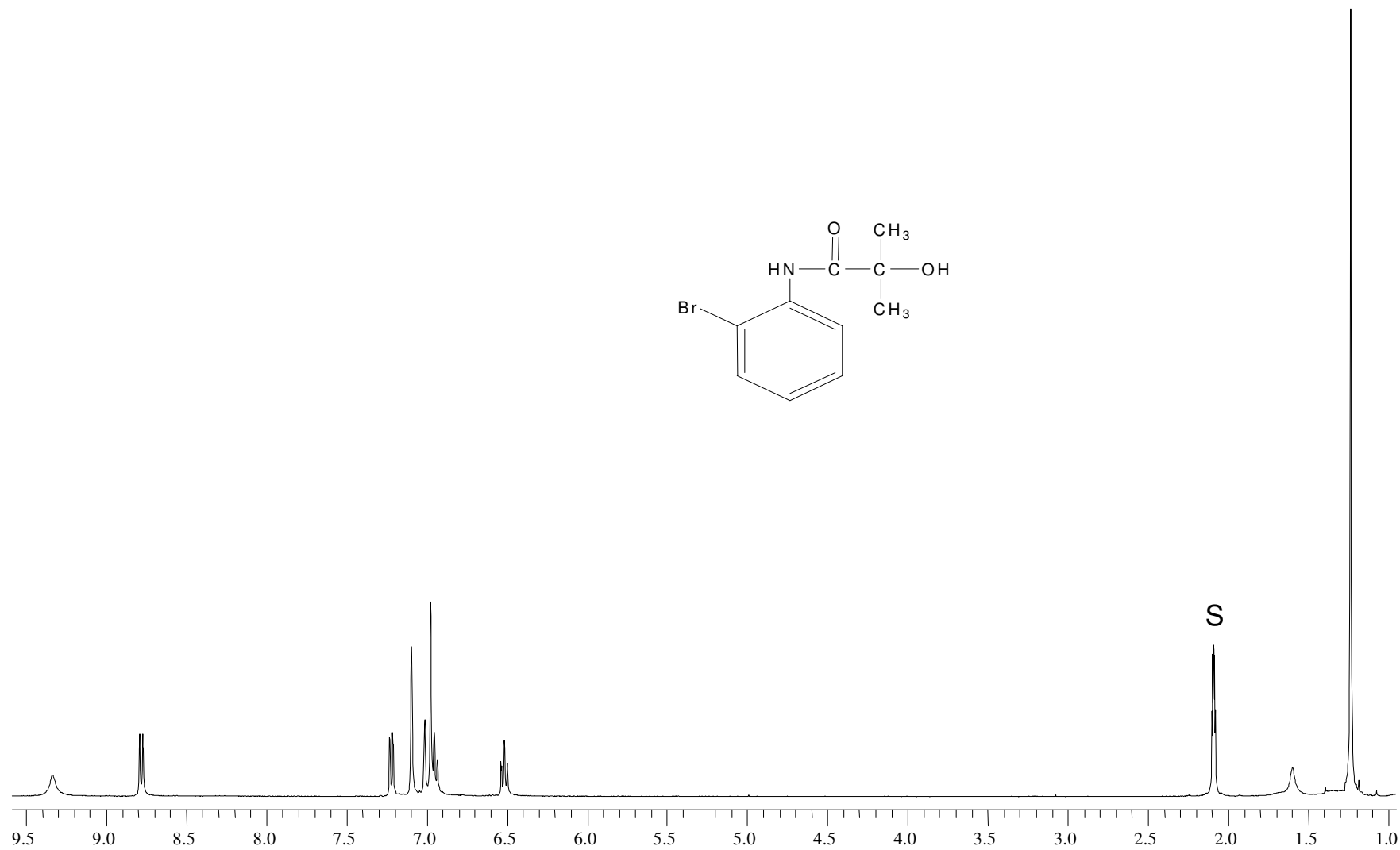


Figure A.16. 400 MHz ¹H NMR spectrum of compound **30** in toluene-d₈. S=solvent

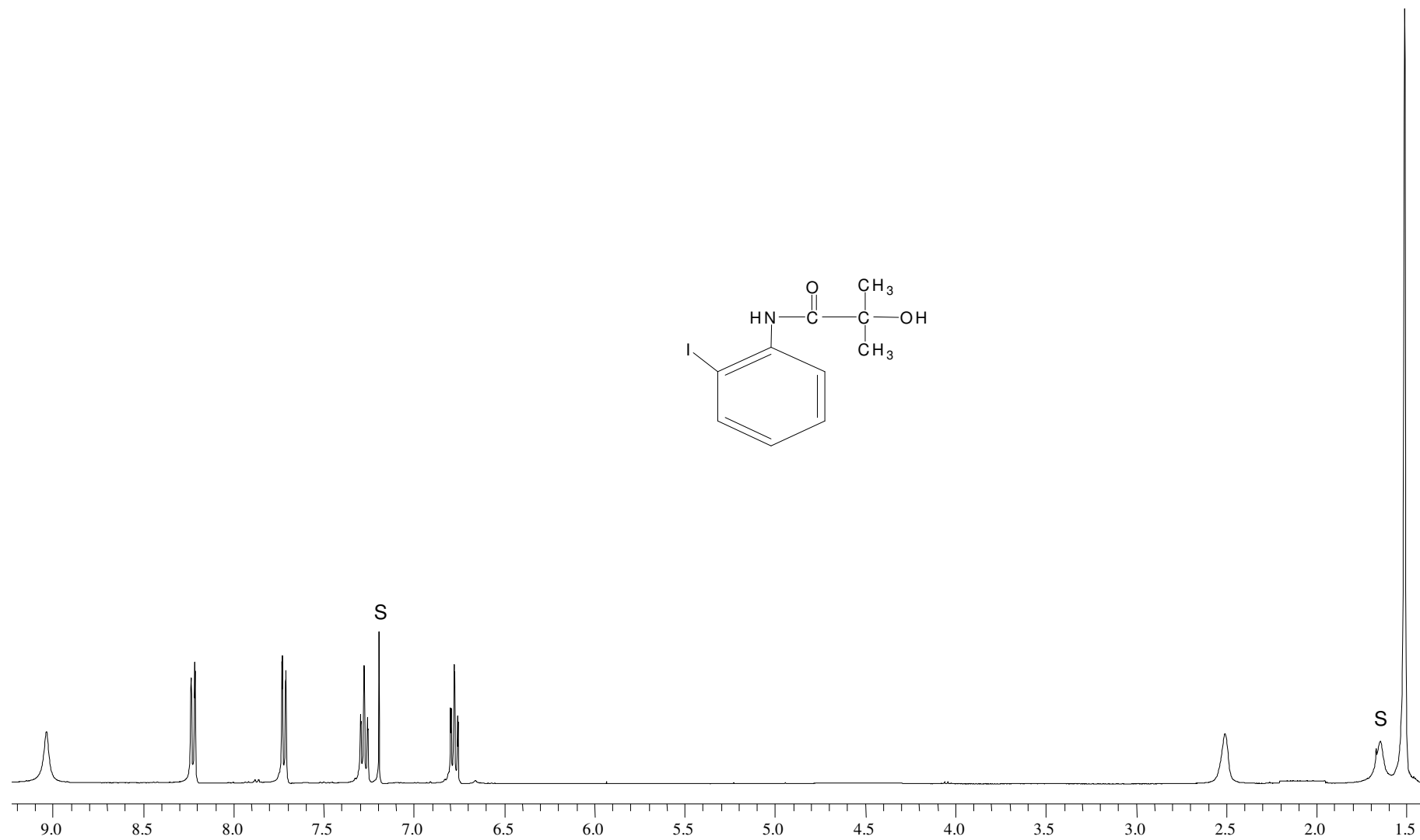


Figure A.17. 400 MHz ^1H NMR spectrum of compound **31** in CDCl_3

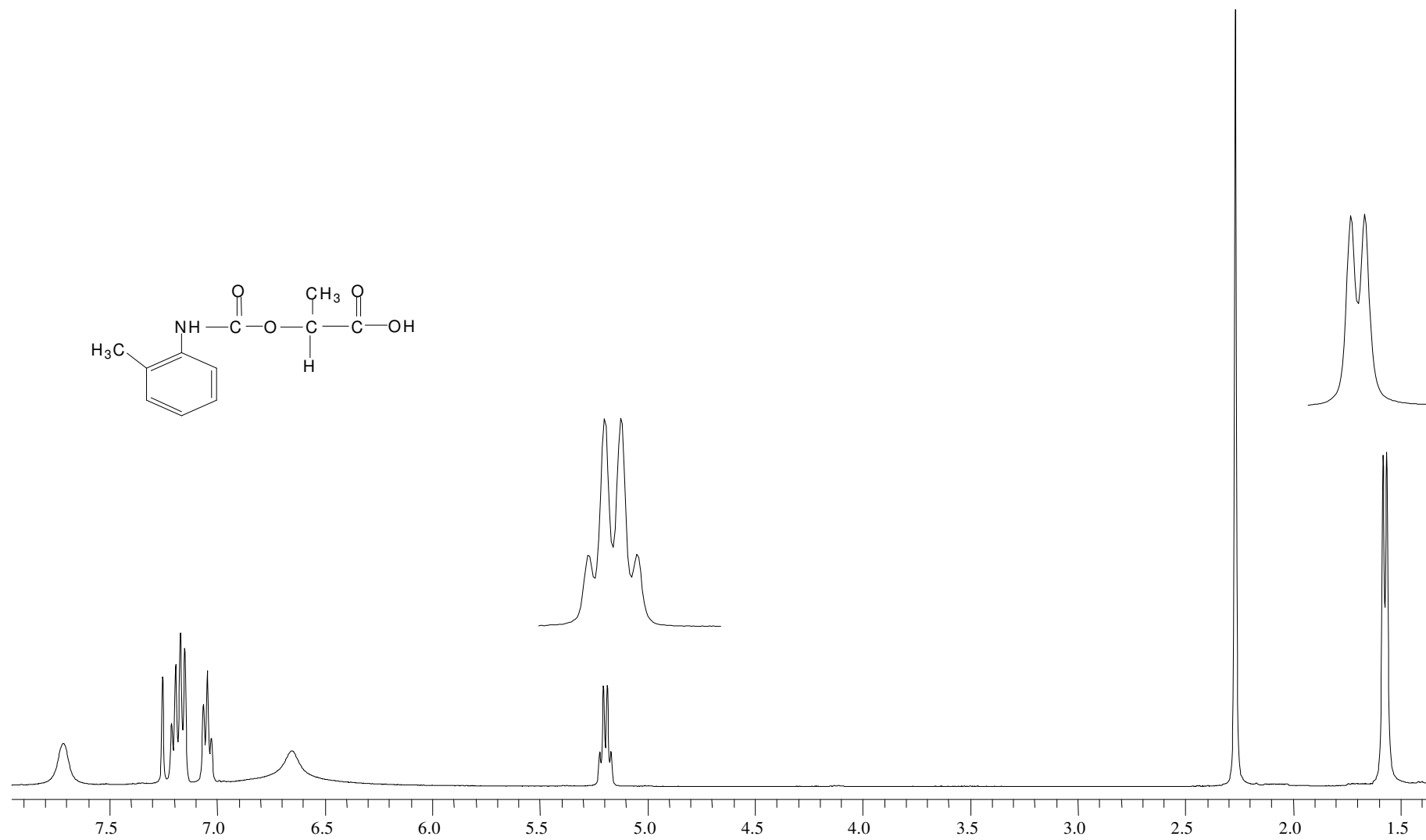


Figure A.18. 400 MHz ^1H NMR spectrum of compound **32** in CDCl_3

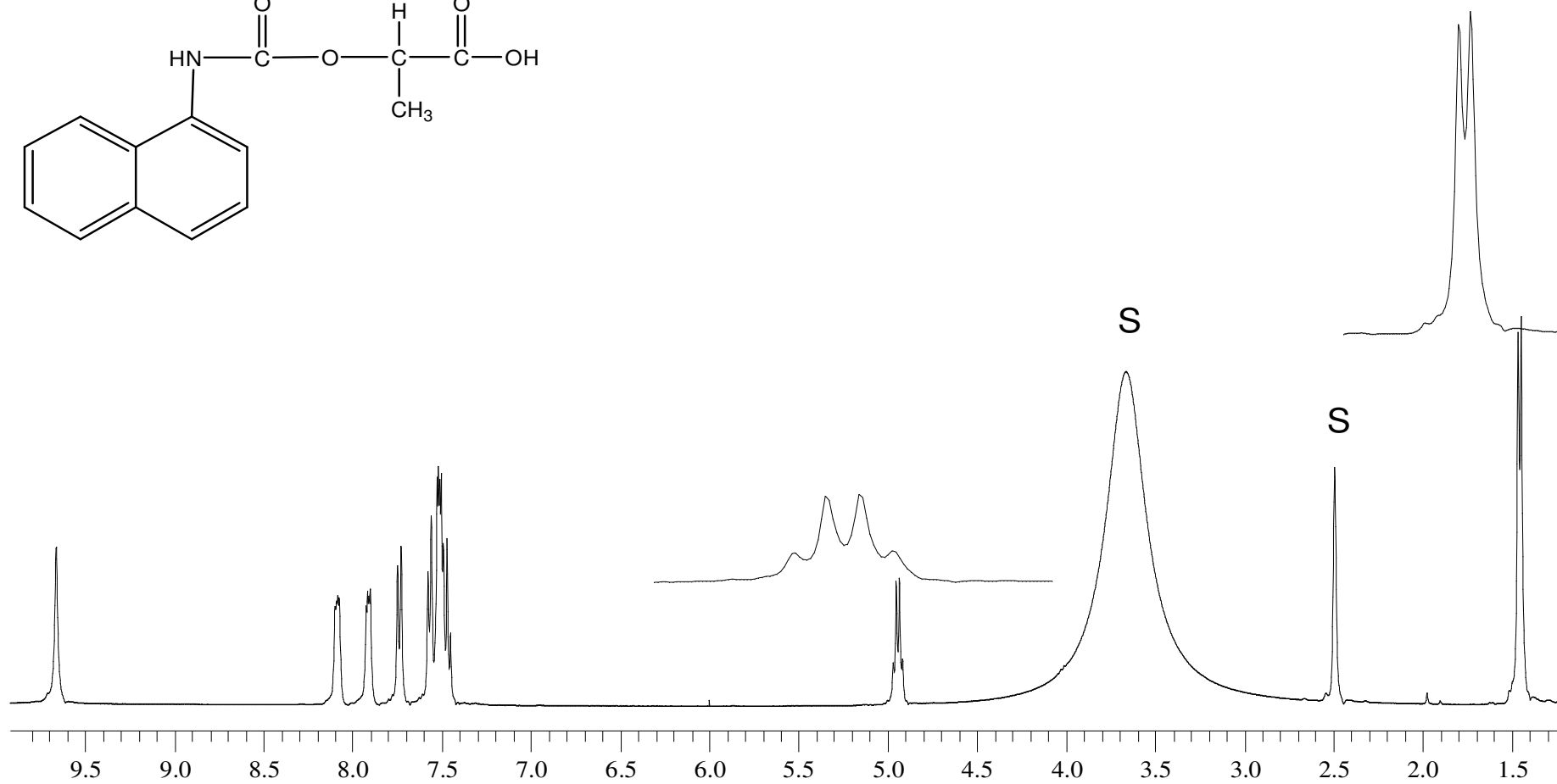
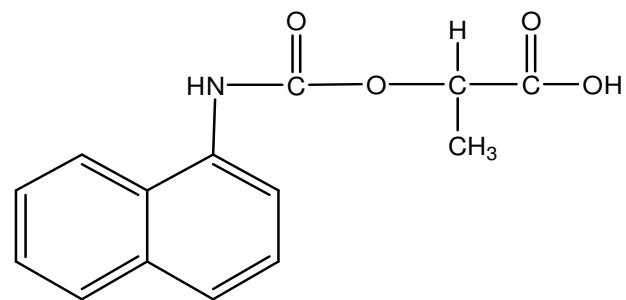


Figure A.19. 400 MHz ¹H NMR spectrum of compound 33 in DMSO. S: Solvent

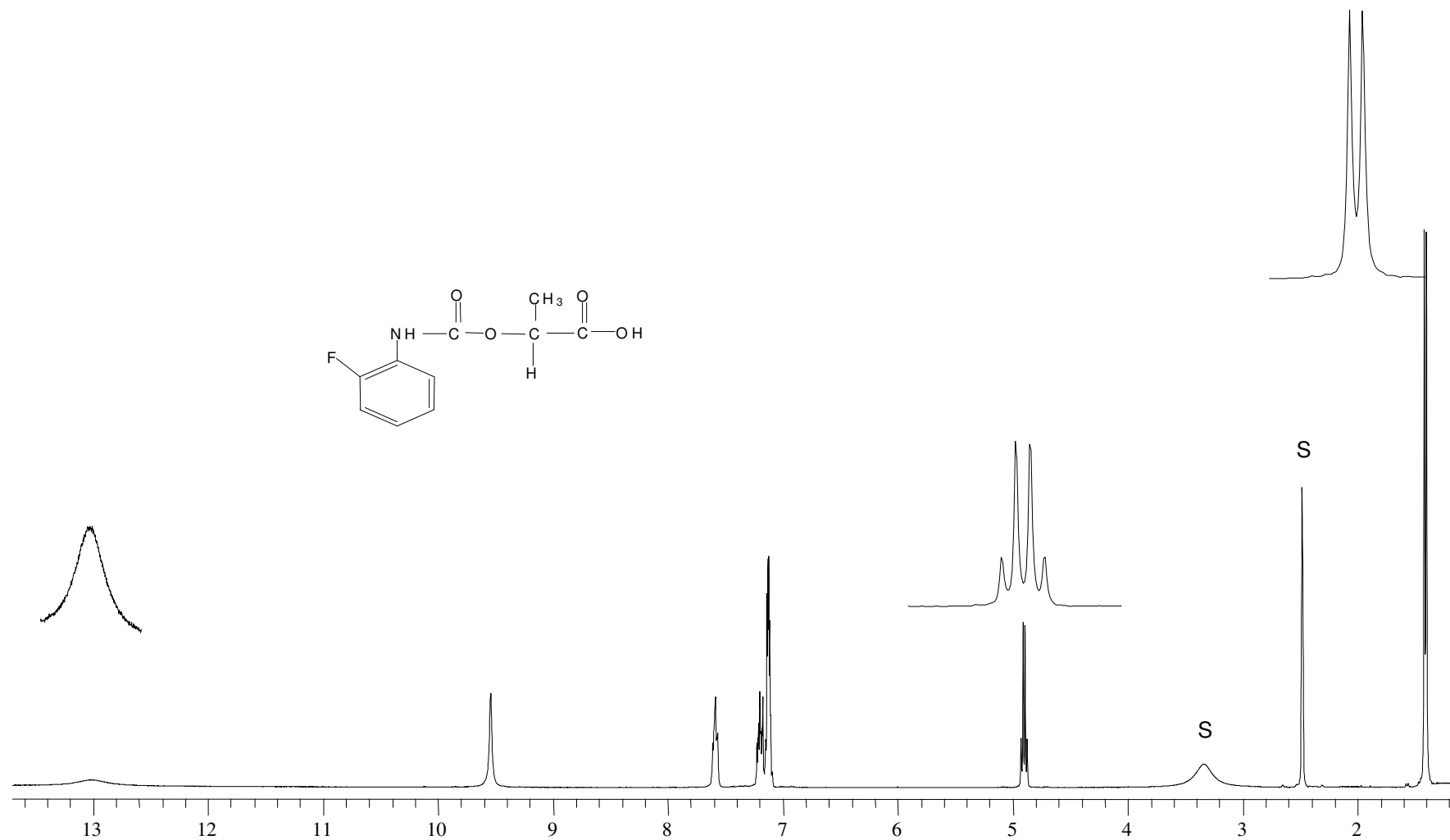


Figure A.20. 400 MHz ¹H NMR spectrum of compound **34** in DMSO. S: solvent

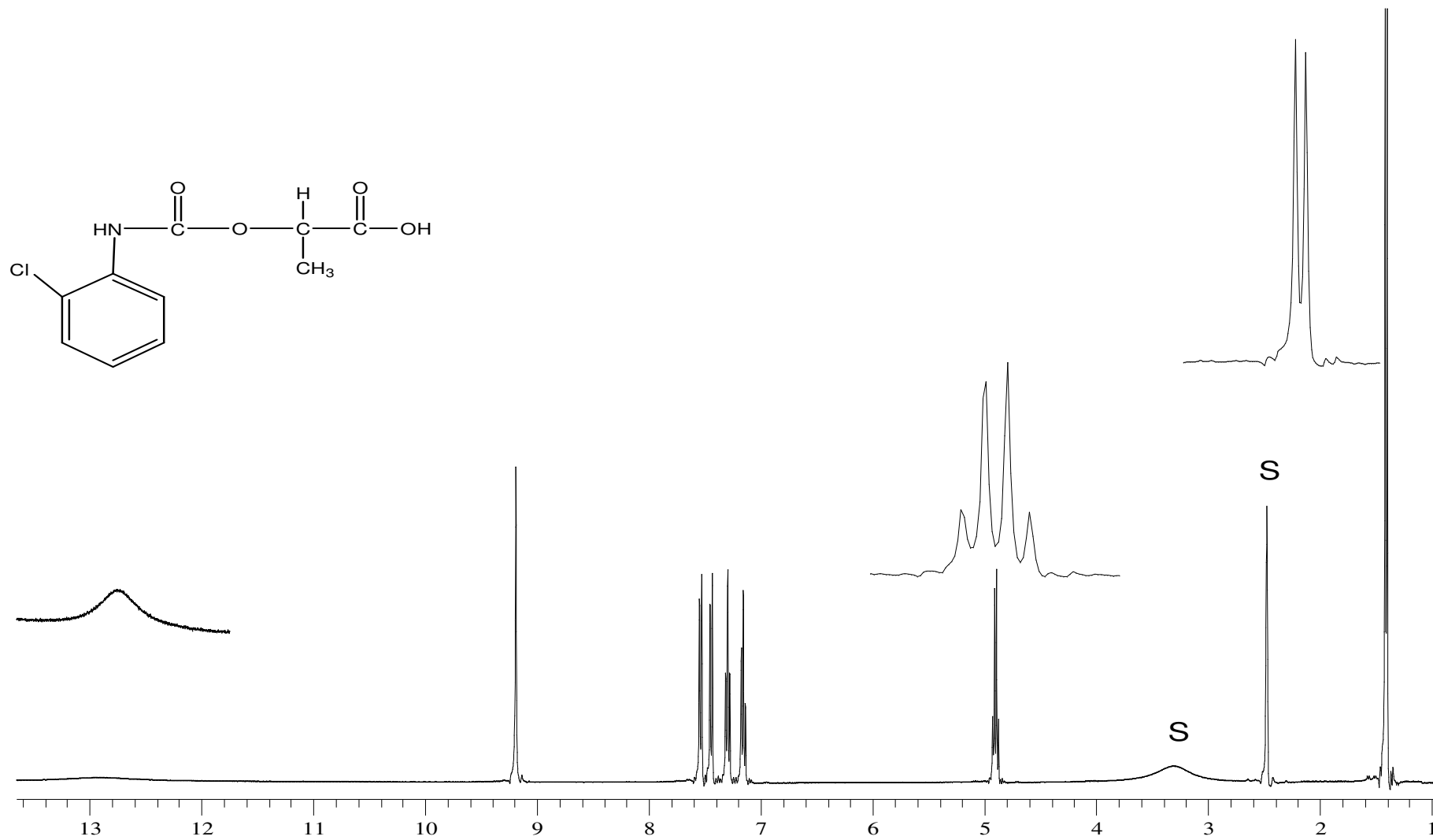


Figure A.21. 400 MHz ¹H NMR spectrum of compound **35** in DMSO. S: Solvent

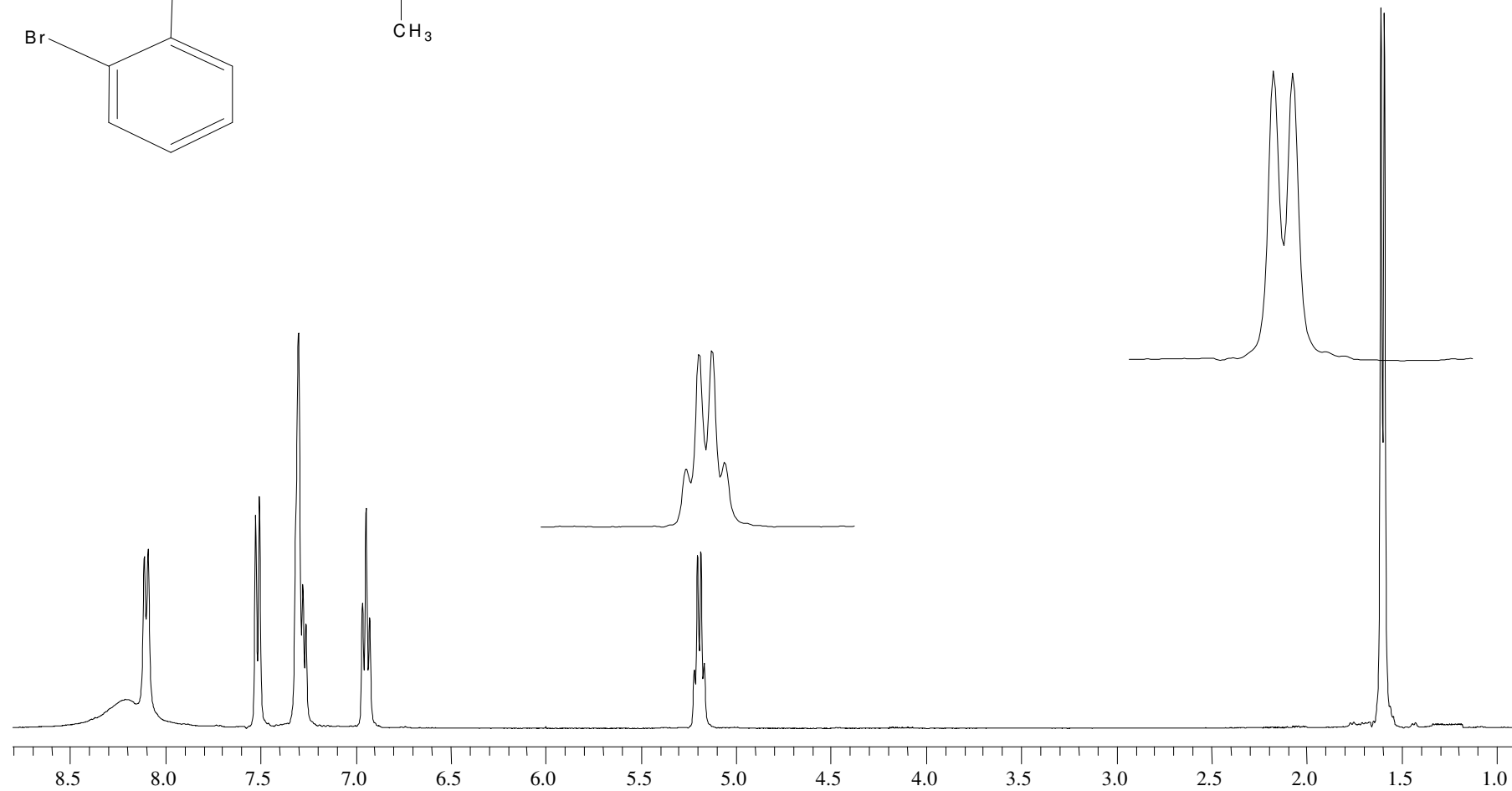
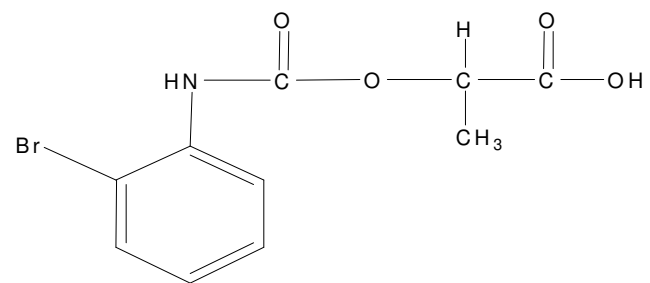


Figure A.22. 400 MHz ¹H NMR spectrum of compound **36** in CDCl₃

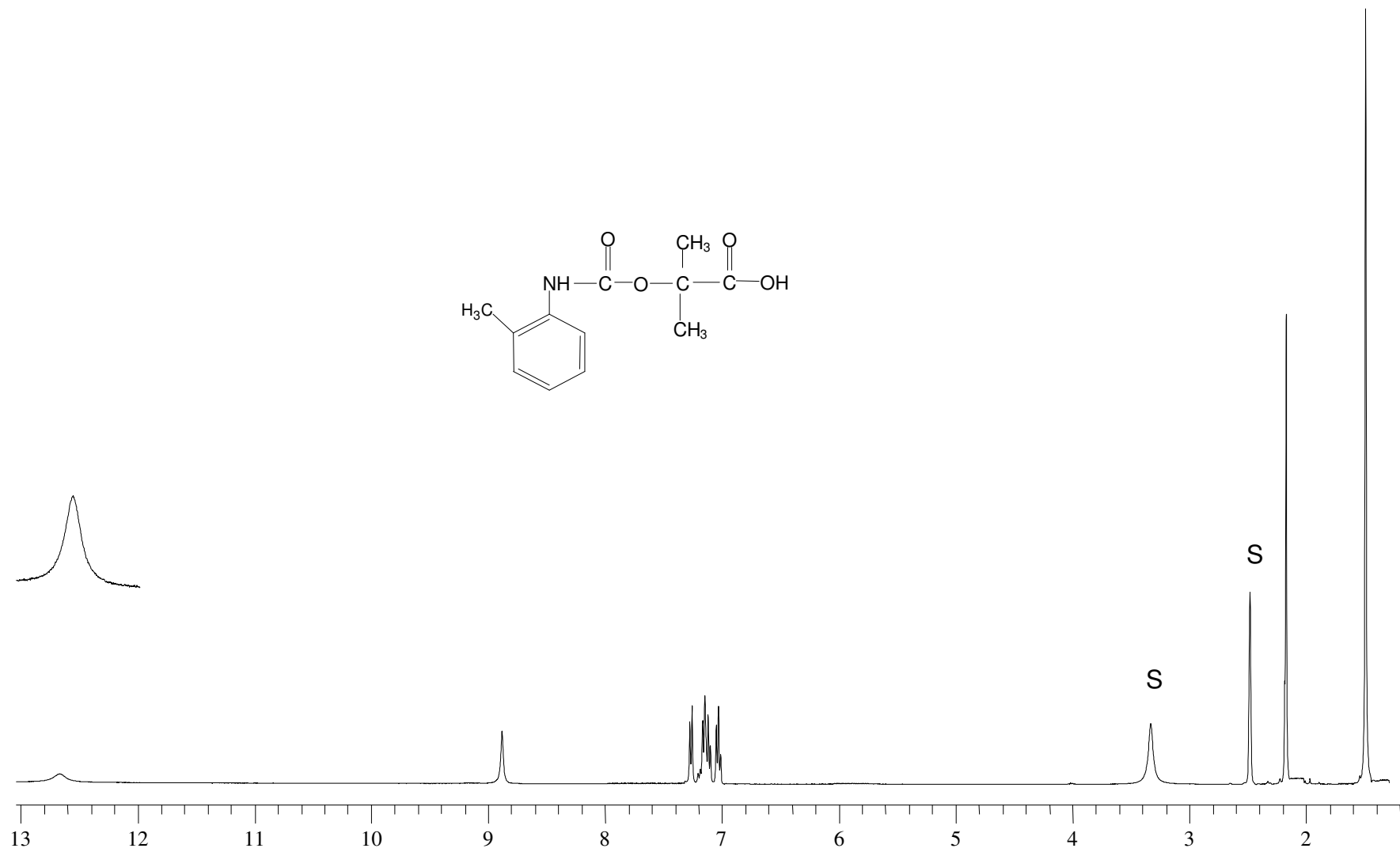


Figure A.23. 400 MHz ¹H NMR spectrum of compound **38** in DMSO. S: Solvent

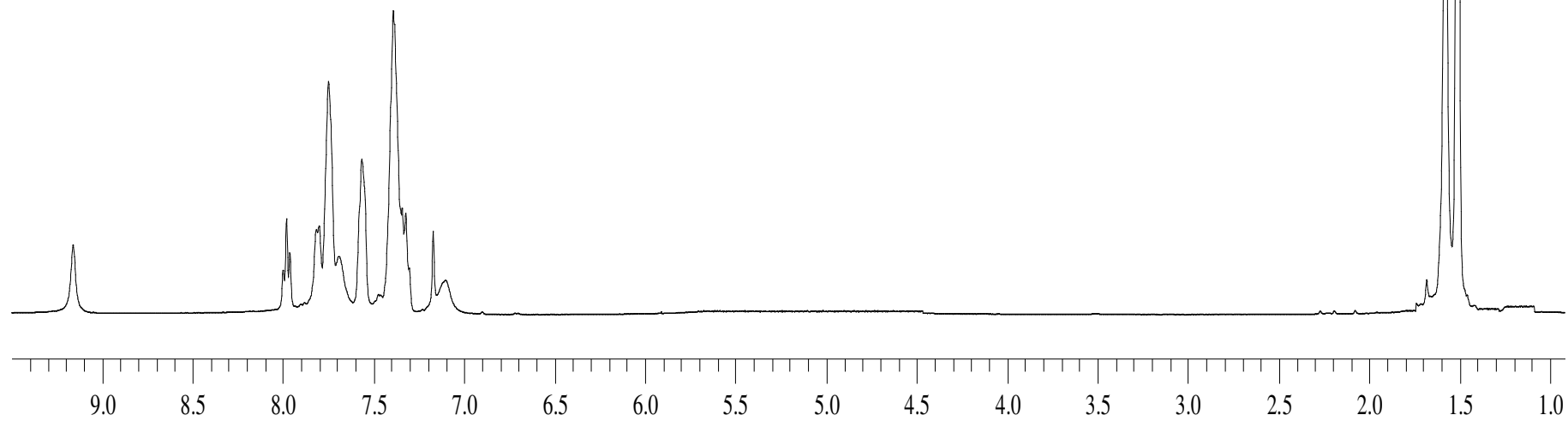
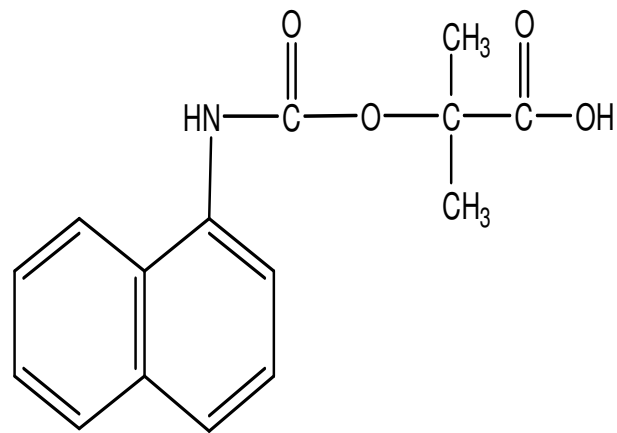


Figure A.24. 400 MHz ¹H NMR spectrum of compound **39** in CDCl₃

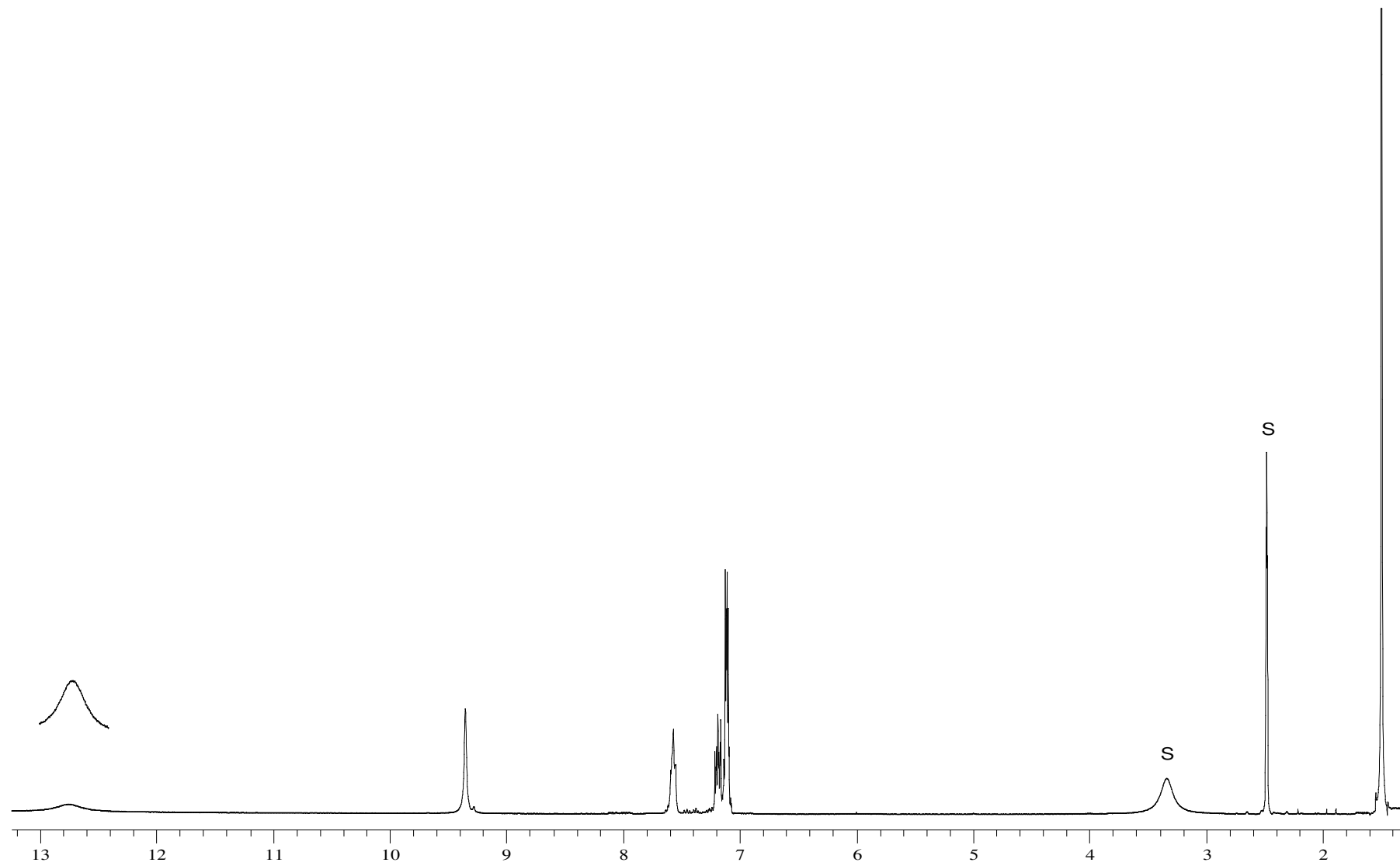


Figure A.25. 400 MHz ^1H NMR spectrum of compound **40** in DMSO. S: Solvent

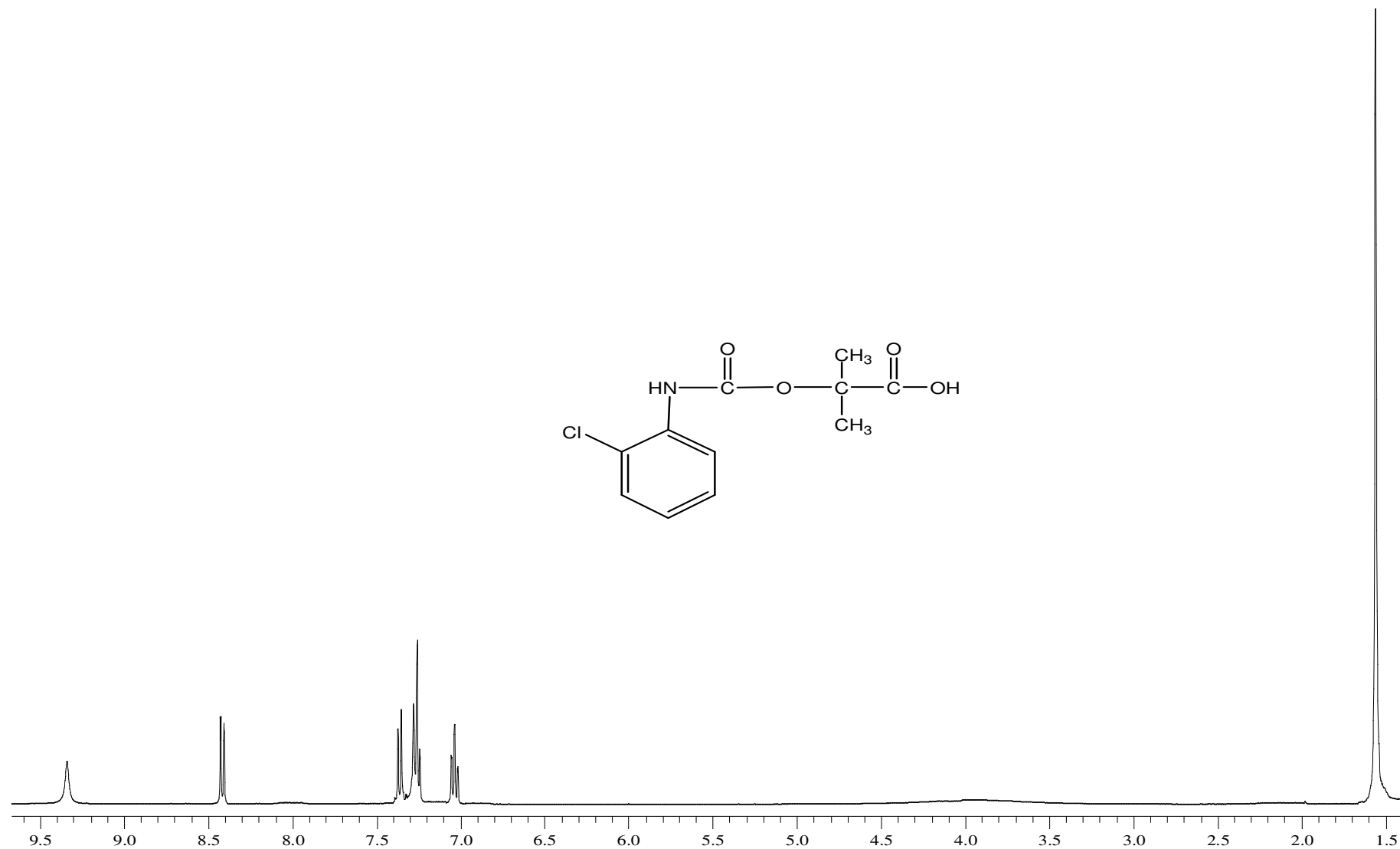


Figure A.26. 400 MHz ¹H NMR spectrum of compound **41** in CDCl₃

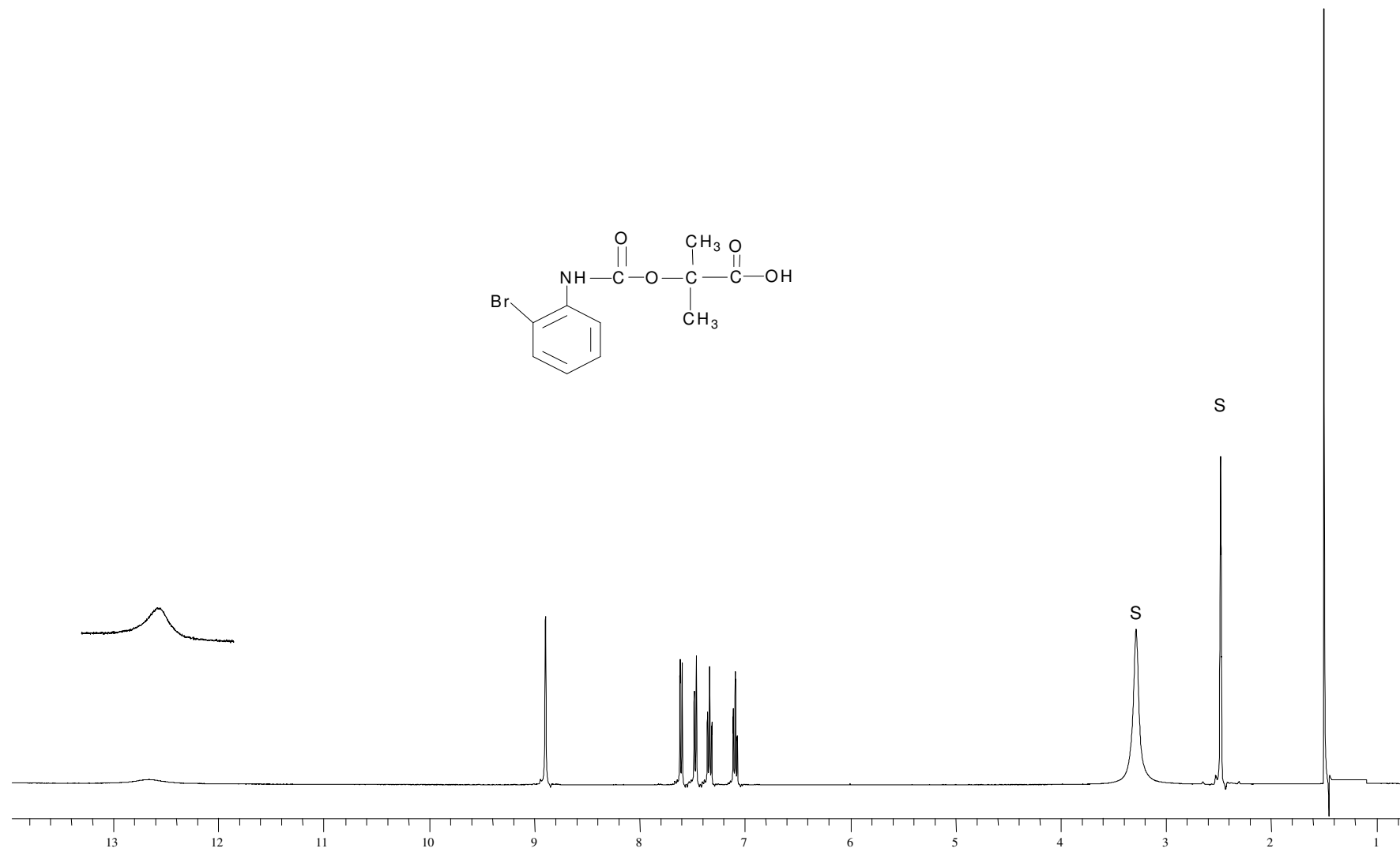


Figure A.27. 400 MHz ¹H NMR spectrum of compound **42** in DMSO. S: Solvent

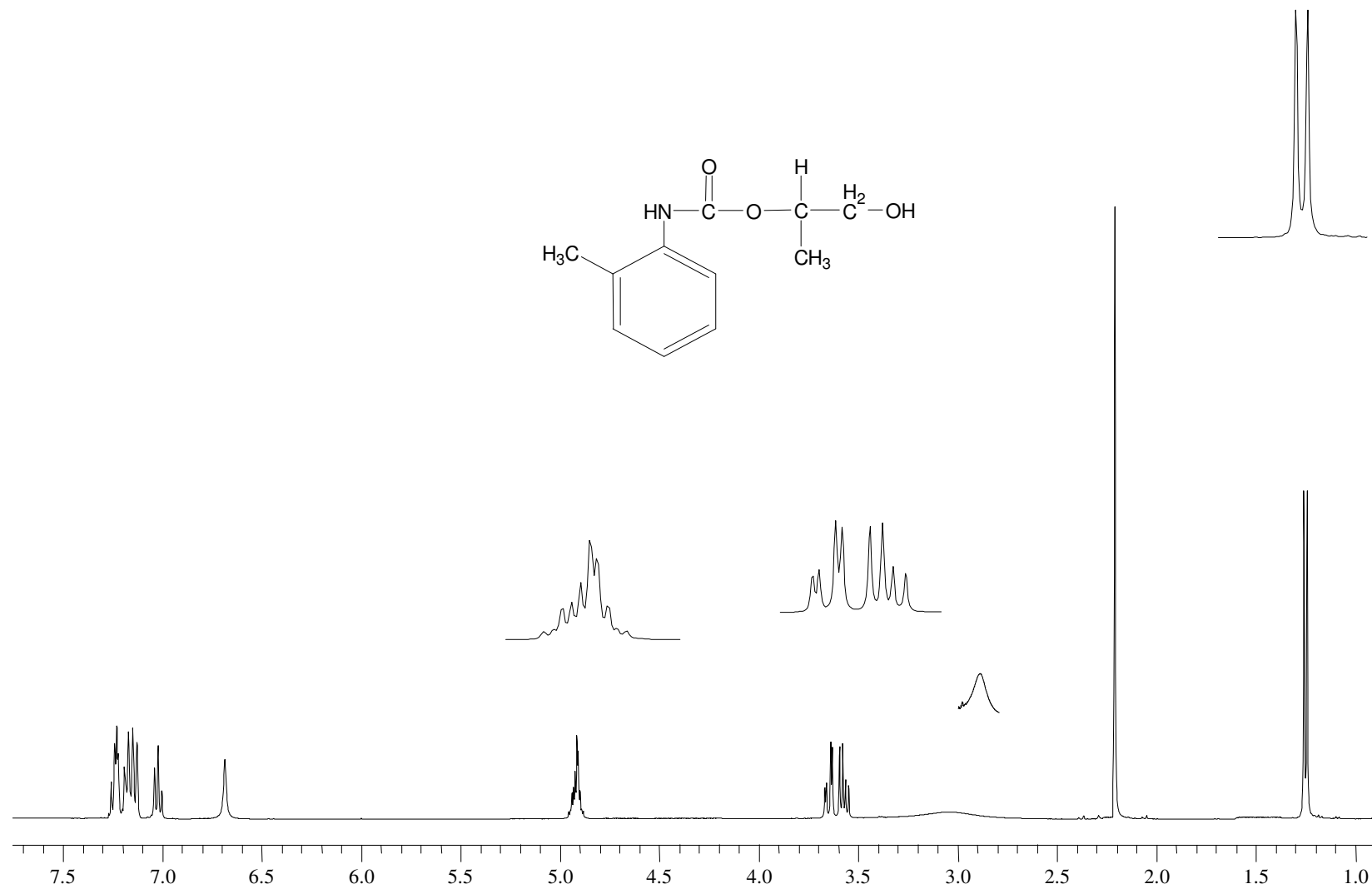
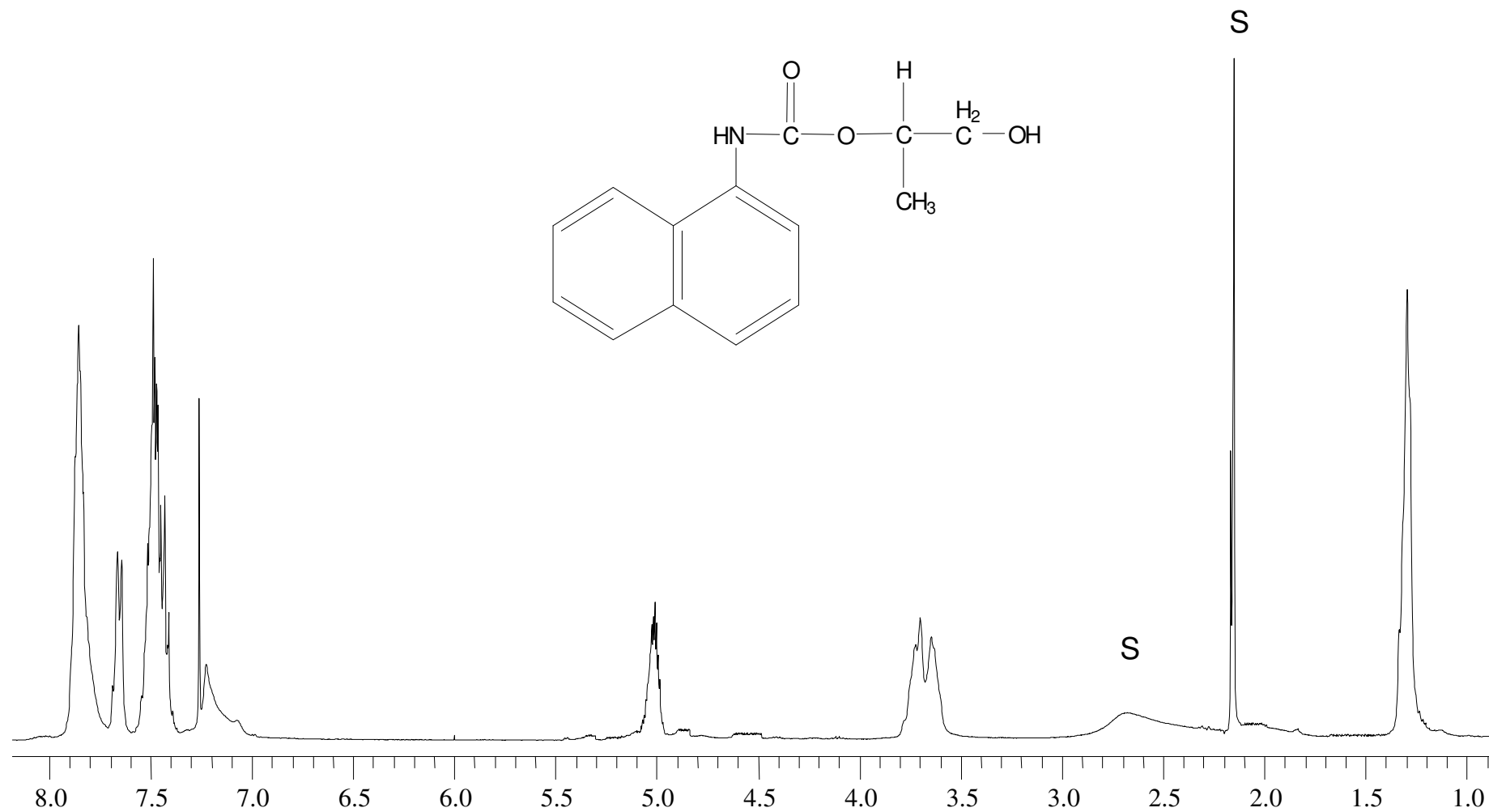


Figure A.28. 400 MHz ^1H NMR spectrum of compound **44** in CDCl_3



FigureA.29. 400 MHz ¹H NMR spectrum of compound **45** in DMSO. S: Solvent

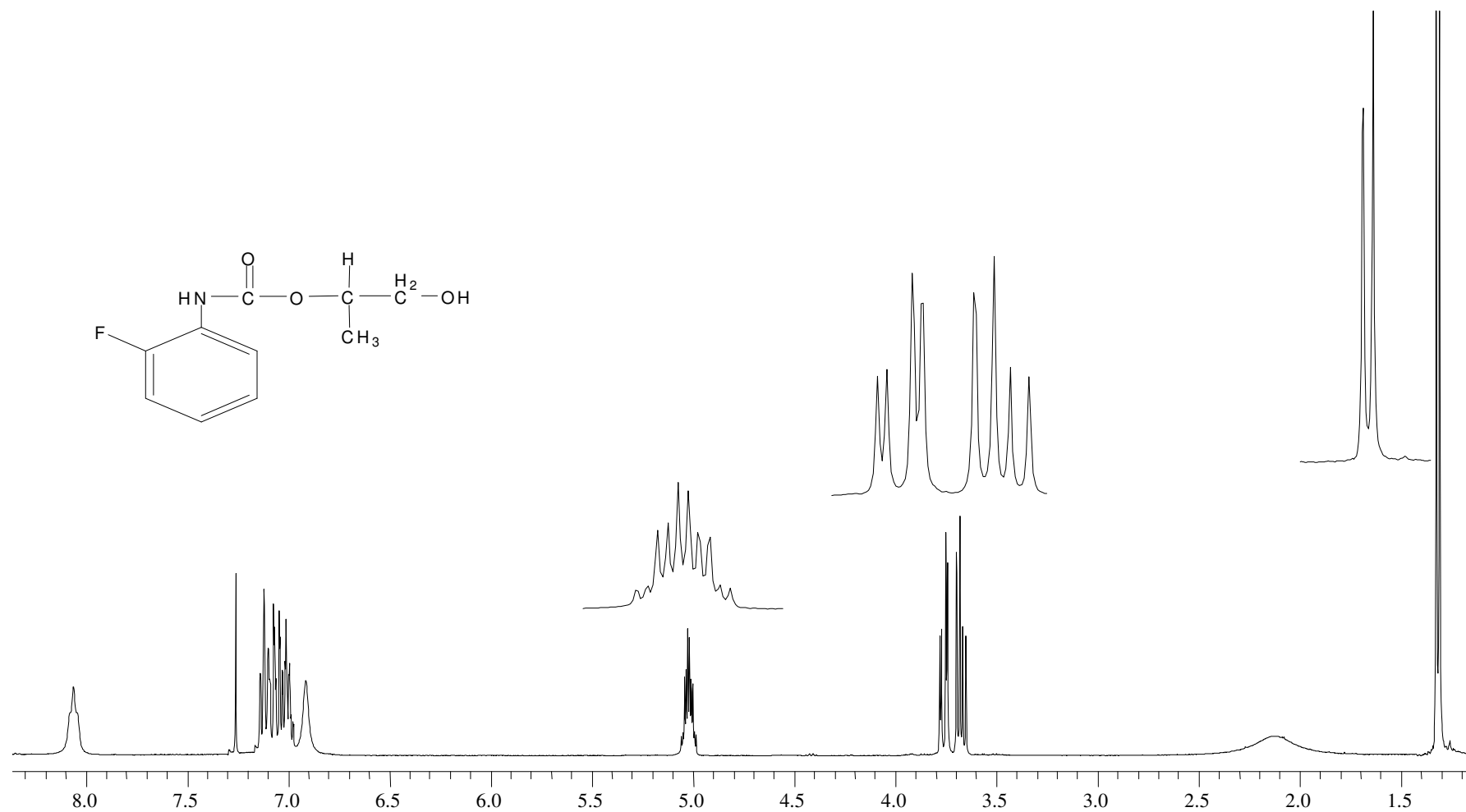


Figure A.30. 400 MHz ¹H NMR spectrum of compound **46** in CDCl₃

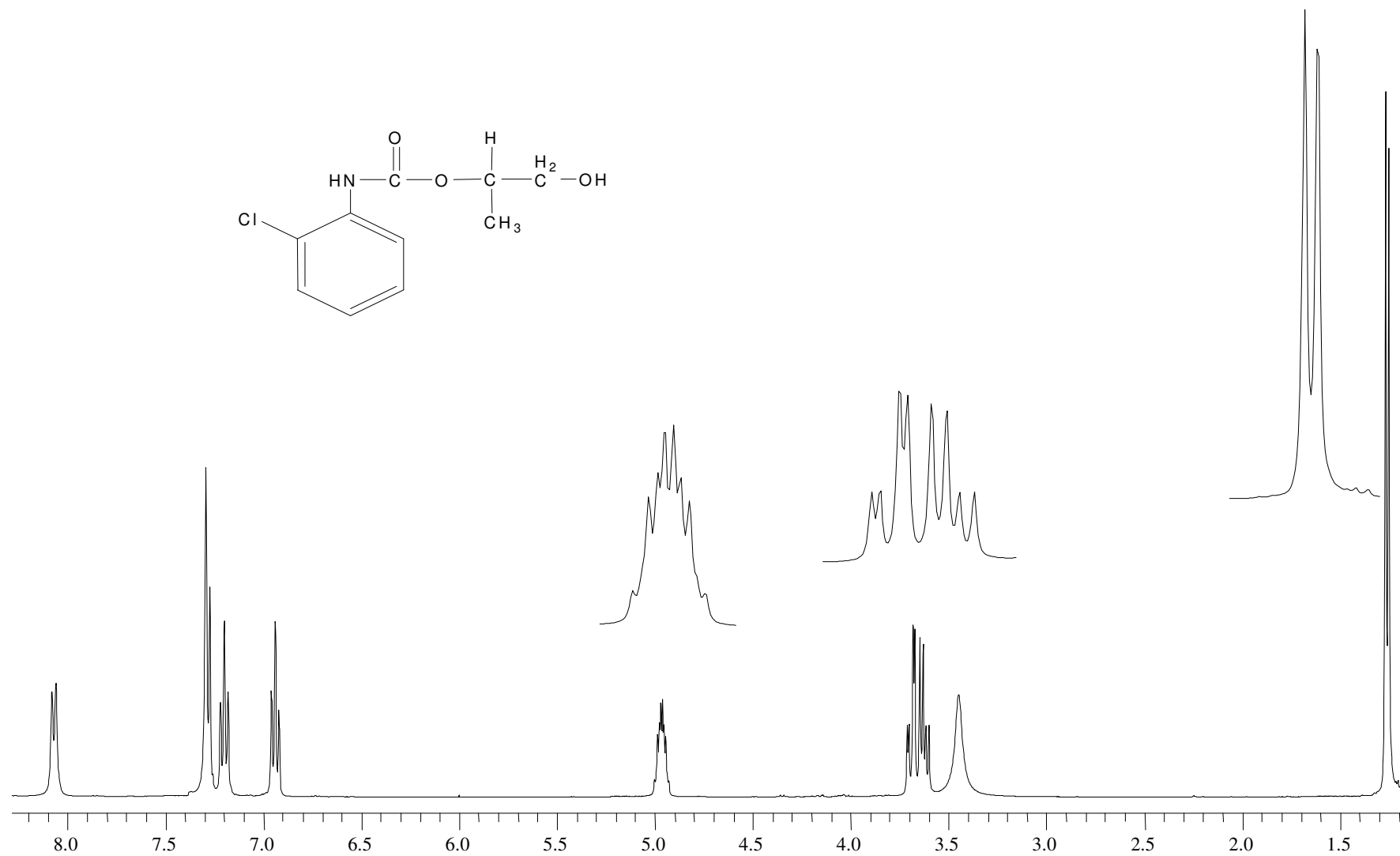


Figure A.31. 400 MHz ^1H NMR spectrum of compound **47** in CDCl_3

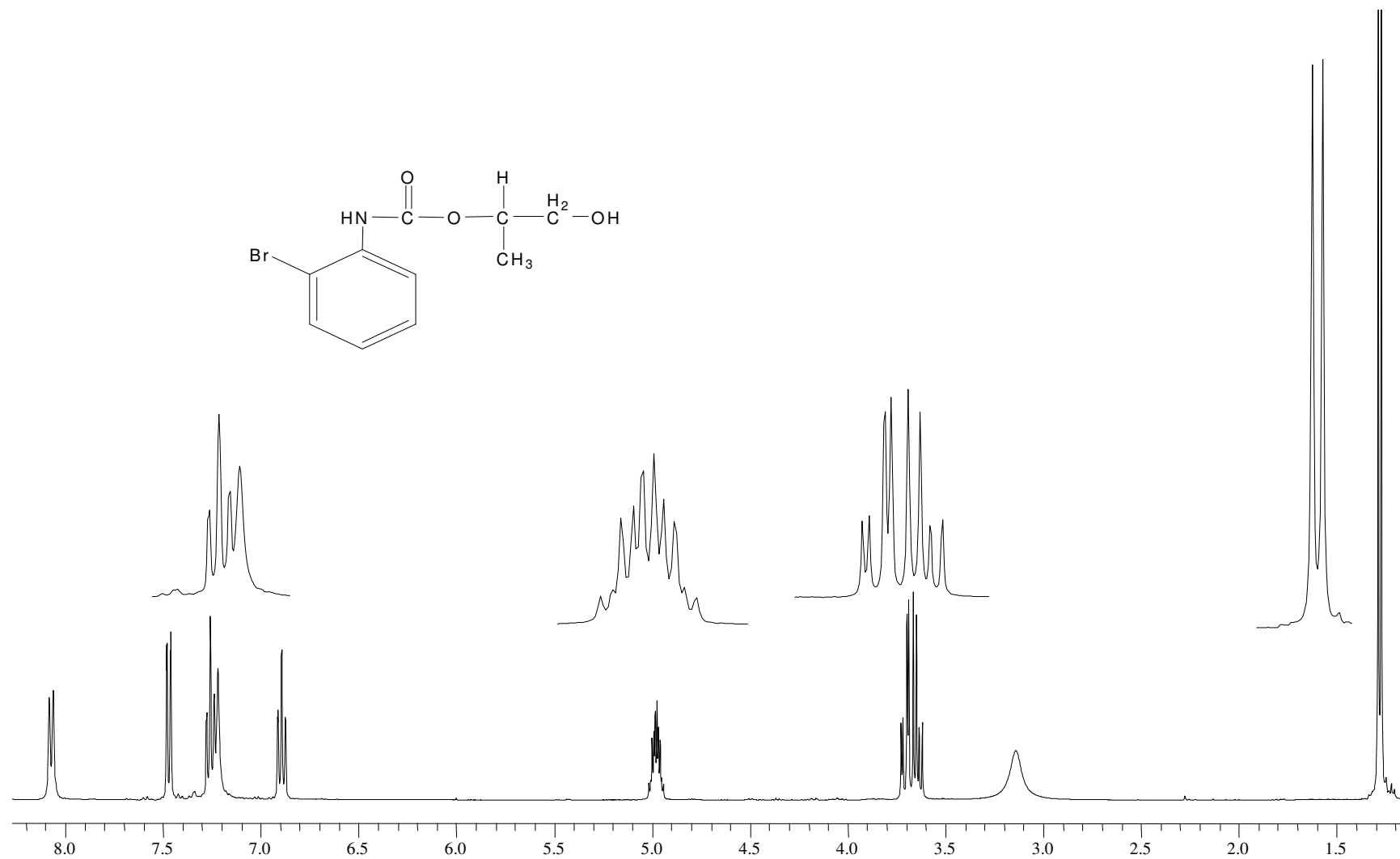


Figure A.32. 400 MHz ¹H NMR spectrum of compound **48** in CDCl₃

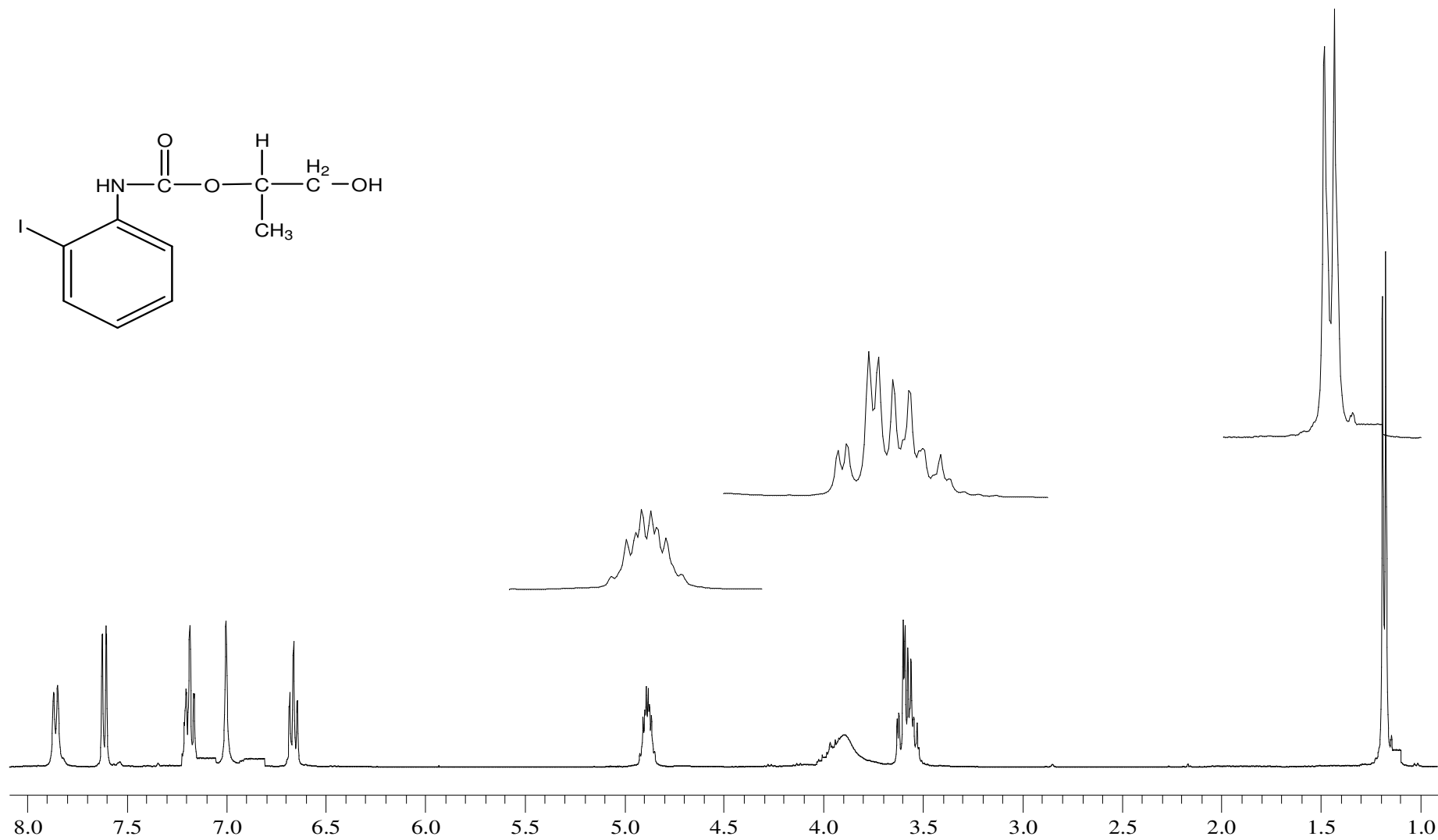
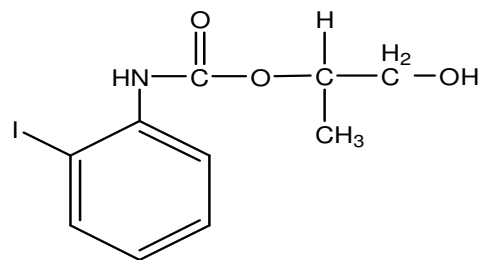


Figure A.33. 400 MHz ^1H NMR spectrum of compound **49** in CDCl_3

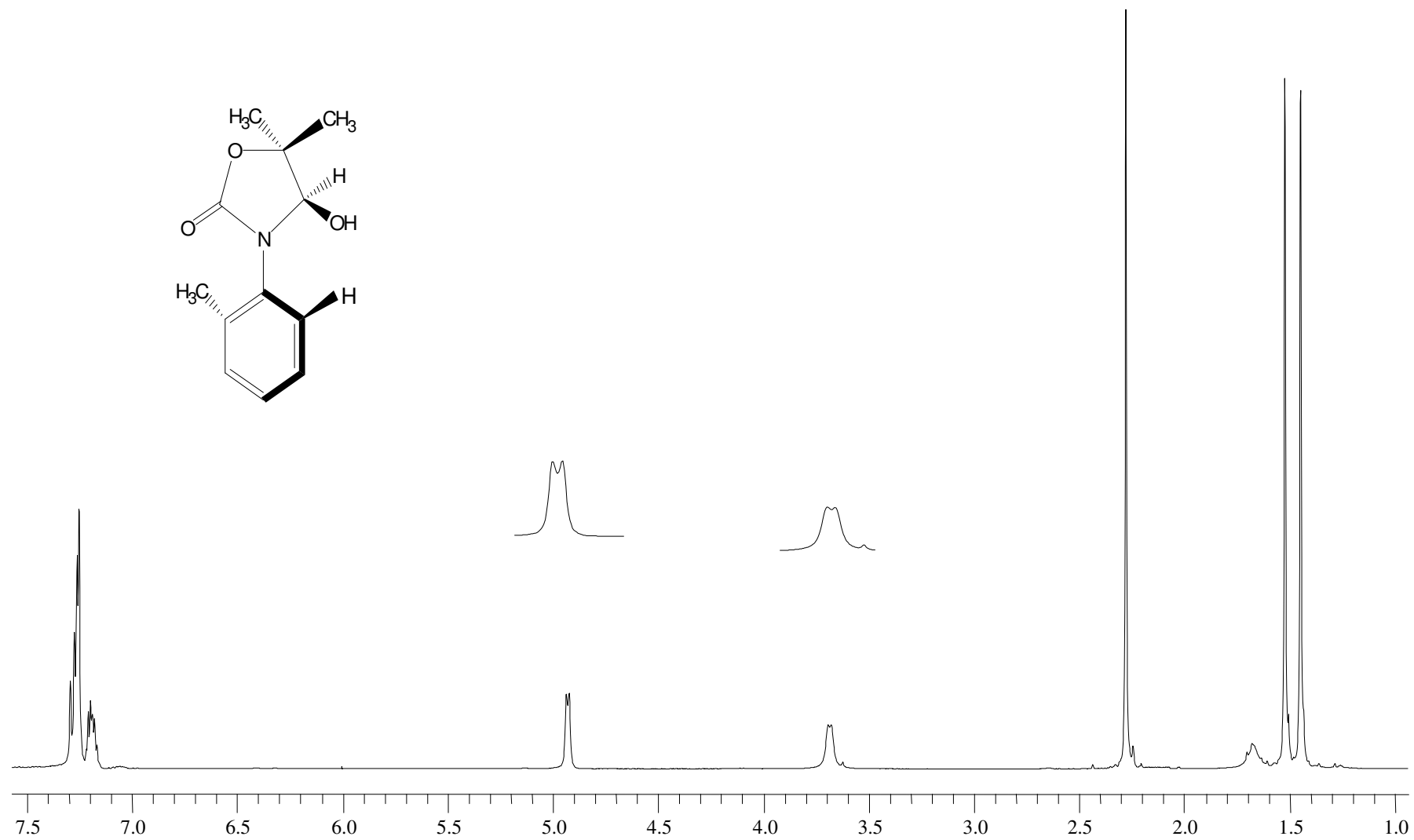


Figure A.34. 400 MHz ¹H NMR spectrum of compound **50** in CDCl₃

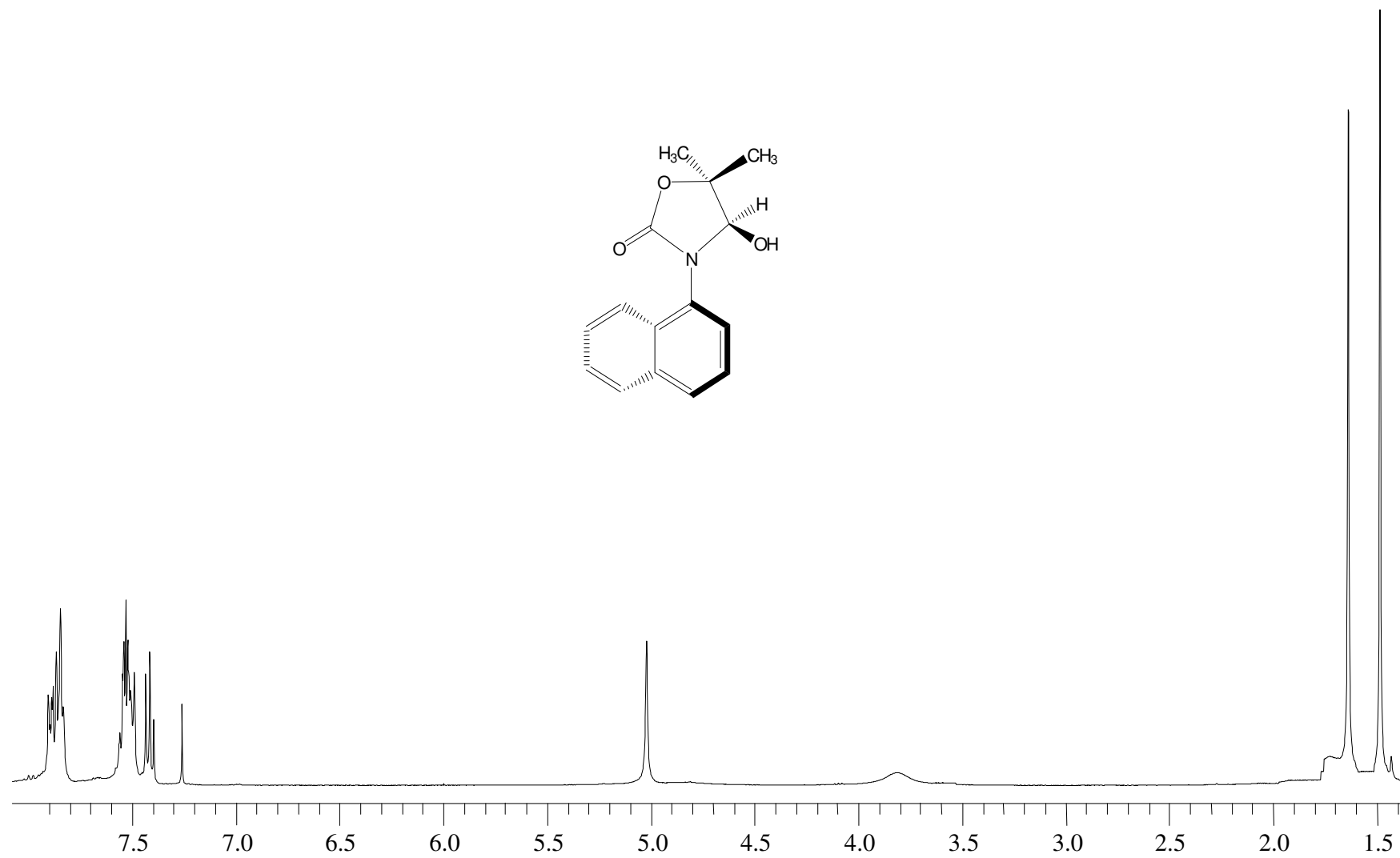


Figure A.35. 400 MHz ¹H NMR spectrum of compound **51** in CDCl₃

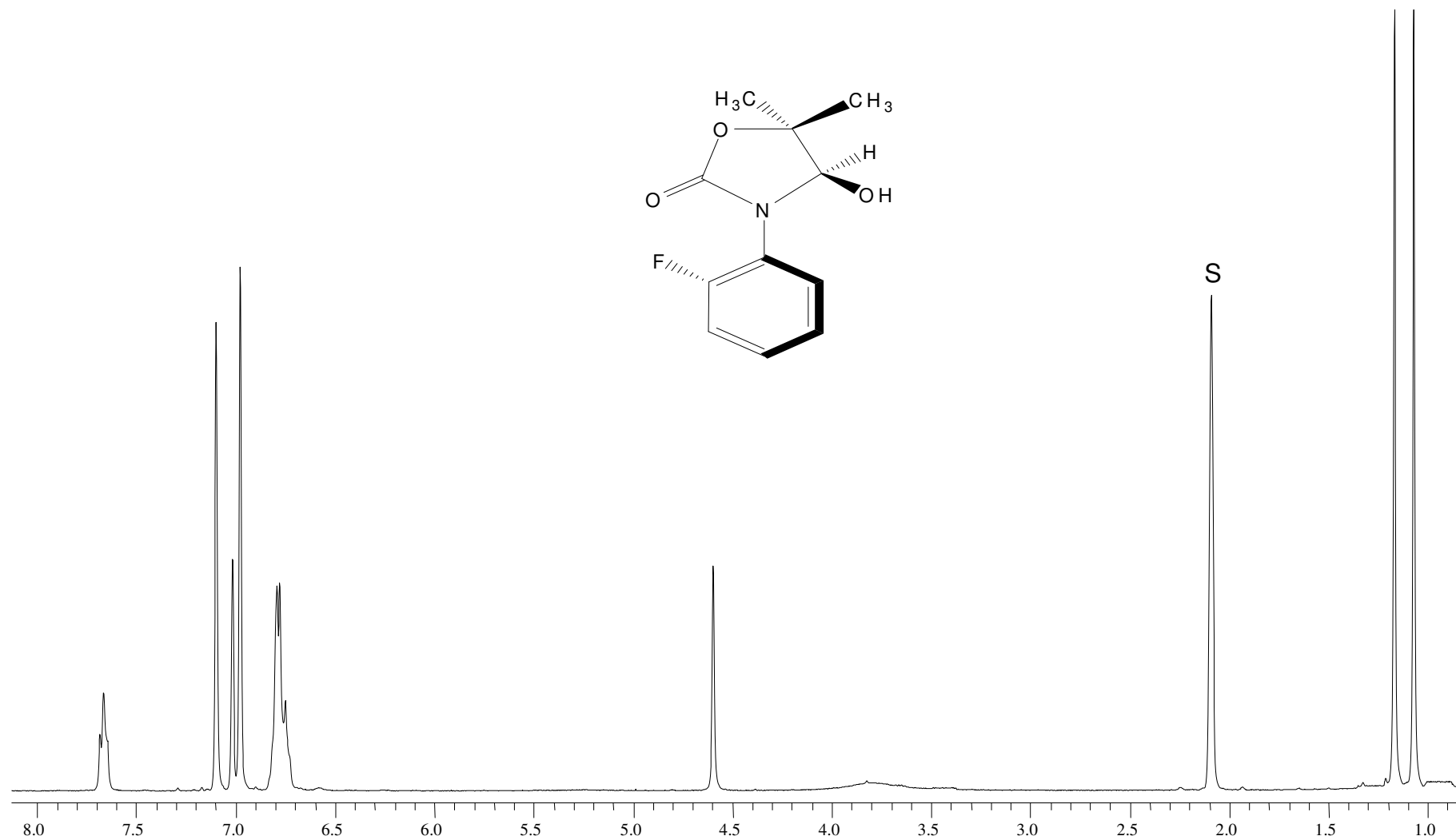


Figure A.36. 400 MHz ^1H NMR spectrum of compound **52** in toluene-d_8 . S:Solvent

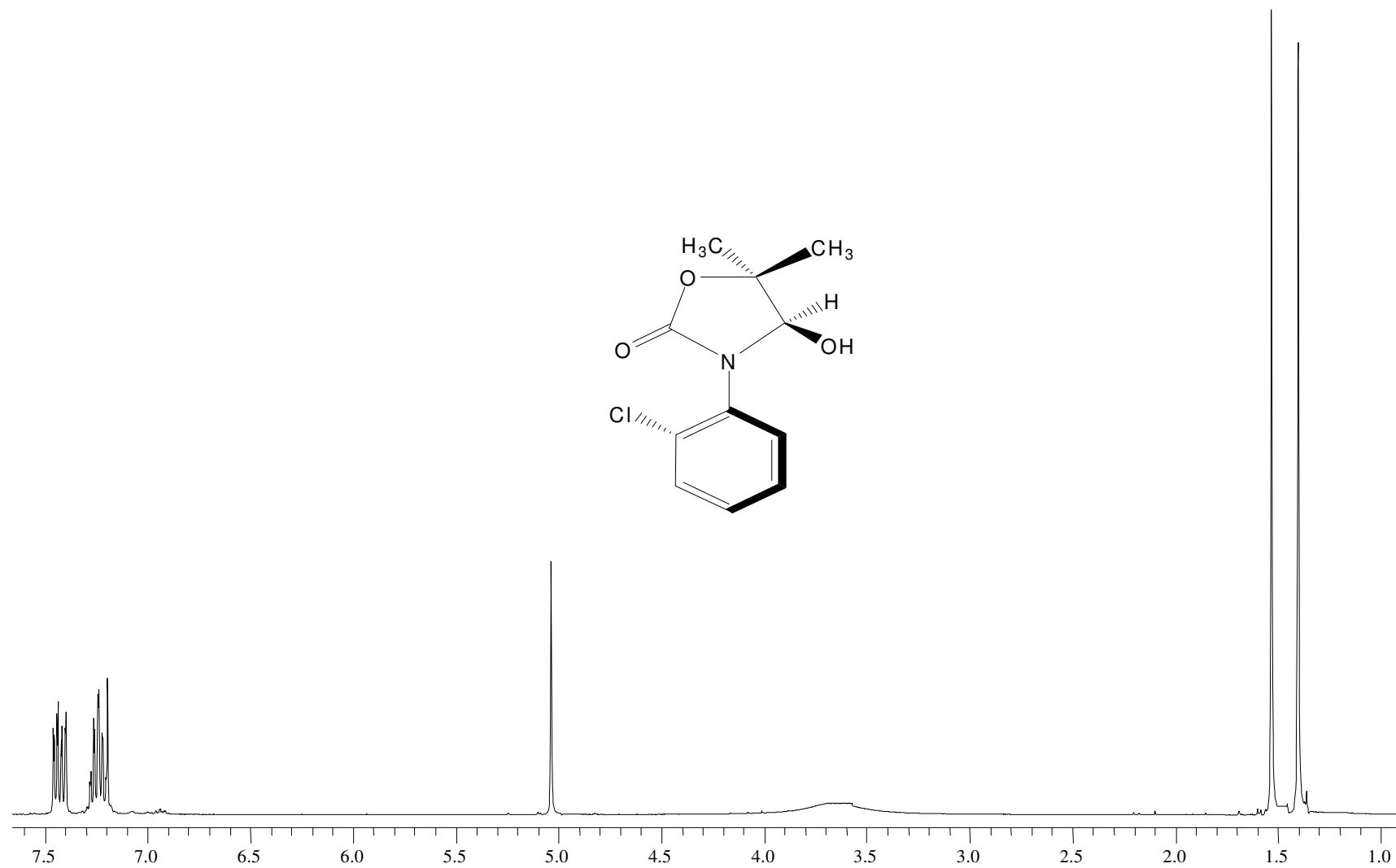


Figure A.37. 400 MHz ^1H NMR spectrum of compound **53** in CDCl_3

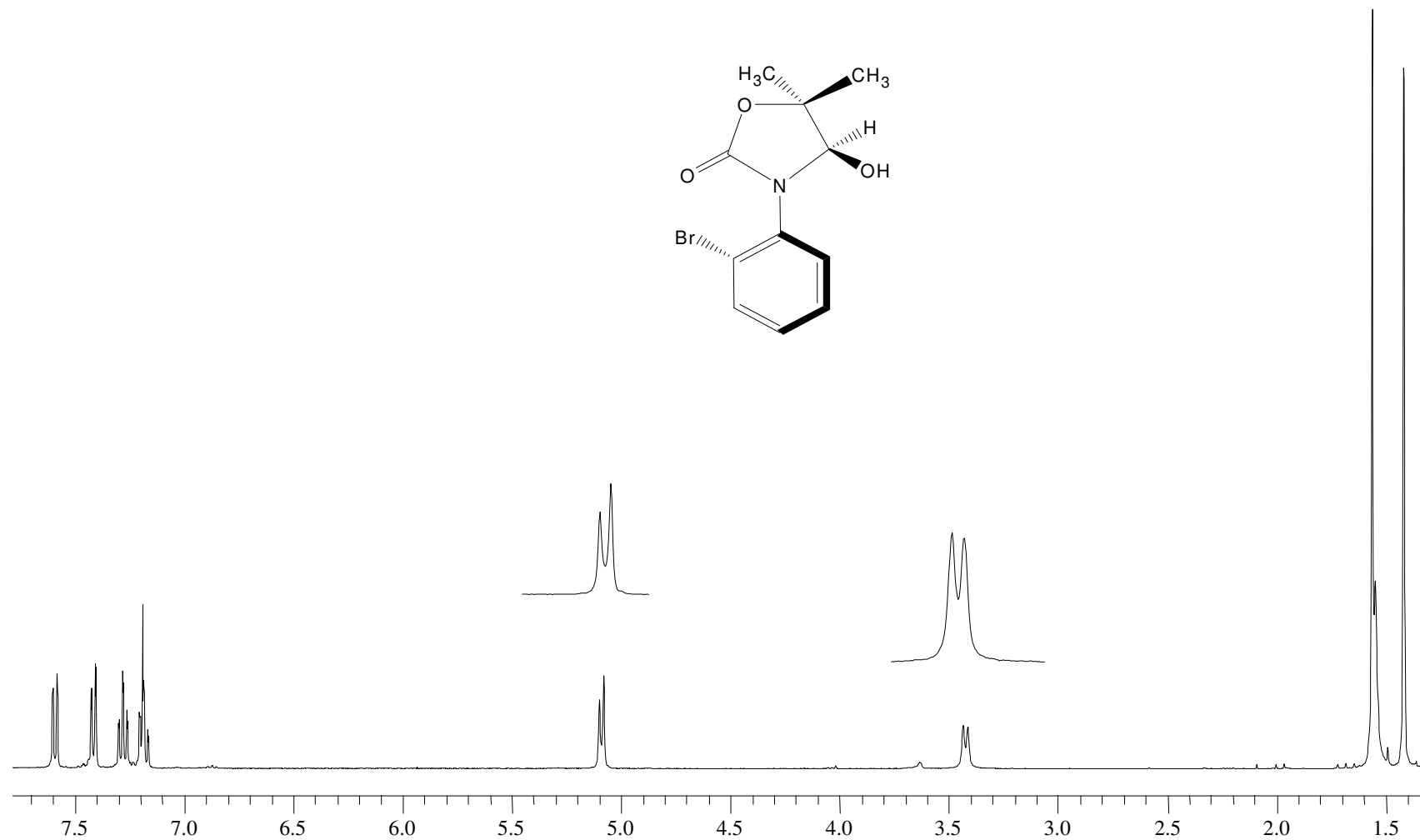


Figure A.38. 400 MHz ^1H NMR spectrum of compound **54** in CDCl_3

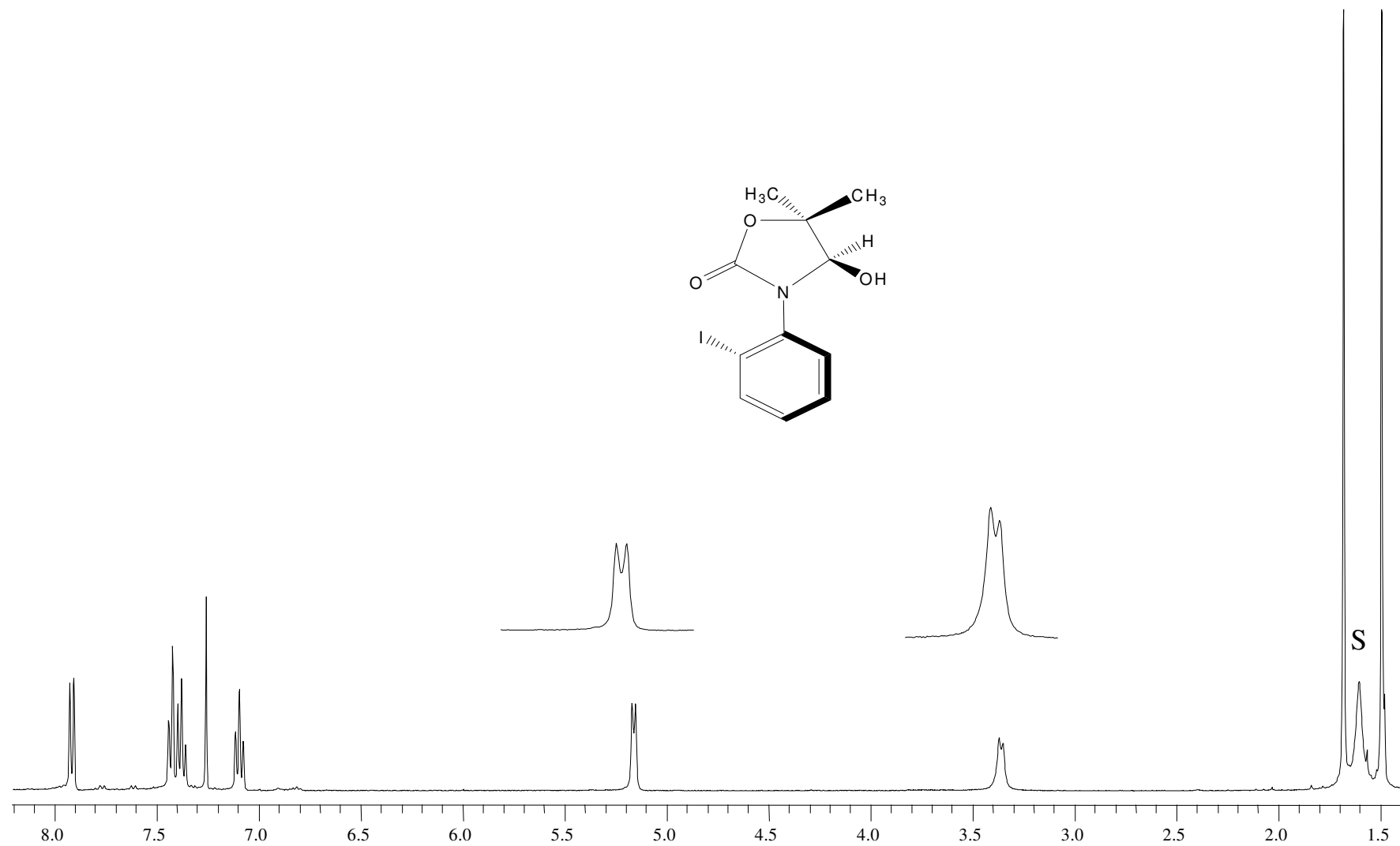


Figure A.39. 400 MHz ¹H NMR spectrum of compound **55** in CDCl₃. S:Solvent

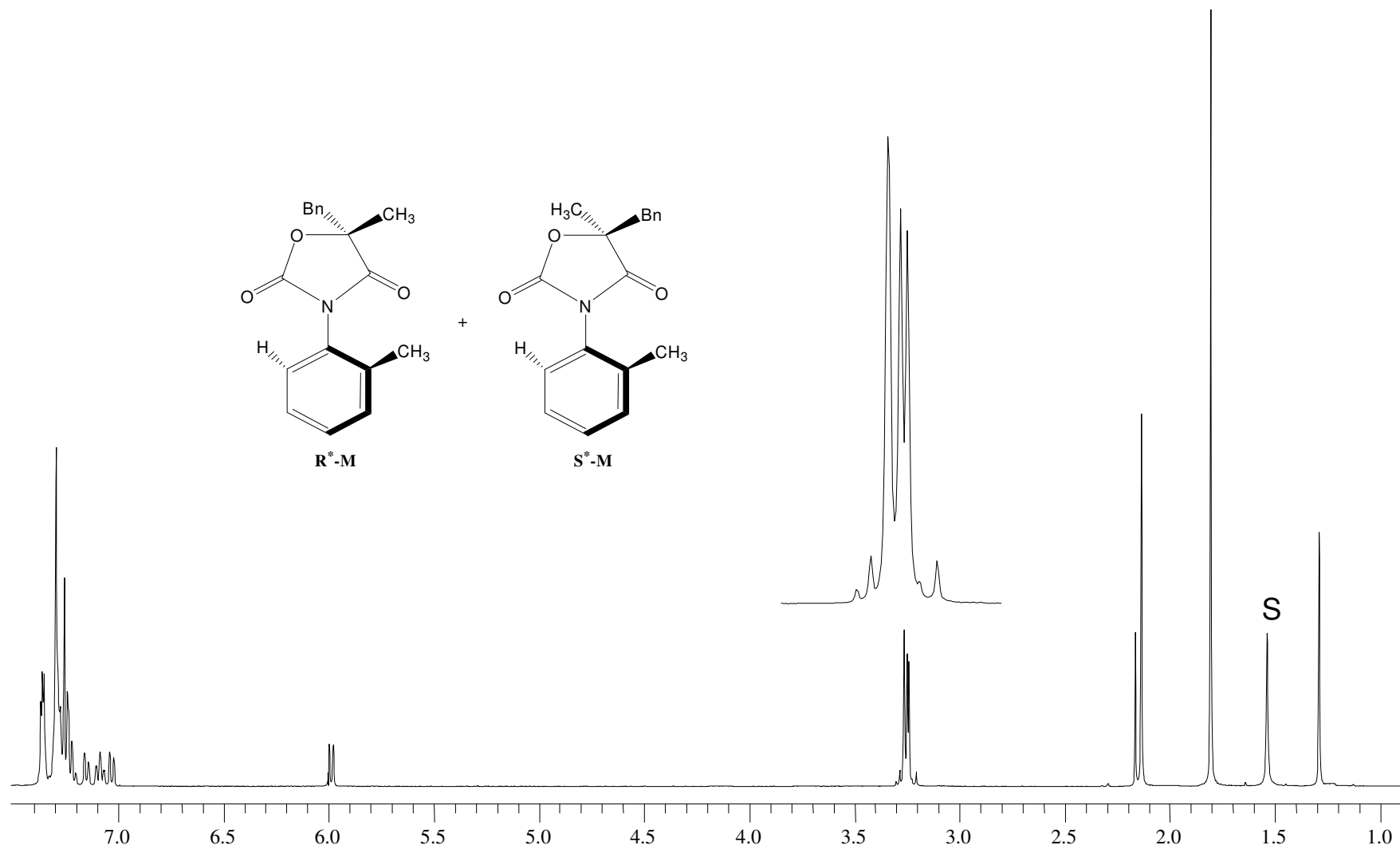


Figure A.40. 400 MHz ¹H NMR spectrum of compound **56** in CDCl₃. S: Solvent

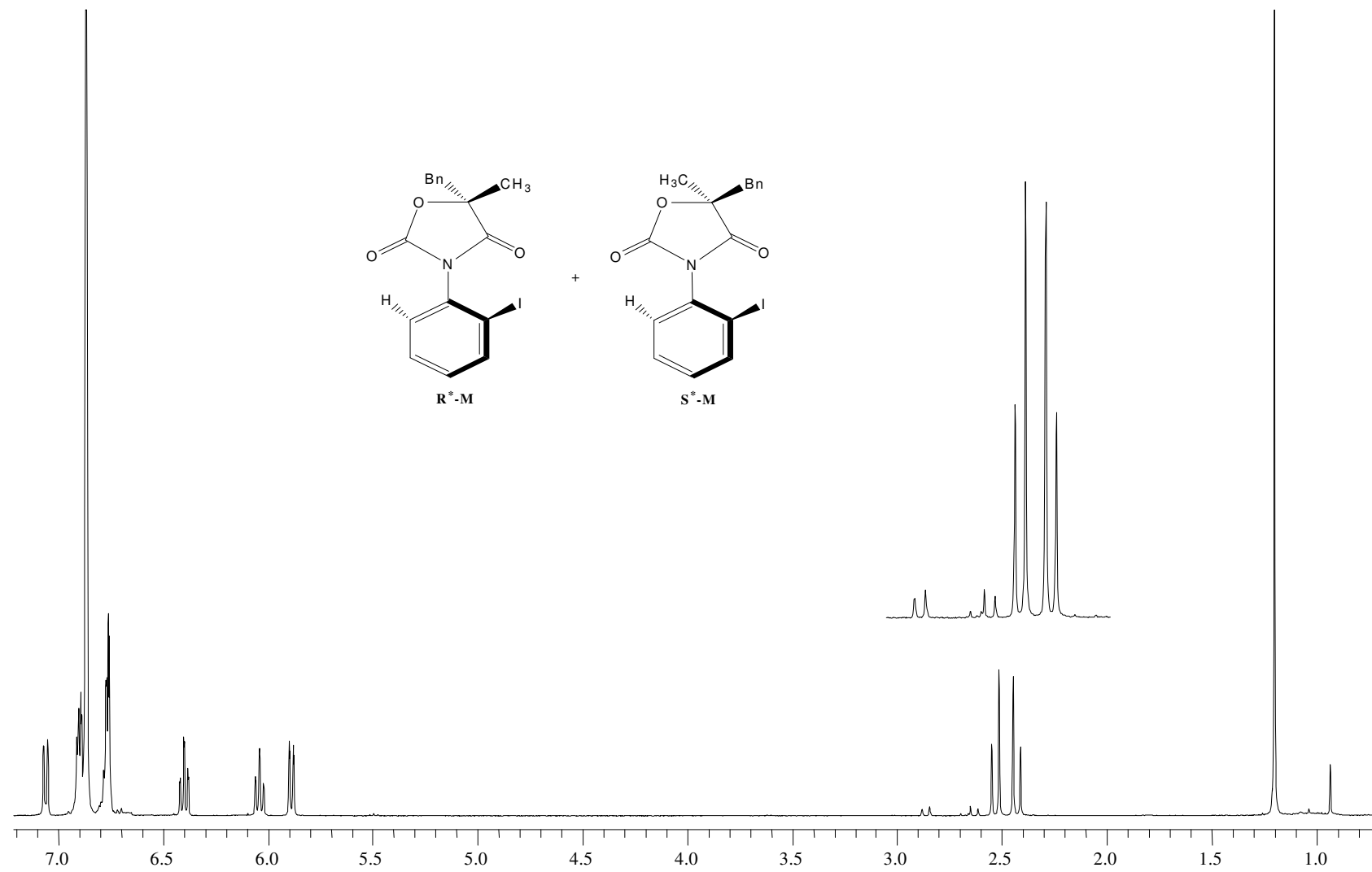


Figure A.41. 400 MHz ¹H NMR spectrum of compound **57** in CDCl₃

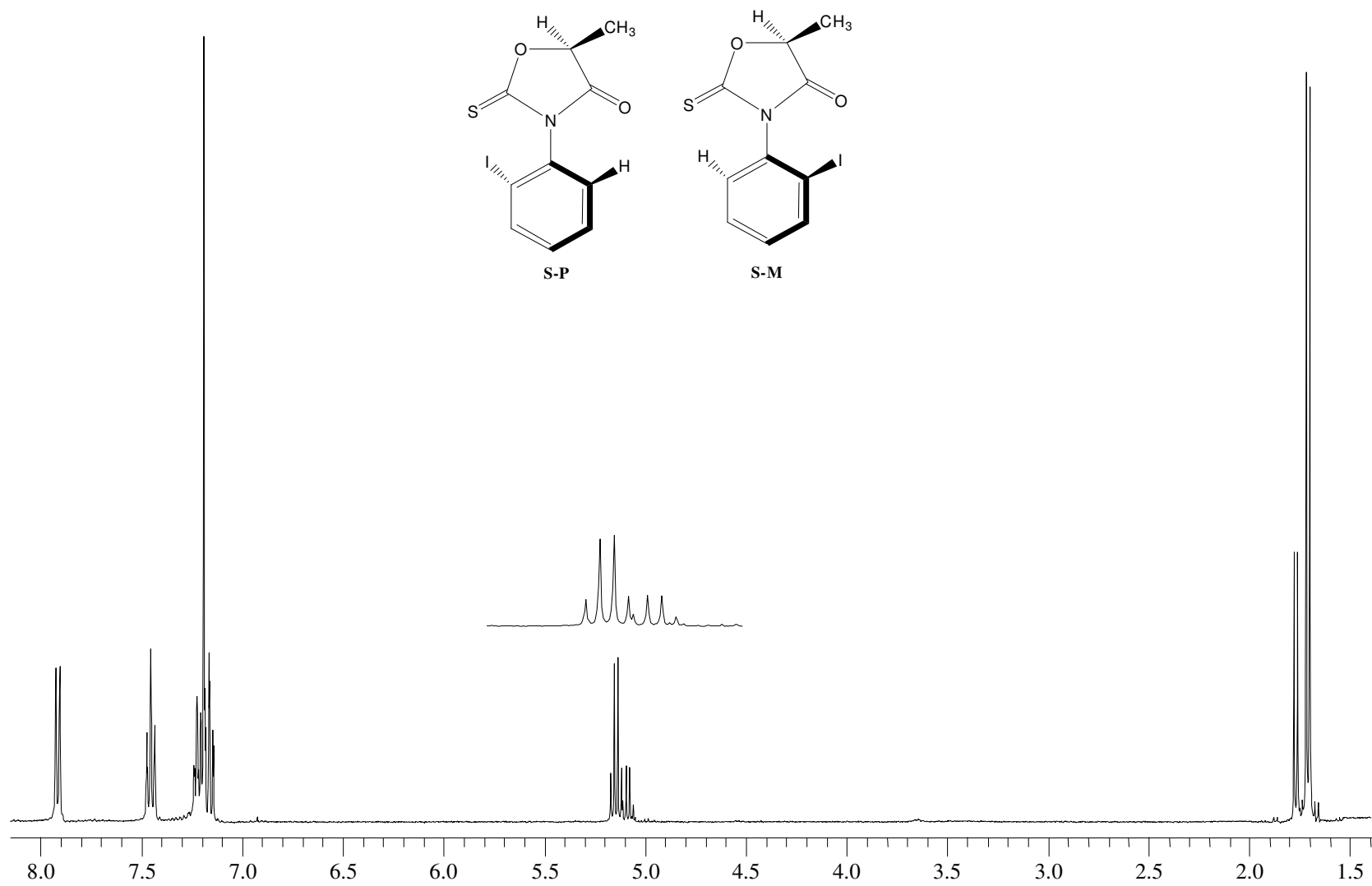


Figure A.42. 400 MHz ^1H NMR spectrum of compound **58** in CDCl_3 (Before equilibrium)

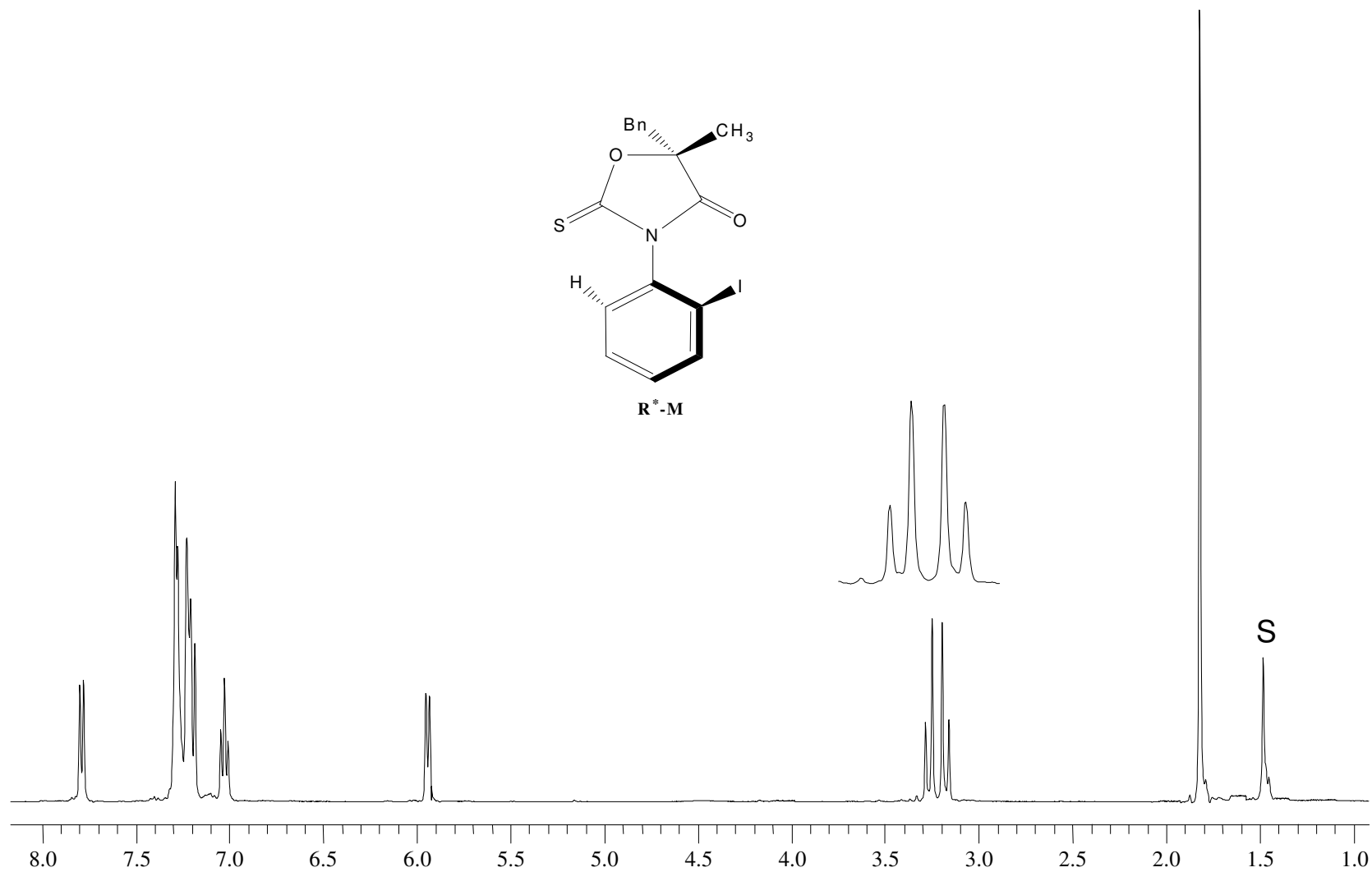


Figure A.43. 400 MHz ¹H NMR spectrum of compound **59** in CDCl₃. S: Solvent

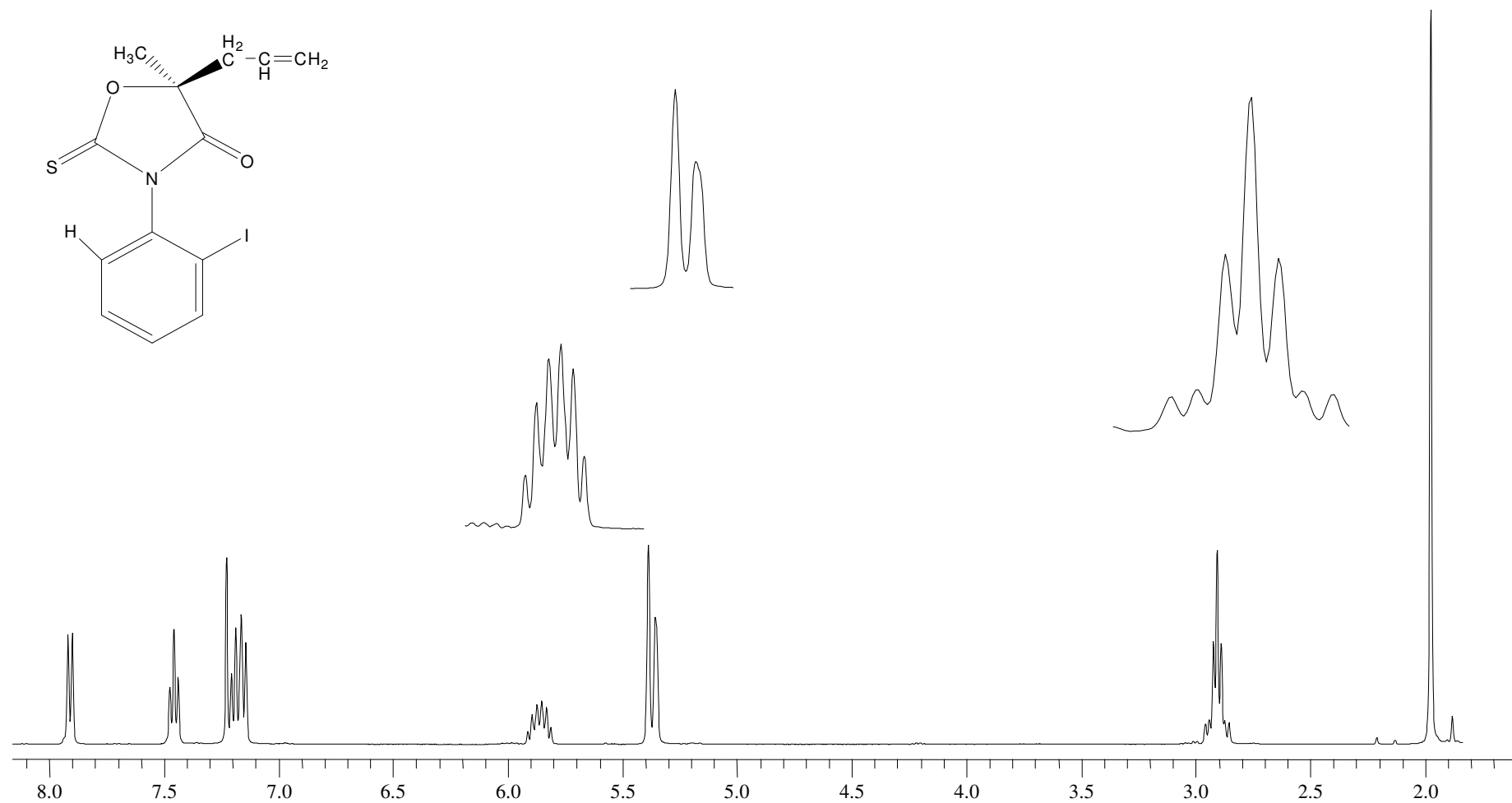


Figure A.44. 400 MHz ^1H NMR spectrum of compound **60** in CDCl_3

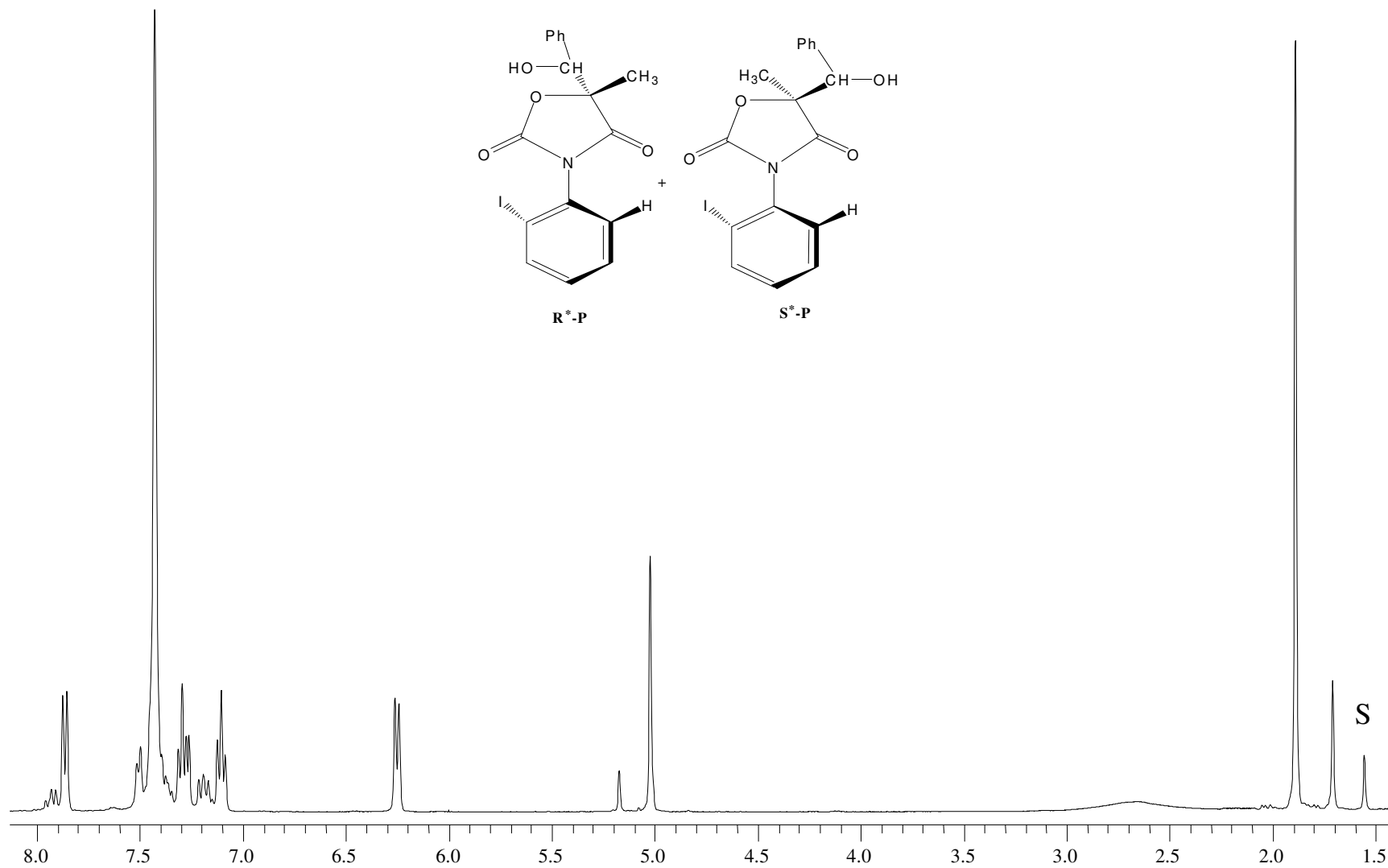


Figure A.45. 400 MHz ^1H NMR spectrum of compound **61** in CDCl_3 . S: Solvent

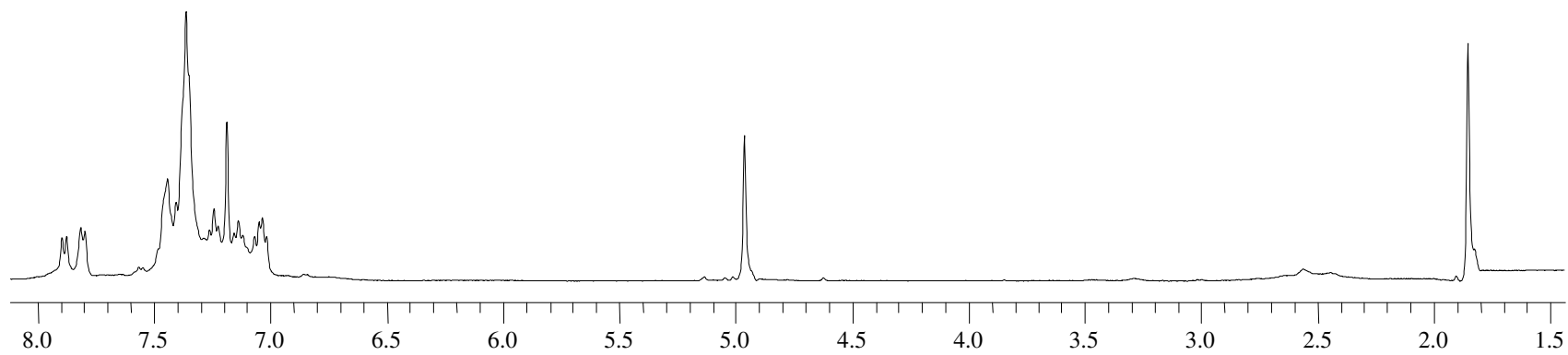
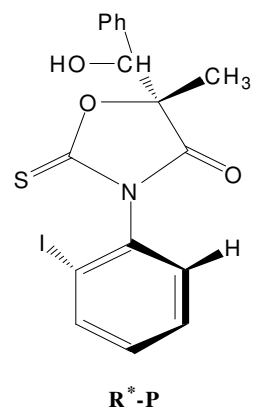


Figure A.46. 400 MHz ¹H NMR spectrum of compound **62** in CDCl₃

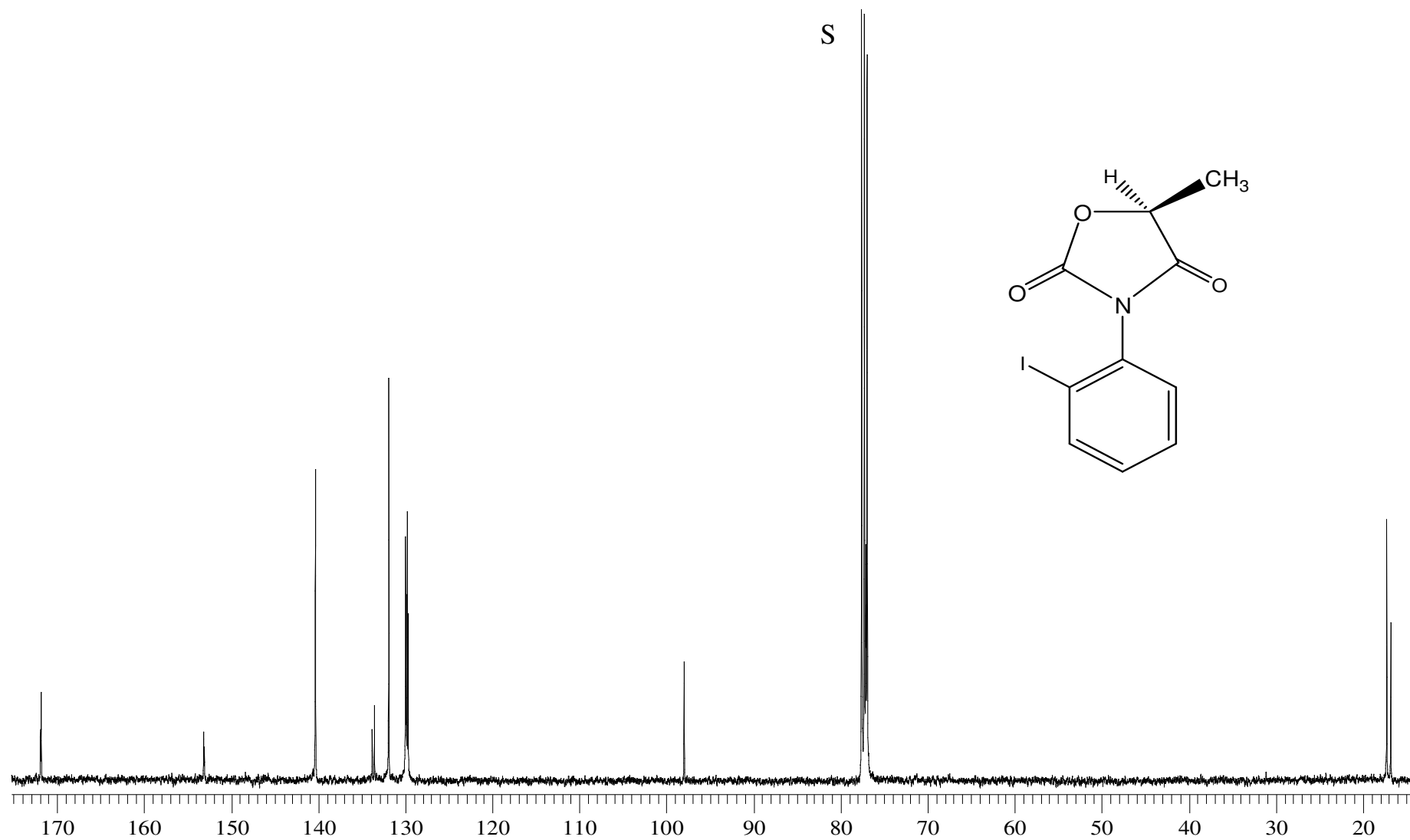


Figure A.47. 100 MHz ^{13}C NMR spectrum of compound **3** in CDCl_3 . S: Solvent

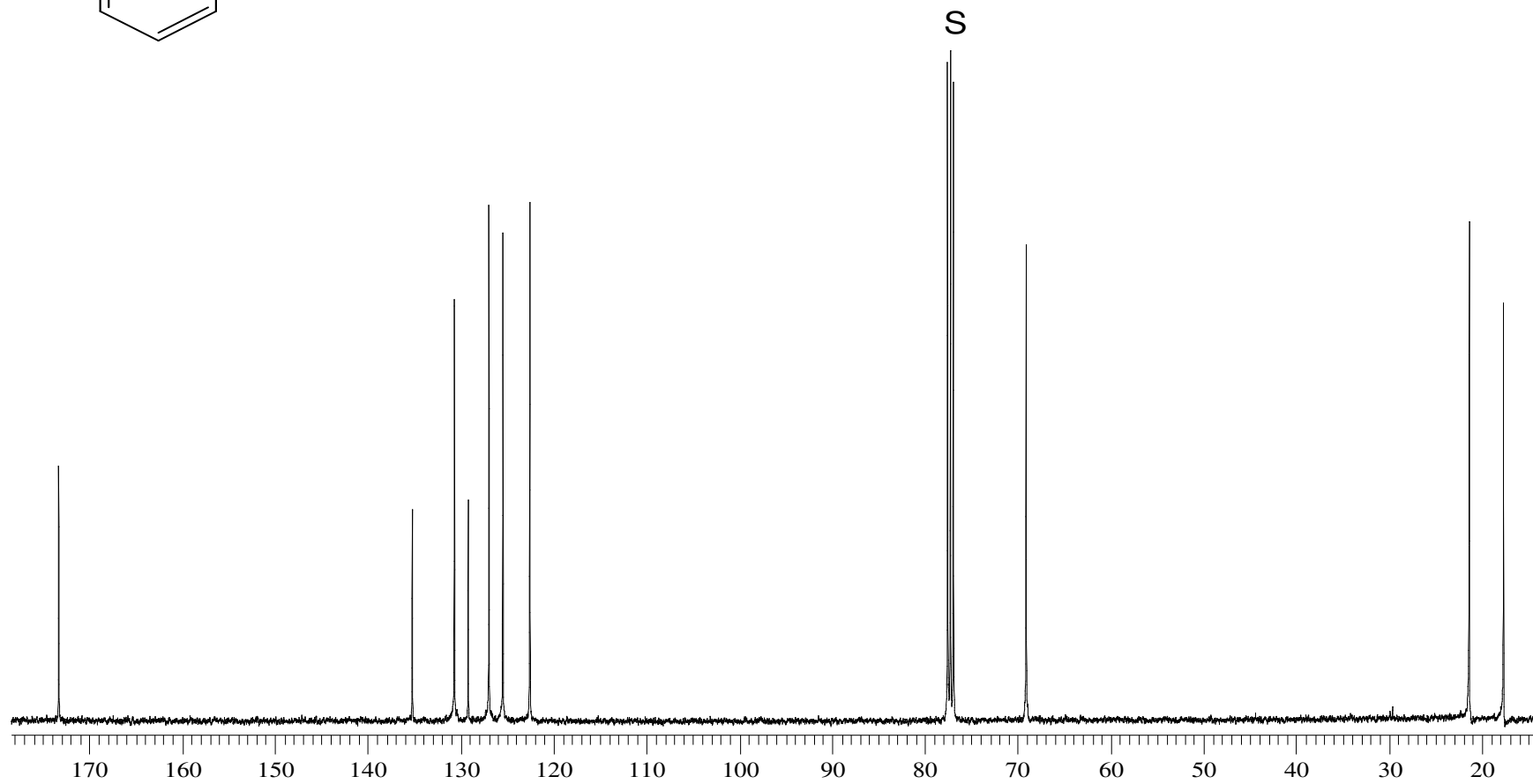
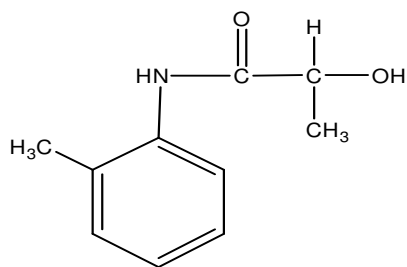


Figure A.48. 100 MHz ¹³C NMR spectrum of compound **20** in CDCl₃. S: Solvent

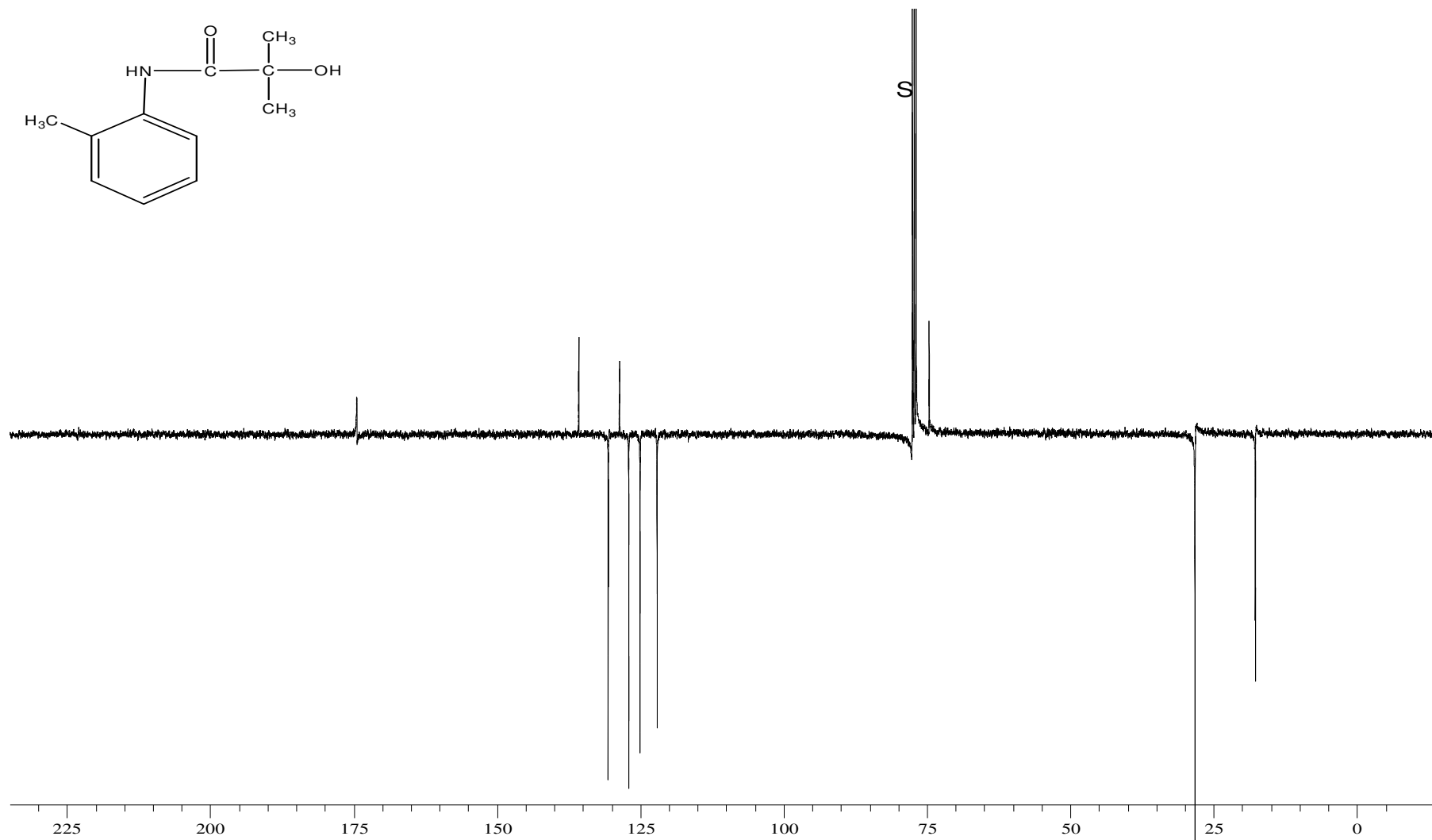
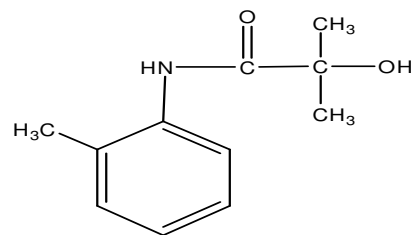


Figure A.49. 100 MHz ¹³C NMR spectrum of compound **26** in CDCl₃. S: Solvent

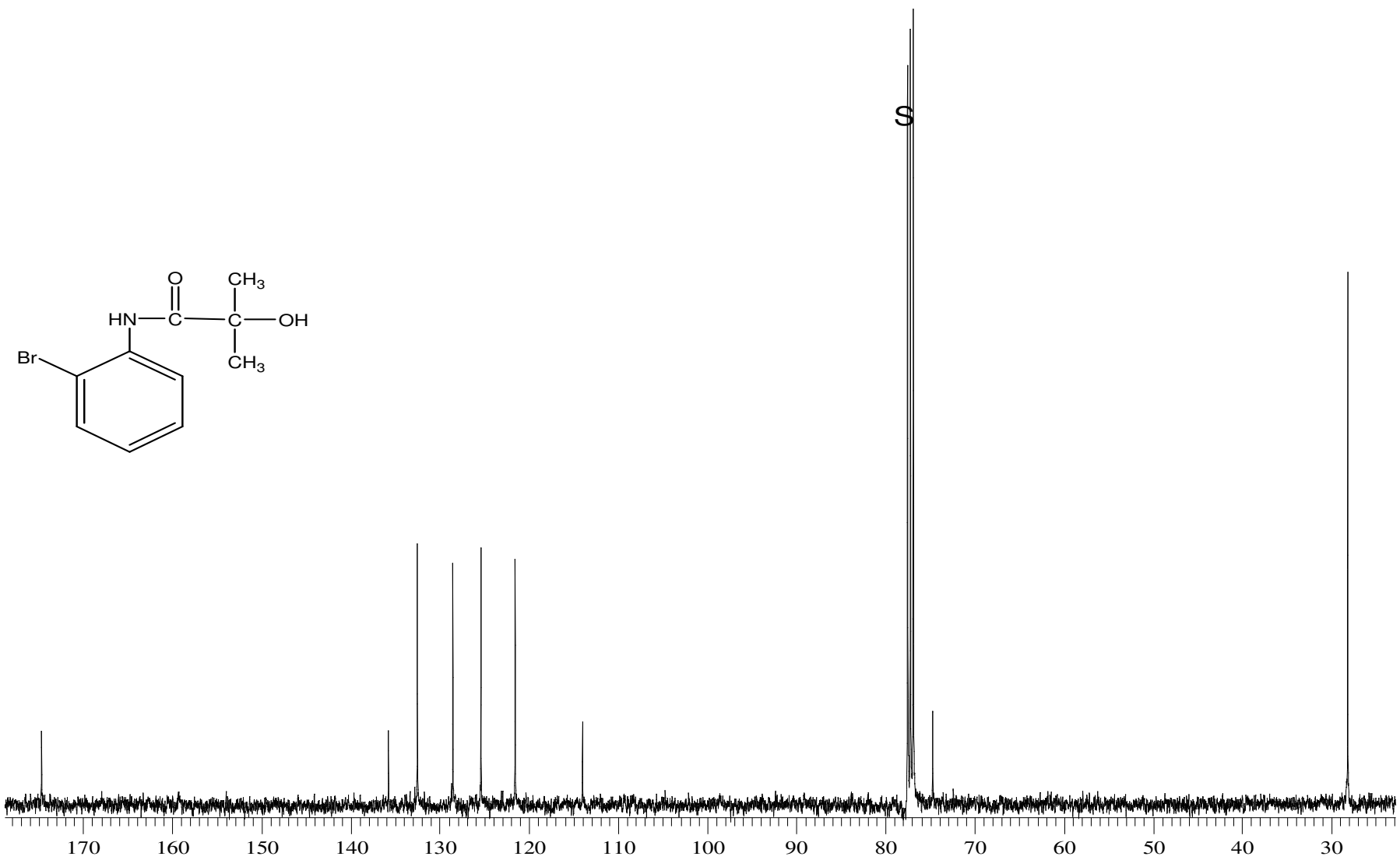


Figure A.50. 100 MHz ¹³C NMR spectrum of compound **30** in CDCl₃. S: Solvent

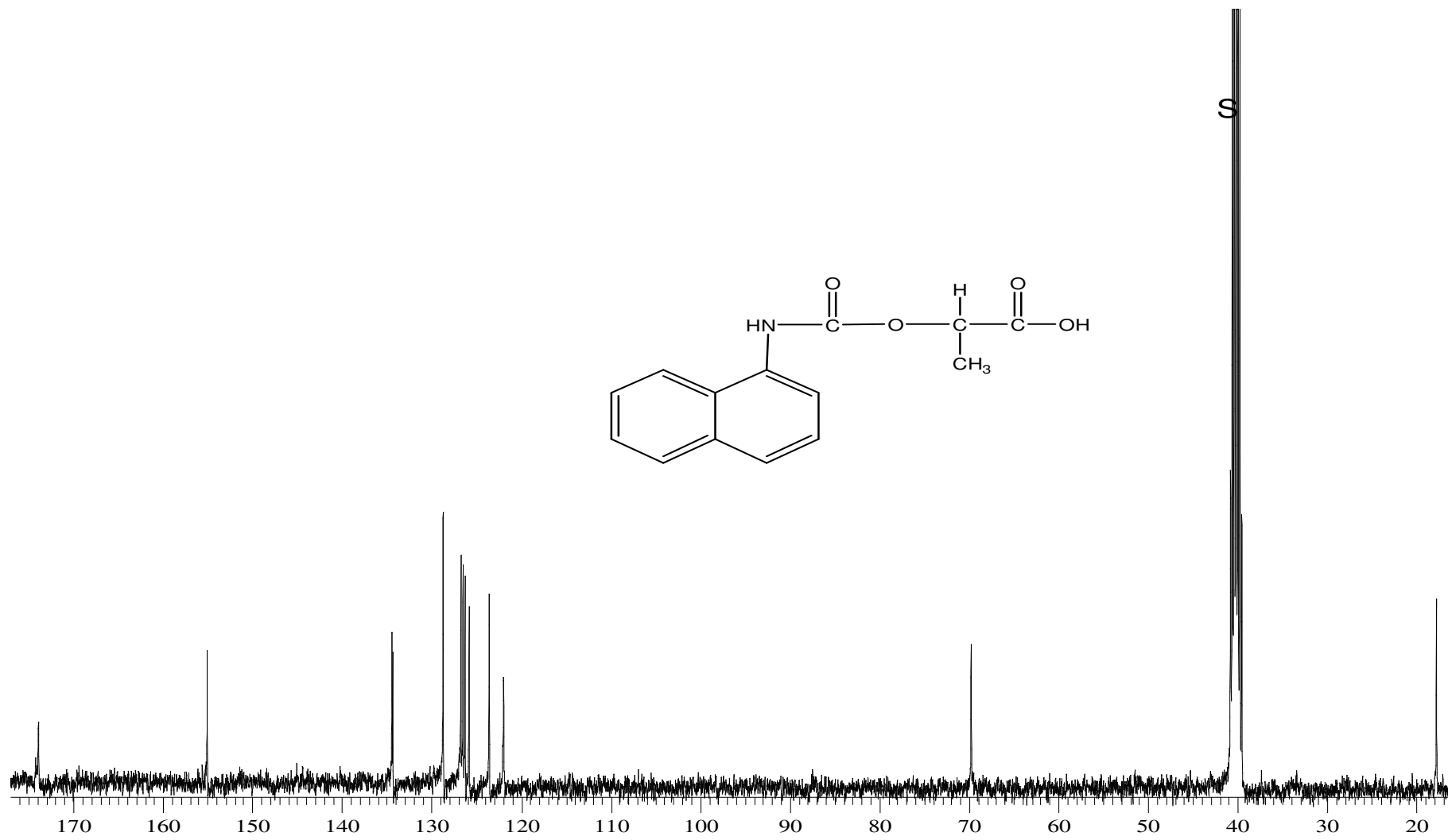


Figure A.51. 100 MHz ¹³C NMR spectrum of compound **33** in CDCl₃. S: Solvent

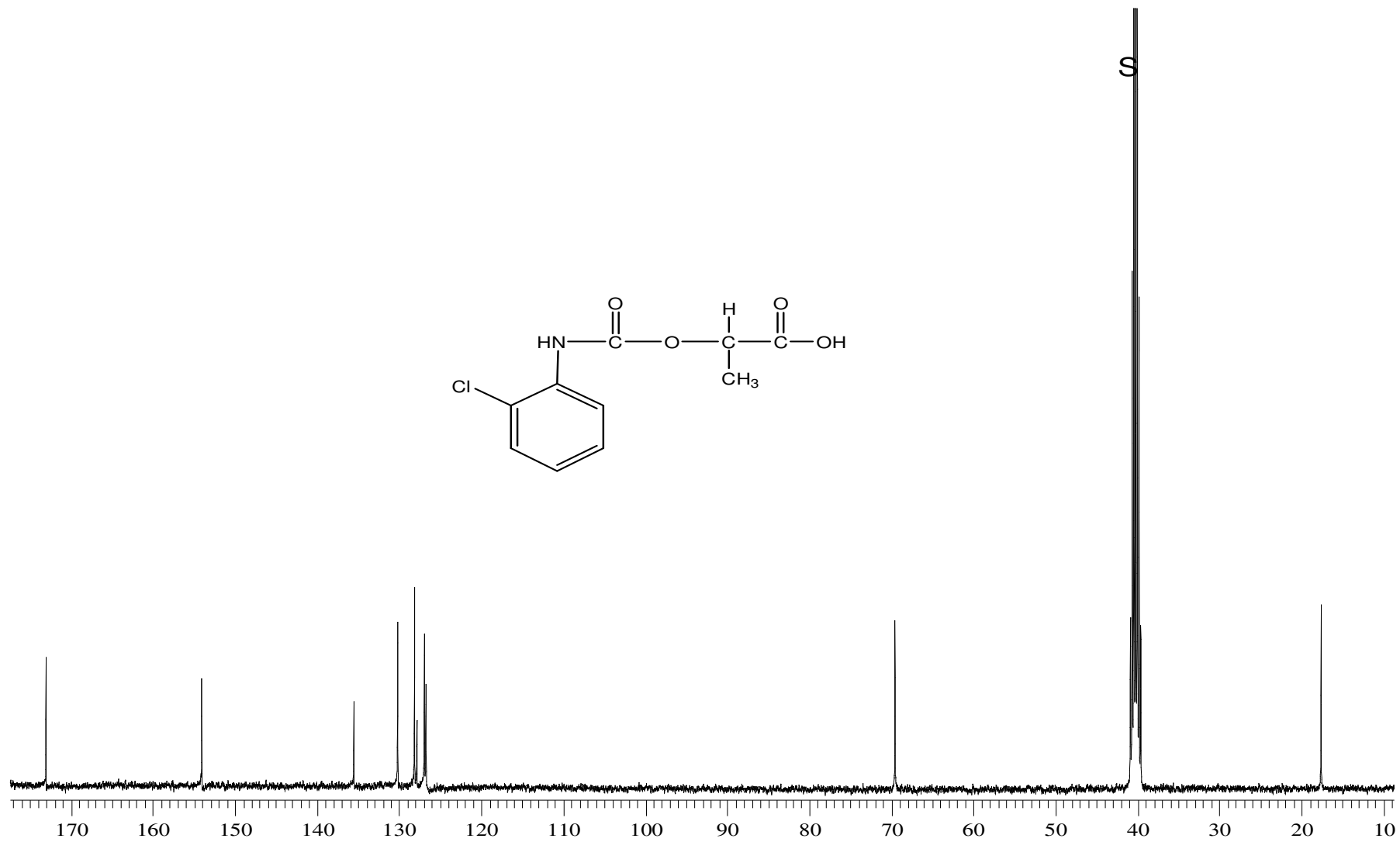


Figure A.52. 100 MHz ^{13}C NMR spectrum of compound **35** in CDCl_3 . S: Solvent

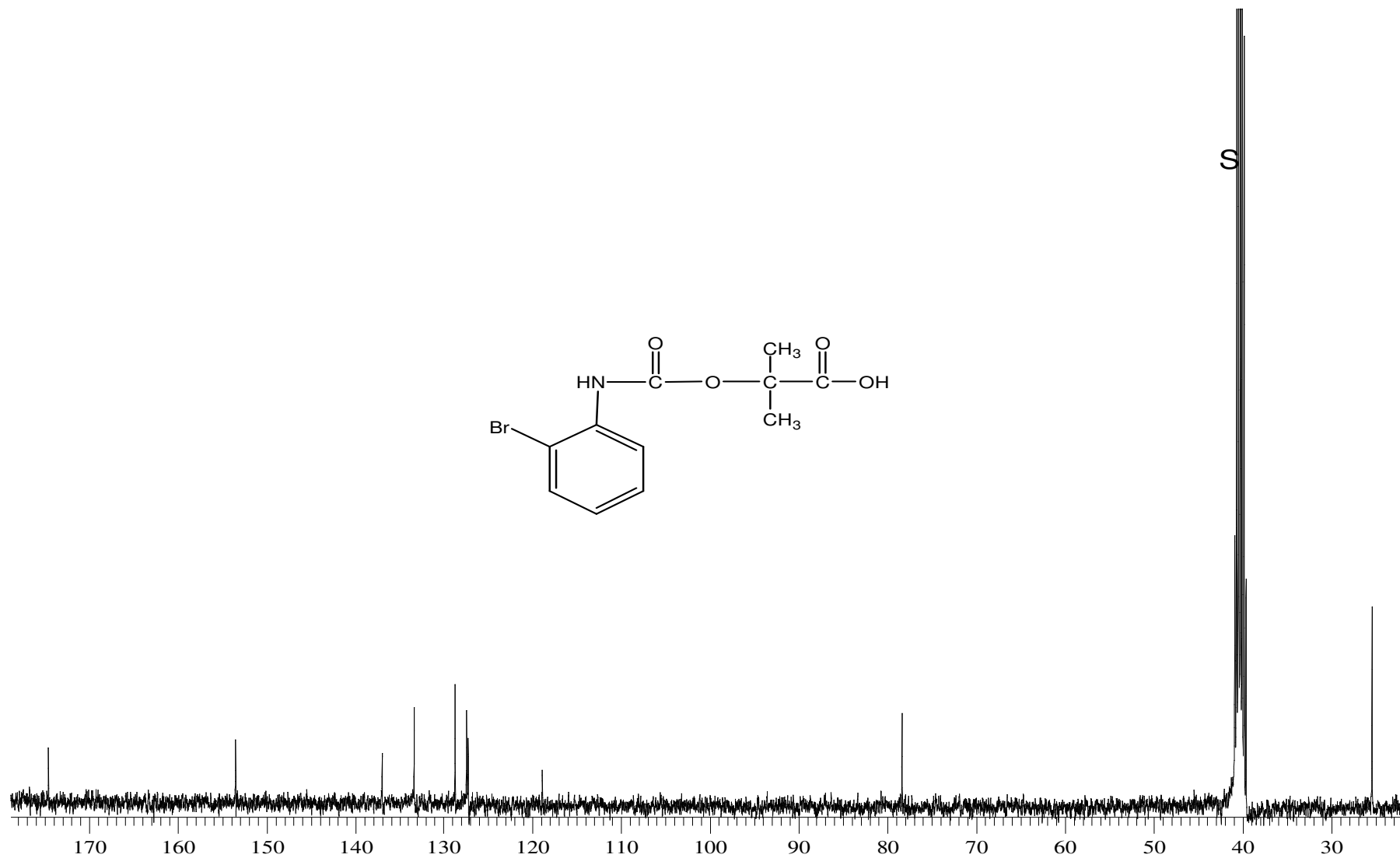


Figure A.53. 100 MHz ^{13}C NMR spectrum of compound **42** in CDCl_3 . S: Solvent

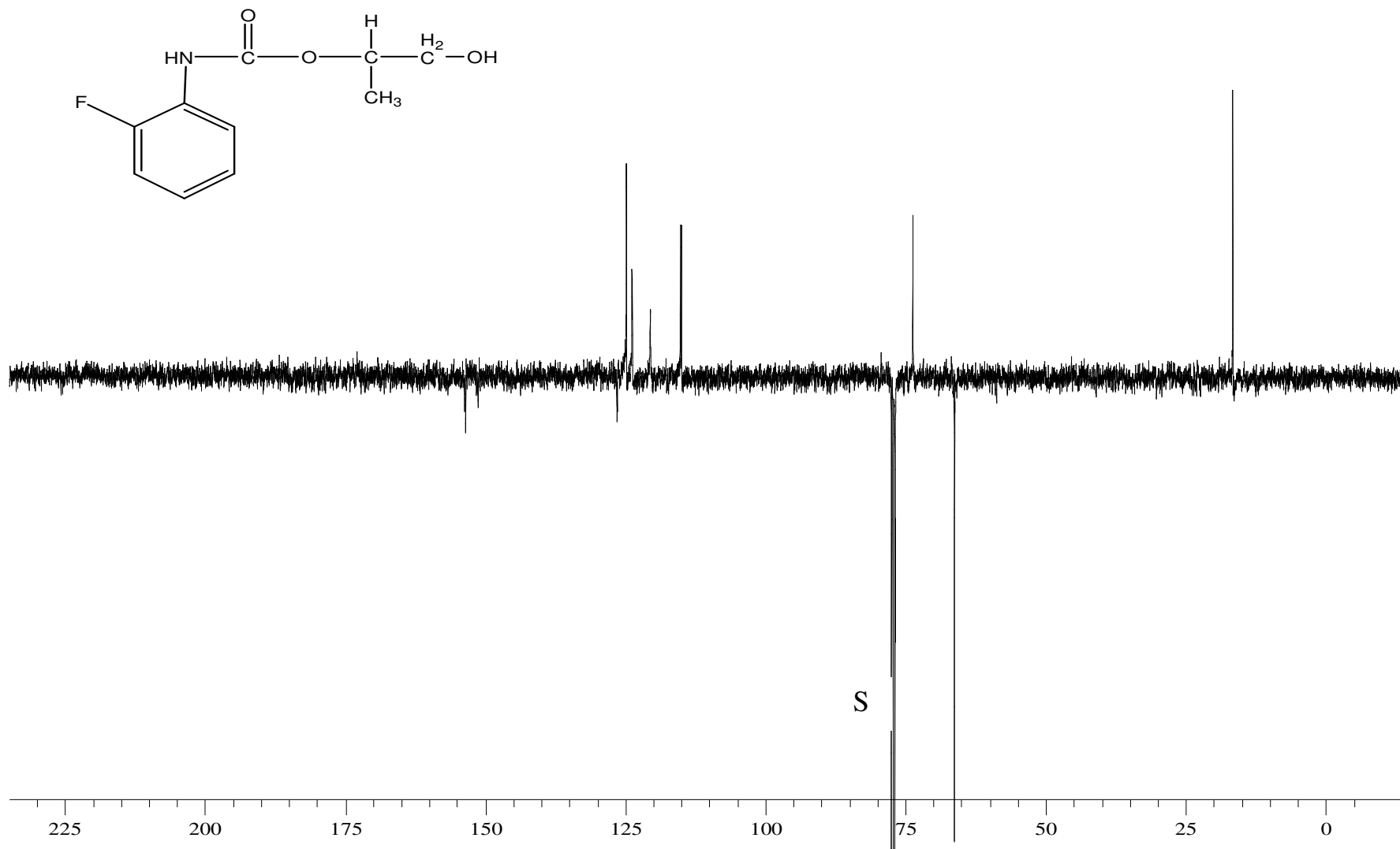


Figure A.54. 100 MHz ¹³C NMR spectrum of compound (±)46 in CDCl₃. S: Solvent

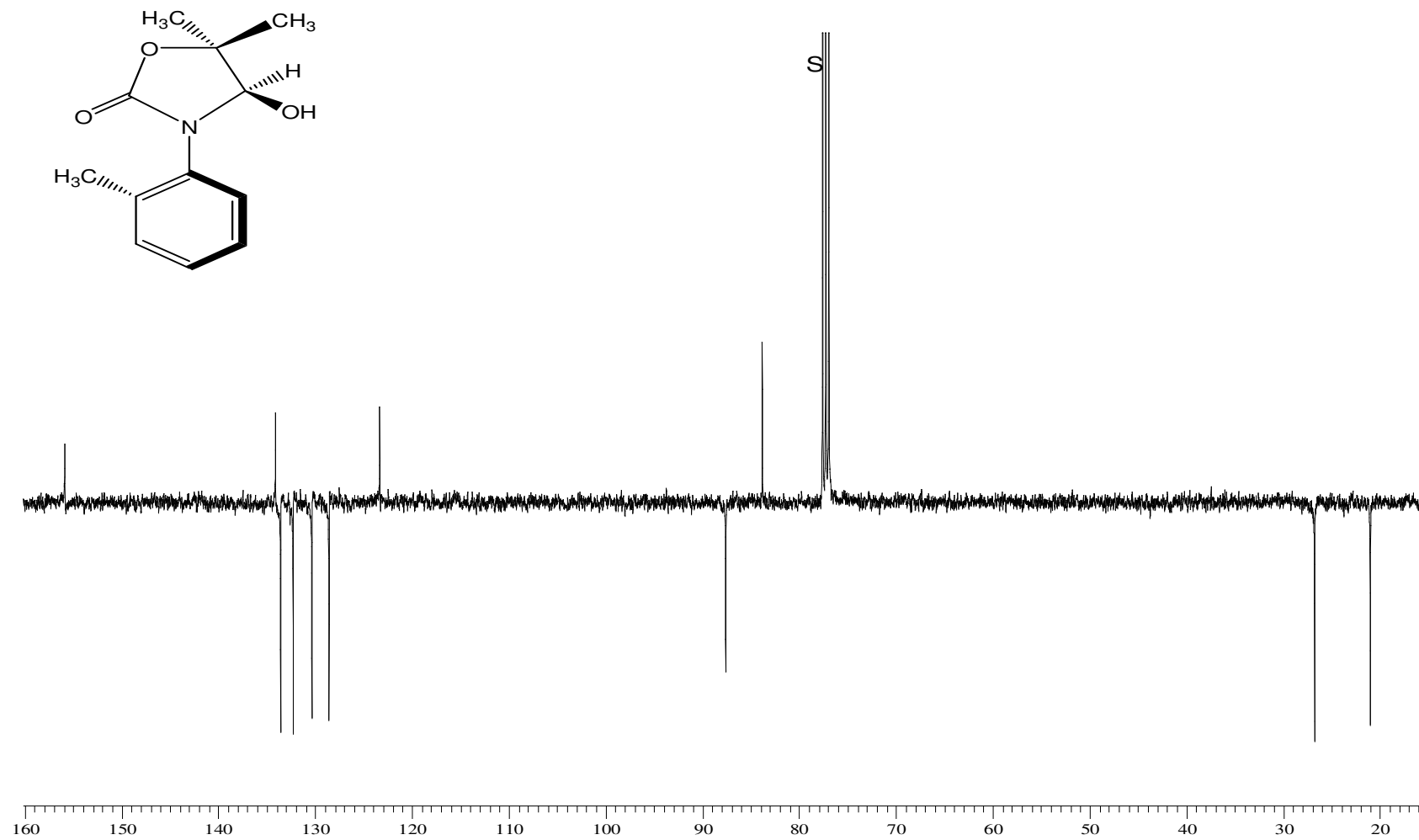


Figure A.55. 100 MHz ^{13}C NMR spectrum of compound **50** in CDCl_3 . S: Solvent

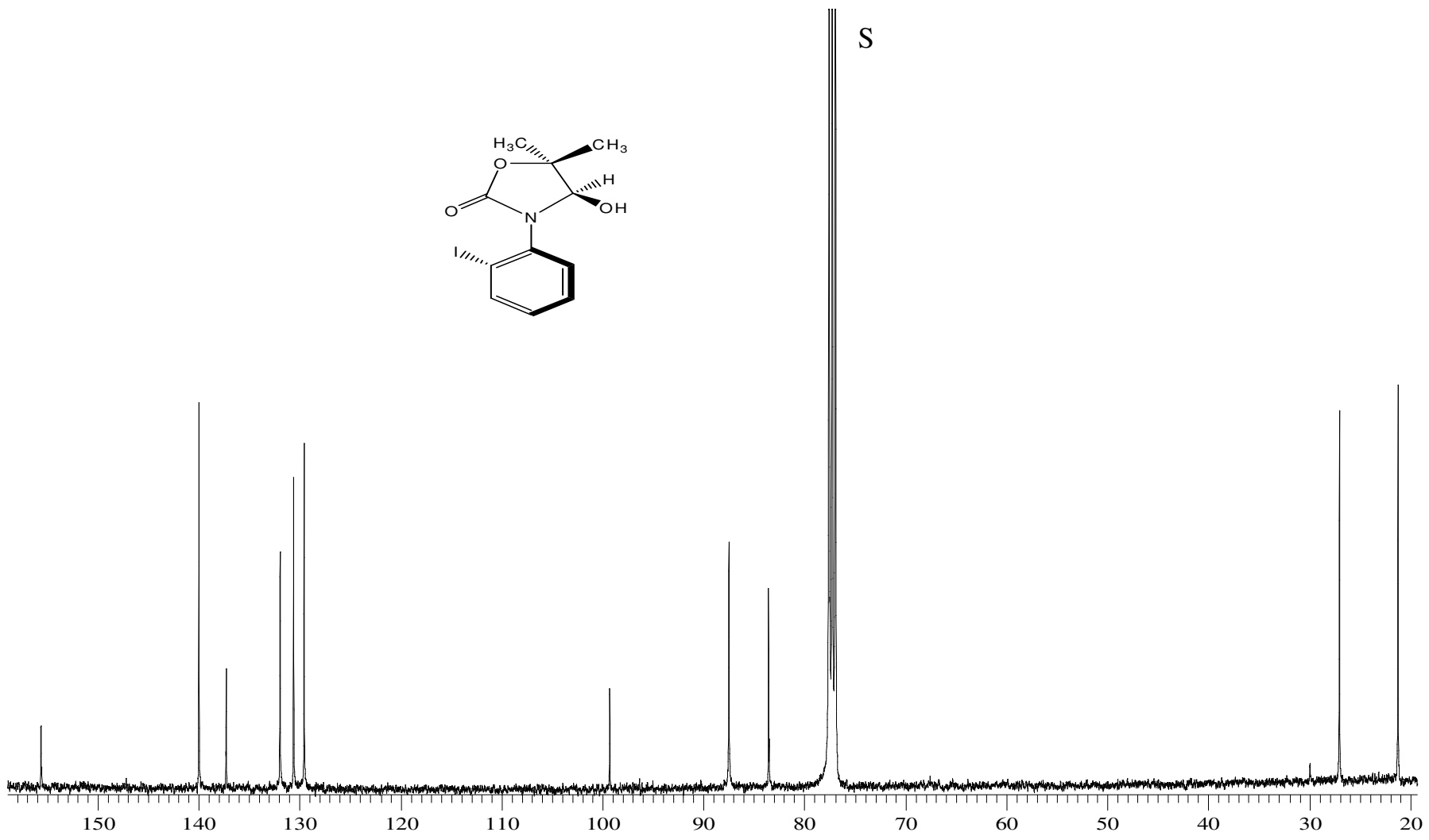


Figure A.56. 100 MHz ¹³C NMR spectrum of compound **55** in CDCl₃. S: Solvent

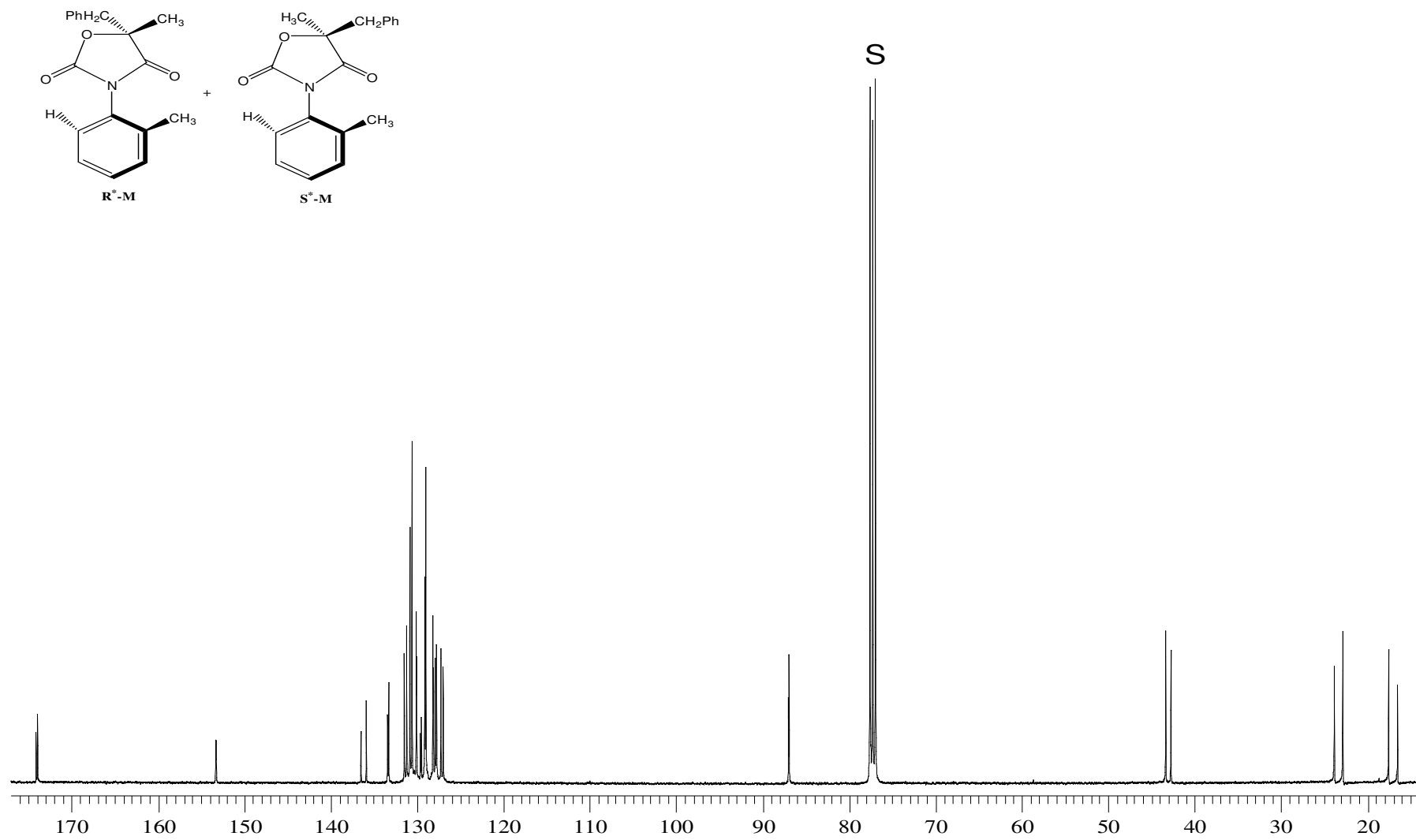


Figure A.57. 100 MHz ¹³C NMR spectrum of compound **56** in CDCl₃. S: Solvent

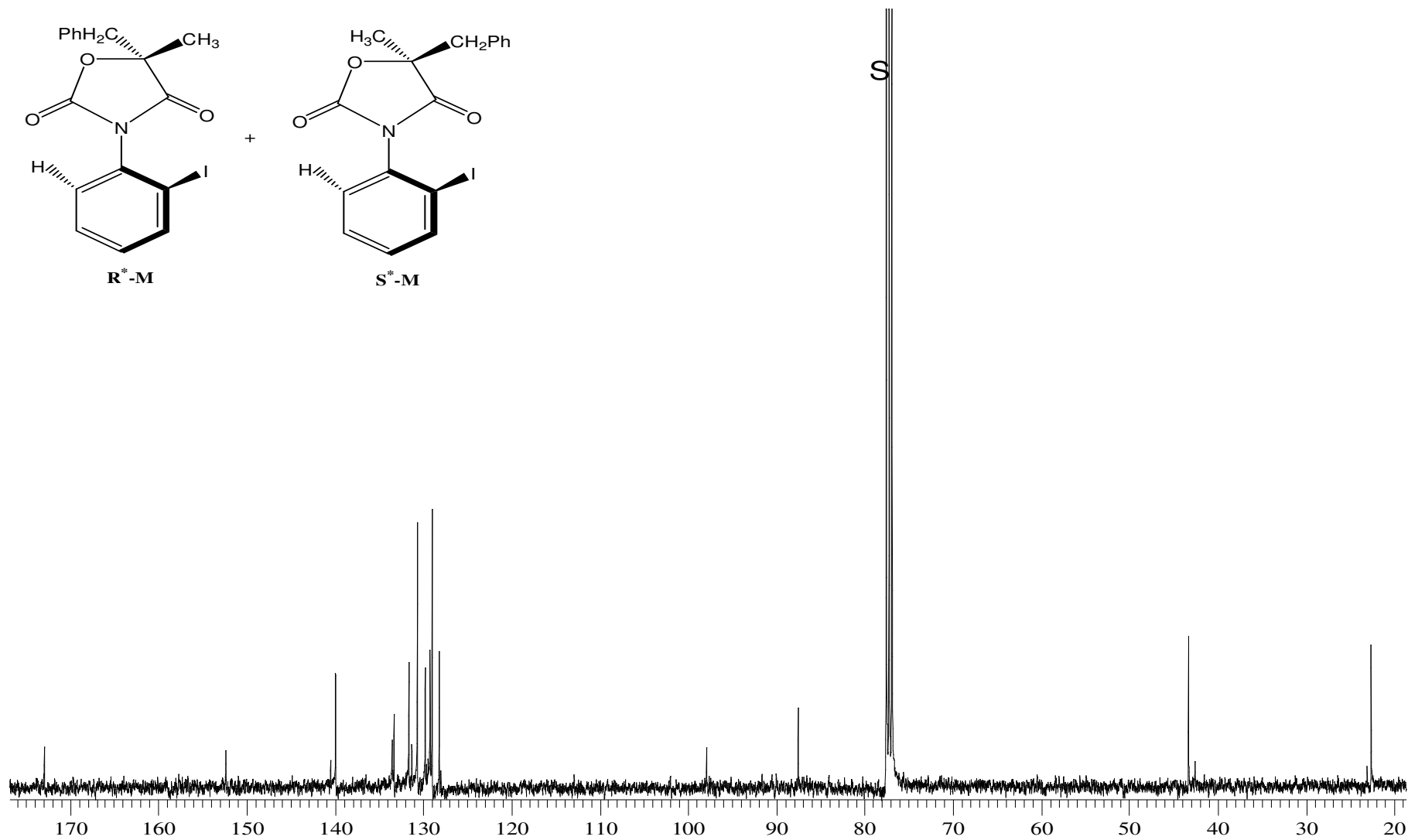


Figure A.58. 100 MHz ^{13}C NMR spectrum of compound **57** in $CDCl_3$. S: Solvent

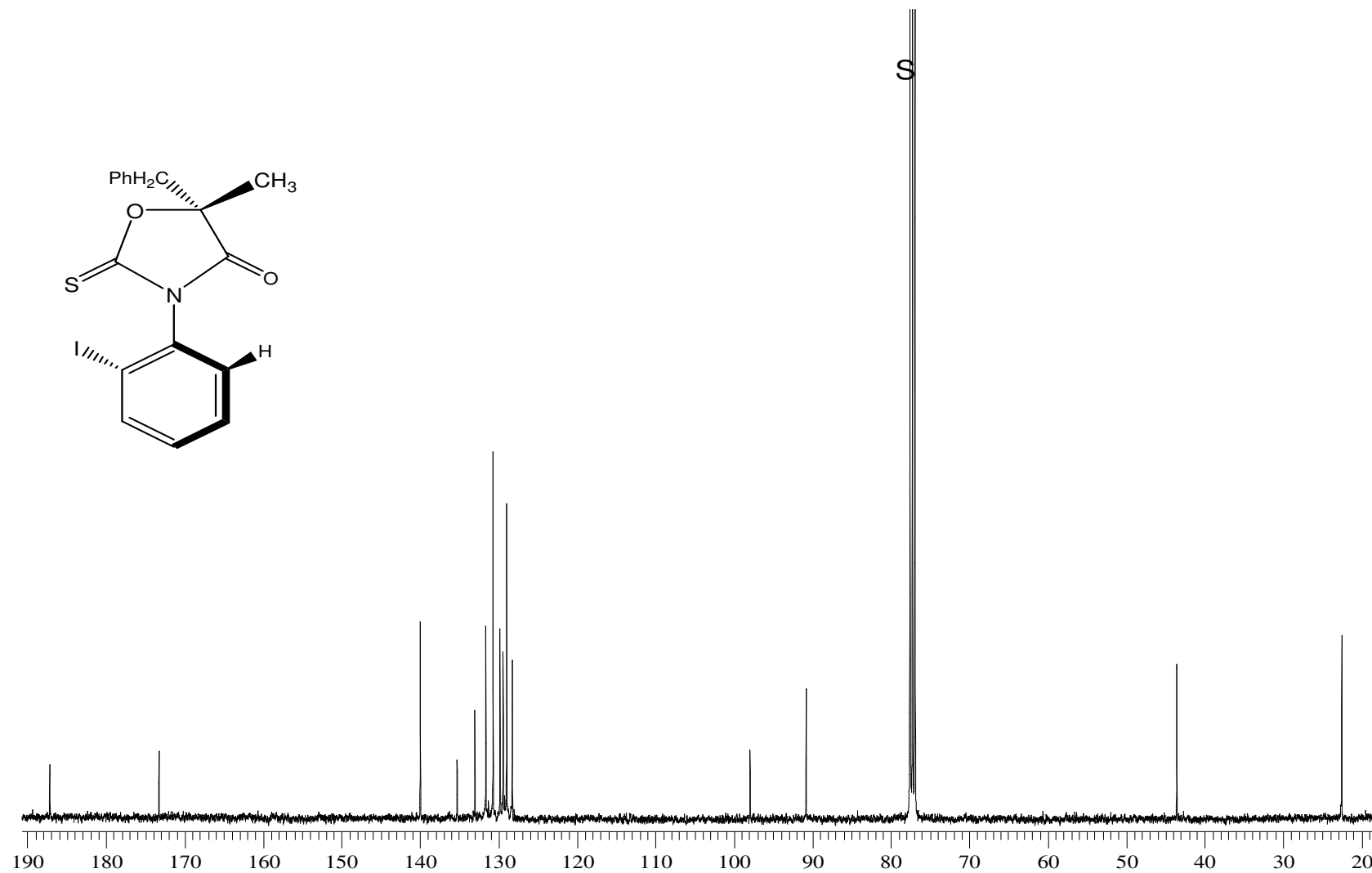


Figure A.59. 100 MHz ^{13}C NMR spectrum of compound **59** in CDCl_3 . S: Solvent

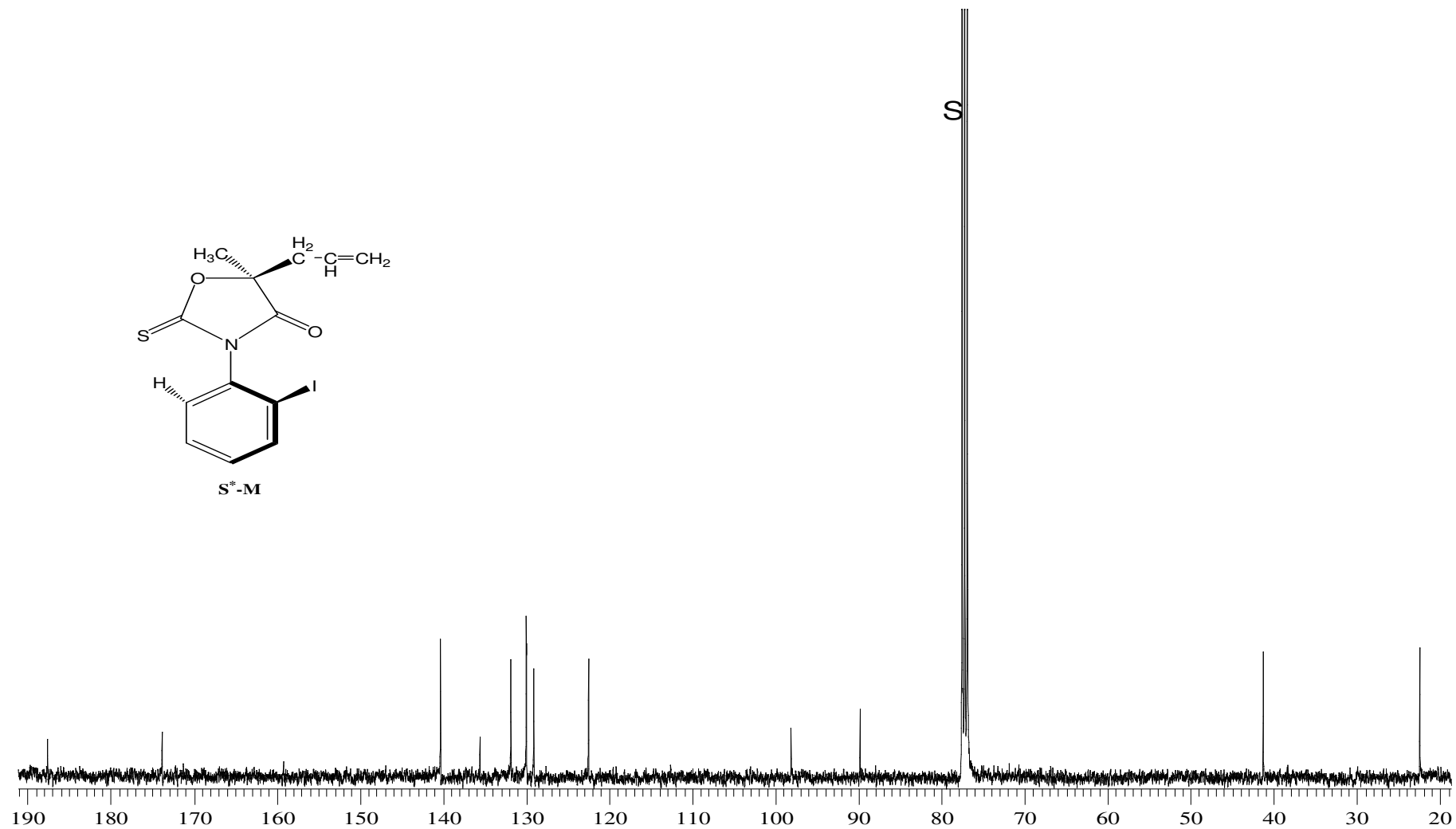


Figure A.60. 100 MHz ^{13}C NMR spectrum of compound **60** in CDCl_3 . S: Solvent

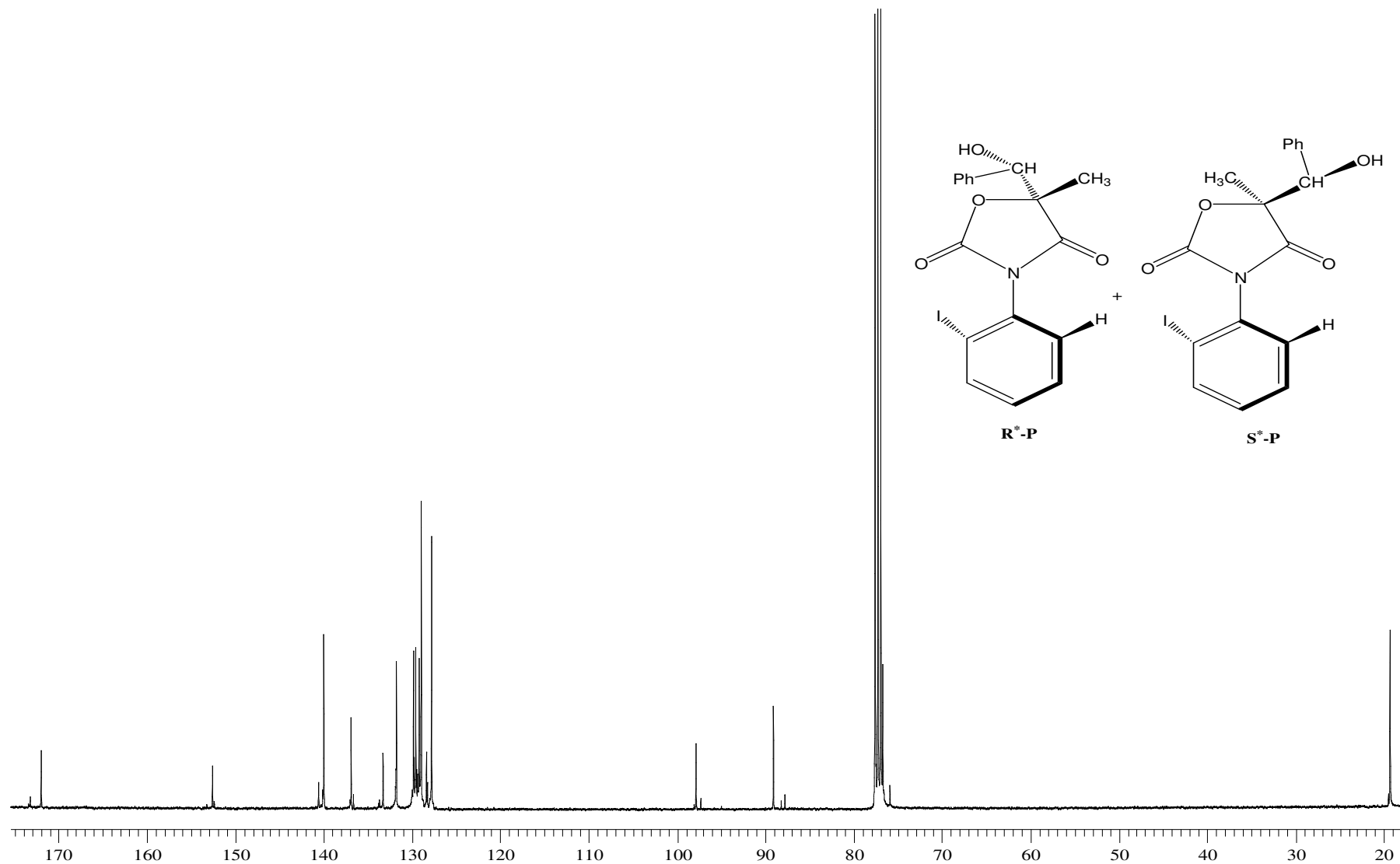


Figure A.61. 100 MHz ^{13}C NMR spectrum of compound **61** in CDCl_3 . S: Solvent

REFERENCES

1. Masamune, S., S. Choy, W. Kerdesky, F. A. J. Imperiali, "Stereoselective Aldol Condensations. Use of Chiral Boron Enolates", *J. of Am. Chem. Soc.*, , Vol.103, pp. 1566-1568, 1981.
2. Shapiro, S. L., I. M. Rose, F. C. Testa, E. Roskin, L. Freedman, "N-substituted Oxazolidinediones", *J. Am. Chem. Soc.*, Vol.81, pp. 6498-6504, 1959.
3. İçli, S. "¹H NMR and ¹³C NMR Studies on 3-Aryl-5-alkyl-2,4-oxazolidinediones. The Magnetic Non-equivalence of Isomeric Nuclei", *Organic Magnetic Resonance*, Vol. 12, No. 3, pp. 178-182, 1979.
4. Adams, R. and R.W. Stoughton, "Stereochemistry of Diphenyl Compounds. The Preparation and Resolution of 2-Methyl-6-nitro-2'-carboxydiphenyl", *J. American Chemical Society*, Vol. 52, pp. 5263-5267, 1930.
5. Chan, R. S., C. Ingold and V. Prelog, "Specification of Molecular Chirality", *Angew. Chem. Internat. Edition*, Vol. 5, No. 4, pp. 385-415, 1966.
6. Allinger, N. L., E. L. Eliel and S. H. Wilen, *Topics in Stereochemistry*, New York: John Wiley & Sons, 1982.
7. Pirkle, W. H. and D. L. Sikkenga, "The Use of Chiral Solvating Agent for Nuclear Magnetic Resonance Determination of Enantiomeric Purity and Absolute configuration of Lactones. Consequences of Three-Point Interactions", *J. Org. Chem.*, Vol. 42, pp. 1370-1374, 1977.
8. Lin G-Q., Y-M. Li and A.S.C. Chan, *Principles and Applications of Asymmetric Synthesis*, John Wiley, New York.
9. Rainer M., *Modern Aldol Reactions*, Wiley-VCH Verlag GmbH&Co. KGaA, 2004.

10. Ager D. J. and M. B. East, *Asymmetric Synthetic Methodology*, CRC Press LLC, 1996.
11. Evans, D. A., J. Bartroli and T. L. Shih, "Enantioselective Aldol Condensations. 2. Erythro Selective Chiral Aldol Condensation via Boron Enolates", *J. Am. Chem. Soc.*, Vol. 103, pp. 2127-, 1981.
12. Prashad M., D. Har, H-Y. Kim and O. Repic, "A New, Economical, Practical and Racemization Free Method for the Reductive Removal of 2-Oxazolidinones from N-acyloxazolidinones with Sodium Borohydride", *Tetrahedron Letters*, Vol. 39, pp. 7067-7070, 1998.
13. Thornton R. and M. P. Bonner, "Asymmetric Aldol Reactions. A new Camphor-Derived Chiral Auxiliary Giving Highyl Stereoselective Aldol Reactions of both Lithium and Titanium(IV) Enolates", *J. American Chemical Society*, Vol. 113, pp. 1299-1308, 1991.
14. Demir Ö. and İ. Doğan, "Conformational Preferences in Diastereomeric (5S)-Methyl-3-o-aryl-2,4-oxazolidinediones", *Chirality*, Vol. 15, pp. 242-250, 2003.
15. Sohar P., *Nuclear Magnetic Resonance Spectroscopy*, Boca Raton, FL, CRC, 1984.
16. Alberty R.A. and R. J. Silbey, *Physical Chemistry*, Newyork: Wiley, 1992.
17. Eliel E.L. and S. H. Wilen, *Stereochemistry of Organic Compounds*, New York:Wiley, 1994.
18. Gruttadauria N. R. and M. Pace, "NMR Analysis of Restricted Internal Rotation in 2-Substituted-2,3-dihydro-3-o-toly(chlorophenyl)-4(1H)-quinazolinones", *J. of Heterocyclic chem.*, Vol. 33, pp. 1067-1071, 1996.

19. Demir Ordu, Ö. and İ. Doğan, "Determination of Energy Barriers to Rotation and Absolute Conformations of Thermally Interconvertible 5,5-Dimethyl-3-(*o*-aryl)-2,4-oxazolidinedione Enantiomers", *Tetrahedron: Asymmetry*, Vol. 15, pp. 925-933, 2004.
20. Bürkle, W., H. Karfunkel and V. Schurig, "Dynamic Phenomena During Enantiomer Resolution by Complexation Gas Chromatography : A Kinetic Study of Enantiomerization" *Journal of Chromatography A*, Vol. 288, pp. 1-14, 1984.
21. Mannschreck, A and L. Kiebi, "Enantiomerization During HPLC on an Optically active Sorbent. Deconvolution of Experimental Chromatograms", *Chromatographia*. Vol. 28, pp. 263-266, 1989.
22. Wolf, C., W. H. Pirkle, C. J. Welch, D. H. Hochmuth, W. A. König, G. L. Chee and J. L. Charlton, "Determination of the Enantiomerization Barrier of Arylnaphthalene Lignans by Cryogenic Subcritical Fluid chromatography and Computer Simulation", *Journal of Org. Chem.*, Vol. 62, pp. 5208-5210, 1997.
23. Okamoto, Y.; Kaida, Y. "Resolution by High-performance Liquid Chromatography Using Polysaccharide Carbamates and Benzoates as Chiral Stationary Phases", *Journal of Chromatography A*, Vol. 666, pp. 403-419, 1994.
24. Doğan, I., T. Burgemeister, S. Icli and A. Mannschreck, "Synthesis and NMR Studies of Chiral 4-Oxazolidinones and Rhodanines", *Tetrahedron*, Vol. 48, pp. 7157-7164, 1992.
25. Jullian, J. C., X. Franck, S. Latypov, R. Hocquemiller and B. Figadere, "NMR Determination of Absolute Configuration of α -acyloxy Ketones", *Tetrahedron: Asymmetry*. Vol. 14, pp. 963-966, 2003.
26. Pirkle, W. H. and J. M. Finn, "Chiral High Pressure Liquid Chromatographic Stationary Phases. 3. General Resolution of Arylalkyl Carbinols", *J. Org. Chem.*, Vol. 46, pp. 2935-2938, 1981.

27. Lipkowitz, K. B., D. A. Demeter and C. A. Parish, "Enantioselective Binding of 2,2,2-Trifluoro-1-(9-anthryl)ethanol on a Chiral Stationary Phase: a Theoretical Study", *Anal. Chem.*, Vol. 59, pp. 1731-1733, 1987.
28. Karataş, M., S. Koni and İ. Doğan, "Chiral N-(o-aryl)-thiazolidinediones: Synthesis from Rhodanines and Investigation on Rotational Enantiomers by NMR Spectroscopy", *Can. J. Chem.*, Vol. 76, pp. 254-259, 1998.
29. Beaufour, M.; Merelli, B.; Menguy, L.; Cherton, J. C. "Determination of the Enantiomeric Composition of Chiral Delta-2-oxazolines-1,3 by ^1H and ^{19}F NMR Spectroscopy Using Chiral Solvating Agents", *Chirality*, Vol. 15, pp. 382-390, 2003.
30. Demir Ordu, Ö., E. M. Yılmaz and İ. Doğan, "Determination of the Absolute Stereochemistry and the Activation Barriers of Thermally Interconvertible Heterocyclic Compounds Bearing Naphthyl Substituent", *Tetrahedron: Asymmetry*, Vol. 16, pp. 3752-3761, 2005.
31. Evans, D. A., K. T. Chapman, D. T. Hung and A. T. Kawaguchi, "Transition State π -Solvation by Aromatic Rings: An Electronic Contribution to Diels-Alder Reaction Diastereoselectivity", *Angew. Chem., Int. Ed. Engl.*, Vol. 26, pp. 1184-1186, 1987.
32. Pirkle, W. H., T.C. Pochapsky, "Chiral Molecular Recognition in Small Bimolecular Systems: A Spectroscopic Investigation into the Nature of Diastereomeric Complexes", *J. Am. Chem. Soc.*, Vol. 109, pp. 5975-5982, 1987.
33. Cochran, J. E., T. J. Parrot, B. H. Whitlock and H. W. Whitlock, "Pi Hydrogen Bonds as a Design in Molecular Recognition", *J. Am. Chem. Soc.*, 114. 2269-2270, 1992.
34. Pirkle, W. H., S. D. Beare and R. L. Muntz, "Assignment of Absolute Configuration of Sulfoxides by NMR. A Solvation Model", *Tetrahedron Letters*, Vol. 26, pp. 2295-2298, 1974.

35. Hanna, G. M. and F. E. Evans, "Optimization of Enantiomeric Separation for Quantitative Determination of the Chiral Drug Propranolol by ^1H NMR Spectroscopy Utilizing a Chiral Solvating Agent", *Journal of Pharmaceutical and Biomedical Analysis*, Vol. 24, pp. 189-196, 2000.
36. Guckian, K. M., B. A. Schweitzer, R. X.-F. Ren, C. J. Sheils, D. C. Tahmassebi and E. T. Kool, "Factors Contributing to Aromatic Stacking in water: Evaluation in the Context of DNA", *J. Am. Chem. Soc.*, Vol. 122, pp. 2213-2222, 2000.
37. Rotello, V. M., E. A. Viani, G. Deslongchamps, B. A. Murray and J. Rebek, "Molecular Recognition in Water: New Receptors for Adenine Derivatives", *J. Am. Chem. Soc.*, Vol. 115, pp. 797-798, 1993.
38. Muehldorf, A. V., D. V. Engen, J. C. Warner and A. D. Hamilton, "Aromatic-aromatic Interactions in Molecular Recognition: A Family of Artificial Receptors for Thymine that Shows both Face-to-Face and Edge-to-Face Orientations", *J. Am. Chem. Soc.*, Vol. 110, pp. 6561-6562, 1988.
39. Walker, R. B., L. D. Fitz, L.M. Williams, H. Linton and C. C. Smith, "The Effect of Ephedrine Isomers and Their Oxazolidines on Locomotor Activity in Rats", *General Pharmacology: The Vascular System.*, Vol. 24, pp. 669-673, 1993.
40. Momose, Y., T. Maekawa, T. Yamano, M. Kawada, H. Odaka, H. Ikeda and T. Sohda, "Novel 5-Substituted 2,4-Thiazolidinedione and 2,4-Oxazolidinedione derivatives as Insulin Sensitizers with Antidiabetic Activities", *J. Med. Chem.*, Vol. 45, pp. 1518-1534, 2002.
41. Aitken, R. A.; Kilenyi, S. N. *Asymmetric Synthesis*; London: Blackie Academic & Professional, 1992; pp. 83-140.
42. Beesley, R. M., C. K. Ingold and J. F. Thorpe, "The Formation and Stability of Spiro-compounds. Part 1. Spiro-compounds from Cyclohexane", *J. Chem. Soc. Trans.*, Vol. 107, pp. 1080-1106, 1915.

43. Kaneti J., A. J. Kirby, A. H. Koedjikov and I. G. Pojarlieff, "Thorpe–Ingold Effects in Cyclizations to Five-membered and Six-membered Rings Containing Planar Segments. The Rearrangement of N(1)-alkyl-substituted Dihydroorotic acids to Hydantoinacetic Acids in Base", *Organic and Biomolecular Chemistry*, 2, pp. 1098-1103, 2004.
44. For the synthesis of the compounds see references 14 and 19.
45. Seyden-Penne J., *Reductions by the Alumino- and Borohydrides in Organic Synthesis*, Wiley-VCH, 1997.

